Fall 12-2011

Design of Covalently Dynamic Films and Coatings: Analysis of Biocatalyzed Kinetic Behavior in Soft Condensed Matter

Pirro Cipi
University of Southern Mississippi

The University of Southern Mississippi

DESIGN OF COVALENTLY DYNAMIC FILMS AND COATINGS: ANALYSIS OF BIOCATALYZED KINETIC BEHAVIOR IN SOFT CONDENSED MATTER

by

Pirro Cipi

A Dissertation
Submitted to the Graduate School
of The University of Southern Mississippi
in Partial Fulfillment of the Requirements
for the Degree of Doctor of Philosophy

December 2011

ABSTRACT

DESIGN OF COVALENTLY DYNAMIC FILMS AND COATINGS:

ANALYSIS OF BIOCATALYZED KINETIC BEHAVIOR IN

SOFT CONDENSED MATTER

by Pirro Cipi

December 2011

Reversibly adjusting surface and bulk properties of materials is advantageous to many applications and will vastly expand current polymer capabilities. A novel strategy was developed to render materials capable of "smart" surface and bulk properties with the aid of embedded biocatalyst and latent functional groups that are selectively activated in the presence of biocatalyst to undergo chemical transformation. The research presented herein focused on systematically characterizing the activity of lipase catalysts embedded in poly (alkyl methacrylate)s simultaneously with functionalized components, either as diffusing within the polymeric matrix or tethered to the matrix. Lipase activity, ester forming (synthetic) or ester breaking (hydrolytic), provided the pathway for the polymer matrix to self-tune its properties by catalytic transformation of untethered or tethered functionalized component. Therefore, the primary research goal was to understand and quantify embedded biocatalyst mediated transformation rates of functional species, diffusing or covalently tethered in films and coatings, as a function of polymer physical parameters and processing conditions.

In vivo, biocatalysts mediate complex biochemical reactions and pathways in macromolecular crowded environments. The excluded volume established by macromolecular complexes largely controls cellular enzyme turnover rates by establishing concentration gradients and diffusion regimes within cells. Initially, three poly (alkyl methacrylate) free-standing films were embedded with Porcine Pancreas Lipase and –OH and –COOH functional small molecules capable of undergoing lipase catalyzed acyl transfer reactions. Design of films with embedded functionality along with embedded biocatalyst was inspired by the confined nature of cellular microenvironments.

A systematic study was conducted to understand how initial confining matrix properties influence transformation rates of embedded functionality mediated by embedded enzymes in amorphous matter. Biocatalytic activity in films embedded with enzyme and functionality was diffusion-limited relative to both free enzyme and enzyme-only embedded films with surface exposure to small molecule functionality. The diffusion-limited biocatalytic activity exhibited linear dependency on the fraction of polymer free volume in glassy and rubbery films at < 8% by weight (8.8 - 9.7% by volume) loadings of stoichiometric amounts of functionality. The biocatalytic activity in the glassy state increased linearly with film thickness, which suggested the fugitive solvent left behind more free volume sites within the confining matrix at higher film thicknesses facilitating the transport of the functionality within the matrix.

Temperature studies confirmed that biocatalytic activity in the glassy state was dependent on small molecule migration in kinetically trapped excess free volume within interconnected OA and 1-NN rich regions. Solvents in the glassy systems behaved as transient templates during film formation as determined by the correlation of biocatalytic activity with the difference between the solubility parameters of the film and the solvent. Poly (alkyl methacrylate) films with embedded biocatalyst alongside functionality manifested reversible conversion of octanoic and 1-nonanol to nonyl octanoate based on the equilibrium water content. These formulations exhibit potential as hybrid materials with switchable bulk properties via reaction equilibrium control of the functionality by altering environmental conditions.

We also investigated an approach to engineer materials capable of reversible crosslinking by immobilizing enzymes in matrices containing multifunctional comb-like –COOH and –OH copolymers for adhesives, elastomers, composites, and laminates applications. Coatings comprised of the polyfunctional polymer blend and lipase at 1-4 wt% on solids were cast on glass and aluminum substrates. Acid equivalents, final molecular weight, and T_g, progression over time were used to quantitatively assay the enzyme-catalyzed reaction between the two functionalized components up to 250 hours. In rubbery systems, the consumption of acid functionality corresponded to an increase in molecular weight with similar reactivity rates.

Finally, immobilized lipase B from *Candida Antarctica* was used to synthesize novel poly (ester amide)s with pendant and backbone amides. Polymerization kinetics, molecular weight, and structure of the resulting poly (ester amide)s were determined via gel permeation chromatography and nuclear magnetic resonance spectroscopy. Rate constants for lipase from *Candida Antarctica* -catalyzed polyesterifications were examined as a function of monomer structure. Polymerization kinetics were characterized by initial linear molecular weight growth and a plateau in the later stages of polymerization. Thermal analysis of poly (ester amide)s suggested that the pendant amide improved thermal stability. In addition, the polymerization of γ-acetamido-ε-caprolactone was carried out by a two-step, one-pot process, despite lower reactivity relative to the unsubstituted analog, ε-caprolactone. Initially, base catalyzed ring opening was conducted in methanol at room temperature followed by bulk polymerization in the presence of *Candida Antarctica* lipase acrylic resin at 60 °C for 150 h. The resulting polymer was determined to be amorphous in nature due to the presence of pendant groups along the polyester backbone.

The University of Southern Mississippi

DESIGN OF COVALENTLY DYNAMIC FILMS AND COATINGS: ANALYSIS OF BIOCATALYZED KINETIC BEHAVIOR IN SOFT CONDENSED MATTER

by

Pirro Cipi

A Dissertation
Submitted to the Graduate School
of The University of Southern Mississippi
in Partial Fulfillment of the Requirements
for the Degree of Doctor of Philosophy

Approved:

_James W. Rawlins_____
Director

_Robson F. Storey_____

_Sergei I. Nazarenko_____

_Lon J. Mathias_____

_Gordon C. Cannon_____

_Susan A. Siltanen_____
Dean of the Graduate School

December 2011

DEDICATION

In memory of Spiro Cipi (1909 – 1987) and Josif Popa (1927 – 1996).

This dissertation is dedicated to my family for their love and support:

To my grandmother, Elvira Popa, for her wisdom, fortitude, and discipline;

To my parents, Bardhyl and Margarita Cipi for their sacrifice and perseverance to facilitate my absolute success;

To my brother, Rezart Cipi, for his encouragement and inspiration; and

To the Strickland family (Larry, Regina, Leah, Leisa, and Sam) for generously providing home away from home.

For everyone, I am eternally grateful.

ACKNOWLEDGMENTS

I am profoundly grateful to my advisor, Dr. James W. Rawlins, for providing the opportunity to learn and mature personally and professionally under his guidance. His scientific and business acumen, broad knowledge, pragmatic approach, and strong work ethics have been a great source of inspiration during my graduate career. I would also like to acknowledge my committee members for their time, guidance, and expertise: Dr. Robson F. Storey, Dr. Sergei I. Nazarenko, Dr. Gordon C. Cannon, and Dr. Lon J. Mathias. I would also like to thank the School of Polymers and High Performance materials for providing funds during my first year as a graduate student.

I would like to thank all of the Thames-Rawlins Research Group, my fellow graduate students, and my first year class. In particular, I would like to thank Kim Brandon, Kim Luck, Sharathkumar Mendon, Michael Blanton, Richard Ferguson, David Delatte, Dwaine Braasch, Eric Williams, Andrew Jones, Melvin Tucker, Brandon Achord, Jeremy Swanson, James Whittemore, Hussein and Eylem Tas, Sam Tucker, Justin Chan, Andrew Magenau, Mukul Kaushik, and Luke Kwisnek for providing vast insight, fruitful discussions, and endless support throughout my graduate career.

TABLE OF CONTENTS

LIST OF FIGURES

Figure

LIST OF TABLES

Table

CHAPTER I

INTRODUCTION

Enzymes are biopolymers that catalyze reactions in all living systems. They belong to the protein class of biomolecules, but are distinguished from other proteins by the presence of active sites that facilitate catalysis *(1)*. Enzyme catalysis provides an excellent method for chemical transformations at a wide range of temperatures with great efficiency and virtually no side reactions. Enzymes accept a vast library of chemical functionality with high specificity and selectivity and are an efficient tool in the preparation of pharmaceuticals, natural products, fine chemicals, and food ingredients *(2,3)*. The rediscovery that most enzymes can function perfectly well in near anhydrous conditions has dramatically widened the scope of their use in synthesis applications since the vast majority of organic compounds are not water soluble *(4,5)*. Steady increases in commercial availability, coupled with advances in directed evolution techniques and aqueous extraction methods, have yielded enzymes with superior properties relative to the wild type counterparts for use in catalysis, separation, and sensor applications *(6)*. The common focus of these applications is developing methods to obtain desired enzyme activity while maintaining or improving biocatalyst stability and longevity under the end-use conditions.

There are two broad approaches to biocatalyst stabilization for industrial applications: carrier-free and carrier-bound enzyme immobilization *(7,8)*. The term ‘immobilization’ in open literature refers to incorporating an enzyme molecule in a distinct phase while allowing exchange with the bulk phase *(9)*.

Immobilized enzymes consist of a catalytic component that converts target molecules (enzyme substrates) within the desired timeframe, and a non-catalytic component that stabilizes the catalyst and aids in controlling substrate transfer to and from the catalytic components *(8)*. The non-catalytic component is an inert organic or inorganic polymeric matrix in carrier-bound systems and an insoluble protein in carrier-free systems. Traditionally, immobilized enzymes have applications as catalytically active materials in heterogeneous catalysis, analytical and biomedical devices, and selective sorbents for bioseparation *(3,10,11)*. Recently, interests have developed in the utilization of biocatalyst embedded in materials for applications as protective, decorative, biodegradable, antifouling, self-cleaning and detoxifying coatings, and in films and fabrics where "smart" surface properties are desirable *(12,13,14,15,16)*. This dissertation describes materials capable of "smart" surface and bulk properties with the aid of embedded biocatalyst and latent functional groups that are selectively activated in the presence of biocatalyst to undergo chemical transformation.

Membranes, films, coatings, and multilayer compositions are derived from diverse chemistries and additives to achieve the desired processing and end-use mechanical and/or aesthetic properties *(17)* (Table 1).

Table 1

Typical Composition of Membranes, Films, Coatings, and Multilayer Systems

Phase	Component	Type
Continuous	Polymer	polyesters, polyurethanes, acrylics, epoxy resins, phenolic resins, natural resins
	Solvent	nonpolar, polar (aprotic/protic)
Discontinuous	Additives	catalysts, driers, flow agents

Embedding active enzymes is an attractive approach to enhance mechanical and chemical properties of materials via biotransformation of embedded latent functionalities in the post-cure polymer phase. The functional groups capable of undergoing biocatalyzed transformations to achieve bulk mechanical and chemical properties modification must also be embedded alongside the biocatalyst in the host material of interest. The simultaneous embedding of biocatalyst and functional groups distinguishes this research from the general literature on immobilization enzyme technology (Figure 1).

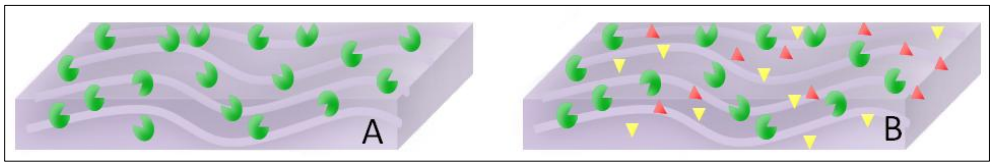

Figure 1. A) Catalyst-only embedded material as described in the literature obtained via adsorption, covalent attachment, entrapment, or encapsulation of the biocatalyst (ᗧ) in an inorganic or organic matrix (rectangle) in various geometries, and B) biocatalyst (ᗧ) and latent functionality (▲and ▼) embedded in polymer films/coatings/membranes (rectangle) where the functionality is freely diffusing or tethered to the matrix as described in this research.

Engineering a biocomposite material is challenging since microenvironment chemical and physical properties must be tailored to optimize biocatalyst activity. Physical and chemical properties of the matrix limit biocatalyst activity by imposing diffusional resistance on the starting functional groups and biotransformation products. Optimizing biocatalyst activity to match shifts in material properties during end use requires answering the following questions: *what* degree of biocatalyst activity enhancement or reduction is achieved by each polymer physical and chemical property, and *what* is the final physical and chemical character of the polymer. Incorporation of an active

enzyme confers the ability to conduct selective chemistry at a range from room temperature to boiling temperatures in organic media *(18)*. Moreover, biocatalyst mediated chemistries are reversible and thus, can be designed to respond to specific stimuli. These features make them particularly attractive for film, coating, and membrane applications that occupy specialty niches in dissimilar environments during material life cycle.

Biocomposite material activity, synthetic or hydrolytic, is a fundamental parameter to evaluate the utility of embedded enzymes in specific film, coating, and membrane applications. Biocatalyst activity is proportional to the catalyzed zero order reaction rate. Enzymes lower the activation energy required to transform functional groups by non-covalent stabilization of the target molecules. The active site binding energy accounts for the loss of activation entropy due to abating translational and rotational motion of the reacting species. An enzyme is thereby able to proportionally increase the rate of the forward and reverse reactions. Specific activity and catalytic efficiency are biocatalyst intrinsic parameters obtained by determining the binding affinity (K_m) and maximal reaction rate (V_{max}) of the biocatalyst. However, embedded enzymes present a case where microenvironment conditions dictate biocatalyst intrinsic parameters. Thus, biocatalyst activity is dependent on the interplay of intrinsic biocatalyst parameters and extrinsic microenvironment factors. To modulate enzyme activity, it is necessary to fully understand the impact of physical and chemical characteristics on enzyme-catalyzed reactions. Understanding the interplay between variables allows the matrix and processing conditions, e.g., polymer

type, porosity, solvent type, temperature, polymer geometry, and crosslink density, to be tuned to produce the desired activity and end-properties.

In catalyst-only immobilization systems, investigations have provided insight into the mechanisms and molecular interplays of these complex systems. Empirical theories have been put forth to account for some of the experimental results. While these results have implications for films and coatings where surface property modification is desirable, they do not fully extend to scenarios where both biocatalyst and functional groups are embedded in the same host matrix. Therefore, the objective of this research was to provide an experimental and theoretical framework from which to understand and predict how various microenvironment conditions affect enzyme activity in cases where biocatalyst and functional groups are embedded simultaneously in a host matrix.

This dissertation is organized into three major sections. Section 1 (Chapters I, II, and III) provides the introduction, objectives, and applications for enzyme activated materials, as well as, experimental methods including polymer synthesis, active film/coatings preparation, and characterization techniques. Section 2 (Chapter IV) presents the kinetic behavior of enzyme catalyzed reactions in dilute and viscous organic media as baseline experiments for comparison with systems that have increasing diffusional constraints of the functionalized species. Section 3 (Chapters V and VI) extends kinetic models developed in the previous section to thermoplastic systems with embedded biocatalyst and small molecule functionalities. Section 4 (Chapters VII and VIII) describes kinetic behavior of catalyzed reactions and the thermal properties of

coatings containing copolymer blends with embedded enzyme and tethered functional groups. In addition, enzyme catalyzed polymerization of novel monomers to yield poly (ester amide)s and the results from studies evaluating the effects of sterically hindered functionality on biocatalysis are included in this section. Finally, Section 5 (Chapter IX) presents the concluding remarks and recommendations resulting from this work.

Background

Biocatalysis in confined environments

To understand the behavior of enzymes in confined environments, one can turn to studies of viscous media in aqueous environments where enzymatic and ligand binding properties have been studied to understand cellular physiology. It is well known that k_{cat} (turnover rate) is proportional to the inverse of viscosity to the β power, where $0 < \beta < 1$ is a function of cosolvent molecular weight *(19,20,21,22)*. As the cosolvent molecular weight increases, β shifts toward zero, and the reaction rate does not depend on solvent viscosity since larger cosolvents (diluents) cannot penetrate into the enzyme.

In films and coatings, mass transfer limitations are a prominent factor in enzyme-catalyzed reactions since functionalized species must overcome significant diffusional resistance from polymer chains prior to active site sequestration. Currently, little to no evidence is available in the literature to correlate enzyme activity to mass transfer limitations imposed by the host polymer matrix, whether the matrix is rubbery, leathery, or glassy in nature.

A few studies evaluated the stability of food products, mainly various polysaccharides, in the presence of enzymes that catalyzed hydrolysis. The impact of food glass transition on enzymatic and non-enzymatic rates has been explored, and in some cases, finite rates have been reported in the glassy regime *(23)*. Bell and White reported that non-enzymatic rates of thiamin hydrolytic degradation increased as the degradation temperature increased above the glass transition temperature (T_g) *(24)*. Kouassi and Roos evaluated the impact of T_g on enzyme-catalyzed hydrolysis of semi-crystalline carbohydrate mixtures as model food systems *(25)*. It was determined that hydrolysis occurred at reasonable rates in the rubbery state due to the increased molecular mobility that minimized diffusion limitations *(25)*. Increasing the water content validated the role of moisture as a factor that trumps T_g, and the sudden increase in the rate of hydrolysis was attributed to a threshold where enzyme and carbohydrate mixtures are compatible *(23,25,26)*.

From an organic polymer material perspective, it is well known that relaxation processes display universal behavior in their time-temperature dependence. Above the T_g, macromolecular dynamics dependence on temperature is best described by a two-energy of activation model, such as the Vogel-Tammann-Fulcher (VTF) and the Williams-Landen-Ferry (WLF) expressions. Below the T_g, the temperature dependence on macromolecular dynamics exhibits a single energy of activation, i.e., Arrhenius behavior, due to lack of long range molecular motions *(27,28)*. This universal temperature

dependency translates to important material parameters such as modulus, viscosity, thermal, mechanical, and electrical relaxations.

Host matrix physical properties: Design requirements

Physical parameters become prominent controlling factors when the matrix imposes mass transfer limitations that affect enzyme-catalysis reaction rates by lowering the diffusion rates of reactants and products. The driving force for the net diffusive events of reactants and products are the concentration gradients at the surface and throughout the confining matrix. Reactants diffuse through the unstirred media until an active site is encountered, followed by the catalyzed conversion. Once the product has been formed in the active site, it will diffuse in the surrounding media down its concentration gradient freeing up the active site.

The diffusive events can be expressed as external and internal mass transfer events for both reactants and products. External mass transfer occurs when reactants and products diffuse towards the outside of the confining matrix down their concentration gradient. Internal mass transfer occurs when reactants diffuse throughout the confining matrix towards enzyme active site or as products migrate away from the active site during synthetic or hydrolytic catalyzed events. Both diffusive events occur simultaneously and contribute to the formation of reactant and product concentration gradients within the film.

A study of the adsorption characteristics of *Rhizomucor Miehei* lipase on inorganic supports established a correlation between mesh size and lipase activity *(29)*. It was determined that pores with diameters less than 25 nm were

inaccessible to the lipase; at least a 35 nm size pore was necessary for the internal surface area of the pore to be usable as an adsorption site. It was also found that activity was highly dependent on pore size when <100 nm pores were used, presumably due to limitation in the rate of reactant diffusion. In pore sizes >100 nm, no change in activity was observed indicating that catalysis by lipase was not diffusion-limited *(29)*.

Other studies have addressed the minimum pore size necessary to overcome diffusional constraints. Reactant diffusion inside pores is determined by the 20 nm partition layer, p_L, and above 20 nm, the diffusion constraint by the partition layer can be neglected. To overcome diffusional constraints, the distance from the enzyme layer on the pore wall to the pore center should be greater than 20 nm (d_L). The minimum pore size should be double the pore radius, r_P, i.e., 40+2d_E *(8)*. If one considers the size of a typical enzyme as 6 nm, the minimum pore size would be 62 nm (Figure 2).

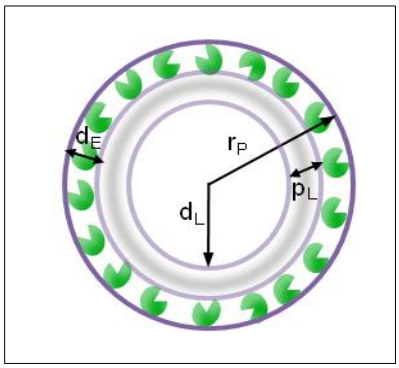

Figure 2. Pore size configuration in catalyst-only immobilized carrier to overcome diffusional constraints where d_E – enzyme diameter (●), d_L - diffusion layer, p_L - partition layer, and r_P – pore radius.

Lipase experiments in controlled pore glass have shown similar pore size values beyond which the reaction was not diffusion controlled *(30)*. Esterification

assays exhibited conversion even when pore diameters were less than 25 nm. Studies with penicillin G acylase and other enzymes have shown that pore sizes 8-10 times the enzyme diameter do not show diffusion-limited kinetics *(31)*. When diffusional constraints have an effect on enzyme catalysis, the intrinsic enzyme kinetic parameters are affected. In one study, it was found that the K_m value of acid phosphatase immobilized in bovine serum albumin-poly (ethylene glycol) increased two to five fold, depending on the polyethylene glycol (PEG) chain length and bead size *(32)*.

Particle size is an important parameter in immobilization technology especially when a non-porous media is used. Generally, the smaller the particle size, the greater the amount of enzyme that will be loaded in a given media resulting in higher activity because of added surface area covered/saturated with the enzyme. However, there are some practical limitations associated with end-use applications. Enzymes immobilized in an inert carrier, whether by adsorption or covalent conjugation, are used as heterogeneous catalysts for bioreactors. Particle sizes <100 μm result in problems with separation and pressure design in reactors. Typically, commercially available non-porous carriers are designed with particle sizes of approximately 100 μm *(2)*.

Novick and Dordick studied the impact of diffusional constraints by copolymerizing a vinyl-functionalized α-chemotrypsin with a series of multifunctional vinyl monomers to form bioactive networks that were pulverized to determine solution activity. Apparent activities 6.25 fold higher were observed in 6:1 than 1:1 solvent:monomer formulations when used as transesterification

catalyst for 1-propanol and *N*-acetyl-phenylalanine-ethyl ester. Increasing the mesh size via plasticization translated to an increased reactant diffusion rate and resulted in higher enzyme activity. Increasing the crosslink length (lower crosslink density and lower modulus) resulted in greater activity, which corroborated the concept that a larger mesh size supports higher diffusivity rates for the reactants and leads to higher observed catalytic activity *(33)*.

In another study, Gross and coworkers demonstrated the influence of diffusional constraints on reaction rates for enzyme-catalyzed polymerizations via crosslinked PMMA-based solid-resin beads with immobilized enzymes across a range of bead sizes. Constant pore diameter and bead surface area were maintained resulting in increased lengths of the tortuous pathway in higher diameter beads. When smaller bead sizes were loaded with immobilized catalyst, the enzyme-catalyzed polymerization rates were higher because of reduced pathway length and minimized migration of monomers and polymer products *(34)*.

Host matrix chemical properties: Design requirements

Molecular constitution and various substituents affect solubility parameter values. These chemical parameters are the result of the intrinsic polarity of each component and the interaction and combination of enzyme/matrix or functionality/matrix. They are described quantitatively by Hansen solubility parameters, which algebraically express the energy associated with the net attractive interaction or by logarithm of partition (log P) values for each type of interaction *(35)*. These interactions can lead to preferential crystallization of

reactants or products that can effectively increase or decrease accessibility to the active site. Abe and coworkers showed that copolymer compositions from (*R*)-3-hydroxybutyric and 6-hydroxyhexanoic acids demonstrated higher rates of erosion for amorphous compositions than crystalline ones when exposed to the aqueous solution of lipase from *Rhizopus Delemar* at 25 °C and pH 7.4 *(36)*. The results indicate that preferential crystallization in compositions with higher (*R*)-3-hydroxybutyric content led to diminished accessibility to the active site.

Chemical interactions also influence the diffusive behavior of reactants and products. Thermodynamically unfavorable interactions within a confining matrix have diminished probability of occurrence and lead to the formation of reactant and product gradients that result in varying observed enzyme activity versus polymer-reactant, polymer-product interaction parameters. Novick and Dordick incorporated chymotrypsin in polystyrene, poly (methyl methacrylate), and poly (vinyl acetate) films and investigated the degradation activity of chymotrypsin towards the milk protein, casein. The highest activity was observed in the hydrophilic poly (vinyl acetate) films. Results indicated that hydrophobic/hydrophilic interactions drive preferential reactant partitioning and result in either higher or lower activity that is directly proportional to enzyme active site accessibility *(37)*. Favorable interactions between casein and the hydrophilic surface increased casein's accessibility to the enzyme resulting in higher degradation rates *(37)*.

In addition, noncovalent interactions can impact the manner in which an enzyme interacts with a matrix. These interactions can affect enzyme

conformation and/or lead to ineffective adsorption to material interfaces. Lipase adsorbed on hydrophilic Celite® or Spherosil®, had more hydrolytic activity than lipase immobilized on Duolite® XAD 761 *(38)*. Celite and Spherosil are silica based, while Duolite XAD 761 is based on a phenol-formaldehyde polymer resin *(38)*. The highest synthetic activity was obtained using Duolite XAD 761 as the inert carrier *(38)*. The data revealed that the enzyme remained active when adsorbed on both carriers and exhibited 12.2 fold higher synthetic activity than the free enzyme when Duolite XAD 761 was used as an inert carrier *(38)*. However, enzyme adsorbed on hydrophilic carriers exhibited activity exclusively in aqueous media *(38)*. These results suggest that enzyme active conformations are directly dependent on the chemical nature of the carrier. Such data is common in published literature and confirm how all variables are seemingly important; and yet enzymes are also very robust for activity in a wide variety of environments *(39)*.

In other cases, the chemical nature of the carrier is important for the adsorption capacity of the carrier and the total enzyme activity i.e., product of total amount adsorbed and specific activity. It was found that the adsorption capacity of trypsin on copolymers of styrene and 2-hydroxyethyl methacrylate was dependent on the amount of hydroxyl functional comonomer *(40)*. Increased 2-hydroxyethyl methacrylate content led to reduced loading of trypsin due to the carrier's hydrophilic character *(40)*. Despite achieving 65% higher loading capacity in hydrophobic carriers, the specific activity measured by monitoring the

hydrolysis of *N*-α-benzoyl-*L*-arginine ethyl ester was diminished presumably due to autolysis or denaturation of trypsin induced by the hydrophobic surface *(40)*. Many researchers have included a spacer molecule between the enzyme and the inert carrier to fix the distance between active site and carrier. The addition of spacers minimizes enzyme conformational changes caused by nonspecific adsorption on the inert matrix and ensures minimal steric hindrance for optimal access during catalysis. Incorporation of a spacer arm also overcomes the issue of incompatible matrices *(39)*. For example, rennin type II from *Mucor Miehei* was immobilized on agarose supports conjugated with dextran. The activity of rennin on casein was determined to be 15-fold higher than the activity of the directly immobilized rennin. The data suggested that the presence of the hydrophilic spacer minimized steric hindrance from the support surfaces, and enabled the catalyst to exhibit high activity towards biological macromolecules *(41)*.

Applications as Bioactive Films, Membranes and Coatings Biocomposites

Antifouling surfaces

Biofouling is a term used to describe accumulation of biological materials on surfaces. The fouling organisms range from single proteins to bacteria, algae, and marine animals on the surface of structures immersed in seawater. Marine biofouling leads to aesthetic and structural damage of surfaces and coatings, but more problematically, fouling causes higher weight and drag resistance on surfaces, e.g., ship's hulls. The US Navy has estimated that biofouling costs

over $150 million annually in extra fuel consumption and cleaning costs for naval vessels *(42)*.

Metal oxides or organometallic compounds such as copper, mercury, lead, and tributyltin have been found to prevent biofouling and are commercially employed as biofouling additives in coatings. Recent concerns about heavy metal impact and long-term toxicity on the marine environment have provided an impetus for alternative and environmental friendly technologies. Several organisms found in nature employ enzymes to resist biofouling. Enzymes have proven attractive as active and yet broad range antimicrobial and antifouling materials. Since enzymes biodegrade in aqueous conditions, both leaching and long-term exposure to marine environments are not considered persistent, bioaccumulative, or toxic in nature according to current EPA standards *(43)*.

Any biological additive needs to be capable of surviving contact, storage, processing, application, and cure of coatings to be considered useful. Specific requirements for biocidal additives include compatibility with polymer, solvent and additives, collectively referred to as coating chemistries, and sustained activity over a definable lifetime for the applied coating. Hydrolases, glycosylases, and oxidases are considered as excellent candidates for anti-fouling purposes due to their activity and biodegradability *(44)*. Hydrolases catalyze the hydrolytic degradation of ester or amide containing functionality that comprise the adhesive layer of marine microorganisms, while glycosylases act on glycolytic bonds, a major cell wall component. Oxidases function by converting compounds present

in seawater or coatings into potent oxidizing agents that have biocidal effects on marine microorganisms.

Enzymes have been incorporated into polyurethanes, acrylates, polystyrene, alkyds, acrylamides, and rosin-based emulsions to serve as active static surface modulators or time-release active coatings, termed functional films in many recent literature references *(44,45,46)*. Research has confirmed that certain enzymes are active towards only specific microorganisms in terms of biocidal activity and/or reduction in adhesion strength for organisms on surfaces. Alternatively, certain enzymes are capable of producing and/or releasing organic molecules that abate the conventional biofouling processes from occurring on surfaces *(44)*. Mixing different classes of enzymes for both range and duration of activity half-life have failed to result in broader biofouling resistance *(44)*.

Albeit sound in principle, the studies presented to date often lack statistically relevant correlation for enzyme activity to coating system parameters, and therefore miss the objective of ascertaining activity variation among different coating systems. Within the open literature, a systematic investigation and understanding of coating formulation, processing, application, film-forming, and curing parameters on enzyme activity is not available and continues to hinder the rational design for active functional films.

Antimicrobial coatings

Increasing numbers of antibiotic-resistant strains are contributing to a large number of hospitalizations and deaths in the U.S. and worldwide *(47)*. Surfaces in public areas provide a platform for pathogenic bacteria to settle and

proliferate. One strategy to eliminate pathogen transmission has been to develop coatings with antimicrobial activity *(48,49,50)*. Some of these materials have found applications as coatings for building interiors, ventilation ducts, hospital and medical supplies, consumer products, household goods, kitchen counters, and furniture.

Antimicrobial surfaces with sufficient activity has been conferred by coating formulations based upon biocidal additives ranging from silver to pesticides to antimicrobial peptides to amphipathic polycations designed for controlled environmental release *(51)*. Silver-based coatings are strongly biocidal, however, their activity diminishes drastically as the active silver continues to leach out of the coating over time *(52)*. Also of concern are the unknown but suspected long-term effects from silver nanoparticle accumulation *(53)*. The use of antimicrobial peptides as biocidal coating additives is associated with increased resistance in pathogens and loss of biocidal efficiency over time *(54)*.

Some of the requirements for an effective antimicrobial coating are activity retention throughout the coating lifetime, compatibility with coating systems, and diminished pathogen resistance. Use of bacteriophage-derived enzymes that target pathogen cell walls has emerged as a promising strategy to develop antimicrobial coatings *(55)*. Bacteriophages have developed unique natural mechanisms to ensure their survival by expressing cell lytic enzymes required to exit the host bacterium and allowing them to infect neighboring microbial hosts *(56)*. Bacteriophages such as *Staphylococcus Aureus*, *Streptococcus*

Pneumoniae, and *Bacillus Anthracis* employ amidases, muramidases, and endopeptidases to attack host cell walls *(57,58)*.

Polymeric films containing lysostaphin, a cell lytic enzyme, were tested for bactericidal efficiency in cell culture suspension. Lysostaphin was attached to multiwalled carbon nanotubes (MWNTs) prior to incorporation in films. Experimental results demonstrated that lysostaphin activity was two-fold higher when a PEG linker was used to attach them to MWNTs as compared to direct enzyme attachment. The result suggested that conformational flexibility is important for proper catalytic function of lysostaphin *(59)*.

Decontamination surfaces

Organophosphate-based nerve agents act by blocking acetylcholine receptors that halt muscle activity in the body. Significant attention has been given to strategies to neutralize organophosphate compounds via enzymes that act on phosphoester bonds. Diisopropylfluorophosphatase (DFPase) and organophosphorous hydrolase (OPH) have been tested for their nerve agent decontamination activity in a variety of coating systems *(60,61,62)*. DFPase was incorporated in polyurethane coatings, and it was determined that polyurethane hydrophobicity significantly enhanced enzyme activity *(60)*. Similar improvements in activity were also achieved when porogens were incorporated into the coating, underlining the importance of both chemical and physical modification in achieving higher enzyme activities *(62)*.

OPH has been incorporated into commercial latex coatings and the activity was quantified as a function of surface contamination density versus

drying time of the coating. It was determined that as the drying time of the coating increased, the apparent activity diminished. However, when the coating was rehydrated, more than 85% of the original activity was recovered *(61)*. These two examples illustrate the complexity and diversity in microenvironment allowed by different enzymes that maximizes their utility in films and coatings.

Self-cleaning surfaces

Efforts to develop smart surfaces have led to the incorporation of antibodies in polyurethane coatings (Figure 3). Studies have validated that surface antibody-antigen interactions continue to occur even though the antibody is trapped within the coating. Coatings containing antibodies retained as much as five times more bound antigen than the blank polyurethane coatings *(12)*.

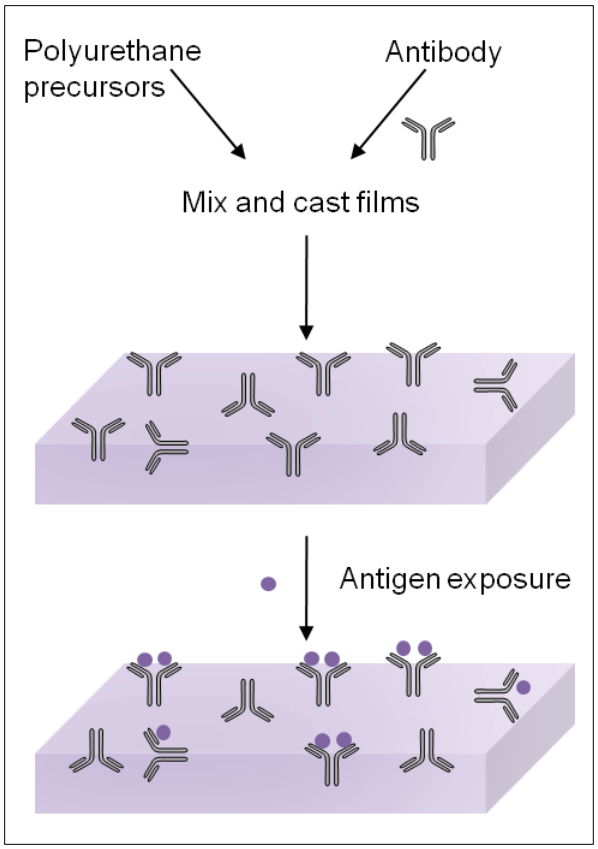

Figure 3. Strategy for antigen-capturing polyurethane surface coating.

Surfaces of films and coatings formulated to contain proteins and active enzymes have shown activities in both wet and dry environments. A protease, *Subtilisin Carlsberg*, was coated on polystyrene films to assess its ability to prevent protein accumulation at the surface. The protease treated films exhibited remarkable activity, specifically, for the hydrolysis of chicken egg albumin in both aqueous solution and on solid-state albumin applied on the protease-active surface *(63)*. This example confirms that enzymes applied over functional surfaces are capable of stimuli responsiveness. Critical to note is the fact that these materials function haphazardly as interactions between active enzymes, reactants, products and the coatings raw materials, e.g., polymer, pigments,

colorants, additives, solvents, fillers, modifiers are not fully understood. These parameters can improve or impede enzyme activity.

Biomedical applications

Recent advances in controlled polymerization techniques have facilitated the development of materials with precise control over monomer-to-monomer connectivity and the resulting polymer architecture for biomedical applications. Biomaterials that change properties in response to applied stimuli, such as temperature, ionic strength, solvent polarity, electric/magnetic field, or light are sought as research and development methods to alter/control material behavior/response once placed *in vivo*. Biomaterials that respond to enzyme catalysis have also been highly investigated due to the selective reactions catalyzed under physiological conditions *(64)*. Figure 4 represents a typical strategy for enzyme-responsive biomaterial hydrogels.

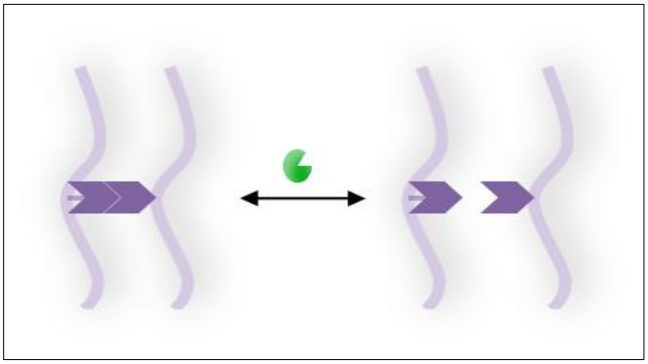

Figure 4. Strategy for development of enzyme-responsive biomaterial hydrogels with tethered functionality that is active in the presence of biocatalysts. Biocatalyst (ᗧ) and covalently tethered bioactive functionality are depicted.

Polymers used in biomedical applications are designed to undergo a sol-gel response or volumetric change via monomer repeat or functional group incorporation that responds to enzyme catalytic activity. The biomaterials

described below have been developed for applications in regenerative medicine, drug delivery, and diagnostics. For regenerative medicine, liquid precursor mixed with cells could be injected into tissue of focus and tissue fluid enzymes could be employed to trigger an *in vivo* gelation event. In contrast, drug delivery systems can be designed to release cargo upon contact with a cleaving enzyme as another method to control delivery kinetics. In diagnostics, sol-to-gel transitions may be incorporated as a method to detect events without relying on expensive equipment *(65)*.

In one example, methacrylic acid based hydrogels were synthesized with covalently tethered glucose oxidase enzyme *(66)*. When glucose was introduced into the hydrogel environment, the catalyzed reaction of glucose and oxygen liberated gluconic acid that caused a decrease in pH. The pH reduction caused protonation of the carboxylic acid groups on the hydrogel, resulting in a hydrogel structural collapse. In another example, peptide-based hydrogels self-assembled upon enzyme-catalyzed coupling of dipeptides to amino acids containing an aromatic fluorenylmethyloxycarbonyl (Fmoc) group. The Fmoc tripeptide self-assembled into high-order aggregates driven by the π-π interactions between the fluorenyl groups *(67)*.

Polymer biodegradation and modification

Polymeric materials have been investigated mainly in solution and film forms for post-synthesis modification via enzymes. The referenced data below focuses on methods to vary existing functionality or investigations targeting controllable polymeric material degradation. Most of the functional group

modification research and development to date for polymeric materials has been conducted using water-soluble biopolymers like polysaccharides *(68,69)*. Xie and Wang grafted ε-caprolactone on water-soluble hydroxyethylcellulose (HEC) using lipase(s) catalysis *(68)*. Hsieh and Xie modified solid cellulose by lipase-catalyzed transesterification of vinyl propionate and vinyl acrylate. Qualitative presence of vinyl ester linkages on the cellulose surface was measured by Fourier transform infrared (FTIR) spectroscopy *(69)*. Enzyme catalyzed modification for synthetic polymers has also been reported *(70,71)*. Polyethylene terephthalate (PET) modification with lipase resulted in improved wetting and absorbency without strength loss for applications in textiles *(70,71)*.

Enzymes have also been employed for the selective degradation of synthetic polymers, albeit primarily in aqueous solutions. Polyester degradation studies focus on quantifying film physical and chemical characteristics that have positive or negative effects on enzyme catalyzed film degradation. Variables shown to affect the rate of polyester degradation are most commonly cited as: monomer and polymer chemical structure, chain mobility, crystallinity, molar mass, and copolymer compositional ratios *(36,72,73)*. Rizarelli *et al.* demonstrated that sebacic acid units in poly(butylene succinate-*co*-butylene sebacate) were preferentially hydrolyzed via lipase and attributed to the more hydrophobic nature of these monomer units compared with other diacids *(72)*. Abe *et al*. studied the enzymatic hydrolysis rate for semi-crystalline poly(hydroxyalkanoic acid) films and concluded that degradation was dictated by lamella thickness and degree of crystallinity *(73)*.

More recently, surfactant paired *Candida Antarctica* Lipase B (CALB) was incorporated in polycaprolactone matrices at 6.5% and 1.65% by weight. Upon immersion in aqueous buffer, complete hydrolysis of polycaprolactone matrix occurred in as little as 24 hours. The number average molecular weight (M_n) diminished from 117,000 to 24,700 as 80% polymer weight loss occurred. Differential scanning calorimetry (DSC) results of the remaining hydrolytically degraded films revealed increased degree of crystallinity as compared to control films, further supporting that CALB induced hydrolysis was preferential to the amorphous regions of the film *(14)*.

Self-repairing polymers

The impetus for self-repairing functionality comes as the result of the inherent loss of properties exhibited by organic-based materials during use and environmental exposure. Materials undergoing constant stress initiate fracture at the molecular level due to events such as chain pullout, chain scission, and bond rearrangement. Fracture and fatigue, micro or macro, have been primarily linked to covalent bond rupture and rearrangement. These events result in more densely, physically or chemically crosslinked regions, and even less interconnectivity across macroscopic scale. Sperling provided keen insight showing that fracture in lower M_n polystyrene latexes, up to 32,000, were almost exclusively due to chain pullout. However, at very high M_n values, greater than 150,000, chain scission events contributed to approximately 90% of fracture events *(74)*.

Several approaches have been put forth to address events that lead to catastrophic failure. UV light stabilizers prevent degradation by capturing the initial excited species before these are able to affect further chain scission and rearrangement. Hindered amine light stabilizers (HALS) scavenge free radicals formed from UV or thermal oxidative degradation processes. HALS trap active radicals and regenerate the amine complex, slowing the degradation process. The data consistently supported that scission points are re-tethered and implicit evidence is available showing improved maintenance of physical and optical properties relative to systems similarly exposed in the absence of HALS *(75)*.

White *et al*. introduced an autonomous healing concept that, unlike prior methods, offers an alternative to manual intervention in the material stabilization process *(76)*. The concept centers on embedding raw materials that are ready for use after a trigger event. The process involves monomer encapsulation in brittle microcapsules that are designed to rupture upon physical fatigue and fracture. Traversing microcracks through capillary driving forces allow the liquid monomer to make direct contact with matrix embedded catalysts. The liquid monomers then polymerize and fill portions of voids in the propagated crack, but not the void remaining from the microcapsule.

Other researchers have utilized Diels-Alder chemistry, hydrogen bonds, metal coordination bonds, and hydrolysis and condensation of boronic esters as self-repairing chemistries; however, absent in the literature are reports of enzyme-mediated polymer self-repair *(77,78,79,80)*. The data presented herein

are focused on quantifying and understanding the variables that support or hinder enzyme catalysis for self-repair.

Research Summary

The research presented herein is focused on experimentally characterizing the activity of lipase catalysts embedded in poly (alkyl methacrylate)s simultaneously with functionality, either as freely diffusing within the polymeric matrix or tethered to the matrix. Lipase activity, ester forming (synthetic) or ester breaking (hydrolytic), will provide the pathway for the polymer matrix to self-modulate its properties by catalytic transformation of the untethered or tethered functionality. The research established that regardless of bond forming or breaking, matrices containing hydroxyl, carboxylic acid, and/or ester groups can be modified *in situ* at ambient. Poly (alkyl methacrylate)s were chosen as model matrices for several reasons. It was desirable to study systems that encompass a wide variety of physical and chemical properties with minor incremental changes in the backbone structure in order to characterize lipase activity with respect to a variety of physical and chemical restrictions. Secondly, by studying poly (alkyl methacrylate)s, changes such as introduction of tethered functional groups or increased crosslink density can be made incrementally without compromising the basic nature of the backbone. Finally, the polymers chosen for the study are common, commercially available, and accessible without using exotic chemistries. These factors are important for developing economically feasible future applications as well as initiating research with extensively characterized materials.

The principal focus of this research was to understand and quantify biocatalyzed transformation rates of untethered or tethered functionality as a function of polymer physical parameters and processing conditions in films and coatings containing both enzyme and functionality. The primary research goal was accomplished by combining several experimental techniques and synthesis methods that will be presented in the following chapters.

Chapter III presents monomer/polymer/copolymer synthetic techniques, film/coating casting and characterization methods, and methods to characterize enzyme activity. Chapter IV presents results of kinetic behavior of enzyme-catalyzed reactions in dilute and organic viscous media. Chapters V and VI present results on the physical and interaction effects of the matrix on lipase activity towards freely diffusing functionality. Chapter VII extends the concept and presents results of lipase activity in matrices where the functionality is tethered to the polymer backbone. Chapter VIII presents results from enzyme-catalyzed polymerization of novel monomers and explores the catalytic behavior as a function of monomer structure.

The multipronged approach of this work has allowed us to extract information and understand the ramifications across a wide range of conditions in a manner that provides greater insight into the complex activity behavior in embedded catalysis systems. The research reported herein seeks to answer the fundamental questions: *what* major and minor factors limit enzyme catalytic activity in bulk polymeric materials, and *how* each of these impact the physical properties of the final polymer matrix compared to each system's starting point.

These questions are of great practical importance and provide a route to understanding the complexity of controlling polymer properties by tuning variables that directly affect performance. From an academic viewpoint, new approaches were developed to determine lipase activity in embedded systems to further the general understanding of these complex systems.

CHAPTER II

OBJECTIVES

This dissertation describes a novel strategy to render materials capable of "smart" surface and bulk properties with the aid of embedded biocatalyst and latent functional groups that are selectively activated in the presence of biocatalyst to undergo chemical transformation. The research presented herein focused on characterizing the activity of lipase catalysts embedded in poly (alkyl methacrylate)s alongside functionalized component, either diffusing within the polymeric matrix or tethered to the matrix. Lipase activity, ester forming (synthetic) or ester breaking (hydrolytic), provided the pathway for polymer matrix to self-tune its properties by catalytic transformation of untethered or tethered functionalized component. Therefore, the primary research goal was to understand and quantify biocatalyzed transformation rates of untethered or tethered functionality as a function of polymer physical parameters and processing conditions in films and coatings containing both enzyme and functionality. Specific objectives were as follows:

1. develop kinetic models to quantify enzyme-catalyzed reaction kinetics in increasingly constrained environments from liquid, viscous liquid, to rubbery and glassy solid;
2. to characterize the enzyme-catalyzed reaction kinetics to verify the kinetic models and to understand properties that control the kinetic behavior in systems with diminishing degrees of freedom; and

3. to characterize the chemical and physical properties of polymers resulting from the enzyme-catalyzed transformation of the blended or covalently attached functionality.

The first objective provided an understanding of kinetic behavior of enzyme-catalyzed transformations to determine the controlling mechanism across systems with increasing excluded volume. Much of the experimental work reported in literature has focused on characterizing immobilized biocatalyst particles for use upon exposure to liquid reactant media, organic or aqueous, for applications in the synthesis of pharmaceuticals, natural products, fine chemicals, and food ingredients. In coatings and thin films, the focus has been to characterize the activity of embedded enzyme by challenging the surface with reactants whether liquid, organic, or aqueous. It has been shown experimentally that these processes have a dimensionality dependence based on the application method, whether coated or immersed in aqueous or organic solutions of reactants. Since we were interested in embedding the biocatalyst and the functionalities in the same matrix, it was important to develop kinetic models using current literature understanding and compare it across systems with diminishing degrees of freedom.

The attainment of the second objective served to advance the previously developed kinetic models for enzyme-catalyzed transformation across systems with increasing excluded volume. Our hypothesis was that the ability of enzymes to catalyze reactions in polymer systems with embedded with biocatalyst alongside functionality depended on the polymer matrix free volume, functionality

degrees of freedom, and interactions: functionality-film, enzyme-film, and enzyme-functionality. Consequently, a series of poly (alkyl methacrylate)s with embedded biocatalyst and functionalized components, diffusing or tethered to the backbone, were investigated. These experiments quantified the effects of total free volume, reactant degrees of freedom, polymer microstructure, polymer relaxation times, and distance of functional tether from polymer backbone on the enzyme-catalyzed transformation rate.

Finally, we evaluated the effect that enzyme-catalyzed transformations had on the chemical and physical properties of the polymer systems. We expected that in systems with embedded functionalities and biocatalyst, biotransformation of the functionality from free –COOH and –OH to the ester would impact the elastic modulus and toughness of the material. In polymers with covalently attached functionalities, shifting from coupled to uncoupled system would impact the crosslink density, coefficient of thermal expansion, T_g, and, the elastic behavior of the material. In addition, the experiments validated the effect of water on the reversibility of the enzyme-catalyzed transformations confirming the switchable nature of the chemistry in these materials.

CHAPTER III

EXPERIMENTAL

Materials and Instrumentation

Materials

Lipase (from porcine pancreas) Type II E.C. 3.1.1.3 (PPL), lipase acrylic resin from *Candida Antarctica* (CAAR), and lipase from *Candida Antarctica* (≥ 1.0 units/mg) (CALB) were obtained from Sigma Chemical Co. (St. Louis, MO). Lipolase E.C. 3.1.1.3, was provided by Reactive Surfaces Ltd. (Austin, TX) and *Pseudomonas Fluorescence* lipase E.C. 3.1.1.3 (PFL) were obtained from Sigma Chemical Co. Octanoic acid (OA), octanoyl chloride, triethylamine (TEA), and 2,6-di-*tert*-butyl-4-methyl phenol were purchased from Acros Organics (Geel, Belgium), while 1-nonanol (1-NN) was purchased from Alfa Aesar (Ward Hill, MA). 1,6-hexanedithiol was obtained from Sigma Chemical Co. Methyl methacrylate (MMA) and butyl acrylate (BA) were purchased from Fisher Scientific (Fairlawn, NJ). Butyl methacrylate (BMA) and ethyl methacrylate (EMA) were obtained from Acros Organics, while polymethyl methacrylate (PMMA) M_w 996,000 was purchased from Sigma Chemical Co. Azobisisobutyronitrile (AIBN) was purchased from Sigma Chemical Co. and recrystallized twice from methanol prior to use. 1,12-dodecanediol, dodecanethiol, and acryloyl chloride were purchased from Sigma Chemical Co. 11-(methacryloylamino) undecanoic acid (11AUDA) was obtained from Key Organics (Cornwall, UK). 1,4-Dioxane was purchased from Sigma Chemical Co. Adipic acid divinyl ester (DVA) was purchased from TCI America. HPLC grade

acetone (99.9%), methanol, methylene chloride, ethyl acetate, tetrahydrofuran (THF), and acetonitrile were purchased from Fisher Scientific. THF was distilled from CaH_2 over molecular sieves. All other reagents and organic solvents were of the highest grade or purity commercially available and were used as received.

Instrumentation

Colorimetric endpoint titration (–COOH equivalent weight): A procedure based on ASTM D1639 was used to quantify the –COOH functionality in films, coatings, and liquid media at fixed times using a Metrohm, 719 S Titrino automatic titrator. In a typical procedure, the specimen (liquid or solid) mass, S, was weighed into a scintillation vial, at a final concentration of 2.5-5% w/v in methylene chloride, THF, or THF:CH_3OH (1:1 by volume) as determined from ASTM D1639, Table 1, and based on the initial –COOH value. Once S was dissolved, a 2% w/v phenolphthalein in methanol was added to achieve a final concentration of 0.5% v/v. A standardized 0.1000 N potassium hydroxide solution in methanol was used as the titrant. Functional equivalent weight was determined using the following expression:

$$FEW_{COOH} = \frac{V_{KOH} \cdot N_{KOH}}{FW_{KOH} \cdot g_S} \qquad \text{Equation 1}$$

where FEW_{COOH} is the functional equivalent weight of –COOH functionalized species (mol/g), V_{KOH} is the volume of the standardized KOH solution in mL, N_{KOH} is the normality of the standardized KOH solution in mg/mL, FW_{KOH} is the molecular weight of KOH in mg/mol, and g_S is the solids content of the specimen in grams.

Potentiometric endpoint titration (hydroxyl equivalent weight): A procedure based on ASTM E1899 was used to quantify the concentration of hydroxyl functionality in films and coatings using Denver Instrument Model 352. In a typical procedure, the specimen mass, S, was weighed in a beaker using an optimum sample weight as determined by the following expression:

$$S = \frac{40}{HV_{exp}} \qquad \text{Equation 2}$$

where S is the specimen weight in grams, and HV_{exp} is the expected hydroxyl value of the specimen in mg KOH per gram of sample. The specimen was dissolved in 10 mL of anhydrous THF and 10 ± 0.1 mL *p*-toluenesulfonyl isocyanate (TSI) was added. The beaker was covered and the solution was stirred for 5 min. 0.5 mL deionized (DI) water was used to react with the excess TSI reagent and after stirring for 1 min, an additional 30 mL of THF was added to the beaker. The solution was titrated potentiometrically using a potassium hydrogen phthalate (KHP) standardized solution of tetrabutylammonium hydroxide (TBA). Hydroxyl equivalent weight was determined using the following expression:

$$FEW_{OH} = \frac{\left| V_2 - V_1 \right| \cdot N_{TBAOH} \cdot 56.1}{FW_{KOH} \cdot g_S} \qquad \text{Equation 3}$$

where FEW_{OH} is the functional equivalent weight of hydroxyl functionalized species (mol/g), V_1 is the first potentiometric endpoint of the standardized TBA solution in mL, V_2 is the second potentiometric endpoint of the standardized TBA solution in mL, N_{TBAOH} is the normality of the standardized KOH solution in mol/L, 56.1 is the multiplication factor to convert the normality from mol/L to mg/mL,

FW_{KOH} is the molecular weight of KOH in mg/mol, and g_S is the solids content of the specimen in grams.

Gas chromatography - mass spectroscopy (GC-MS): The developed protocols were used to determine the concentration of small molecules in dilute solutions or dispersed in films and coatings at fixed times. GC-MS analysis was performed on a Hewlett-Packard Agilent 6890-5972A GC-MS workstation equipped with an Agilent DB-1 high resolution column. The thermal program used was: initial oven temperature 50 °C for 3 min, ramp to 150 °C at 10 °C/min, hold for 1 min, ramp to 250 °C at 50 °C /min, hold for 14 min. The injector temperature was 200 °C with 1 µL injection volume and the carrier gas was helium. The samples (liquid or solid) were dissolved in HPLC grade acetone to a final volume of 1.5 mL. Functional equivalent weight of the analyte was determined using the following expression:

$$FEW = \frac{Area \cdot V}{RS \cdot g_S} \qquad \text{Equation 4}$$

where Area is the integrated analyte response area, RS is the area response slope determined from a range of known concentrations of each analyte, V is total solution volume, and g_S is specimen weight in grams.

Differential scanning calorimetry (DSC): DSC experiments were performed to determine polymer T_g, in film or powder form, by monitoring the heat rate differential between reference and sample pans over a preset temperature range. The analysis was performed on a TA instrument Q-1000 differential scanning calorimeter using a nitrogen-purged cell at a flow rate of 80 mL/min. Protocols consisted of heat/cool/heat cycles at 10 °C/min heating rate and 5 °C/min cooling

rate. The data was analyzed using TA Instruments software Universal Analysis 2000 Version 4.0©. T_g was determined by identifying discontinuities in the heat flow versus temperature curves and using software assistance to set the onset and endset points of the curve discontinuities. The midpoint temperature corresponding to the peak maximum of the first derivative of heat flow curve was taken as the T_g.

Thermogravimetric analysis (TGA): A TGA Q5000 from TA Instruments was employed to determine weight loss temperature profiles for the synthesized polymers. The analysis was conducted by heating the sample at 50 °C/min from 25 °C to 500 °C in a nitrogen environment. Mass loss and the onset of degradation temperature were analyzed using TA Instruments software Universal Analysis 2000 Version 4.0©.

Thermal mechanical analysis (TMA): TMA experiments were performed on a TA instrument Q400 using a cylindrical expansion probe with a flat end (3 mm in diameter as determined with a digital caliper). TMA records sample geometric changes using a weighted probe in direct contact with the sample. Coefficient of thermal expansion was determined by analyzing film specimen deformation under constant load of 0.02 N over a set temperature range. The specimen was annealed above T_g and heated at 2 °C/min from 25 °C to 120 °C. The modulus was determined by analyzing sample deformation under isothermal conditions over a set force range. The modulus was calculated by applying the Hertz equation from the indentation of the rigid, circular, and flat ended probe on a flat sheet as shown in ASTM E2347:

$$E = \frac{3F}{4 \cdot D \cdot p} \qquad \text{Equation 5}$$

where E is the complex modulus in MPa, F is the force applied on the sample in N, D is the probe diameter in mm and p is the penetration depth in mm.

Nuclear magnetic resonance (NMR): Solution ^{1}H and ^{13}C nuclear magnetic resonance spectra were collected on a Varian Gemini 300 spectrometer at 75.47 MHz spectral frequency for carbon. NMR spectra were recorded at ambient using $CDCl_3$ or DMSO with tetramethyl silane (TMS) as the internal reference. All chemical shifts were referenced to the $CDCl_3$ and DMSO peaks. Weight percent residual content of small molecules in polymers was determined using the following expression:

$$Wt\% = \frac{\frac{Area_{res}}{no_H} \cdot FW}{\frac{Area_{pol}}{no_H} \cdot MW_{rep} + \frac{Area_{res}}{no_H} \cdot FW} \qquad \text{Equation 6}$$

where $Area_{res}$ represents the integrated area of the residual compound protons while FW represents the compound's formula weight, $Area_{pol}$ represents the integrated area of the polymer matrix protons, MW_{rep} is the molecular weight of the repeat unit, and no_H is the number of structural protons that corresponds to the integrated area. Mole percent incorporation of functional repeat unit in copolymerizations was determined using the following expression:

$$\text{mol\%} = \frac{\frac{\text{Area}_{\text{func}}}{\text{no}_{\text{H}}}}{\frac{\text{Area}_{\text{nf}}}{\text{no}_{\text{H}}} + \frac{\text{Area}_{\text{func}}}{\text{no}_{\text{H}}}} \cdot 100\% \qquad \text{Equation 7}$$

where $\text{Area}_{\text{func}}$ represents the integrated area of protons emanating from functional portion of the copolymer, Area_{nf} represents the integrated area of protons originating from non-reactive acrylate portion of the copolymer, and no_{H} is the number of protons that corresponds to the specific integrated area.

Gel permeation chromatography (GPC): GPC studies were performed on a Varian PL GPC-50 equipped with dual angle light scattering, differential pressure and refractive index detectors. THF was used as the eluent at a flow rate of 0.8 mL/min at 40 °C with a series of four Polymer Laboratory columns (three Polypore and one 50 Å PLGel column). Toluene was used as an internal standard, and GPC data was determined from calibration curve generated from polystyrene molecular weight standards.

GPC was also performed on a Waters 515 HPLC pump equipped with a Waters 2414 refractive index detector. The column system consisted of two PLGel Mixed B columns in series with a total length of 600 mm. A solution of 0.5 N sodium nitrite in *N*,*N*'-dimethyl acetamide was used as the eluent at a flow rate of 1.0 mL/min at 70 °C. Molecular weight calculations were based on a polystyrene molecular weight standard curve.

Near-Infrared Spectroscopy: Spectroscopic analysis of films was conducted on a Antaris II FT-NIR Analyzer from Thermo Fisher Scientific to determine the

relative water content. Absorbance scans were carried out before and after films were exposed to 0 or 100% relative humidity. The peak absorbance at 7000 cm^{-1}, which corresponds to vibration modes of water and methylene groups, was normalized to absorbance at 6000 cm^{-1} corresponding to vibration modes of methylene groups only.

Positron Annihilation Lifetime Spectroscopy (PALS): Free volume was determined via PALS using ^{22}Na as positron source. Film coupons (diameter 10 mm, thickness 1 mm) were sandwiched between the positron source. Measurements were taken at ambient with a total of 1 x 10^6 counts for each film. The average hole sizes were determined from the longest lifetime (τ_3) of the orthopositronium (positron/electron pair) species which was described elsewhere in the literature (*81*).

Film thickness and density determination: Dry film thickness was determined via a digital caliper, and density was determined using a Mettler-Toledo XS104 microbalance using a density determination kit (Part# 11106706, accuracy 0.002 cm^3/g). Measurements were conducted at ambient temperature (21-23 °C). Dry films ca. 1-2 g were serially weighed in air and deionized water (auxiliary liquid). Water was selected since it exhibits little affinity for poly (alkyl methacrylate)s. Film density, ρ in g/cm^3, was calculated using the following expression:

$$\rho = \frac{W_{air}}{W_{air} - W_{liq}}\left(\rho_{liq} - \rho_o\right) + \rho_o \qquad \text{Equation 8}$$

where W_{air} is film weight in air (in grams), W_{liq} is film weight in the auxiliary liquid (in grams), ρ_{liq} is the density of auxiliary liquid in g/cm^3, and ρ_o is the density of air (0.0012 g/cm^3).

Synthesis

Synthesis of nonyl octanoate (NOc)

Nonyl octanoate standard to construct calibration curves was synthesized by charging 1-nonanol (18.75 g, 0.13 mol) and triethylamine (17.19 g, 0.17 mol) into a 500 mL three-neck flask equipped with thermometer and an addition funnel. 100 mL of dichloromethane was added and the reaction mixture was placed in an ice bath. Octanoyl chloride (26.0 g, 0.16 mol) in 50 mL of dichloromethane were added dropwise to the reaction mixture while maintaining the temperature under 4 °C. The reaction was continued for 24 h and filtered via Whatman standard filter paper No.4 to remove the triethylamine chloride salt. The resulting solution was washed three times with saturated sodium bicarbonate solution. The organic layer was dried over $MgSO_4$ and dichloromethane was removed by rotatory evaporation. The oily product (98% purity) was confirmed by ^{1}H NMR ($CDCl_3$) δ: 0.8 (t, 6H), 1.2 (m, 18H), 1.54 (m, 6H), 2.21 (t, 2H), 3.98 (t, 2H) (Figure 5) and ^{13}C NMR ($CDCl_3$) δ: 173.6 (-CH_2-*C*O-O-CH_2), 64.1 (-CH_2-CO-O-*C*H_2-), 34.2 (-*C*H_2-CO-O-CH_2-), 31.7 (-*C*H_2-CH_2-CH_3), 29.1 (-CH_2-*C*H_2-CH_2-), 25.8 (-CO-O-CH_2-CH_2-*C*H_2), 24.9 (*C*H_2-CH_2-CO-O-), 22.5 (-CH_2-*C*H_2-CH_3), 13.9 (-CH_2-CH_2-*C*H_3) (Figure 6).

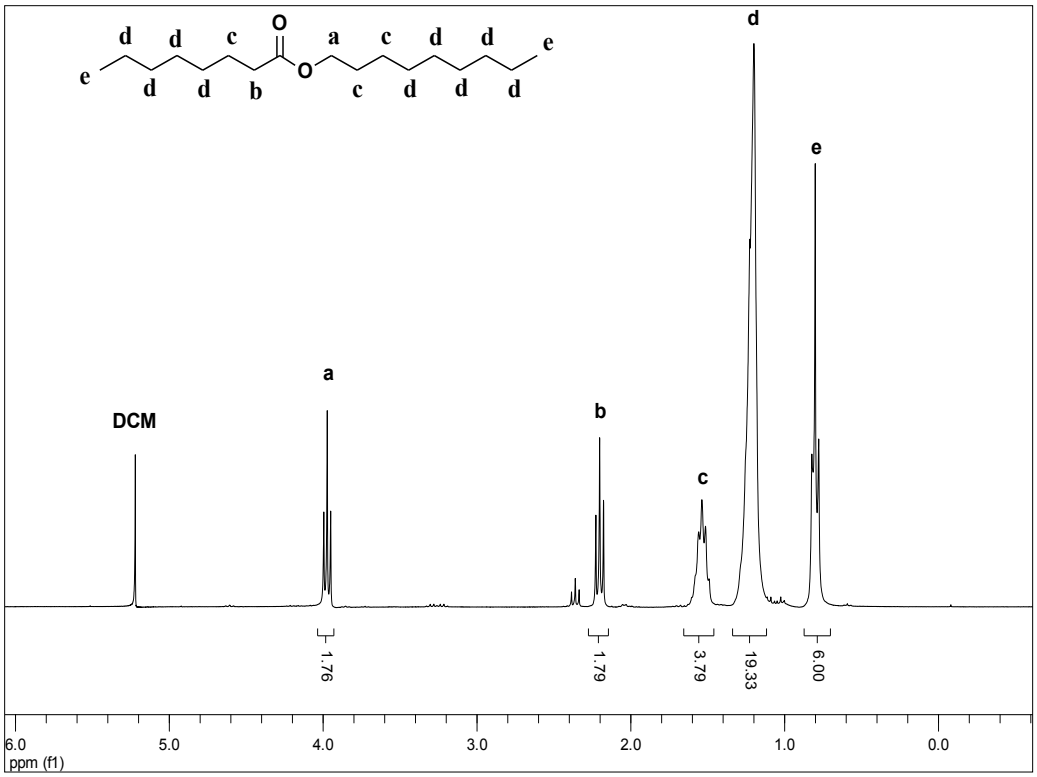

Figure 5. ^{1}H NMR of nonyl octanoate.

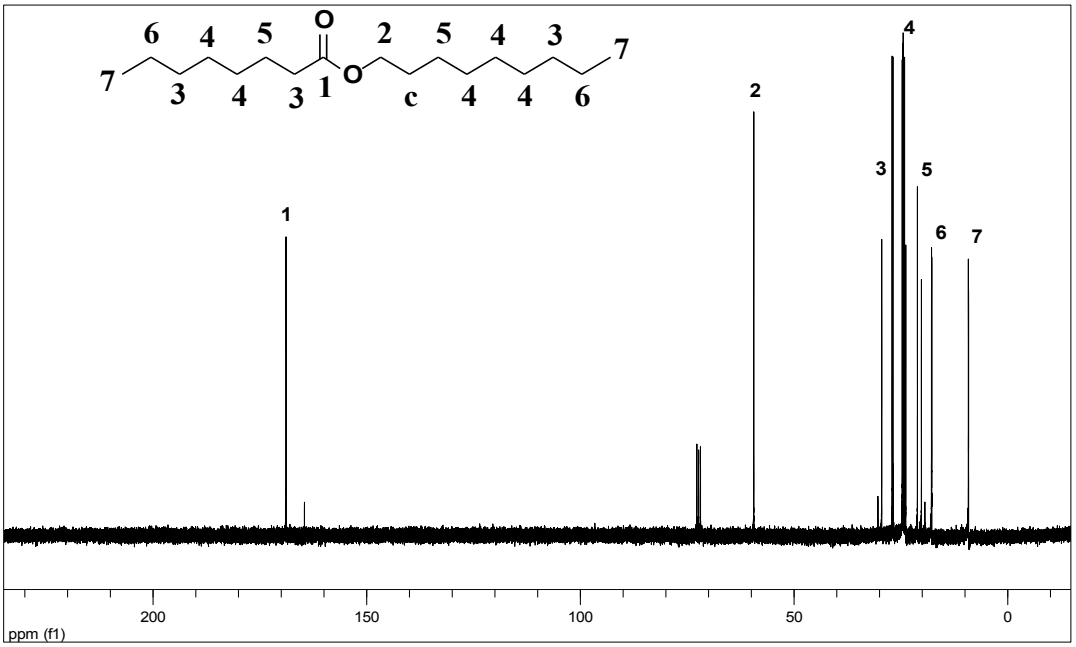

Figure 6. ^{13}C NMR of nonyl octanoate.

Synthesis of poly alkyl (methacrylate)s

Polyethyl methacrylate (PEMA) and polybutyl methacrylate (PBMA) were synthesized by free radical solution polymerization targeting similar molecular weights for each polymer. *PEMA synthesis*: EMA (50 g, 0.44 mol) and toluene (193 mL) were placed in a 500 mL three-neck flask equipped with a condenser, thermocouple, and a nitrogen purging line. The vessel was sealed and purged overnight. The solution was heated to 60 °C and initiated with AIBN (0.164 g, 1 mmol). The reaction was continued for 24 h and terminated by slow precipitation in excess methanol. The white flaky product that formed was dried under vacuum at ambient to remove residual solvent. The product was confirmed by ^{1}H NMR ($CDCl_3$) δ: 0.75-1.10 (-$CH_2C\mathit{H_3}$, 3H), 1.20-1.30 (-$CC\mathit{H_3}$, 3H), 1.75-2.10 (-$CC\mathit{H_2}$, 2H), 3.09-4.10 (-$OCOC\mathit{H_2}$, 2H) (Figure 7). M_n determined by GPC analysis was 38,000 g/mol. T_g determined by DSC analysis was 58 °C and was acquired from the second heating cycle.

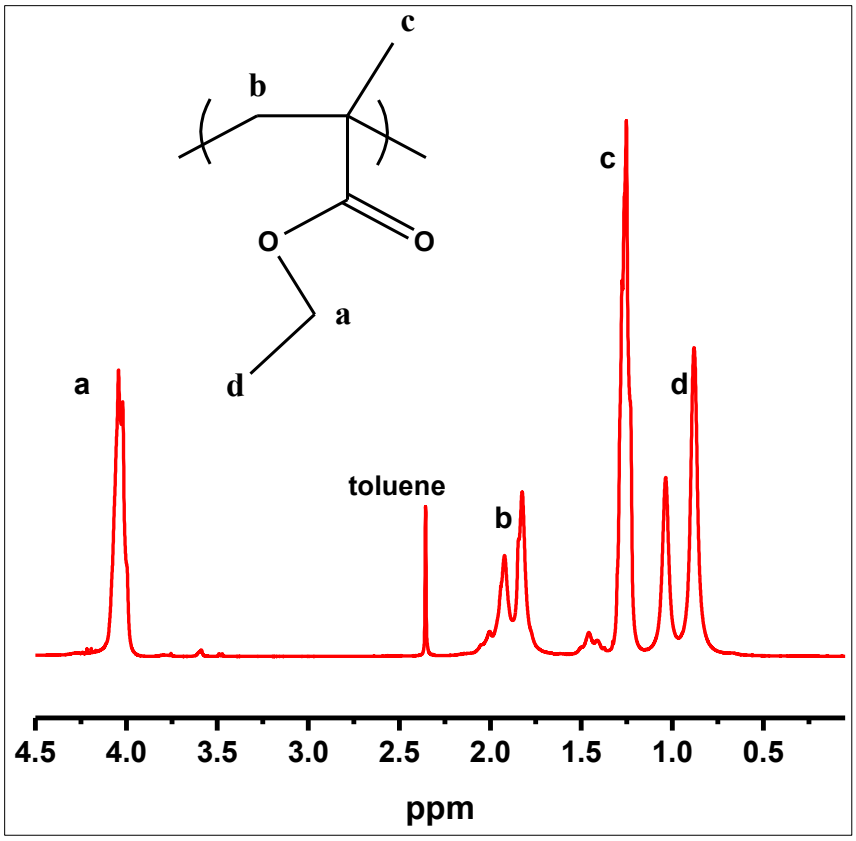

Figure 7. ^{1}H NMR of poly ethyl methacrylate.

PnBMA synthesis: n-BMA (50 g, 0.35 mol) and toluene (193 mL) were placed in a 500 mL three-neck flask equipped with a condenser, thermocouple, and a nitrogen purging line. The vessel was sealed and purged overnight. The reaction was initiated with AIBN (0.164 g, 1 mmol). The reaction was continued for 24 h at 60 °C and subsequently terminated by slow precipitation in excess methanol. The white flaky product that formed was dried under vacuum at ambient to remove residual solvent. The product was confirmed by ^{1}H NMR ($CDCl_3$): 0.75-1.15 (-C*H*$_3$, 6H), 1.3-1.5 (-C*H*$_2$CH$_3$, 2H), 1.5-1.7 (-OCH$_2$C*H*$_2$, 2H), 1.75-2.15 (-CC*H*$_2$, 2H), 3.80-4.1 (-OCOC*H*$_2$, 2H) (Figure 8). M_n as determined by GPC analysis was 40,000 g/mol and its T_g was 23 °C.

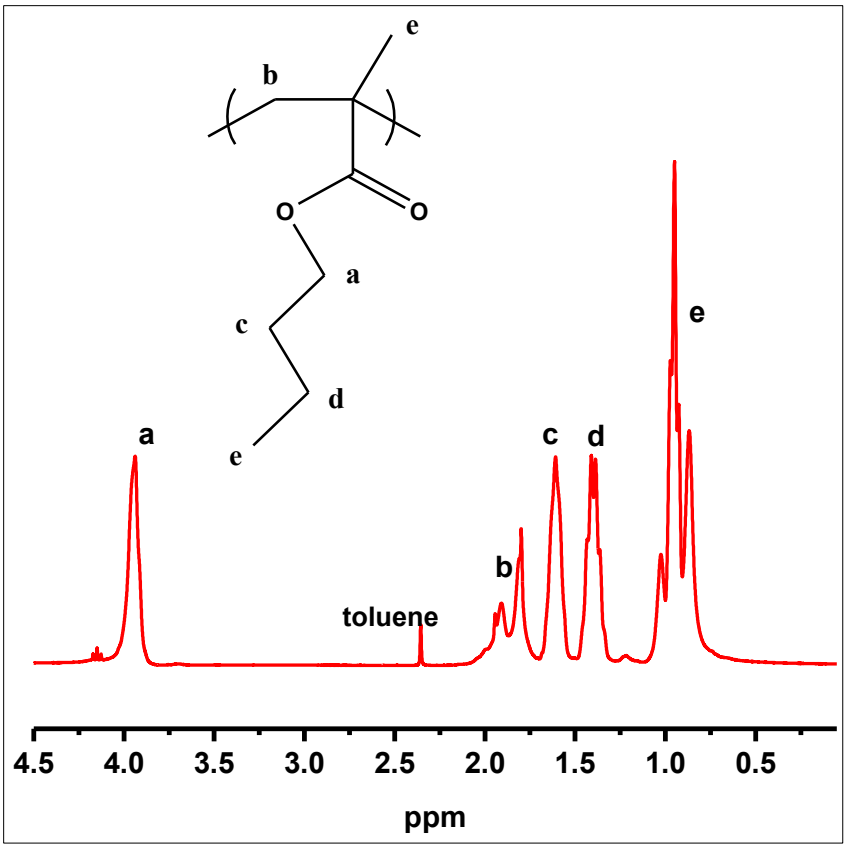

Figure 8. ^{1}H NMR of poly-N-butyl methacrylate.

Synthesis and characterization of –OH functionalized vinyl monomers

Hydroxyl functional vinyl monomers were synthesized following the general synthesis scheme shown in Figure 9.

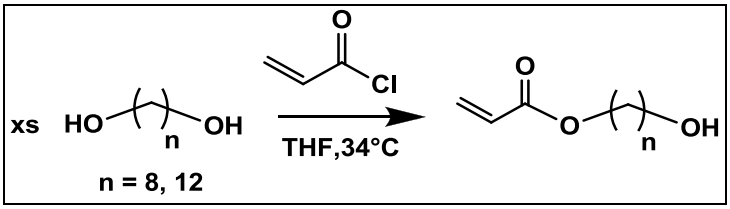

Figure 9. Synthesis of hydroxyl functional vinyl monomers.

Synthesis of 12-(acryloyloxy)-1-dodecanol (12A1D): The procedures used in literature were modified as follows (*82-83*): triethylamine was used as a base catalyst instead of pyridine, and the molar ratio of glycol to acyl chloride was 10

to 1 instead of 2.5 to 1. A 500 mL three neck flask equipped with a thermocouple and an addition funnel was charged with 1,12-dodecanediol (50 g, 0.239 mol), triethylamine (3.51 g, 0.035 mol), 2,6-di-*tert*-butyl-4-methyl phenol (0.01 g) and 400 mL THF. The reaction mixture was dissolved by heating to 34 °C. The addition funnel was charged with acryloyl chloride (2.24 g, 0.025 mole) and 80 mL THF. The acryloyl chloride solution was added dropwise to the reaction flask over 3-4 hours. The reaction was continued for 24 h at 34 °C. The TEA chloride salt was filtered off and an equal volume of $CHCl_3$ was added. The solution was washed sequentially several times with saturated bicarbonate solution and DI water, and the solvents were removed under reduced pressure. The product was dissolved in 200 mL of $CHCl_3$ and placed in dry ice to filter off the unreacted glycol. The remaining solution was dried over $MgSO_4$ and purified via a silica gel column using a solvent blend ($CHCl_3$:CH_3OH 95:5 by volume) as the eluent. An oily product was obtained (yield 40-60%). ^{1}H NMR ($CDCl_3$) *δ* 6.35-6.41 (d, vinyl, 1H), 6.10-6.20 (q, vinyl, 1H), 5.74-5.78 (d, vinyl, 1H), 4.10-4.18 (t, OCOC*H*$_2$, 2H), 3.61-3.65 (t, HOC*H*$_2$, 2H), 1.62-1.66 (br, CH_2, 8H), 1.26 (s, CH_2, 12H) (Figure 10). ^{13}C NMR ($CDCl_3$) δ: 166 (=CH-*C*O-O-CH_2-), 130 (*C*H_2=CH-CO-O-), 129 (CH_2=*C*H-CO-O-), 64.6 (=CH-CO-O-*C*H_2-), 62.7 (CH_2-*C*H_2-OH), 32.7 (*C*H_2-CH_2-OH), 28.5-29.5 (-CO-O-CH_2-*C*H_2), (-CH_2-*C*H_2-CH_2-), 25.7 (-CO-O-CH_2-CH_2-*C*H_2), (*C*H_2-CH_2-CH_2-OH) (Figure 11).

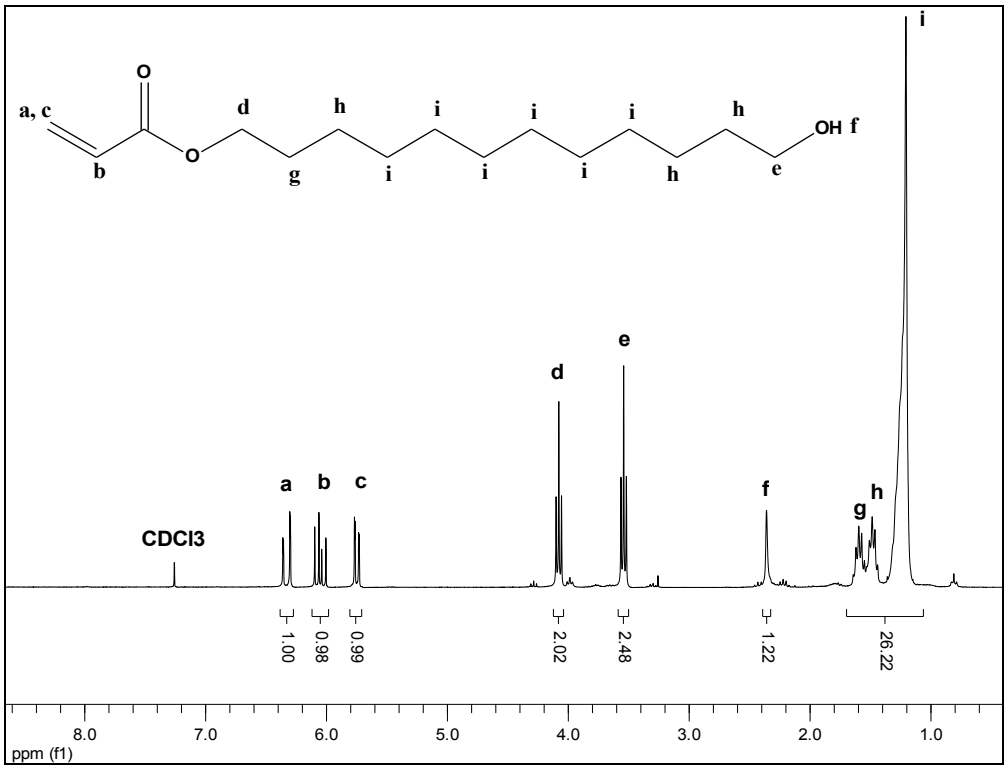

Figure 10. ^{1}H NMR of 12-(acryloyloxy)-1-dodecanol.

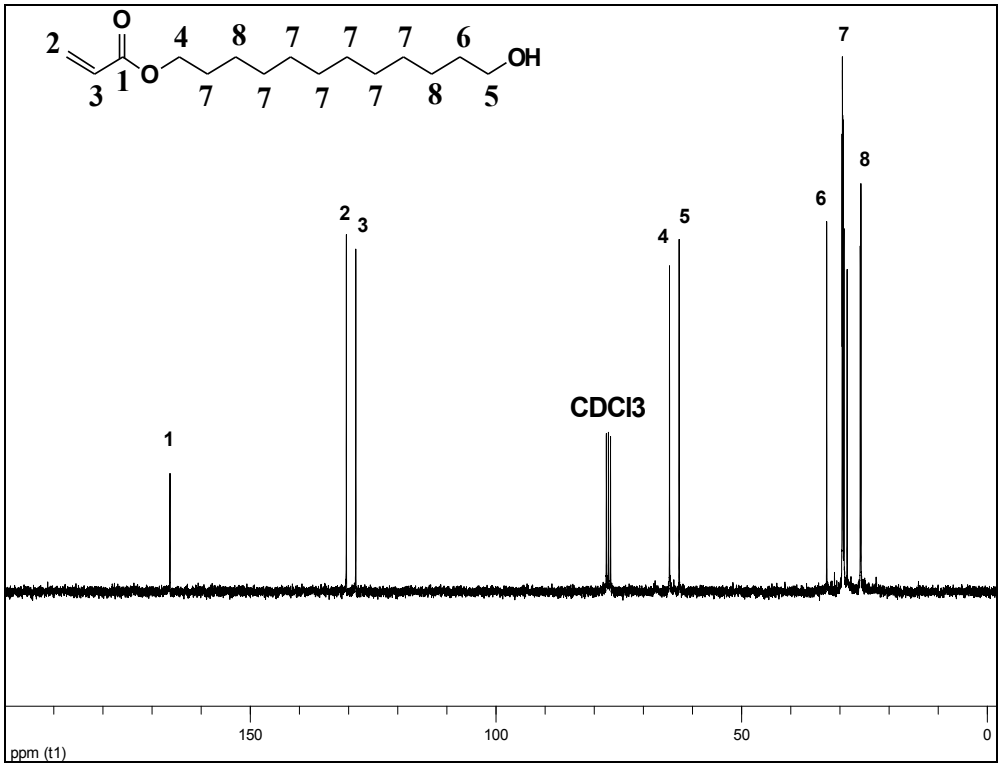

Figure 11. ^{13}C NMR of 12-(acryloyloxy)-1-dodecanol.

Synthesis of 8-(acryloyloxy)-1-octanol (8A1O): A 500 mL three neck flask equipped with nitrogen line, thermocouple, and an addition funnel was charged with 1,8-octanediol (49.3 g, 0.34 mol), triethylamine (4.65 g, 0.046 mol), 2,6-ditertbutyl-4-methyl phenol (0.01 g), and THF (350 mL). The addition funnel was charged with acryloyl chloride (3.28 g, 0.034 mol) and 40 mL THF. The system was sealed and purged with nitrogen for 30 min. The acryloyl chloride solution was added dropwise to the reaction flask over 3-4 hours. The reaction proceeded for 24 h at room temperature. The TEA chloride salt was removed via filtration. The THF was evaporated under reduced pressure and the mixture was solubilized in 200 mL of $CHCl_3$. The solution was placed in an ice bath to induce the precipitation of unreacted glycol. After filtering the unreacted glycol, the remaining solution was dried over $MgSO_4$. The product was purified via a silica gel column using a solvent blend ($CHCl_3$:CH_3OH 98:2 by volume) as the eluent. An oily product was obtained (95% yield). ^{1}H NMR ($CDCl_3$) δ 6.25-6.35 (d, vinyl, 1H), 6.00-6.10 (q, vinyl, 1H), 5.70-5.79 (d, vinyl, 1H), 4.00-4.05 (t, OCOCH_2, 2H), 3.45-3.51 (t, HOCH_2, 2H), 1.62-1.51 (br, CH_2, 8H), 1.10-1.30 (s, CH_2, 4H) (Figure 12).

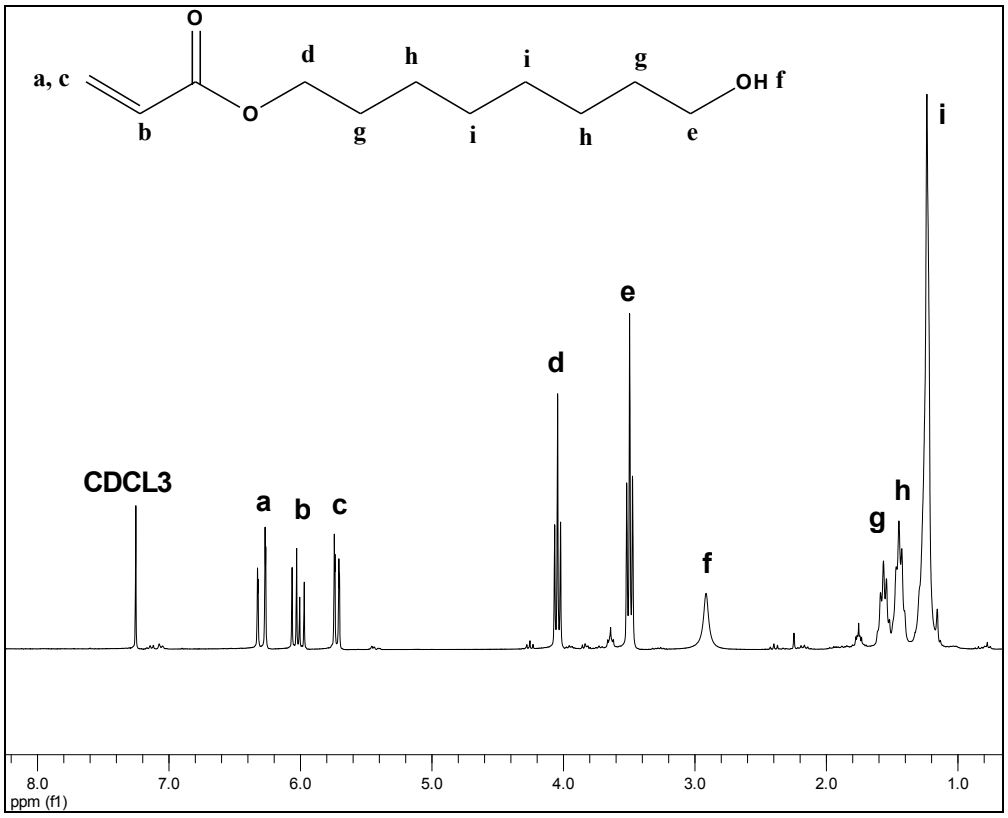

Figure 12. ^{1}H NMR of 8-(acryloyloxy)-1-octanol.

Synthesis and characterization of –COOH functionalized vinyl monomers

Synthesis of 12-(acryloyloxy)octadecanoic acid (Figure 13): A 500 mL three neck flask equipped was charged with 12-hydroxystearic acid (40 g, 0.13 mol), triethylamine (17.8 g, 0.18 mol), THF (110 mL), and cooled with an ice bath. Acryloyl chloride (14.5, 0.16 mol) was added slowly dropwise while maintaining the reaction temperature between 0 °C and 4 °C. The resulting salt was removed via gravity filtration. THF was removed under reduced pressure and the mixture was dissolved in 100 mL of CH_2Cl_2. The solution was placed in an ice bath to induce the precipitation of unreacted glycol. After filtering the unreacted glycol, the solution was washed several times with brine solution to remove unreacted acid chloride. The remaining solution was dried over $MgSO_4$. CH_2Cl_2

was removed under reduced pressure to yield an oily product. ^{1}H NMR ($CDCl_3$) δ 6.35-6.45 (d, vinyl, 1H), 6.15-6.19 (q, vinyl, 1H), 5.71-5.80 (d, vinyl, 1H), 4.80-5.0 (m, OCOC*H*-, 1H), 2.20-2.50 (m, HOOCCH_2, 2H), 1.40-1.71 (br, CH_2, 6H), 1.10-1.40 (b, CH_2, 22H), 0.80-0.92 (m, CH_3, 3H) (Figure 14)

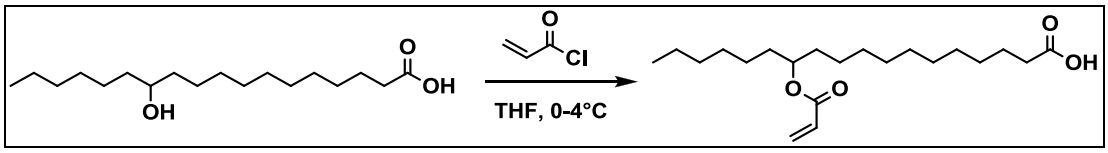

Figure 13. Synthesis of 12-(acryloyloxy)octadecanoic acid.

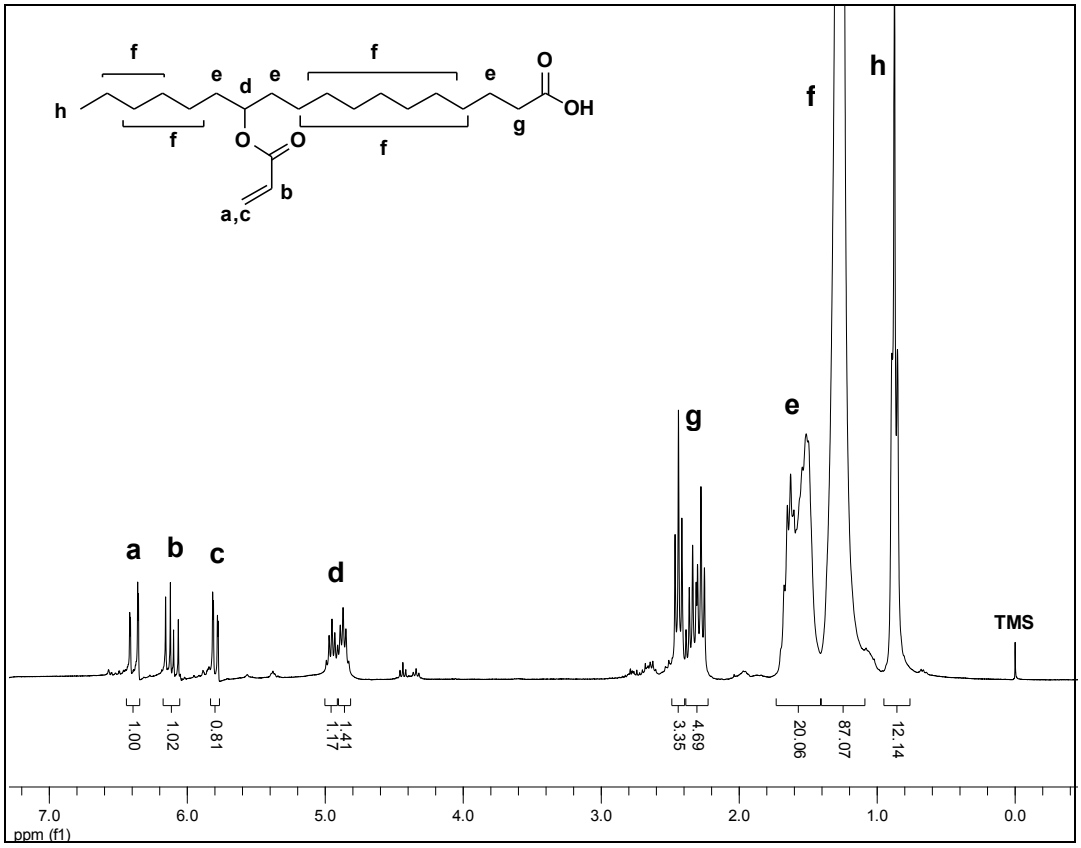

Figure 14. ^{1}H NMR of 12-(acryloyloxy)octadecanoic acid.

Synthesis of N-methyl acrylaminoundecanoic acid (Figure 15): A 500 mL three neck flask equipped was charged with aminoundecanoic acid (100 g, 0.5 mol), NaOH (40 g, 1 mol), hydroquinone (0.5 g) and DI water (140 mL). The

suspension was cooled with an ice bath. Methacryloyl chloride (52.3 g, 0.5 mol) was added slowly dropwise over 30 min while maintaining the reaction temperature between 0 °C and 4 °C. The solution was neutralized with 35 mL concentrated HCl and the product was extracted with ethyl acetate. The solution was washed sequentially several times with dilute HCl and DI water and dried over $MgSO_4$. The solvent was removed under reduced pressure and the oily product was covered with a layer of ether. Upon cooling to -5 °C, product crystals were obtained. ^{1}H NMR ($CDCl_3$) δ 9.30-9.80 (b, COO*H*, 1H), 6.10-6.25 (b, CON*H*, 1H), 5.60-5.65 (s, vinyl, 1H), 5.10-5.30 (s, vinyl, 1H), 3.10-3.30 (m, CONHCH_2, 2H), 2.10-2.31 (m, HOOCCH_2, 2H), 1.80-1.96 (s, CH_3, 3H), 1.39-1.60 (m, CH_2, 4H), 1.19-1.36 (b, CH_2, 12H) (Figure 16).

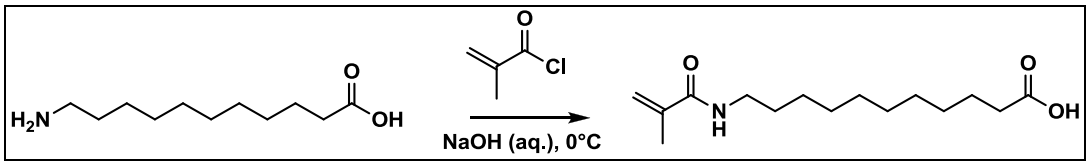

Figure 15. Synthesis of *N*-methyl acrylaminoundecanoic acid.

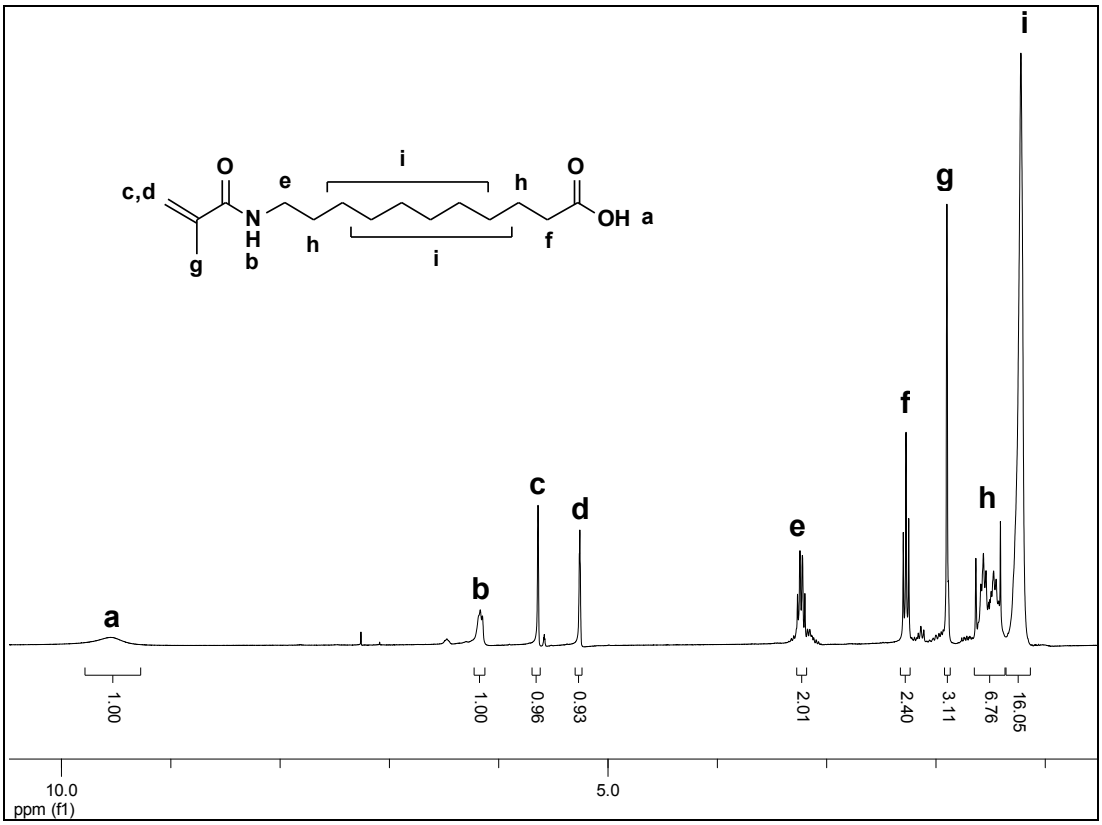

Figure 16. ^{1}H NMR of *N*-methyl acrylaminoundecanoic acid.

Synthesis and characterization of –OH pendant functionalized polymers

Hydroxyl pendant functionalized monomers were synthesized following the general synthesis scheme shown in Figure 17.

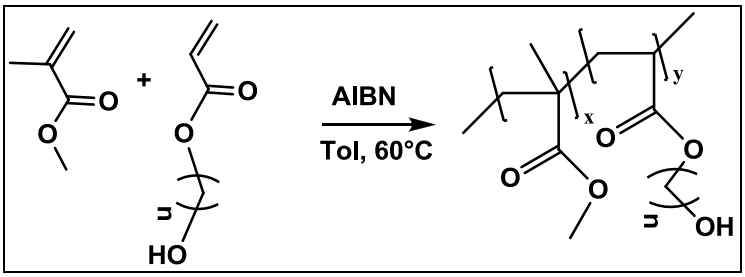

Figure 17. Synthesis of hydroxyl pendant functionalized polymers.

Synthesis of hydroxyl ethyl methacrylate-methyl methacrylate-butyl acrylate copolymer (AC(CH$_2$)$_2$OH-MMA-BA): A 500 mL three neck flask equipped with a nitrogen line, condenser, and a thermocouple was charged with MMA (15.4 g,

0.15 mol), BA (24.3 g, 0.19 mol), HEMA (8.71 g, 0.067 mol) in THF (250 mL). The flask was purged with nitrogen for 30 min and heated to 60 °C. A THF solution of AIBN (3.88 g, 0.024 mol) was injected to initiate polymerization. The polymerization was quenched after 24 h by exposing to air. The polymer solution was precipitated in 10 times volumetric excess of hexanes to yield (74%) a white flaky product with a T_g of -2.2 °C. Results were summarized in Table 2. ^{1}H NMR ($CDCl_3$) *δ*: 3.89-4.36 (2H), 3.70-3.90 (3H), 3.50-3.70 (2H), 1.75-2.45 (2H), 1.40-1.65 (2H), 0.79-1.20 (2H) (Figure 18). ^{13}C NMR ($CDCl_3$) *δ*: 175-180 (-*C*O-O-CH_2-), 67-68 (-CO-O-*C*H_2-),64-66 (CH_2-*C*H_2-OH), 60 (backbone, -*C*H_2-), 52 (backbone, -*C*H_2-), 43-46 (backbone, -O-OC-*C*(CH_3)(CH_2)$_2$), 29-31 (-CO-O-CH_2-*C*H_2), 19-20 (-CO-O-CH_2-CH_2-CH_2), 14 (-CO-O-CH_2-CH_2-*C*H_2) (Figure 19).

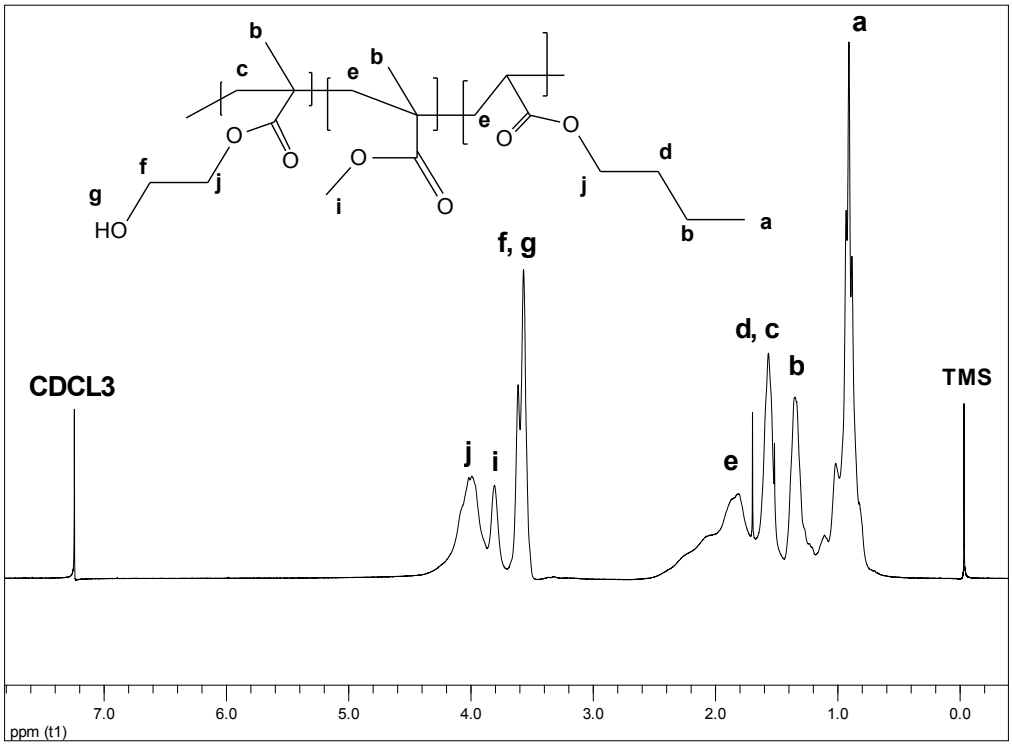

Figure 18. ^{1}H NMR of AC(CH_2)$_2$OH-MMA-BA copolymer.

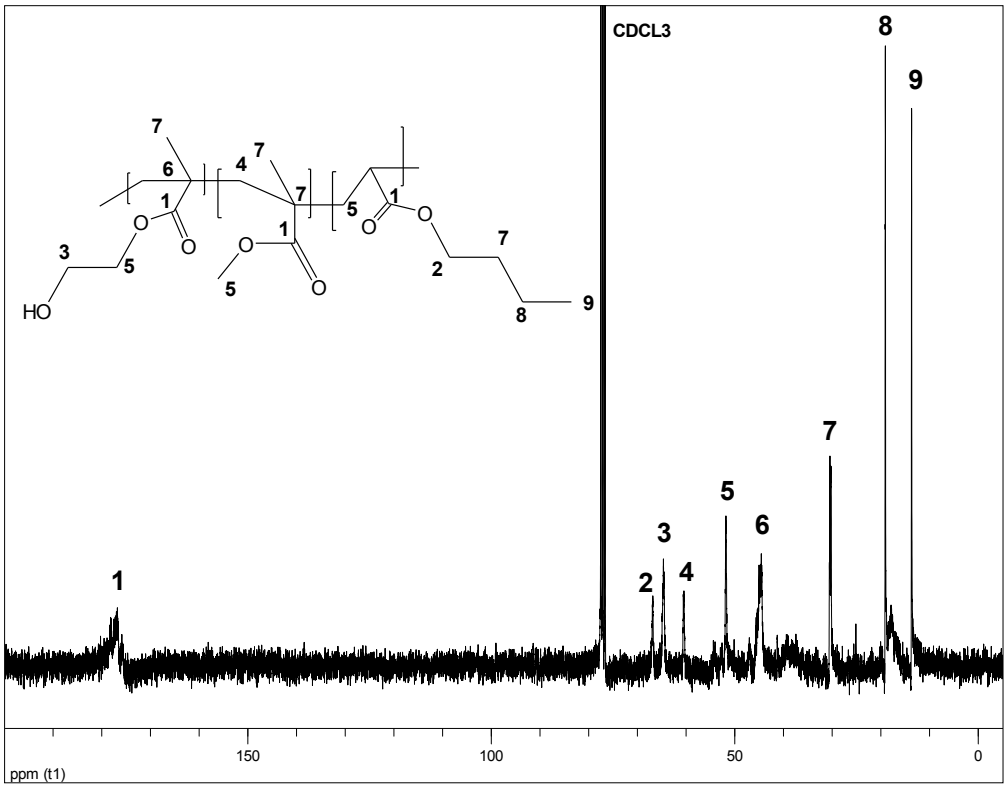

Figure 19. ^{13}C NMR of $AC(CH_2)_2OH$-MMA-BA copolymer.

Table 2

Properties of $AC(CH_2)_2OH$-MMA-BA

Polymer (ID)	Mole %	M_n	M_w	PDI	T_g (°C)
$AC(CH_2)_2OH$-MMA-BA	16.5	9,500	14,000	2.31	-2.2

Synthesis of 12-acryloyloxy-1-dodecanol-methyl methacrylate-butyl acrylate copolymer ($AC(CH_2)_{12}OH$-MMA-BA): A three neck flask equipped with nitrogen line, thermocouple, and condenser was charged with 12A1D (1.04 g, 4.1 mmol), MMA (0.5 g, 5 mmol), BA (0.5 g, 4 mmol), dodecanethiol (0.0132 g, 0.065 mmol) in 8 mL of toluene. The flask was sealed and sparged overnight with nitrogen. The reaction was initiated by adding AIBN (0.167 g, 1.02 mmol) at 60 °C. The polymerization was quenched after 24 h by exposing to air. The polymer solution

was precipitated by dropwise addition into 10 times volumetric excess of heptane. The product was dried under vacuum at room temperature with 30% yield. Results were summarized in Table 3. ^{1}H NMR (DMSO-d_6) δ: 4.29-4.40 (1H), 3.85-4.09 (2H), 3.42-3.62 (3H), 3.30-3.40 (2H), 1.45-2.00 (15H), 1.15-1.40 (16H), 0.70-1.00 (3H) (Figure 20).

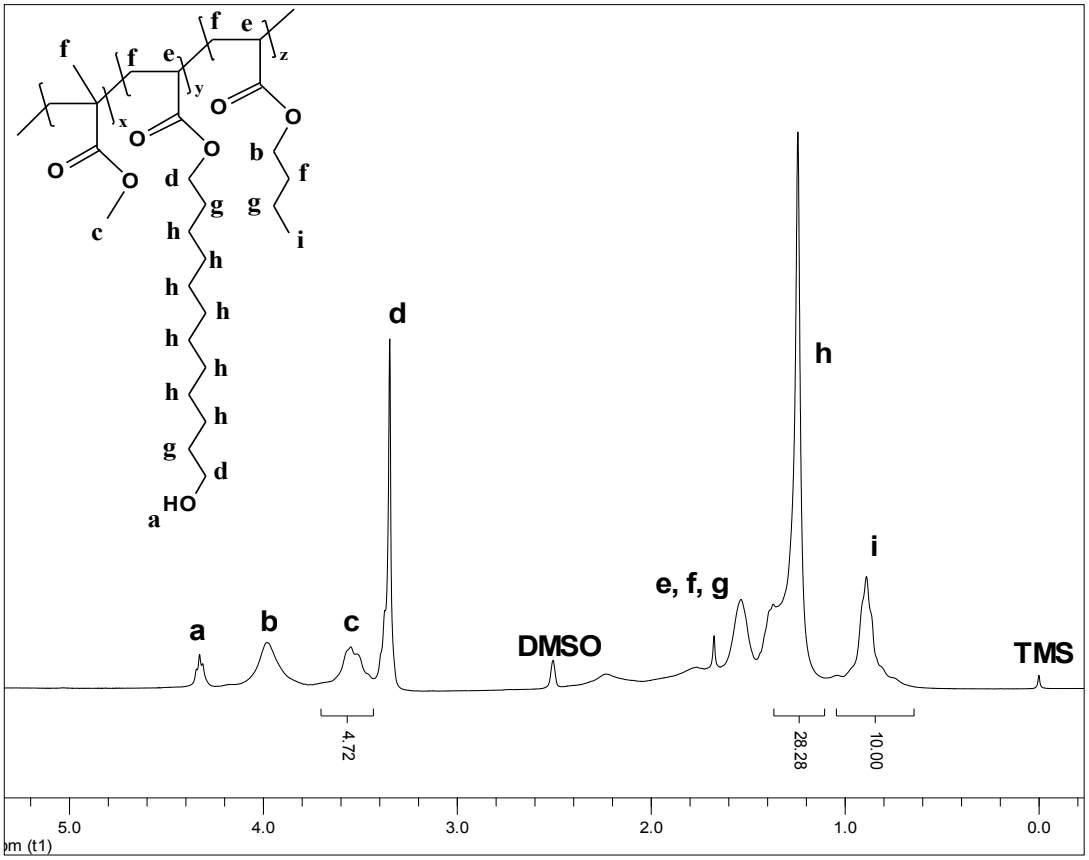

Figure 20. ^{1}H NMR of $AC(CH_2)_{12}OH$-MMA-BA.

Table 3

Properties of $AC(CH_2)_{12}OH$-MMA-BA Copolymer

Polymer (ID)	Mole%	FEW[a]	FEW[b]	M_n	T_g (°C)
$AC(CH_2)_{12}OH$-MMA-BA	26.1	990	1,170	13,100	n/a

[a]Determined by ^{1}H NMR
[b]Determined by potentiometric titration for hydroxyl groups

Synthesis of 12-acryloyloxy-1-dodecanol-methyl methacrylate copolymer (AC(CH_2)$_{12}$OH-MMA): In a typical formulation, a 250 mL three neck flask equipped with a thermocouple, a condenser and nitrogen line was charged with 12A1D (5 g, 19.5 mmol) and MMA (8.03 g, 80.2 mmol) in 150 mL toluene. The system was sealed and purged with N_2 for 30 min. The reaction was initiated by injection of AIBN (0.21 g, 1.3 mmol) toluene solution at 60 °C. The reaction was quenched after 24 h by exposing to air and cooling to room temperature. The polymer solution was precipitated by dropwise addition into 10 times volumetric excess of hexanes. This procedure was repeated until unreacted monomers could not be detected by ^{1}H NMR achieving final yields 18-23%. Results were summarized in Table 4. The product was dried under vacuum at room temperature. ^{1}H NMR ($CDCl_3$): 0.95 (6H), 1.4 (2H), 1.61 (2H), 1.8 (2H), 3.94 (2H) (Figure 21).

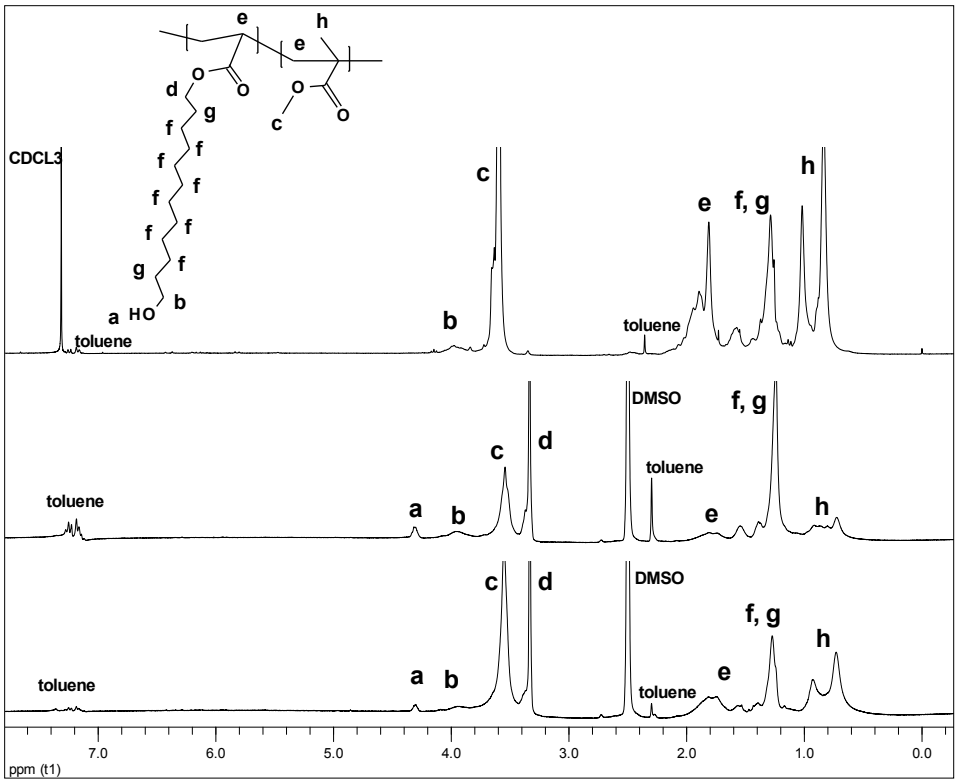

Figure 21. ^{1}H NMR of AC$(CH_2)_{12}$OH-MMA copolymer series with various functional monomer incorporation: top curve corresponds to AC$(CH_2)_{12}$OH-MMA 12%, middle curve corresponds to AC$(CH_2)_{12}$OH-MMA 15%, and bottom curve corresponds to AC$(CH_2)_{12}$OH-MMA 46%.

Table 4

Properties of AC$(CH_2)_{12}$OH-MMA Copolymer Series

Polymer (ID)	Mole%	FEW[a]	FEW[b]	M_n	M_w	PDI	T_g (°C)
AC$(CH_2)_{12}$OH-MMA 12%	12.1	2,560	3,026	9,500	14,000	1.47	55
AC$(CH_2)_{12}$OH-MMA 15%	14.6	1,862	n/a	20,760	30,200	1.45	59
AC$(CH_2)_{12}$OH-MMA 46%	46.1	560	n/a	10,750	30,305	2.82	-29

[a]Determined by ^{1}H NMR
[b]Determined by potentiometric titration for hydroxyl groups

Synthesis and characterization of –COOH pendant functionalized polymers

Carboxyl pendant functionalized monomers were synthesized following the general synthesis scheme shown in Figure 22.

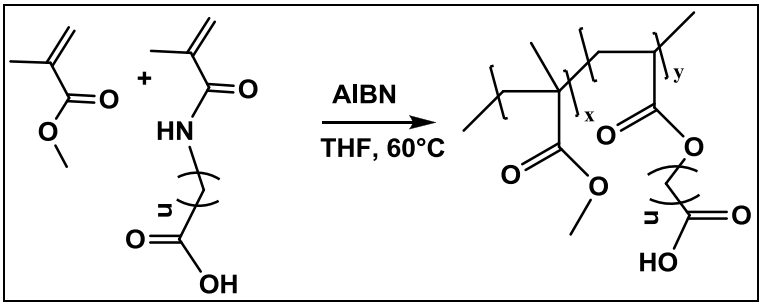

Figure 22. Synthesis of –COOH pendant functionalized polymers.

Synthesis of 11-(methacryloylamino) undecanoic acid -methyl methacrylate - butyl acrylate copolymer (AM(CH_2)$_{10}$COOH-MMA-BA): A three-neck flask equipped with nitrogen line, thermocouple, and condenser was charged with 11AUDA (4.9 g, 18.2 mmol), MMA (3.64 g, 36.4 mmol), BA (6.99 g, 54.6 mmol), and dodecanethiol (0.111 g, 0.055 mmol) in 58 mL anhydrous THF. The flask was sealed and sparged overnight with nitrogen. The reaction was initiated by injecting AIBN (1.28 g, 7.8 mmol) solution at 60 °C. The reaction was quenched after 24 hours by cooling to room temperature and exposing to air. CH_3OH (50 mL) was added to the reaction vessel followed by dropwise precipitation into 10 times volume excess of ether. The product was dried in vacuum at room temperature. The final product had a T_g of 0.83 °C and a yield of 42% (Table 5). ^{1}H NMR ($CDCl_3$) δ: 5.70-6.10 (1H), 3.85-4.02 (2H), 3.50-3.70 (3H), 3.0-3.30 (2H), 2.30-2.40 (2H), 1.50-1.80 (23H), 1.20-1.40 (8H), 0.80-1.10 (3H) (Figure 23).

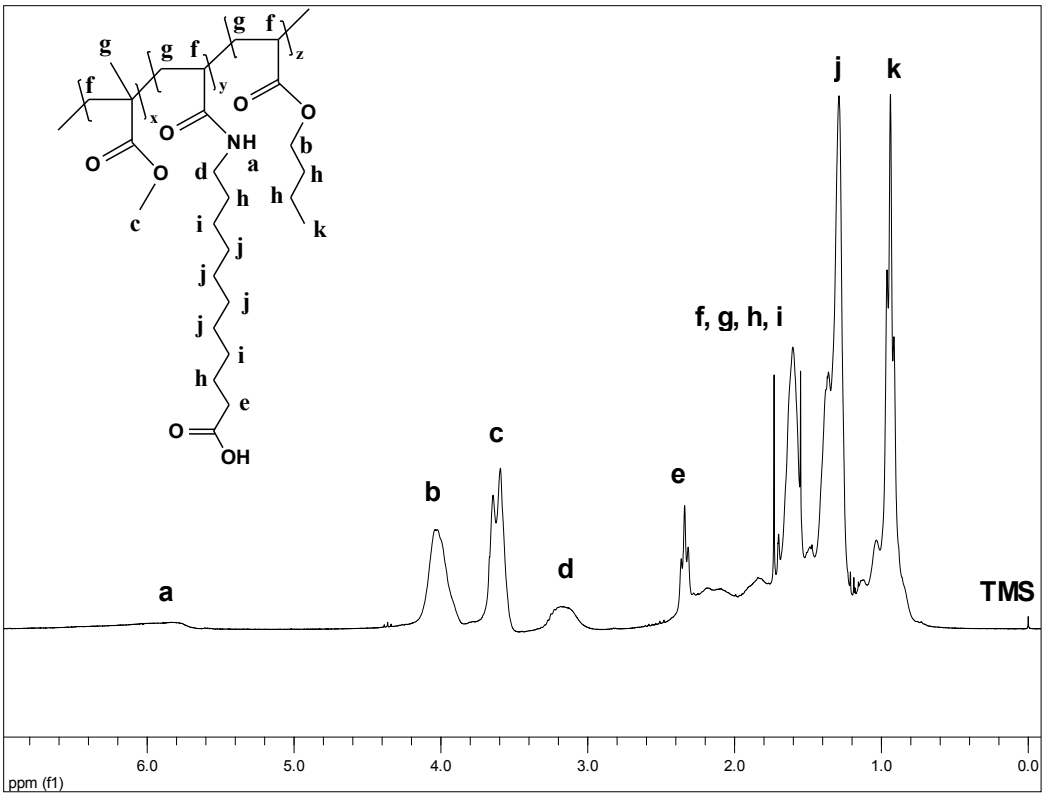

Figure 23. ^{1}H NMR of AM$(CH_2)_{10}$COOH-MMA-BA.

Table 5

Properties of AM$(CH_2)_{10}$COOH-MMA-BA Copolymer

Polymer (ID)	Mole%	FEW[a]	FEW[b]	M_n	M_w	PDI	T_g (°C)
AM$(CH_2)_{10}$COOH-MMA-BA	8.7	3,102	1,250	6,700	9,500	1.42	-18.30

[a]Determined by ^{1}H NMR
[b]Determined by end-point titration for carboxylic acid groups

Synthesis of 11-(methacryloylamino) undecanoic acid-methyl methacrylate copolymer series (AM$(CH_2)_{10}$ COOH-MMA): A three-neck flask equipped with a thermocouple and condenser was charged with 11AUDA (4.99 g, 18.5 mmol), MMA (7.38 g, 74 mmol), and dodecanethiol (0.093 g, 0.5 mmol). The system was sealed and 143 mL of anhydrous THF were pumped into the flask via a nitrogen line. The reaction was initiated by injecting AIBN (0.2 g, 1.2 mmol) solution at 60 °C. The reaction was quenched after 24 h by exposing to air and

cooling to room temperature. The product was dissolved in equal volume of methanol and precipitated by dropwise addition in 10 times volumetric excess ether. This procedure was repeated until unreacted monomers could not be detected by ^{1}H NMR. The product was dried in a vacuum oven and final yields from 18.6-35.3% were achieved. Results were summarized in Table 6. ^{1}H NMR (DMSO-d_6): 0.95 (6H), 1.4 (2H), 1.61 (2H), 1.8 (2H), 3.94 (2H) (Figure 24).

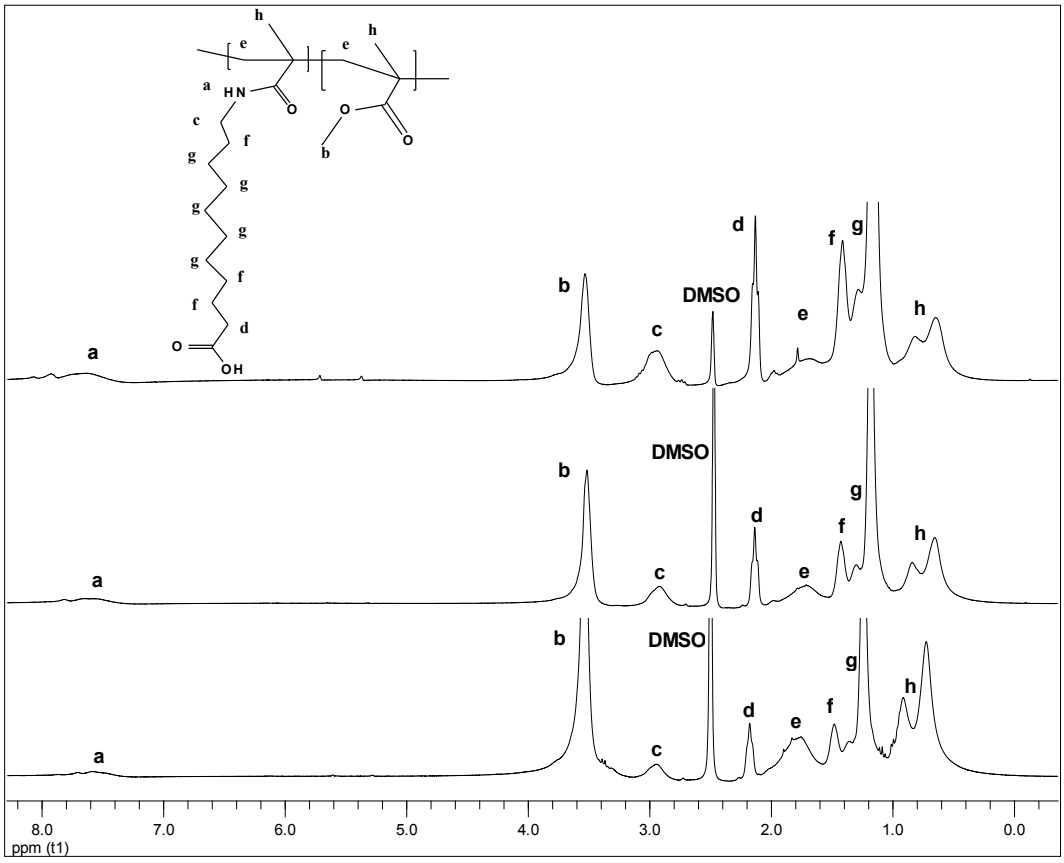

Figure 24. ^{1}H NMR of AM$(CH_2)_{10}$ COOH- MMA copolymer series with various functional monomer incorporation: bottom curve corresponds to AM$(CH_2)_{10}$ COOH- MMA 10%, middle curve corresponds to AM$(CH_2)_{10}$ COOH- MMA 30%, and top curve corresponds to AM$(CH_2)_{10}$ COOH- MMA 50%.

Table 6

Properties of AM(CH_2)$_{10}$ COOH-MMA Copolymer Series

Polymer (ID)	Mole%	FEW[a]	FEW[b]	M_n	M_w	PDI	T_g (°C)
AM(CH_2)$_{10}$ COOH-MMA 10%	9.9	2,700	873	16,800	23,200	1.38	86
AM(CH_2)$_{10}$ COOH-MMA 30%	30.3	900	505	7,400	9,800	1.32	80
AM(CH_2)$_{10}$ COOH-MMA 50%	47.8	540	378	4,000	4,100	1.10	31

[a]Determined by ^{1}H NMR
[b]Determined by end-point titration for carboxylic acid groups

Synthesis of 5-Acetamidooxepane-2-one (AcCL, Compound 6)

AcCL and the corresponding adducts, e.g., AcCL/EA, CL/EA, AcCL/HMDA CL/HMDA, were provided by Eylem-Tarkin Tas (*84*). The following expand upon the synthesis with detailed ^{1}H NMR and ^{13}C NMR analysis of the adducts.

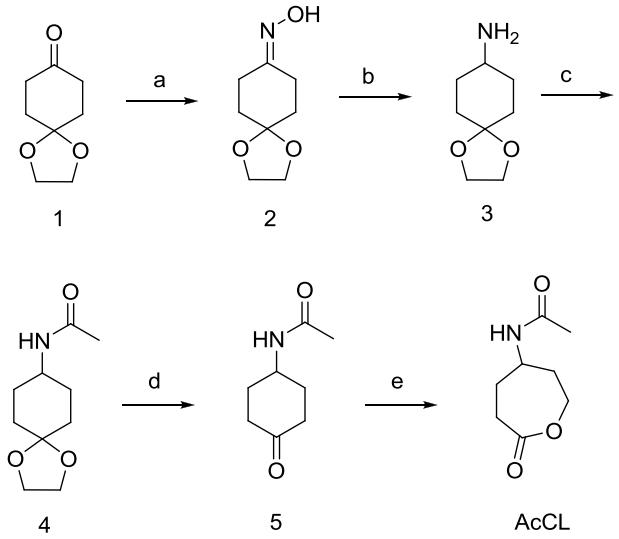

Figure 25. Synthesis of γ-acetamido-ε-caprolactone. a) $NH_2OH.HCl$, NaOAc, CH_3OH:H_2O, 85 ºC, 3h, 98% b) $LiAlH_4$, THF, 80 ºC, 48h, 90% c) AcOAc, THF, 25 ºC, overnight, 96% d) HCl (aq), 25 C, overnight, 80% e) m-CPBA, CH_2Cl_2, 25 ºC, overnight 98%.

Synthesis of 4-Acetamido-6-hydroxy-n-(2-hydroxyethyl)hexanamide (AcCL/EA, 7)

Compound 6 (1.0 g, 5.8 mmol) and ethanolamine (1.1 equivalents) were dissolved in 20 mL of CH_2Cl_2. The reaction was continued overnight at ambient temperature with stirring. The oily product (1.3 g, 99% yield) was purified by trituration from CH_2Cl_2, mp 96 °C. The product was confirmed by ^{1}H NMR (DMSO-d_6) δ: 1.5 (m, 2H), 1.6 (m, 2H), 1.8 (s, 3H), 2.0 (t, 2H), 3.1 (t, 2H), 3.35 (m, 4H), 3.7 (m, 1H), 4.6 (s, 2H), 7.6 (s, 1H), 7.8 (s, 1H); ^{13}C NMR (DMSO-d_6) δ: 172.6 (-CH_2-NH-*C*O-CH_2-), 169.8 (-CH-NH-*C*O-CH_3), 60.1 (HO-*C*H_2-CH_2-NH-), 58.1 (-CH_2-*C*H_2-OH), 45.6 (-*C*H-NH-CO-CH_3), 41.7 (HO-CH_2-*C*H_2-NH-), 37.8 (-*C*H_2-CH_2-OH), 32.4 (-NH-CO-*C*H_2-CH_2-), 30.8 (-NH-CO-CH_2-*C*H_2-), 22.8 (-NH-CO-*C*H_3).

Synthesis of 6-Hydroxy-n-(2-hydroxyethyl)hexanamide (CL/EA, 8)

ε-Caprolactone (1.0 g, 8.8 mmol) and ethanolamine (1.1 equivalents) were dissolved in 20 mL of CH_2Cl_2. The reaction was continued overnight at ambient temperature with stirring. The oily product (1.5 g, 97% yield) was purified by trituration from CH_2Cl_2, mp 77°C. The product was confirmed by ^{1}H NMR (DMSO-d_6) δ: 1.23 (m, 2H), 1.39 (m, 4H), 2.05 (t, 2H), 3.1 (t, 2H), 3.36 (t, 2H), 3.55 (m, 4H), 7.77 (s, 1H); ^{13}C NMR (DMSO-d_6) δ: 172.6 (-CH_2-NH-*C*O-CH_2-), 60.7 (-CH_2-*C*H_2-OH), 60.0 (HO-*C*H_2-CH_2-NH-), 41.5 (HO-CH_2-*C*H_2-NH-), 35.5 (-NH-CO-*C*H_2-CH_2-), 32.3 (-CH_2-*C*H_2-CH_2-OH), 25.3 (-CO-CH_2-*C*H_2-*C*H_2-CH_2-).

Synthesis of hexamethylene bis(6-hydroxy-4-acetamido hexanamide) (AcCL/HMDA, 9)

Compound 6 (1.88 g, 11 mmol) and 1,6-hexamethylenediamine (0.58 g, 5 mmol) were dissolved in 50 mL of dioxane in a 100 mL round bottomed flask containing a magnetic stirrer. The reaction mixture was refluxed overnight. The solvent was removed under reduced pressure and the product was washed with acetonitrile to remove unreacted compound 6. The white solid product (2.0 g, 90% yield) was purified by recrystallization from dioxane, mp 144 °C. The product was confirmed by ^{13}C NMR (DMSO-d_6) δ: 172.0 (-CH_2-NH-*C*O-CH_2-), 169.4 (-CH-NH-*C*O-CH_3), 58.0 (-CH_2-*C*H_2-OH), 45.6 (-*C*H-NH-CO-CH_3), 38.5 (-*C*H_2-NH-CO-CH_2-), 37.7 (-*C*H_2-CH_2-OH), 32.4 (-NH-CO-*C*H_2-CH_2-), 30.8 (-NH-CO-CH_2-*C*H_2-), 29.1 (-CH_2-*C*H_2-CH_2-NH-CO-), 26.2 (-*C*H_2-*C*H_2-CH_2-NH-CO-), 22.7 (-NH-CO-*C*H_3).

Synthesis of hexamethylene bis(6-hydroxy hexanamide) (CL/HMDA, 10)

ε-Caprolactone (1.88 g, 11 mmol) and 1,6-hexamethylenediamine (0.58 g, 5 mmol) were placed in a 100 mL round bottomed flask containing a magnetic stirrer. 50 mL of dioxane was added and the reaction mixture was refluxed overnight. The solvent was removed under reduced pressure and the product was washed with acetonitrile to remove unreacted 1,6-hexamethylenediamine. The white solid product (1.6 g, 95% yield) was purified by recrystallization from dioxane, mp 100°C. The product was confirmed by ^{1}H NMR (DMSO-d_6) δ: 1.21 (m, 4H), 1.35 (m, 4H), 2.01 (t, 2H), 3.00 (t, 2H), 3.35 (t, 2H), 3.68 (s, 1H), 7.78 (s, 1H); ^{13}C NMR (DMSO-d_6) δ: 171.9 (-CH_2-NH-*C*O-CH_2-), 60.6 (-CH_2-*C*H_2-OH), 38.3 (-*C*H_2-NH-CO-CH_2-), 35.5 (-NH-CO-*C*H_2-CH_2-), 32.3 (-*C*H_2-CH_2-OH), 29.2 (-

CH_2-*C*H_2-CH_2-NH-CO-), 26.3 (-*C*H_2-*C*H_2-CH_2-NH-CO-), 26.13 (-NH-CO-CH_2-*C*H_2-) 25.3 (-NH-CO-CH_2-*C*H_2-).

Biocatalytic synthesis of poly(ester amide)s (PEAs)

Poly(ester amide)s were prepared both as neat mixtures and in solution using acrylic resin immobilized lipase from *Candida Antarctica*. *Neat formulation*: Amide-functionalized substituted and unsubstituted diols were combined directly with DVA in a 1:1 molar ratio in a 50 mL round bottom flask. Amide containing unsubstituted diols were heated to 70 °C for the mixture to reach the melt state. Amide-functionalized substituted diols were heated to 95 °C for the mixture to melt. Immobilized enzymes were added to the reaction mixture while stirring with a magnetic bar. The reactions were terminated after 48 hours by removing from heat and fully dissolving in methanol at ambient temperature. The lipase beads were removed by gravity filtration using medium porosity filter paper. The solvent was removed under reduced pressure. The resulting PEAs were further purified by dissolving in minimal amounts of DMSO and precipitating in acetone. *Formulations in dioxane*: Amide-functionalized substituted and unsubstituted diols and DVA (1:1 molar ratio) were dissolved in 1,4-dioxane at 10% w/v of monomers. Immobilized lipase from *Candida Antarctica* was added to the solution at 10% w/w of monomer. The reaction vessels were incubated at 65 °C for 48 hours and 80 °C for 212 hours. The reactions were terminated and the resulting PEAs were purified as described above.

Two-step, one pot lipase-catalyzed polycondensation reaction

Compound 6 (1.0 g, 5.8 mmol) was dissolved in excess methanol and TEA was added as a catalyst (1 mol%). The mixture was allowed to react overnight at room temperature with continuous stirring. Unreacted methanol was removed under reduced pressure, and the reaction flask was attached to a vacuum line. 50 mg of lipase from *Candida Antarctica* acrylic resin was added to the flask and polymerization was conducted at 60 °C for 150h with continuous stirring. The polymer product was characterized with GPC, NMR, DSC and TGA and will be discussed in detail in Chapter VIII.

Enzyme Extraction to Organic Media

Lipase from *Aspergillus Niger* (Lipolase) was modified by adding two times more by volume of 1,4-dioxane to lipolase propylene glycol aqueous buffer (2% w/v) slowly with stirring over a 10 min period. The resulting slurry was centrifuged at 5000 x *g* for 2 min at RT. The supernatant was decanted and the pellet was dried using a flowing nitrogen stream and resolubilized in the appropriate solvent prior to use.

Lipase from *Candida Antarctica* was initially solubilized in a 20 mM sodium acetate buffer (pH 4.5), 9 mM $CaCl_2$, and 0.25% v/v isopropyl alcohol to make 0.5 mg/mL enzyme solution. An equal volume of 2 mM dioctyl sodium sulfosuccinate (AOT) in isooctane was added to the enzyme solution and the blend was mixed for 15 min using an orbital shaker (100 rpm) at 30 °C. The mixture was centrifuged for 10 min at 3,000 rpm to separate the organic and aqueous layers. The organic phase was collected and the isooctane was

removed under reduced pressure. The surfactant-paired enzyme was resolubilized in the appropriate solvent prior to use.

Enzyme Activity in Dilute and Viscous Organic Media

Rapid activity screening: Spectroscopic determination of relative activity

The relative activity was determined visually by monitoring the color change associated with the enzyme-catalyzed hydrolysis of *p*-nitrophenyl acetate in solution relative to negative control solutions (no enzyme). 100 µL of 2.9 mM *p*-nitrophenyl acetate in isopropanol (IPA) was added to 890 µL of 20 mM TRIS buffer (pH 7.1). 10 µL of 0.5 mg/mL enzyme solution (aqueous or organic) was added to initiate the reaction. 10 µL of similar solution composition, as above, was added to the buffer mixture in negative control samples. The enzyme was deemed active and suitable for further characterization when clear-to-green color change (405 nm absorbance using UV spectrophotometer) was observed in the enzyme containing mixture relative to the neat mixture.

Determination of enzyme activity via end-point titration

Enzyme activity was determined by monitoring the concentration change over time of OA associated with the enzyme-catalyzed synthesis of nonyl octanoate from the reaction of OA and 1-NN. Scintillation vials containing 0.1-1 M of stoichiometric amounts of OA and 1-NN in toluene or 1-20% PMMA solids in toluene were prepared. The reaction was initiated by the addition of 0.67 wt% PPL to the solution and placing in an orbital shaker at 250 rpm and 40 °C. Time 0 h was taken as the time prior to the addition of catalyst. 100 µL aliquots were taken at fixed times and solubilized in dichloromethane to yield 1 wt% solutions.

2% w/v phenolphthalein in methanol was added to a final concentration of 0.5% v/v. End-point titration at fixed times to determine –COOH equivalents was conducted as described earlier in the chapter. PPL activity was computed from the zero-order consumption of –COOH functionality via linear regression and was expressed in μmol/g/h or μM/h.

Determination of enzyme activity via GC-MS spectroscopy

Enzyme activity was determined by monitoring the concentration changes over time of OA, 1-NN, and nonyl octanoate associated with the enzyme-catalyzed synthesis of nonyl octanoate from the reaction of OA and 1-NN. Scintillation vials containing 0-150 mM of stoichiometric amounts of OA and 1-NN in various organic solvents were prepared. The reaction was initiated by the addition of 1 wt% PPL to the solution and placing in an orbital shaker at 250 rpm and 40 °C. Time 0 h was taken as the time prior to the addition of catalyst. 100 μL aliquots were taken at fixed times and added to 1.7 mL dram vials (National Scientific, Rockwood, TN) containing 1,400 μL of cold acetone to induce enzyme precipitation. The GC-MS procedure to determine the concentration of OA and 1-NN during the enzyme-catalyzed reaction is described earlier in the chapter. PPL activity was computed from the zero-order increase of nonyl octanoate via linear regression and was expressed in μmol/g/h or μM/h.

Film Preparation and Characterization Methodologies

Formation of free-standing functional biocatalytic films

Enzyme and functionality embedded in film: In a typical formulation, stoichiometric amounts of OA and 1-NN (6 wt% total on solids) were added to a 5

mL of 10% w/v polymer solution in toluene. The solutions were shaken on a vibratory mixer and subsequently lipase was added at 1 wt% of the solid content. The heterogeneous mixtures were vortexed for 10 seconds, poured into 50 mm diameter glass dishes, and covered with a box to limit rapid solvent evaporation. Samples were kept at ambient for 9 h, then cut into 6 mm diameter circles using a round punch, weighed and placed in scintillation vials. The films with average thickness of 200 μm were incubated at 40 °C and assayed periodically by GC-MS. The film thickness was controlled by the amount of polymer solution added to each glass dish and was measured by a digital caliper. Parameters that varied from system to system are listed below:

1. the polymeric matrix (PMMA, PnBMA and PEMA);
2. the combined OA and 1-NN loading (4-16% by weight);
3. enzyme loading (0.5-4% by weight);
4. casting solvent (toluene, chloroform, tetrahydrofuran, methyl ethyl ketone, dichloromethane, and 1,4-dioxane);
5. assay temperature (30-70 °C); and
6. relative humidity (0-100%).

Enzyme embedded in film with functionality coated on the topside film surface: In a typical formulation, PPL comprising 0.67 wt% of the solid content was added to a premixed 10 wt % solution of PMMA (M_w 996,000 g/mol) in toluene. The solution was vortexed for 10 sec, poured onto 50 mm bottom diameter glass mold, and covered with a box to limit rapid solvent evaporation. Samples were kept at ambient for 9 h, then cut in 6 mm diameter circles by a

hole punch, weighed, and placed in scintillation vials. The enzyme active small molecules, OA and 1-NN were coated on the topside surface of each pre-weighed film using a micropipette with a stoichiometric blend of OA and 1-NN (6 wt% total of the film). The resulting functional films were incubated at 40 °C and assayed periodically by GC-MS.

Rapid activity screening: Spectroscopic determination of relative activity

The relative activity was determined visually by monitoring the color change associated with the enzyme-catalyzed hydrolysis of *p*-nitrophenyl acetate in solution relative to negative control solutions (no enzyme). 100 µL of 2.9 mM *p*-nitrophenyl acetate in IPA was added to 800 µL of 20 mM TRIS buffer at pH 7.1. 100 µg of 1 wt% enzyme embedded film or coating was added to initiate the reaction. 100 µg of similar film or coating composition as above was added to the buffer mixture in negative control samples. The enzyme was deemed active and suitable for further characterization when clear-to-green color change (405 nm absorbance by UV spectrophotometer) was observed in the enzyme containing mixture relative to the neat mixture.

Determination of free-standing film enzyme activity

Enzyme activity was determined by monitoring the concentration changes over time of OA, 1-NN, and nonyl octanoate associated with the enzyme-catalyzed synthesis of nonyl octanoate from the reaction of OA and 1-NN. Coupons (6 mm diameter) were weighed at fixed times during the reaction and placed in dram vials (1.7 mL) and solubilized in cold acetone. The final volume of the solution was adjusted to 1.5 mL. Time 0 h was taken as the time after

enzyme-functionality loaded films were dried for 9 h at ambient prior to exposure to higher temperatures. The GC-MS procedure to determine the concentration of reactants and products during the enzyme-catalyzed reaction is described earlier in the chapter. PPL activity was computed from the zero-order increase of nonyl octanoate via linear regression and expressed in μmol/g/h or μM/h.

Formation of polyfunctional coatings

MMA-BA and functional component copolymer blends: Two master batches were prepared with 1:1 molar functional equivalents of both -COOH and hydroxyl functional copolymers corresponding to a total weight of 1.05 g. Both batches were solubilized in 10 mL THF. 10 mg of previously *Candida Antarctica* lipase acrylic resin was added to one of the batches, while the other served as the negative control. 2 mL of solution from the master batches was dispensed into multiple scintillation vials for film formation to occur. Coatings were dried under vacuum for 48 hours and placed in an oven at 70 °C for the reaction to proceed.

MMA and functional component copolymer blends: In a typical experiment, two master batches were prepared with stoichiometric amounts both –COOH and –OH functional copolymers, which corresponded to a total of 0.45 grams of blended copolymers in THF:DMF (9:1 by volume). 890 μL of 2% w/v lipolase aqueous solution was precipitated in dioxane as described earlier in the chapter to yield 4 wt% of enzyme on total resin solids. The precipitate was mixed with copolymer blend solution. 45 μL of the solution was pipetted in pre-weighed standard DSC aluminum pans, and the resulting coatings were dried at ambient

for 48 h. The coated pans were exposed to cure temperature ranging from 40-70 °C and periodically tested for their thermal properties, coefficient of thermal expansion and molecular weight at pre-determined intervals for up to 250 h.

Determination of coating biocatalytic activity

MMA-BA and functional component copolymer blends: Biocatalytic activity was determined by monitoring concentration changes over time of –COOH functional equivalents associated with the enzyme-catalyzed synthesis. Scintillation vials containing 210 mg of coating blend were solubilized in THF to give a final 2.1% w/v solution. Time 0 h was taken as the time after coatings with no enzyme were dried under vacuum for 48 h. 2% w/v phenolphthalein in methanol was added to achieve a final concentration of 0.5% v/v. End-point titration at fixed times to determine –COOH equivalents was conducted as described earlier in the chapter. PPL activity was computed from the zero-order consumption of –COOH functionality via linear regression and was expressed in μmol/g/h or μM/h. GPC samples for molecular weight determination were prepared by solubilizing coatings blends in dry THF at a final concentration of 10 mg/mL at pre-determined times.

MMA and functional component copolymer blends: Activity was determined by monitoring the average molecular weight (M_n) changes over time due the enzyme-catalyzed synthesis reaction. GPC samples were prepared by solubizing coatings blends in 0.05 N sodium nitride N,N-dimethyl acetamide solution at a final concentration of 10 mg/mL at pre-determined times. Enzyme

activity was computed from the zero-order increase over time of degree polymerization via linear regression and was expressed in 1/h.

Free-standing films sorption rate determination

Poly (alkyl methacrylate) films cast from toluene solutions and dried at ambient for 24 h were prepared with dimensions of ca. 20 mm x 20 mm x 0.3 mm and conditioned in an oven for 24 h at 40-90 °C. Specimens were exposed to OA and 1-NN baths at constant temperature of 40 °C. Specimens were removed from baths at different times to quantify OA and 1-NN uptake measurement. Excess OA or 1-NN on the specimen surface was removed with dry, clean KimWipes®. After each uptake measurement was performed gravimetrically, the individual film specimens were placed back into the original and corresponding baths to continue uptake measurements until an equilibrium endpoint was reached.

CHAPTER IV

THE KINETIC BEHAVIOR OF ENZYME-CATALYZED REACTIONS IN DILUTE AND VISCOUS ORGANIC MEDIA

The vast majority of enzymes are proteins with primary structure determined by a deoxyribonucleic acid (DNA) sequence. Each distinct amino acid residue contains a functionality that exhibits a wide range of polarity and ionizability in aqueous environments. Backbone non-covalent interactions, such as hydrogen bonding and Van der Waals (VDW) interactions, drive the enzyme secondary structure(s) in the form of α helices, β sheets, and β turns. Additional structural complexity arises from the 3D spatial configuration of these local conformations, termed tertiary structures. Crevice sites that arise from the specific combination of structures and folding serve as catalytic sites of enzymes *(1)*.

Catalytic sites or active sites generally contain a series of ~10 amino acid residues that solvate the substrate(s) to form an enzyme-substrate complex and subsequently, direct the dissociation of the enzyme-substrate complex to yield the product(s) and free enzyme (Figure 26). The local conformation of the active site develops a congruous conformation that fits the transient configurations adopted by the functionality during their conversion to products *(85)*. Progress of the functionality to the transition state is favored by non-covalent stabilization (hydrogen bonding and electrostatic interactions) of the transition state species by the active site. Hence, the binding energy accounts for the loss of activation entropy as a consequence of abating translational and rotational motion of

reacting species *(85)*. An enzyme is thereby able to proportionally lower the activation energy of the forward and backward reactions and increase the reaction rate. Enzymes only decrease the time necessary to establish equilibrium conditions, and do not directly shift the equilibrium between reactants and products *(1)*. Enzymes carry nominal amounts of water even when introduced to hydrophobic organic media. Embedding enzymes in hydrophobic polymers will lead to higher water content than in the absence of enzymes.

Serine Hydrolase Structure and Mechanism

The Nomenclature Committee appointed by the International Union of Biochemistry in 1984 categorized enzymes into six main reaction catalysis classes. Enzymes classes that have found commercial applications are oxido-reductases, hydrolases, and transferases (*85-86*). Oxido-reductases catalyze the transfer of oxygen, hydrogen or electrons between molecules. Hydrolases catalyze the transfer of acyl groups in ester, peptide, and glycosidic chemistries. Transferases catalyze the transfer of atoms between substrate molecules *(87,88,89,90,91).*

The serine hydrolase class is one of the most studied enzyme families and includes serine proteases (trypsin, chymotrypsin), esterases (lipases), acetylcholinesterase, thioesterases and phospholipases *(92)*. For the research described in this dissertation, lipases were chosen as the model enzyme to test the hypothesis put forth in Chapter II. Lipases have well-defined activity in organic solvents with broad and established tolerance for a variety of functional groups *(93)*. There are several types of lipases based on the organism from

which they are extracted. These include, but are not limited to: Porcine pancreas lipase (PPL), lipase from *Candida Antarctica* (CALB), *Mucor Miehei* lipase*, Pseudomonas Fluorescens* (PFL), *Rhizopus Oryzae*, *Aspergillus Oryzae* (AO), *Aspergillus Niger*, *Candida Rugosa,* and *Pseudomonas Cepacia (85)*.

The active site of lipases is comprised of a serine residue and a catalytic triad, both of which are necessary for the catalytic function (Figure 26). Lipases carry out acyl transfer reactions via a mechanism that is termed ping-pong bi-bi or double displacement mechanism *(94,95)*. Initially, the free enzyme binds to the acyl end of carboxylated species. An acyl-enzyme intermediate (EM) is formed upon the release of the leaving group and frees up the hydroxyl terminal, while the carboxy-terminal remains tethered to the active site. The acyl transfer reaction occurs when a nucleophile enters the active site, cleaves the acyl intermediate, and frees the new acyl containing species *(96)*. The mechanism is the same for hydrolysis, esterification, and amidation reactions; the only difference is the type of nucleophile acting upon the EM. During hydrolysis, the acting nucleophile is water, while in esterification and amidation reactions, the acting nucleophiles are hydroxyls and amines, respectively.

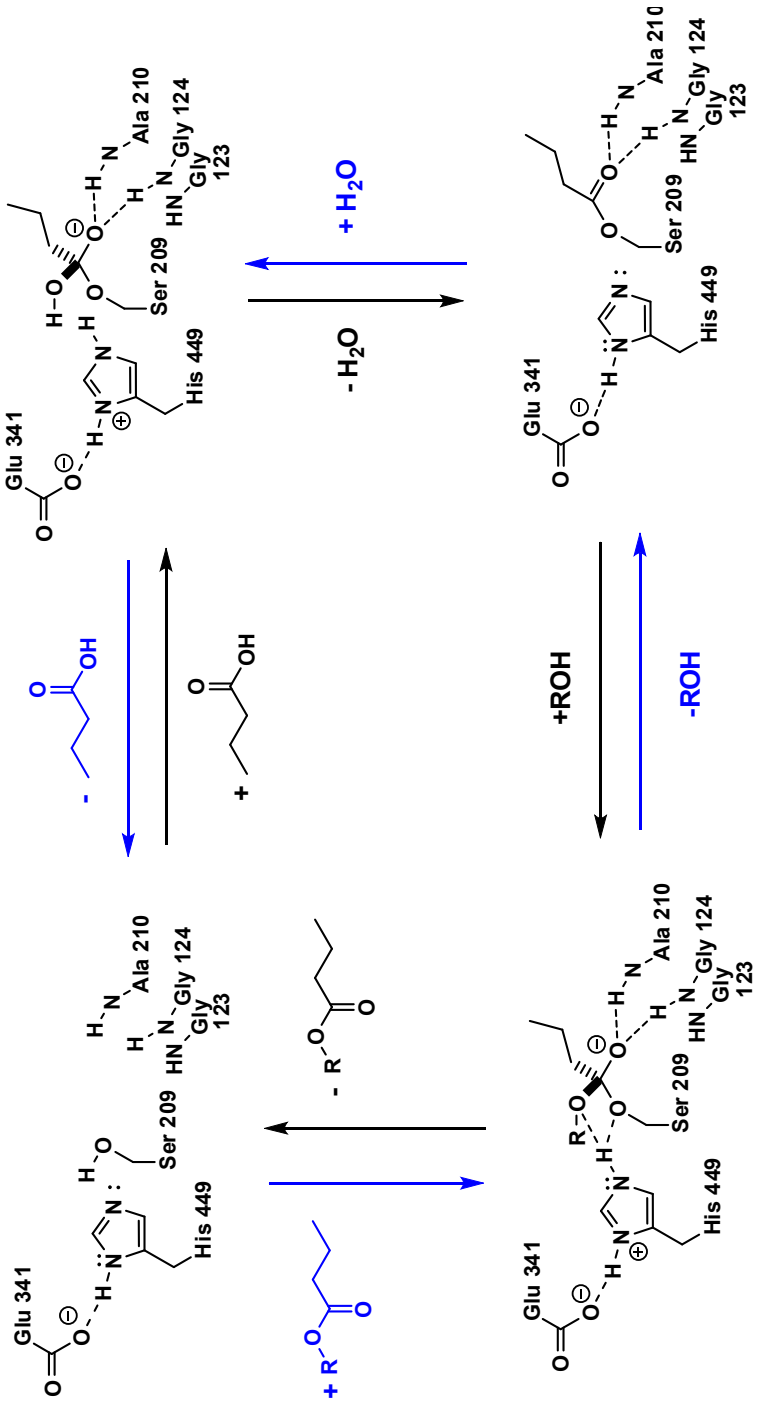

Figure 26. Serine hydrolase catalytic mechanism in esterification and hydrolysis reactions.

Pancreatic lipases consist of a single polypeptide chain 30-50 kDa *(97)*. These enzymes are unique compared to other serine hydrolases; their catalytic site is covered by an amphiphilic lid or flap *(97)*. In the closed lid conformation,

substrate(s) cannot bind to the active site of the enzyme. The open lid conformation exposes the hydrophobic interior of the active site and allows binding of hydrophobic fatty acid chains. The transition from the closed lid to the open lid conformation is an interfacial activated process and requires the adsorption of lipase to a hydrophobic interface *(98)*.

Serine Hydrolase Intrinsic Kinetics

Double displacement kinetics are summarized as shown in the following figure (*99*):

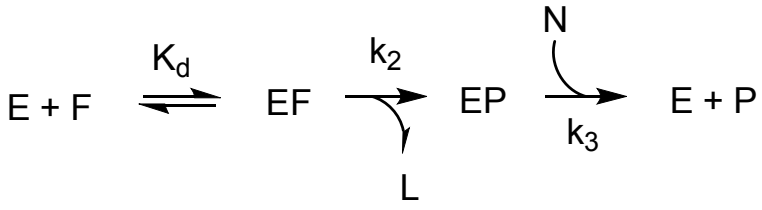

Figure 27. General reaction scheme for ping-pong bi-bi mechanism, F-the initial carboxylated functionality, N-nucleophile, P-product.

To simplify the derivation of the rate law that describes ester biosynthesis, one can assume that F is in a rapid equilibrium with the free enzyme (E) and the enzyme-functionality complex (EF), described by the dissociation constant, K_d, in equation 9.

$$K_d = \frac{[F]\cdot[E]}{[EF]} \qquad \text{Equation 9}$$

The steady-state assumption was also invoked given that E<<F and at initial stages of the reaction, enzymes are continuously in the intermediate stages EF or EP along the reaction pathway. Equations 10 and 11 describe the mass balance between enzyme intermediates and the steady-state condition.

$$\left[E_0\right] = [E] + [EF] + [EP] \qquad \text{Equation 10}$$

$$\frac{d}{dt}[EP] = k_2 \cdot [EF] - k_3 \cdot [EP] \cdot [N] = 0 \qquad \text{Equation 11}$$

Dissociation of EF and EP is assumed as an irreversible process since in the initial stages of the reaction, the product concentration is negligible compared to the initial functional group concentration. The rate laws for product formation have been determined for two main cases: nucleophile concentration much larger than initial functional group concentration (N>>F), and nucleophile concentration equals acyl functionality concentration (N=F). N>>F case is relevant in small molecule transformations such as hydrolysis or transesterification reactions, while N=F case is relevant to enzyme-catalyzed step-polymerization where stoichiometric functional group concentration is necessary to achieve high molecular weights.

Case N>>F

In the initial stages of the reaction, the nucleophile concentration is not changing and k_3 can be written as a pseudo-first-order rate constant and the steady-state equation 11 can be written as follows:

$$\frac{d}{dt}[EP] = k_2 \cdot [EF] - k_3 \cdot [EP] = 0 \qquad \text{Equation 12}$$

Case N>>F, k_2<<k_3: If the rate determining step is the release of the leaving group (k_2<<k_3), the rate law is described by equation 13.

$$\frac{d}{dt}[P] = k_2 \cdot [EF] \qquad \text{Equation 13}$$

The enzyme mass balance expression was written in term of K_d and an expression was obtained for the enzyme intermediate EP.

$$[EP] = \frac{[E_0]\cdot[EF]\,K_d + [F]}{[F]} \qquad \text{Equation 14}$$

Equation 14 was substituted in the steady-state equation 12 and solving for intermediate EF yielded the following expression:

$$[EF] = \frac{k_3\cdot[E_0]\cdot[F]}{k_3\cdot K_d + (k_2 + k_3)\cdot[F]} \qquad \text{Equation 15}$$

Substituting into expression 13 yields the rate law for product formation.

$$\frac{d}{dt}[P] = \frac{\frac{k_2\cdot k_3}{k_2 + k_3}\cdot[E_0]\cdot[F]}{\frac{k_3\cdot K_d}{k_2 + k_3} + [F]} \qquad \text{Equation 16}$$

Equation 16 is the same as the general form of the Michaelis-Menten equation once K_M is substituted for the $k_3\,K_d\,(k_2+k_3)^{-1}$ constant and k_{cat} is substituted for the $k_2\,k_3\,(k_2+k_3)^{-1}$ constant to yield equation 17.

$$\frac{v_0}{[E_0]} = \frac{k_{cat}\cdot[F]}{K_m + [F]} \qquad \text{Equation 17}$$

Case N>>F, k_3<<k_2: If the rate determining step is the release of the newly formed acyl product (k_3<<k_2), the rate law is described by equation 18.

$$\frac{d}{dt}[P] = k_3\cdot[EP] \qquad \text{Equation 18}$$

The enzyme mass balance expression was written in term of K_d and an expression was obtained for the enzyme intermediate EF.

$$[EF] = \frac{[F]\left[E_0\right] - [EP]}{K_d + [F]} \qquad \text{Equation 19}$$

Equation 19 was substituted in the steady-state equation 12 and solving for intermediate EP yielded the following expression:

$$[EP] = \frac{k_2 \cdot \left[E_0\right] \cdot [F]}{k_3 \cdot K_d + \left(k_2 + k_3\right) \cdot [F]} \qquad \text{Equation 20}$$

Substituting into expression 18 yields the rate law for product formation:

$$\frac{d}{dt}[P] = \frac{\frac{k_2 \cdot k_3}{k_2 + k_3} \cdot \left[E_0\right] \cdot [F]}{\frac{k_3 \cdot K_d}{k_2 + k_3} + [F]} \qquad \text{Equation 16}$$

Equation 16 was obtained from both assumptions indicating that product formation will follow the same rate law whether k_2 or k_3 is the rate determining step. This expression can be written as the general form of the Michaelis-Menten equation 17 once K_M is substituted with $k_3\ K_d\ (k_2+k_3)^{-1}$ constant and k_{cat} is substituted with $k_2\ k_3\ (k_2+k_3)^{-1}$

Case N=F

In the initial stages of the reaction, the nucleophile concentration is not changing, however, since there is a stoichiometric amount of functional groups, k_3 is written as a second-order rate constant and the steady-state equation can be written as shown in equation 11.

Case N=F, $k_2 << k_3$: If the rate determining step is the release of the leaving group ($k_2 << k_3$), the rate law is described by equation 13 as the function of intermediate (EF) as shown above and intermediate (EP) is written in terms of K_d

as shown in equation 14. Substituting equation 14 into the steady-state equation 11 and solving for intermediate EF yielded the following expression:

$$[EF] = \frac{k_3 \cdot [E_0] \cdot [F] \cdot [N]}{k_3 \cdot K_d \cdot [N] + k_2 \cdot [F] + k_3 \cdot [F] \cdot [N]} \qquad \text{Equation 21}$$

Substituting into equation 13 and writing $[M]=[N_0]=[F_0]$ yields the rate law for product formation *(100)*.

$$\frac{d}{dt}[P] = \frac{k_2 \cdot [E_0] \cdot [M]}{\frac{k_3 \cdot K_d + k_2}{k_3} + [M]} \qquad \text{Equation 22}$$

Equation 22 can be written as the general form of the Michaelis-Menten equation once K_M is substituted instead of the $(k_3 K_d + k_2) k_3^{-1}$ constant and k_{cat} is substituted with $k_2 k_3 (k_2+k_3)^{-1}$.

Case N=F, $k_3 << k_2$: If the rate determining step is the formation of the new acyl containing product ($k_3 << k_2$), the rate law is described by equation 23.

$$\frac{d}{dt}[P] = k_3 \cdot [EP] \cdot [N] \qquad \text{Equation 23}$$

The intermediate EF is written in terms of K_d as shown in equation 19. Substituting equation 19 in the steady-state equation 11 and solving for intermediate EP yielded the following expression:

$$[EP] = \frac{k_2 \cdot [E_0] \cdot [F]}{k_3 \cdot K_d \cdot [N] + k_2 \cdot [F] + k_3 \cdot [F] \cdot [N]} \qquad \text{Equation 24}$$

Substituting into equation 13 and writing $[M]=[N_0]=[F_0]$ yields the rate law for product formation:

$$\frac{d}{dt}[P] = \frac{k_2 \cdot [E_0] \cdot [M]}{\frac{k_3 \cdot K_d + k_2}{k_3} + [M]} \qquad \text{Equation 22}$$

Equation 22 was obtained from both assumptions indicating that product formation will follow the same rate law whether k_2 or k_3 is the rate determining step. Equation 22 can be written as the general form of the Michaelis-Menten equation once K_M is substituted instead of the $(k_3 K_d + k_2) k_3^{-1}$ constant and k_{cat} is substituted instead of $k_2 k_3 (k_2 + k_3)^{-1}$.

The previous rate law derivation was obtained when N=F by assuming both rapid equilibrium and steady-state conditions. To verify the aforementioned approach, we show that the same rate law can be obtained if only steady-state condition is assumed. The reaction scheme was written in terms of micro-rate constants as shown in Figure 28.

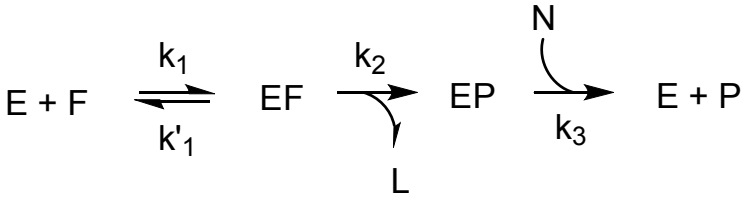

Figure 28. General reaction scheme for ping-pong bi bi reaction where F - initial carboxylated functionality, N - nucleophile, P - product using only the steady-state approximation.

Considering that $[M]=[N]_0=[F]_0$ and $k_3 << k_2$ the following rate laws can be written:

$$\frac{d}{dt}[EF] = k_1 \cdot [E] \cdot [F] - k'_1 \cdot [EF] - k_2 \cdot [EF] = 0 \qquad \text{Equation 23}$$

$$\frac{d}{dt}[EP] = k_2 \cdot [EF] - k_3 \cdot [EP] \cdot [M] = 0 \qquad \text{Equation 24}$$

$$\frac{d}{dt}[P] = k_3 \cdot [EP] \cdot [M] \qquad \text{Equation 25}$$

Solving the steady-state expressions for E and EF and substituting the expression for EF into the expression for E the following are obtained:

$$[E] = \frac{[EF] \cdot \left(k'_1 + k_2 \right)}{k_1 \cdot [M]} \qquad \text{Equation 26}$$

$$[EF] = \frac{[EP] \cdot [M] \cdot k_3}{k_2} \qquad \text{Equation 27}$$

$$[E] = \frac{[EP] \cdot \left(k'_1 + k_2 \right) \cdot k_3}{k_2 \cdot k_1} \qquad \text{Equation 28}$$

Upon substitution of equations 27 and 28 into enzyme mass balance expression, the following is obtained for the intermediate EP:

$$[EP] = \frac{\left[E_0 \right] \cdot k_2 \cdot k_1}{k_3 \left(k'_1 + k_2 \right) + k_1 \cdot k_2 + k_1 \cdot k_3 \cdot [M]} \qquad \text{Equation 29}$$

Substituting into equation 25 and rearranging results in the rate law for product formation yields:

$$\frac{d}{dt}[P] = \frac{k_2 \cdot \left[E_0 \right] \cdot [M]}{\frac{k_3 \cdot K_m + k_2}{k_3} + [M]} \qquad \text{Equation 30}$$

Upon closer examination, it can be seen that this expression is the same as the one obtained using the rapid equilibrium assumption. The only difference is that the dissociation constant K_d in equation 22 represents the limiting case

when $k'_{-1} >> k_2$. The same expression can be obtained for the rate law of monomer consumption following the same procedure as above by substituting in the rate law for monomer consumption shown below:

$$\frac{d}{dt}[M] = k'_1 \cdot [EF] - k_1 \cdot [E] \cdot [M] - k_3 \cdot [EP] \cdot [M] \qquad \text{Equation 31}$$

Equations 22 and 30 can be written as the general Michaelis-Menten equation by writing K^{app} for the ratio of rate constants in the denominator.

$$\frac{v_0}{[E_0]} = \frac{k_{cat} \cdot [F]}{K^{app} + [F]} \qquad \text{Equation 32}$$

Results and Discussion

A model esterification reaction was used to test the derived rate law and determine the activity of this combination in polymer, enzyme, and functionality blends. Octanoic acid (OA) and 1-nonanol (1-NN) were chosen as the model functionality to investigate the biosynthetic activity of lipase (Figure 29). Their aliphatic nature is analogous to naturally occurring lipids and makes them excellent substrate mimics for lipases.

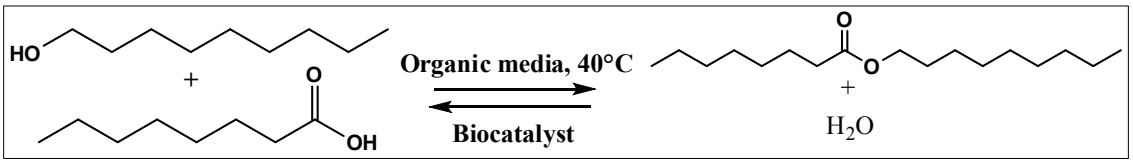

Figure 29. Biocatalyzed synthesis of nonyl octanoate from octanoic acid and 1-nonanol. Porcine Pancreas Lipase was used as biocatalyst unless otherwise specified.

Endpoint titration and GC-MS were employed for conversion and kinetic data characterization to determine the Michaelis-Menten parameters and enzyme activity (Chapter III). Endpoint titration was used to quantify –COOH equivalents

and conversion versus time using a fixed-time assay as described in Chapter III. A typical GC chromatogram is shown in Figure 30 where the retention times of OA, 1-NN, and nonyl octanoate (NOc) were 17.3, 18.0 and 28.3 min.

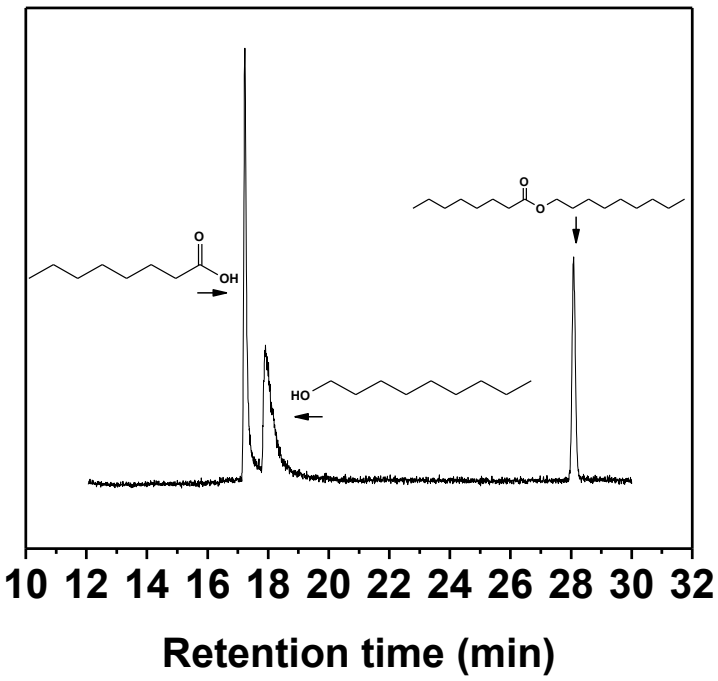

Figure 30. Typical GC-MS traces resulting from OA, 1-NN, and NOc, respectively, from left to right.

Standard calibration curves were prepared from known concentrations of each reaction component as summarized in Figure 31. Each time point was volumetrically controlled and concentrations were calculated from the standard calibration curves.

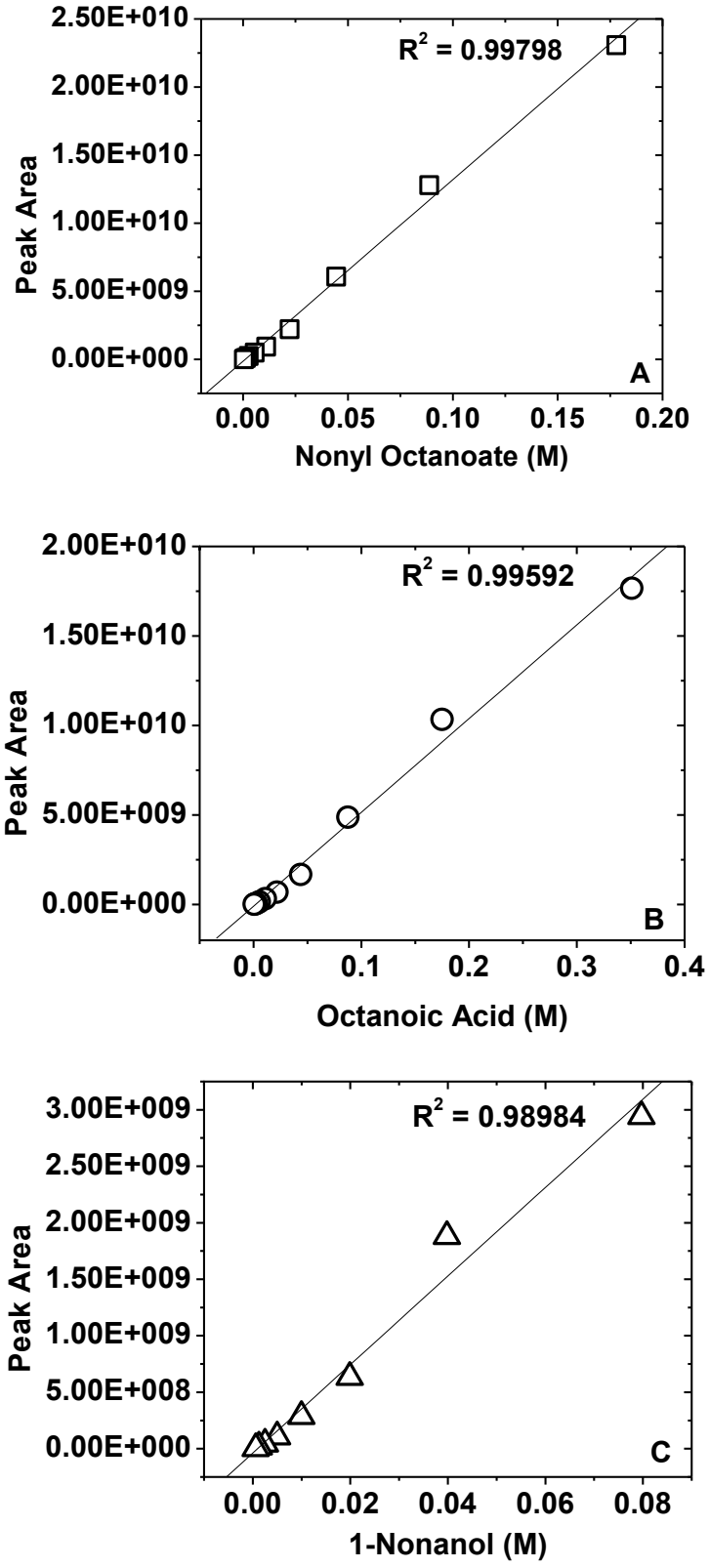

Figure 31. Typical standard calibration curve to determine concentration of (NOc, A), (OA, B), and (1-NN, C).

Determining Porcine Pancreas Lipase (PPL) Michaelis-Menten parameters and activity

To quantify and verify the Michaelis-Menten parameters as derived in equation 32, fixed-time kinetic assays were conducted to determine the optimum initial functionality concentration range and probe zero-order enzyme kinetics. Initial PPL activity was determined by monitoring –COOH concentration over time by endpoint titration (Figure 32). The data revealed an observed time lag before zero-order kinetics were established and a slight but clear dependence of the lag time on the initial –COOH and –OH concentration. For example, at 354 mM, the time lag persisted for ca. 60 h, while at 273 mM, pre-zero order rate consumption of –COOH functional small molecule was observed in the initial 40 h of the kinetic assay.

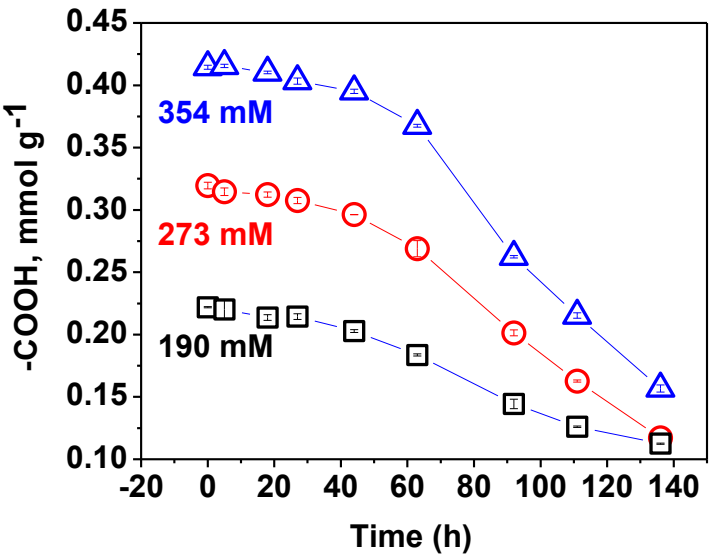

Figure 32. Dependence of the –COOH concentration over time in toluene with stoichiometric amounts of OA and 1-NN at various initial concentrations. The sample was incubated at 40 °C in orbital shaker at 250 rpm where 354 mM corresponds to 0.406 mmol –COOH g^{-1}, 273 mM corresponds to 0.313 mmol –COOH g^{-1}, and 190 mM corresponds to 0.218 mmol –COOH g^{-1}. PPL concentration was 0.66% w/v of toluene, and the assay was performed at 40 °C.

An additional series of experiments were performed specifically to confirm whether the PPL was wetted properly in the assay solvent (Figure 33). PPL was kept in an orbital shaker at 250 rpm for 100 h to exclude the possibility that the observed lag was due to a necessary and conditionally specific “wetting” period, i.e., slow mixing, for the enzyme active site to be exposed to the solution interface. Fixed-time assays were conducted at different levels of initial –COOH and –OH concentration with PPL concentration of 0.66% w/v in toluene. The data revealed that a similar lag time occurred despite wetting PPL in toluene for 100 h. Furthermore, the lag time became more pronounced as the initial concentration of OA and 1-NN increased and confirmed our observations from prior experiments. Specifically, the time to reach zero-order consumption of octanoic acid at an initial concentration of 430 mM was nearly 80 h, compared to the 60 h period to reach zero-order consumption at 350 mM initial concentration of stoichiometric amounts of OA and 1-NN (Figure 33).

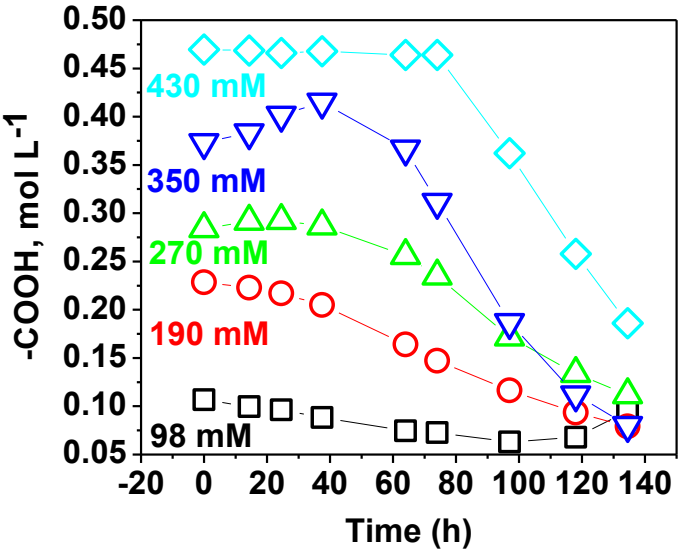

Figure 33. Observed lag in the pre-steady state time course for the consumption of OA and 1-NN, followed by a zero order rate of consumption of OA and 1-NN at various initial OA and 1-NN concentrations, in toluene. PPL concentration in toluene was 0.66% w/v and wetted for 100 h at 40 °C prior to enzyme assay.

The results from the lag time versus wetting experiments supported a natural maturation time for the reaction to proceed and excluded the possibility that slow mixing and solubilization contributed to the lag time. A close look at the mechanism shown in Figure 26 reveals that nucleophile binding to the active site would result in a non-productive enzyme-nucleophile complex. This behavior is referred to as enzyme hysteresis since “locking” the enzyme structure in non-active conformation slows down the enzyme’s response to functional groups *(101)*. This type of enzyme inhibition is reversible and over time, a steady-state conversion is established as confirmed in Figure 33. The hysteresis behavior can be driven by the preferential binding affinity of the nucleophile *(102)*. The slow enzyme response can also be attributed to solution polarity since the enzyme requires nonpolar interfaces for the active site lid to be in the preferred open conformation *(101)*. For our envisioned needs, it is critical to discern

between the possible factors, as each would have implications for the conditions and applications necessary to maintain a fast enzyme response to environmental changes. Another set of experiments were carried out to differentiate between the possibilities listed above. PPL was individually exposed to OA and 1-NN for 100 h prior to the reaction assay for quantifying activity. Fixed-time assays were performed over a series of varying initial stoichiometric OA and 1-NN concentrations with PPL wetted in advance at 0.66% w/v in toluene with either functional group, –COOH or –OH. The experiments confirmed that the same characteristic lag time was present when PPL was wetted in advance of reaction measurements with either functionality as shown in Figures 34 and 35 at concentrations above 200 mM.

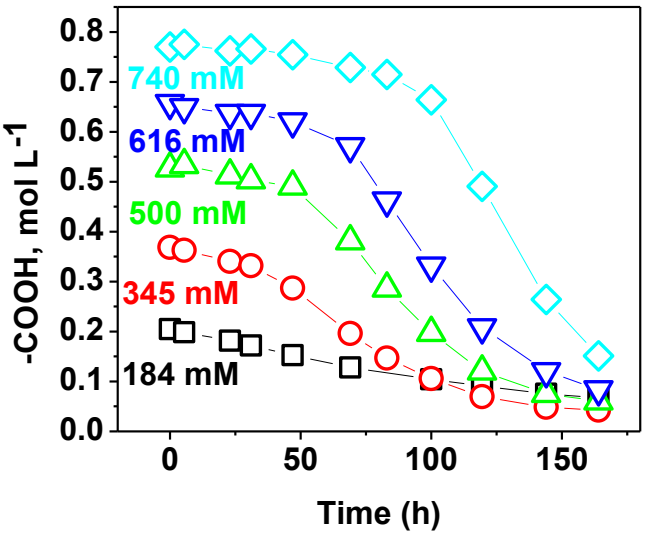

Figure 34. Progress curve with lag in the pre-steady state time course for the consumption of OA and 1-NN, followed by a zero-order rate of consumption at various initial OA and 1-NN concentrations in toluene. PPL assay concentration was 0.66% w/v in toluene and the assay was conducted at 40 °C in orbital shaker at 250 rpm. PPL was exposed to OA/toluene for 100 h at 40 °C prior to enzyme assay.

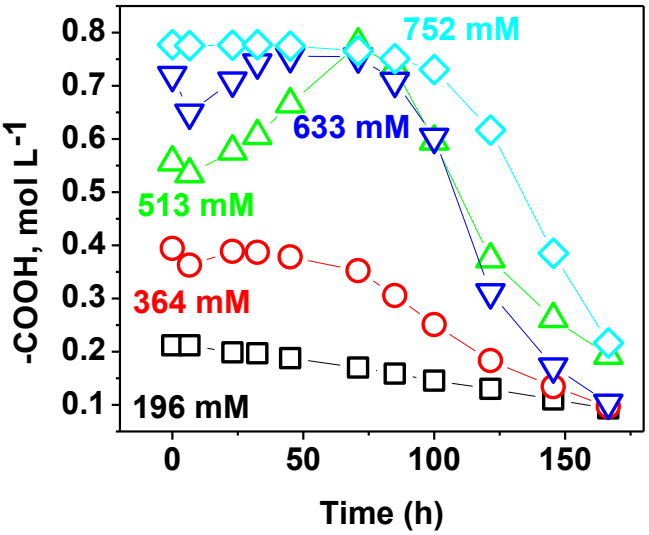

Figure 35. Progress curve with lag time in the pre-steady-state time course for the consumption of OA and 1-NN, followed by zero order rate of consumption at various initial OA and 1-NN concentrations in toluene. PPL assay concentration was 0.66% w/v in toluene, and the assay was conducted at 40 °C in orbital shaker at 250 rpm. PPL was maintained in toluene and 1-NN for 100 h at 40 °C prior to enzyme assay.

The data further support the tenet that the presence of either functional groups triggers the slow switching of the enzyme to its active, open lid form. Under our experimental conditions, the slow response occurs when OA and 1-NN solution concentration exceeds 200 mM (Figures 34 and 35). At these concentrations, we hypothesize that the enzyme must bind to the OA and 1-NN interface, undergo closed to open lid conformational change, and penetrate the OA and 1-NN interface. During the later stages, the enzyme is the open lid conformation and zero-order kinetics are observed. The presence of the lag period in the pre-zero order kinetics, even after the enzyme and functionality were mixed together at a variety of initial OA and 1-NN concentrations, is consistent with literature reports of serine hydrolase catalyzed reaction at interfaces *(103,104,105)*. It has been shown that lag times are not due to

diffusional limitations or slow mixing, but rather directly attributed to relatively slow lipase interfacial penetration as determined by the manner in which functional molecules organize near the catalytic sites *(104,105,106)*. OA and 1-NN binding affinity was quantified using the rate law basis derived in equation 32. PPL activity was determined from the steady-state regime as shown in Figure 36 for each of the different PPL wetting assays.

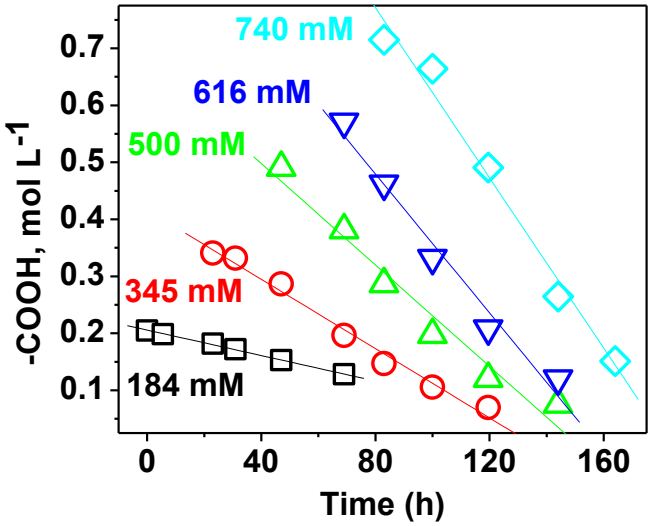

Figure 36. Plotting data to determine enzyme activity from the linear consumption at different initial stoichiometric OA and 1-NN concentrations: (◊) 7.5 μM/h (R^2 0.992), (▿) 6.1 μM/h (R^2 0.988), (Δ) 4.5 μM/h (R^2 0.982), (○) 3.0 μM/h (R^2 0.993), and (□) 1.1 μM/h (R^2 0.999).

The Michaelis-Menten behavior of PPL was evaluated by initial rate versus initial concentration plots in several cases of pre-assay PPL wetting: OA/toluene, 1-NN/toluene, and singularly toluene wetting. The dependence of PPL activity on the initial OA and 1-NN concentration increased linearly when the enzyme was wetted with OA/toluene and neat toluene in advance of the assay (Figure 37). However, the activity of PPL wetted with 1-NN/toluene displayed cooperative behavior (Hill plot), i.e., exposure to one functionality changes the

manner another functionality interacts with the enzyme. Figure 37 also reveals that when PPL was exposed to 1-NN, the activity was lower than the activity observed when PPL was exposed to OA/toluene and toluene at lower initial OA and 1-NN concentrations. The data suggests that OA affinity for the enzyme decreased when PPL was exposed to 1-NN for 100 h prior to the assay. This type of kinetic behavior supports multiple rate dependencies due to interfacial activation and OA and 1-NN inhibition influence the activity at higher initial functionality concentrations.

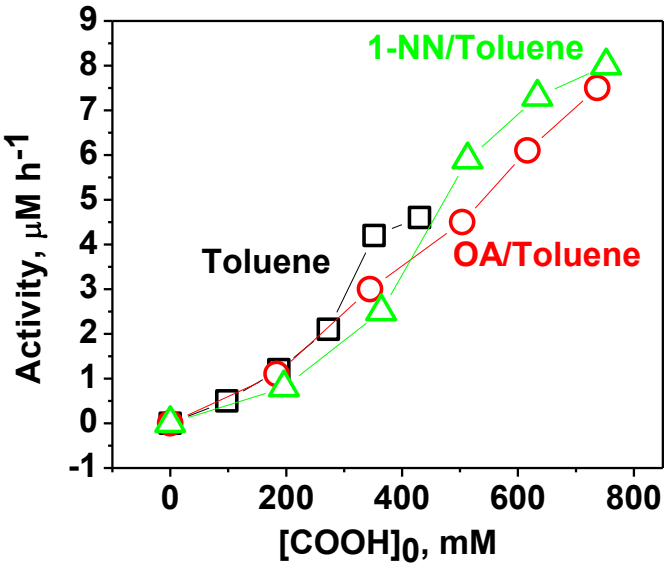

Figure 37. Plot of zero order rate (activity) dependence on the initial –COOH concentration: (-□-), PPL was wetted in toluene for 100 h prior to assay, (-○-) PPL was wetted in OA/toluene for 100 h prior to assay, and (-Δ-), PPL was wetted in 1-NN/toluene for 100 h prior to assay.

To circumvent difficulties in assessing activities that arise as a result of inhibition and/or the presence of lag time due to interfacial activation of lipase, we chose to focus on experiments with initial –COOH and –OH concentrations in the 20-150 mM range and a higher PPL concentration at 1% w/v. Enzyme activities were determined from the initial rate of product formation using GC-MS. The

NOc and OA concentrations were expressed as a fraction of the initial OA concentration to determine the fraction of ester produced and carboxylic acid remaining and quantify each separately to account for the mass balance between reactants and products during reaction progress (Figure 38). For example, a solution containing stoichiometric amounts of OA and 1-NN in toluene to final concentration of 187 mM, yielded 80% NOc ester (20% OA remained) after 600 minutes. Solutions containing stoichiometric amounts of OA and 1-NN at the final concentration of 58.9 mM yielded 35% NOc ester (70 % OA remaining) after 250 minutes. However, solutions with stoichiometric amounts of OA and 1-NN formulated to have a final concentration of 12.97 mM in toluene yielded 80% NOc ester (20% OA remaining) after 5,000 minutes. Control experiments in the absence of enzyme resulted in no detectable NOc ester.

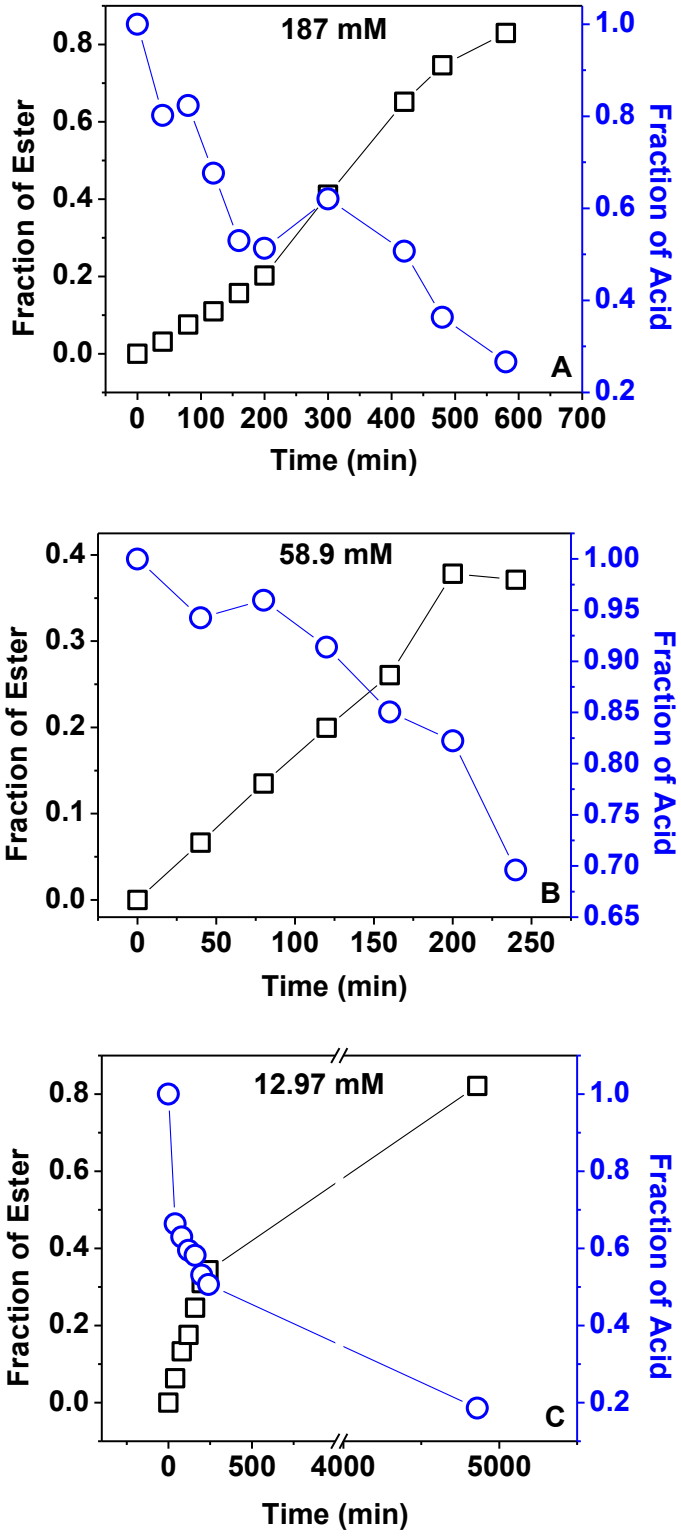

Figure 38. Monitoring OA consumption and NOc production at various initial OA and 1-NN concentrations: A) 187 mM OA and 1-NN, B) 58.9 mM OA and 1-NN, and C) 12.97 mM OA and 1-NN. (-□-) represents fraction of ester, and (-○-) represents fraction of carboxylic acid.

The concentration range we chose to focus on did not display the same time lag as shown in Figures 34-36 further supporting the hypothesis that PPL binds to the OA and 1-NN interface and undergoes a conformation change (not the rate-determining step). The strong correlation between OA consumption and ester formation at the 10-200 mM initial concentration ranges indicate that the enzyme catalyzes the acyl transfer reaction by consuming the acyl donor and producing a new acyl containing species.

Equation 32 was used to model reaction kinetics and determine the intrinsic enzyme parameters, K^{app} and k_{cat}. The initial rate of product formation over the OA and 1-NN concentration range of 20–150 mM is shown in Figure 39. A Michaelis-Menten curve was generated using SOLVER function of Excel®. Nonlinear regression was employed to determine the parameters by minimizing the sum of the square of differences between calculated and experimental values (Figure 39). One advantage of using nonlinear regression analysis is that there is no distortion in error distribution associated with linear transformation of the data, e.g., as occurs when using Lineweaver-Burk or Eadie-Hofstee plots *(107)*. The parameters k_{cat} and K^{app} were determined to be 3.29 μM/h and 115 mM, respectively.

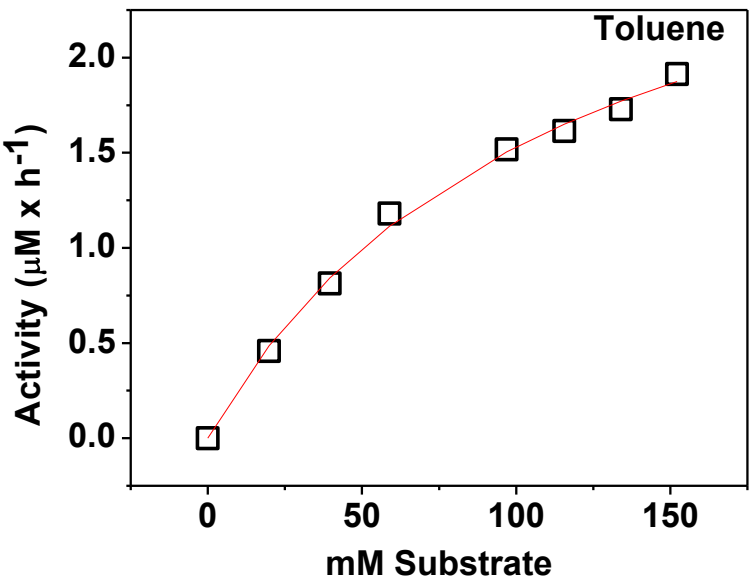

Figure 39. Michaelis-Menten plot for the esterification of OA and 1-NN. (□) represents activity at each initial OA and 1-NN concentration. Line represents the calculated values based on equation 18 by least-square analysis.

Effects of lipase source and modification

Enzymes are typically heterogeneous biocatalysts that are phase separated from the systems designed for catalysis. These catalysts are in the form of lyophilized powder, crosslinked crystals, or as immobilized enzymes on inert supports. Literature sources confirm diminished activity for heterogeneous catalysis when compared with homogeneous forms and attribute it to diffusional barriers of reactants and products as well as the limited accessibility of all available active enzymes *(8)*. Several approaches have been explored to improve biocatalyst solubility through enzyme modification via either hydrophilic polymer covalent attachment or the formation of non-covalent complexes with solubilizing additives for use in polar or nonpolar organic media.

Various methods for modified enzymes result in the same or higher activities as the neat enzyme across a broad range of solvent types and

polarities. For example, direct solubilization of the biocatalyst by adding aqueous enzyme to surfactant containing organic media has been shown to have high levels of enzyme activity in both non-polar and polar solvents *(108)*. Lipase B from *Candida Antarctica* (CALB) was modified via inverse phase extraction from aqueous buffer to organic media. Enzyme activity, determined through the transesterification of bergenin with vinyl butyrate, was four fold greater in both non-polar and polar solvents after enzyme extraction *(108)*. While each enzyme preparation and modification method has its advantages, each method also requires other functional components that might yield side-products and/or interfere with chemical equilibrium.

Lipase from *Aspergillus Niger* (Lipolase) was successfully solubilized while maintaining esterification activity through a protocol described in Chapter III. The activity of organic solvent solubilized Lipolase (P-Lipolase) was compared to the activity of the lyophilized forms of commercial lipases, PPL and *Pseudomonas Fluorescens* lipase (PFL). Suspensions of PPL and PFL in toluene exhibited higher rates of nonyl octanoate synthesis than P-Lipolase and was attributed to higher affinity of functional component and biocatalyst (Figure 40). However, catalyst inhibition and modifications can result in diminished activity as shown in some earlier examples.

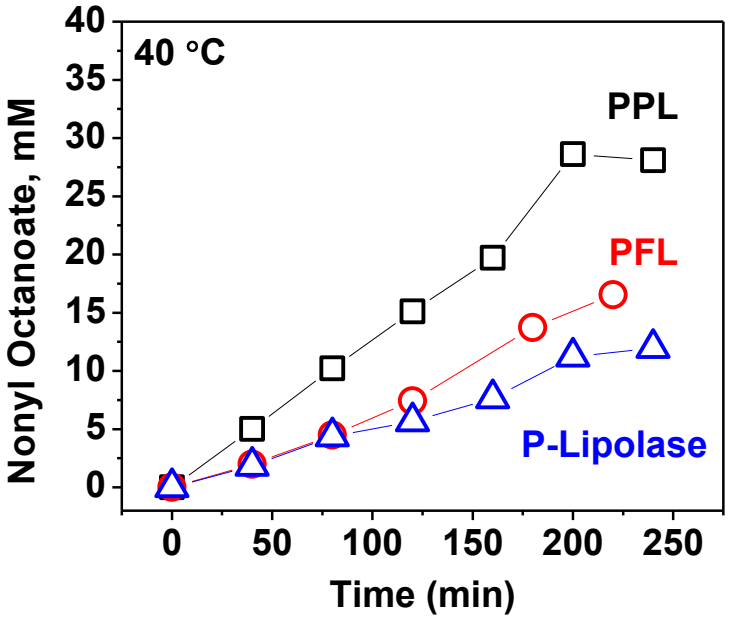

Figure 40. NOc synthesis as a function of time on the source of lipase. 60 mM OA and 1-NN solutions in toluene were incubated at 40 °C in an orbital shaker at 250 rpm containing 1% w/v PPL in toluene.

Effects of polymer matrix precursor functionality

Each polymeric material contains varying functional groups that can aid or hinder enzyme catalytic activity. Polymer-matrix precursor functionality refers to the functional groups that are not designed to participate in the catalytic chemistry but are required for polymerization reactions to proceed at reasonable rates, e.g., thiols are used as reactive functional groups in thermoset and thermoplastic polymer synthesis. Embedding enzymes is often a complex process. Commonly, enzyme and matrix precursors are mixed and cured to form networks that contain embedded catalyst. Prior to biocatalyst use, the effects of the curing protocol and the polymer matrix material on a given enzyme conformation and the resulting enzyme activity must be evaluated.

In the presence of thiol-terminated prepolymers, both PFL and P-Lipolase exhibited lower activities than PPL. The data indirectly suggests that the thiol-disulfide exchange between the prepolymer and the biocatalyst influences the protein structure rendering the biocatalyst inactive, especially after 100 min of continuous exposure. It is known that the thiol-disulfide exchange depends upon the solution acid-base equilibrium and is inhibited at pH values at or below neutral *(109)*. Enzyme microenvironment pH is often adjusted prior to modification procedures and exhibits a pH memory effect, i.e., activity in organic media increases or diminishes based on the pH of the aqueous environment from which the enzyme was extracted (*110*).

Table 7

Biocatalyst Activity Measured after Various Treatment Conditions

Biocatalyst	Solvent	Thiol terminated prepolymer (mM)	Activity ($\mu M \times min^{-1}$)
PPL	Toluene	0	160
	Toluene	10	133
PFL	Toluene	0	78.1
	Toluene	10	31.5
P-Lipolase	Toluene	0	51.7
	Toluene	10	29.5
	Heptane	0	45.7

Table 7 shows biocatalyst activity under the conditions employed in this study. PPL activity was 17% lower in the presence of thiol-terminated prepolymers and 21% lower in the presence of 1,6-hexanedithiol compared to its activity in neat toluene. PFL exhibited greater loss in activity in the presence of thiol-terminated prepolymers while PFL activity was 60% lower relative to neat toluene media. In addition, NOc synthesis reached a plateau 100 min into the

reaction (Figure 41). Similar results were observed with P-Lipolase. In the presence of thiol-terminated prepolymer, its activity was 43% lower relative to its activity in toluene with NOc synthesis reaching a plateau 100 min into the reaction. P-Lipolase exhibited similar activity in heptane and toluene (Table 7).

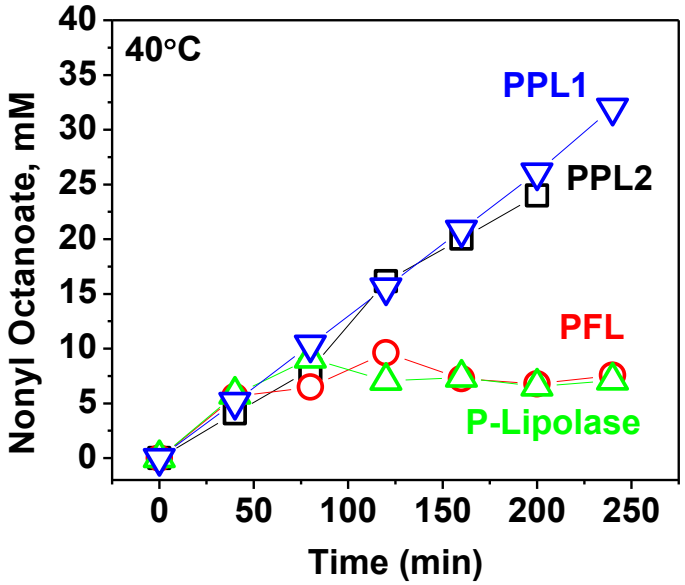

Figure 41. NOc synthesis as a function of time in solutions containing thiol-terminated prepolymers. 60 mM OA and 1-NN solutions in toluene were incubated at 40 °C in an orbital shaker at 250 rpm with 1% w/v PPL in toluene, 10 mM 1,6-hexanedithiol (PPL1) and thiol-terminated prepolymers (PPL2, PFL, and P-Lipolase).

The results validate that the thiol-terminated prepolymer did not have the same impact on PPL activity as it did on PFL and P-Lipolase activity. The observations were consistent with the lower pH values that PPL exhibits upon rehydration relative to PFL. The diminished PPL activity observed in the presence of thiol-terminated prepolymers was similar to the activity in reaction media containing 1,6-hexanedithiol. Thus, the observed reduction in activity among different lipases is not due to solvent partition effects between thiol-terminated species and lipases in organic media (Figure 41).

Effects of media viscosity

Stoichiometric amounts of OA and 1-NN were introduced to toluene containing various amounts of dissolved PMMA with M_n 996,000 g mol^{-1} resulting in final w/w PMMA concentrations of 1.06%, 5.05%, 9.92%, 15.02%, and 20.01% (all w/w in toluene). The sum weight of toluene and PMMA and the ratio of OA and 1-NN to the total weight were kept the same to delineate between the effects of viscosity and concentration on enzyme activity (Figure 42).

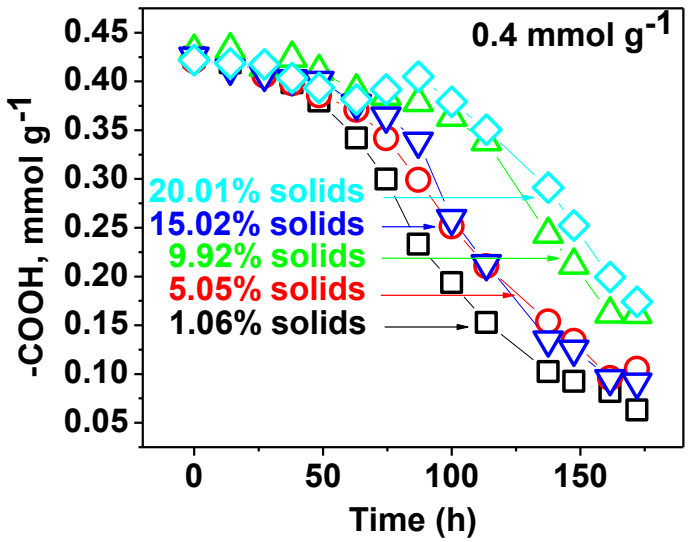

Figure 42. OA consumption as a function of time and viscosity of the organic media for stoichiometric OA and 1-NN (0.4 mmol g^{-1}, 300 mM) and 0.66% w/w PPL. Scintillation vials for fixed-time enzymatic assay were placed in an orbital shaker at 250 rpm and 40 °C.

An initial lag time was observed due to high initial OA and 1-NN concentration (above 200 mM) in the samples. The lag time became more pronounced as the solids content increased, an indication of the influence of increasing PMMA content on OA and 1-NN partition, based on the unfavorable interaction of the polar small molecule functional group and the nonpolar

polymer. Further analysis of the initial rate data for the linear regime is shown in Figure 43.

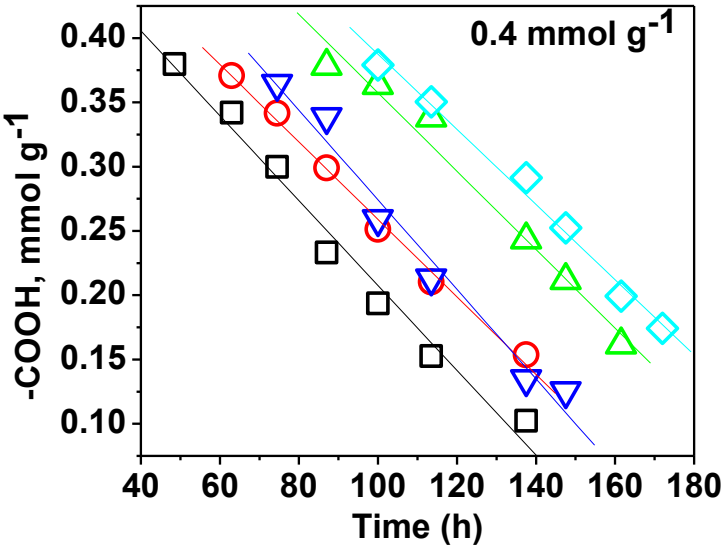

Figure 43. Enzyme activity in the zero-order regime for different media viscosity and the same initial OA and 1-NN concentration (0.4 mmol g^{-1}, 300 mM). Activity values were as follows: (◊), 20.01% PMMA solids, 2.9 µmol/g/h (R^2 0.999), (▿), 15.02% PMMA solids, 3.5 µmol/g/h (R^2 0.977), (Δ), 9.92% PMMA solids, 3.1 µmol/g/h (R^2 0.977), (○), 5.05% PMMA solids, 3.0 µmol/g/h (R^2 0.993), and (□), 1.06% PMMA solids, 3.3 µmol/g/h (R^2 0.981).

These activity data suggested that the OA and 1-NN biotransformation were not diffusion controlled across the drastic viscosity range (macroviscosity) between 1% to 20% polymer solids solution. The observation supported the concept that molecules have a relatively unrestricted diffusional pathway under each of the conditions, although, the macroscopic viscosity varies substantially. The relative diameter of the OA and 1-NN, the diffusing species, is smaller than the screening length of the PMMA chains under these conditions. The diameter of small molecules was determined using equation 33, an expression for volume and assuming that each molecule is spherical.

$$V_M = \frac{FW}{\rho \cdot N_A} \cdot \frac{nm^3}{10^{-21} \cdot cm^3} \qquad \text{Equation 33}$$

V_M - volume per molecule (nm^3/molecule), ρ - density (g/cm^3), N_A - Avogadro's number, and *FW* - molecular weight (g/mol) of the molecule. Similarly, the screening length of PMMA chains was estimated using the following power law for semi-dilute polymer solutions (*28*):

$$\xi = b \cdot \theta^{\frac{-\nu}{3 \cdot \nu - 1}} \qquad \text{Equation 34}$$

where ξ is the mesh size or screening length for PMMA in nm, *b* is the Kuhn statistical length in nm, θ is volume fraction of polymer in the solutions, and *v* is the scaling parameter based on polymer-solvent interactions.

The mesh size for PMMA was estimated to vary from 85 nm in 1% solids solution to 8.4 nm in the 20% solids solution. This indicates that at 1% solids content, any molecules with diameters larger than 85 nm would be excluded by the polymer chains, while at 20% solids content, molecules with diameters larger than 8.4 nm would be screened from the polymer chains.

The diameter of enzyme molecules, ~5 nm, was estimated assuming a density of 1.36 g/mL, standard value for globular protein in solution, and a reported molecular weight value of 50,000 Da (*97, 111-112*). The diameter of OA and 1-NN is 0.8 nm based on equation 33, i.e., one order of magnitude less than the screening length of the polymer chains indicating that the diffusional pathway of OA and 1-NN in solutions containing PMMA is unrestricted by the polymer chains and is the same as in neat toluene. Based on this analysis, the

steady-state reaction rate should remain the same in PMMA solutions with varying solid content, although the solution macroviscosity increases drastically. In fact, the screening length is larger than the calculated diameter of enzyme molecules (5 nm) indicating that enzymes can freely diffuse in the macroviscous solution. This result and our observations were corroborated by similar activities measured in solution and viscous media for the same initial OA and 1-NN concentration (Table 8).

Table 8

PPL in Different Solutions for Esterification of OA and 1-NN
Initial Concentration 0.4 mmol/g in an Orbital Shaker at 250 rpm and 40 °C

Initial OA and 1-NN Concentration (mmol g^{-1})	% PMMA Solids	PPL Exposure Prior to Assay	Activity (μmol g^{-1} h^{-1})
0.40	1.06	none	3.3
0.41	5.05	none	3.0
0.40	9.92	none	3.1
0.40	15.02	none	3.5
0.41	20.01	none	2.9
0.42	0	OA/toluene 100 h	3.5
0.42	0	1-NN/toluene 100 h	3.1
0.41	0	none	2.7

A very interesting point from the kinetic data is that these results were analogous to the enzyme behavior in Ficoll aqueous solutions. Despite macroviscosity changes, enzyme activity does not diminish in aqueous solutions of branched carbohydrates due to the relatively large mesh size of the aqueous carbohydrate (*113*). To the best our knowledge, the observation that enzyme activity remains unaffected in varying PMMA/toluene solutions with macroviscosity differences is the first report of this type of enzyme-catalyzed reaction dependency on organic media viscosity.

Conclusions

In solution, biocatalyzed ester formation followed the rate law derived from theory based on the accepted serine hydrolase (lipase) mechanism. The Michaelis-Menten form of the rate law was shown to be valid regardless of whether one functional component is in excess or the functional components are in stoichiometric proportions. This mathematical treatment and correlation of variables to achieve the same result set the precedent for our expected enzyme intrinsic kinetic behavior of the synthetic or hydrolytic reaction.

In toluene solutions, when the initial OA and 1-NN concentrations were >200 mM, the derived rate law did not hold in the initial stages of the reaction due to a delay in ester production. The observed lag time was partly attributed to the cooperative binding with both functional groups and to inhibitory effects of the nucleophile as determined by end-point titration studies. When OA and 1-NN concentrations were less than 200 mM, GC-MS kinetics indicated initial zero order behavior as expected by the Michaelis-Menten equation. The values for k_{cat} and K^{app} for the model reaction in toluene were determined to be 3.29 μM/h and 115 mM, respectively.

Several enzyme sources were studied for internal comparison and the activity of P-Lipolase was compared to the activity of other commercially available lipases such as PPL and PFL in neat organic solvents and solutions containing multifunctional monomer. Upon solubilization, modified enzymes remained largely active in nonpolar solvents and solutions of multifunctional monomer. The presence of thiol-terminated compounds (polymer precursors)

negatively affected lipase activity, and we suspected that thiols were disrupting biocatalyst conformation via the thiol-disulfide exchange reaction(s).

We demonstrated that PPL catalytic activity in viscous solutions of toluene comprised of 1% solid to 20% solids of PMMA was similar to the PPL activity in neat toluene. By using simple scaling law arguments, we confirmed that the reason for similarity in activity despite higher solution macroviscosity was that the solution mesh sizes established by the excluded volume of polymer segments were larger in diameter than the OA and 1-NN molecules and the enzyme. Since screening did not occur in the 1% to 20% solid PMMA solutions and PPL activity was similar, we suspected that the OA/1-NN and enzyme diffusion rates in polymer solutions were similar to the diffusion rates in neat toluene.

CHAPTER V

FREE VOLUME MEDIATED BIOCATALYSIS INSIDE FREE-STANDING POLYMER FILMS

Abstract

In vivo, biocatalysts mediate complex biochemical reactions and pathways in macromolecular crowded environments. The excluded volume established by macromolecular complexes largely controls cellular enzyme turnover rates by establishing concentration gradients and diffusion regimes within cells *(114)*. We report on three poly (alkyl methacrylate) free-standing films embedded with Porcine Pancreas Lipase and –OH and –COOH functional small molecules capable of undergoing lipase catalyzed acyl transfer reactions. Design of films with embedded functionality and biocatalyst was inspired by the confined nature of cellular microenvironments. We envisioned the biotransformation of the embedded functionality to provide a pathway for the modification of the physical and chemical properties of the confining matrix. Therefore, a systematic study was conducted to understand how initial confining matrix properties influence transformation rates of embedded functionality mediated by embedded enzymes in amorphous matter. Biocatalytic activity in films embedded with enzyme and functionality was diffusion-limited relative to free enzyme and enzyme-only embedded films with surface exposure to small molecule functionality. The diffusion-limited biocatalytic activity exhibited linear dependency on the fraction of polymer free volume in glassy and rubbery films at <8% by weight (8.8-9.7% by volume) loadings of stoichiometric amounts of functionality. In addition, we

demonstrated that biocatalytic activity in the glassy state increased linearly with film thickness suggesting that the fugitive solvent leaves behind more free volume sites within the confining matrix at higher film thicknesses, facilitating the transport of the functionality within the matrix.

Introduction

Using only a few periodic table elements, biological systems provide functions in an integrated fashion over multiple time scales through flawless assembly at the single-cell or multicellular level with superb control of nano- to macro- scale structures. The structural hierarchy is highly dynamic and can be triggered, halted and dormant at a cellular level on a need basis. For the material scientist, examples in nature provide insight in addressing engineering challenges and inspiration in designing the next generation of man-made functional materials. Bridging the gap between functional architectural designs observed in nature and the current state of macromolecular engineering has been increasingly central to designing effective synthetic macromolecular complexes. Stimuli-responsive films, coatings and membranes with autonomic responsiveness to chemical, thermal, optical, electrical, mechanical, and biochemical signals have already initiated advantageous impact in the technology areas of controlled delivery and release systems, “smart” surfaces, transduction systems and micro/nanoactuators *(115)*. Therefore, research and development efforts have focused on mimicking strategies employed by nature to constantly provide the ever changing needs of markets for novel materials.

By leveraging the properties of biological macromolecules, researchers have commenced fundamental developments for the next generation of synthetic/hybrid functional materials. Combining adhesion strategies employed by mussels and geckos has resulted in functional materials that manifest excellent reversible adhesive characteristics in wet and dry environments, and adhere and release over many cycles by using naturally occurring catechol(s) such as 3,4-dihydroxy-phenylalanine and mimicking nanometer scale topographies *(116)*. Similarly, mimicking structural features of insect eyes has inspired optical sensor designs using polymethacrylate(s) *(117)*. Surface features of lotus leaves and the Namib Desert beetle have been mimicked for the development of responsive superhydrophobic and superhydrophilic surfaces *(118,119)*. The shell protein of M13 virus has been used as a site for metal oxide attachment by converting viruses into scaffolds capable of assembling into highly anisotropic nanowires for battery applications *(120)*. Hydrogels containing enzyme responsive peptide motifs have been explored for applications in targeted drug delivery, tissue engineering, and diagnostics *(64)*.

Biocatalysts perform metabolic reactions within the crowded environments of living cells where biological macromolecules can take up as much as 30% of the intracellular space *(114)*. The excluded volume determined by other macromolecules affects enzyme activity by establishing the effective concentration or the diffusional resistance experienced by active enzyme species. The interplay of these factors has broad physiological ramifications in living systems, resulting in vastly different rates and equilibrium for

macromolecular reactions relative to the ones measured *in vitro* in dilute solutions. Intrigued by this capability of living systems and with the goal of creating a platform for adaptable materials via embedded enzymes, we set out to investigate whether novel synthetic-biological hybrid compositions can be formulated to exhibit similar *in situ* biosynthetic activities as a tool to modify bulk and surface properties of free-standing films, coatings, and membranes.

Enzyme engineering has seen tremendous development since the rediscovery that enzymes function well in near anhydrous conditions *(4,5)*. The ability to optimize the highly specific and selective catalytic activity by altering enzyme microenvironment or structure has made them an efficient tool for the preparation of pharmaceuticals, natural products, fine chemicals, and food ingredients. The cholesterol lowering drug, Lipitor®, is currently synthesized using an engineered enzyme via directed evolution techniques that has resulted in a 4000 fold increase in activity compared to the wild type *(6)*. Enzyme immobilization in inert matrices has been widely used in applications demanding heterogeneous biocatalysts, selective adsorbents, controlled released protein drugs, and analytical devices *(8)*. Macroporous materials used in these applications have to be inert and serve as supportive media for immobilization. Several review articles and books thoroughly describe enzyme immobilization technology for applications in the fields of biocatalysis and biosensors *(8,121,122,123)*. By leveraging biocatalyst functionality, we are interested in developing a material platform with embedded functionality and enzyme in the

same matrix that will adapt to an environmental challenge by altering chemical or mechanical properties of the polymer matrix.

Lipase catalyzed reactions are generally accepted to proceed via an acyl-enzyme intermediate (EM) where the propagation step is the nucleophilic attack of a terminal –OH group. Absolute rate theory predicts that reaction rates will depend on interactions and diffusional resistance that arise due to spatial confinement effects. The question we set out to answer was *how* diffusional resistance in amorphous polymers affects catalytic turnover rate, i.e., enzyme activity. Steric repulsions are ubiquitous regardless of the magnitude of any attractive interactions since the available volume is limited and molecules are mutually impenetrable. The diffusional resistance is inherent to crowded systems as the amount of time for diffusion of reactants and products is inversely proportional to their self-diffusion rate. Diminution of diffusion rates will decrease the encounter rate of reactants with enzymes resulting in a lower observed turnover rate.

We examined the catalytic behavior of enzymes in a mechanistic manner within amorphous solids, both rubbery and glassy states, using a simple but relevant model via the catalytic esterification rate of octanoic acid (OA) and 1-nonanol (1-NN) which is termed embedded functionality (Figure 44). Upon condensed phase formation from the corresponding organic solutions, the embedded enzyme remained active towards the embedded functionality in the resulting films. The observed activity was compared to analogous compositions in solution and enzyme-only embedded films. The diffusion-limited nature of

activity in the series of mediums was quantified relative to the films' physical states. We believe that this report is the first comparison between liquid and solid states with an emphasis on the differences between rubbery and glassy systems. The understanding gained revealed that biocatalyzed reactions can occur in glassy films if small molecule functionality is able to permeate through free volume sites of the material. Indeed, it was shown that biocatalytic activity in glassy films was highly dependent on the film thickness. This suggested that the fugitive solvent leaves behind more free volume sites within the confining matrix as the film thickness increases, allowing OA and 1-NN to have improved mobility. The hybrid compositions, i.e., embedded biocatalyst and functionality, could serve as a novel platform for switchable bulk property shifts based upon the facile and reversible nature of enzyme-catalyzed reactions.

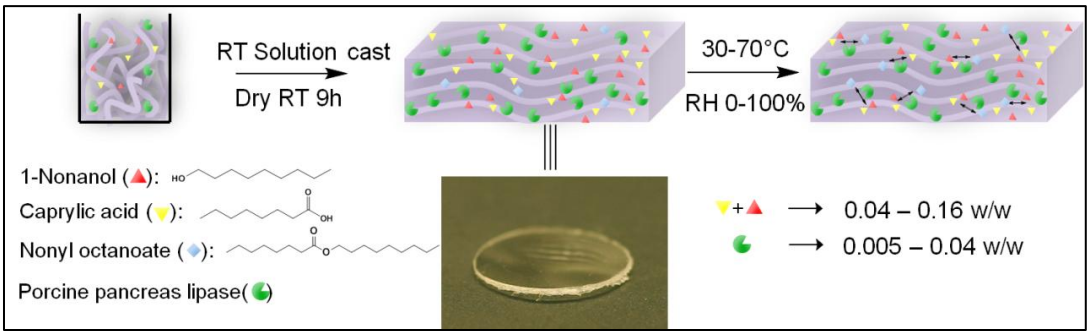

Figure 44. Formation of biocatalytic films upon incorporation of biocatalyst and stoichiometric amounts of small molecule functionality. Photograph shows a typical 6 mm diameter bioactive film.

Results and Discussion

Three methacrylate homopolymers were chosen as host matrix materials. The analogous polymers were chosen for the compositional similarity, varying degree of stiffness relative to exposure temperature (glassy to rubbery state), isotropic nature (amorphous), and the ability to readily form mechanically stable

films from solution casting process (Table 9). OA and 1-NN were chosen as model functionalities to investigate the biosynthetic activity of lipase (Figure 44). The aliphatic nature of OA and 1-NN is analogous to naturally occurring lipids and makes them excellent substrate mimics for lipases. Additionally, OA and 1-NN are low viscosity liquids with low melting temperatures and high boiling points, therefore throughout a variety of experimental conditions, the small molecule functionalities are in the liquid state (not vapor) and able to diffuse within the amorphous polymer for possible interaction with the enzyme active site(s).

Table 9

Physical Characteristics of Poly(alkyl methacrylate)s

Poly alkyl (methacrylate)s	**M_n (g/mol)**	**T_g (°C)**	**Density (g/cm^3)**	**[a]Solubility Parameter $(cal/cm^3)^{0.5}$**
PMMA	996,000	90	1.148	9.3
PEMA	38,000	58	1.102	9.1
PnBMA	40,000	23	1.052	8.7

[a]From ref.*(124)*

Porcine Pancreas Lipase was chosen as the model enzyme due to its well-defined and robust activity in polar and nonpolar organic solvents *(4,5,18)*. Lipases belong to the class serine hydrolase enzymes and their catalytic mechanism for acyl transfer reactions follows a ping-pong bi-bi mechanism *(94,95,96)*. Initially, the free enzyme binds with the acyl end of carboxylated species to form an acyl-enzyme intermediate. Acyl transfer occurs when a nucleophile cleaves the acyl intermediate to form the new acyl-containing product while freeing up the enzyme active site. For esterification, the acting nucleophile is a hydroxyl functional group. The general reaction scheme is represented as

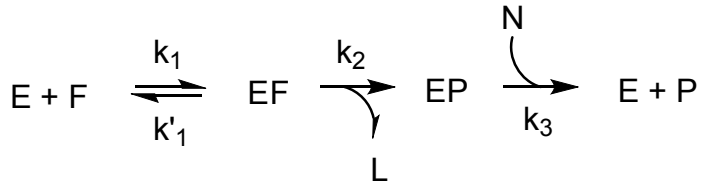

where [F], [N], [E], and [P] denote acyl donor functionality, nucleophile, enzyme, and product, respectively.

Free enzyme (solution activity) vs. enzyme-only embedded film (surface activity) vs. enzyme and functionality embedded film (bulk activity).

By design, we employed small molecule functionality in stoichiometric quantities, i.e. $[F_0]=[N_0]=[M_0]$. Considering OA and 1-NN association with enzyme to be a random process, the product concentration was expressed by the following equation:

$$\frac{dP}{dt} = \frac{k_{cat}\cdot[E]\cdot[M]}{K^{app}+[M]} \qquad \text{Equation 35}$$

where [M] is the concentration of the acyl donor or nucleophiles, [E] represent enzyme concentration, and k_{cat} is the turnover rate. To borrow terms common to Michaelis-Menten kinetics, K^{app} equals ($K_m + k_2/k_3$) where K_m equals (k'_1+k_2/k_1). To obtain the observable reaction rate (k_{obs}), we let

$$k_{obs} = \frac{k_{cat}\cdot[E]}{K^{app}+[M]} \qquad \text{Equation 36}$$

and rewrote equation 35 in a first-order form as

$$\frac{dP}{dt} = k_{obs}\cdot[M] \qquad \text{Equation 37}$$

During the initial stages of the reaction when [M]>>K^{app}, k_{obs} of equation 36 can be regarded as a zero order rate constant. The integrated form of equation 37 was written in terms of product concentration [P] as:

$$[P] = k_{obs} \times t \qquad \text{Equation 38}$$

where k_{obs} is referred to as PPL activity and expressed in μmol/g/h. The observed rate for a reaction catalyzed by a free enzyme in solution is normally higher than the rate observed for an embedded enzyme since OA and 1-NN have to diffuse to the catalytic surface prior to transformation. We evaluated the relative rate diminishment due to the diffusional resistance and concentration gradients of OA and 1-NN within the polymer matrix. Biosynthetic activity was quantified in toluene solutions with free enzyme and functionality, in polymer films with embedded enzyme and coated with liquid functionality, and in polymer films with embedded enzyme and functionality. The relative ratio of functionality to the total material weight across different systems was maintained constant to evaluate the dependence of PPL activity on the degrees of freedom (Figure 45).

Accelerated rates of ester formation were observed from stoichiometric amounts of OA and 1-NN in toluene solution, where 80% conversion was reached in the first 100 min at 40 °C. The rate of ester formation was relatively diminished in films embedded with functionality along with enzymes cast from toluene solutions of PMMA containing 6% by weight stoichiometric amounts of OA and 1-NN with 1% by weight of PPL biocatalyst. Specifically, 80% conversion was reached after 1,600 min (compared with solution rates at 100 min to the same degree of conversion in toluene). Notably, the film with

embedded PPL alongside functionality exhibited higher conversion at the starting point of activity measurement. The film activity cannot be measured in the interim film-forming phase without distorting the results as the material is undergoing a physical state transition from the liquid to solid state. PPL activity assay by our established protocol began after nine hours of drying, which was determined as a necessary flash-off/waiting period for structurally sound films to form, i.e., able to be handled and measured. The end of nine hours was established as t = 0 h and consistently the data revealed that regardless of the polymer or solvent system, at least 20% NOc was already synthesized within the poly (alkyl methacrylate) host matrices by this time.

In addition, we posed limits on the rate of ester formation by casting films embedded only with enzyme (0.67 wt% PPL on solids). Films embedded only with enzymes were challenged by the surface application of a stoichiometric mixture of OA and 1-NN. These data clarified that conversion versus time was slower than the other two examples since OA and 1-NN had to traverse a greater distance through the polymer for mutually locating enzymes and progressing towards esterification. Enzyme activity was initiated by coating stoichiometric amounts of OA and 1-NN on the topside film surface at a final concentration of 0.2 mmol functionality/g and by exposure to 40 °C. Data shown in Figure 45 indicated that 40% NOc was produced catalytically after 4,000 min at 40 °C. The slower biosynthetic rate was attributed to OA and 1-NN access of enzyme only near film surface. The data suggested that biotransformation is controlled by the rate of sorption of OA and 1-NN in the film. We assumed an even biocatalyst

distribution throughout the film, and there are some reasons to question the gradient effects, however, these are not the focus of this chapter. The observed surface activity was consistent with literature reports of biocatalyst surface activity observed upon incorporation of biocatalyst in polymer films. For example, McDaniel *et al.* determined that organophosphorus hydrolase (OPH) remained active upon incorporation in latex-based films, and its activity was dependent on reactant diffusion from surface and sorption/permeation in the film. The higher activity in cases of increased permeation was the result of the reactant being exposed to a larger number active enzyme sites *(61)*.

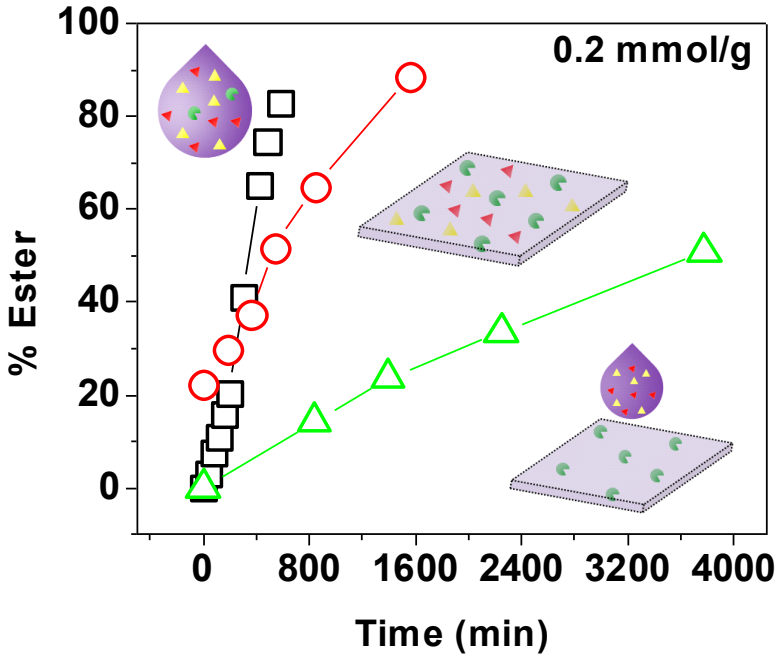

Figure 45. Rate of ester formation dictated by degrees of freedom of enzyme and functionality (free/both embedded/enzyme-only embedded) with 0.2 mmol/g of stoichiometric amounts of OA and 1-NN at 40 °C. (-□-) represents ester formation in toluene (both enzyme and OA and 1-NN free in solution), (-○-) represents ester formation in polymer film (both enzyme and functionality embedded), and (-Δ-) represents ester formation in polymer films with embedded enzyme and topside coated with OA and 1-NN.

Another contributing factor that resulted in lower activity in films with OA and 1-NN placed on the films' topside versus the films with embedded small molecule functionality was the differential in the rate of OA and 1-NN penetration into the host matrix versus the rate of ester synthesis (Figure 45). Our hypothesis was that if the OA and 1-NN uptake rate was faster than the ester conversion rate, the measured activity would be similar to the activity observed in embedded films as OA and 1-NN would be exposed to the same amount of catalyst. However, the surface activity experiments suggested that the rate of OA and 1-NN uptake was much slower than the esterification rate. Additionally for these experiments, the nature of the film, i.e., rubbery, leathery or glassy, did not drastically influence the initial esterification rate. Experiments with films containing the enzyme embedded in PMMA, PnBMA, and PEMA and coated with OA and 1-NN exhibited only slight activity differences, and supported the surface only nature of the activity (Figure 46). Surface activity of films containing embedded biocatalysts has been extensively reported in the literature with substrates coated both in the liquid or dry form *(63,125)*.

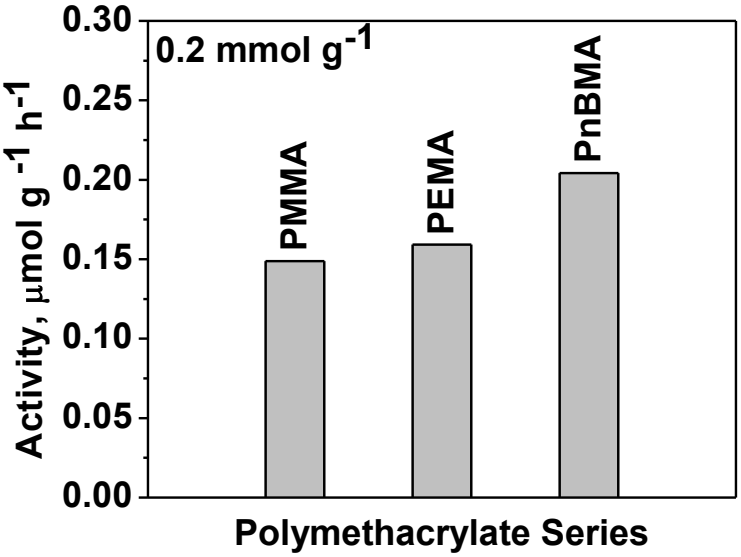

Figure 46. Ester synthesis biocatalyst activity at 40 °C in poly (alkyl methacrylate)s with embedded enzyme at 0.67% by weight with topside liquid deposition of stoichiometric amounts of OA and 1-NN at 0.2 mmol/g.

The observed decrease in PPL activity when assayed in polymer bulk as compared to solution assays is attributed to the increase in diffusional resistance experienced by the OA and 1-NN molecules. In polymer films, OA and 1-NN need to overcome mass transfer resistance from the polymer chains during the translational self-diffusion to arrive at an enzyme active site (Figure 47a). The dimensionless modulus was determined for each small molecule functionality from the diffusivity values in poly (alkyl methacrylate)s and the high modulus values indicate a diffusion-limited reaction (see supplemental information, Figure 59 and Tables 13-15).

Figure 47b summarizes the ^{1}H NMR spectra of PMMA films with embedded biocatalyst and small molecule functional components. A distinct triplet appeared at 4.1 ppm upon exposure at 40 °C for 192 h and was attributed to the NOc oxomethylene protons labeled **a**. The NOc distinct proton peak resonance was observed in PMMA films embedded with biocatalyst and small

molecule functionality only after the prescribed time for reaction progress. The small peaks overshadowed by the prominent PMMA ester peak observed in the negative control were attributed to the α-protons of 1-NN. The pendant methacrylic esters are sterically hindered due to the proximity of the ester functional group to the polymer backbone. Therefore, host matrix polymers remain catalytically neutral in presence of the biocatalyst. The catalytic neutrality of the host matrix polymers was also confirmed from several control experiments (Figure 47). These observations were consistent with literature reports of the α-chymotrypsin catalyzed hydrolysis of the *p*-nitroanilidine group in acrylamide copolymers where it was shown that the rate decreased sharply when the reactive site was less than five methylene units away from the polymer backbone *(126)*.

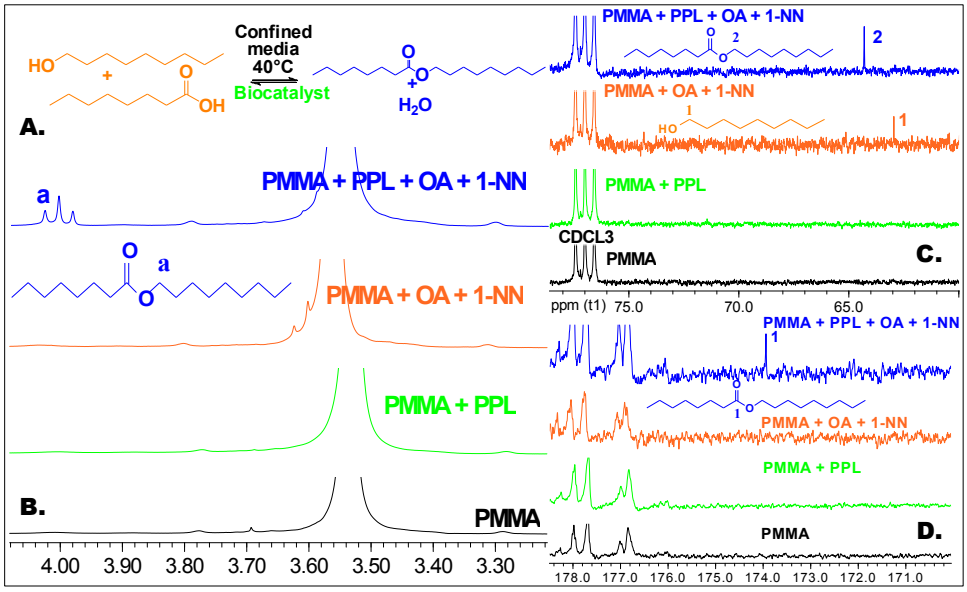

Figure 47. A) Biocatalyzed conversion of OA and 1-NN, B) ^{1}H NMR, C) ^{13}C NMR (60-80 ppm), and D) ^{13}C NMR (170-180 ppm) plots of PMMA films in $CDCl_3$ containing combined 13.3 wt% stoichiometric amounts of OA and 1-NN and 0.67 wt% PPL (top); combined 13.3 wt% stoichiometric amounts of OA and 1-NN; 0.67 wt% PPL; and PMMA neat (bottom). Films were exposed at 40 °C for 192 h.

The ^{13}C NMR spectra of PMMA films with embedded biocatalyst and small molecule functional additives provide further support for the biosynthetic activity of PPL in PMMA films under these conditions (Figures 47c and 47d). The peak resonance at 174 ppm corresponds to the acyl carbon (ester carbonyl) of NOc labeled **1** upon exposure at 40 °C for 192 h (Figure 47d). In addition, the peak resonance shift from 63 ppm to 64.5 ppm suggests that the α carbon (labeled **1** of 1-nonanol) converted to the oxomethylene carbon labeled **2** (Figure 47c). These distinct signals were not present in PMMA films embedded with small molecule functionality (negative controls).

Several important control experiments were conducted in PMMA films embedded only with one functionality and biocatalyst to confirm that the NOc synthesis occurs only when both functional groups are embedded in the film (Figure 48). ^{1}H NMR data confirmed that NOc synthesis occurs only in cases when PMMA films are embedded with the biocatalyst and two functional small molecules, –OH and –COOH.

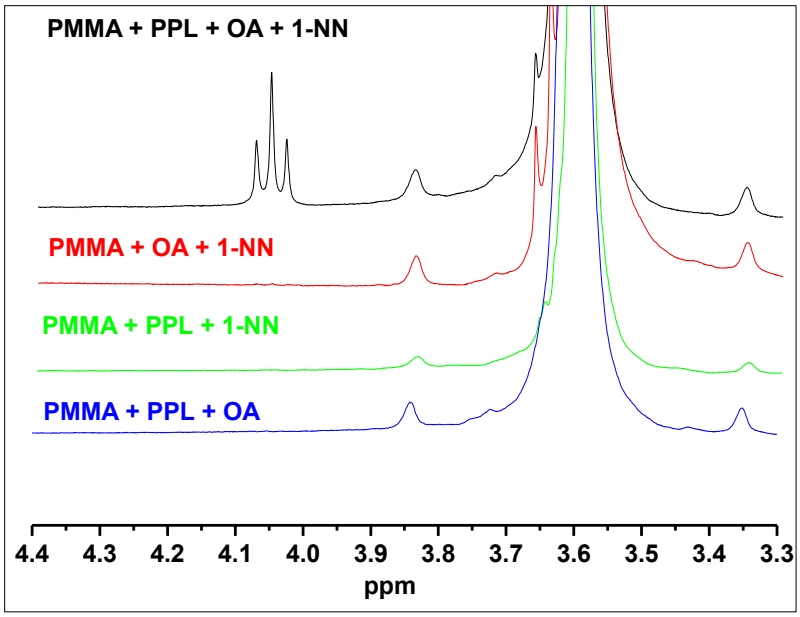

Figure 48. ^{1}H NMR plots of PMMA films in $CDCl_3$ containing combined 13.3 wt% stoichiometric amounts of OA and 1-NN and 0.67 wt% PPL; combined 13.3 wt% stoichiometric amounts of OA and 1-NN; 6.67 wt% 1-NN; and 6.67 wt% OA. All films were exposed at 40 °C for 192 h.

Reaction progress curves consistently displayed a linear increase during the initial stages of the reaction. Our typical reaction progress curve revealed a zero order regime with an eventual plateau in PMMA and PnBMA films. The diffusion limits for the glassy and the rubbery regime dictated rates mathematically described by equation 38 (Figure 49). PPL activity was lower by a factor of 2 in the glassy PMMA host matrix as compared to the rubbery PnBMA host matrix containing 4% and 8% by weight of stoichiometric amounts of OA and 1-NN (Figure 49). Linear increase in ester synthesis was also observed in glassy and rubbery host matrices embedded with different weight fractions of small molecule functional components, OA and 1-NN (supplemental information, Figures 60-62). When rubbery films were used as host matrices, linear increase in ester synthesis occurred during the initial stages of the reaction immediately

after exposure at 40 °C. However, in glassy PMMA films upon exposure at 40 °C, two-stage kinetics were consistently observed with an initial linear increase in ester synthesis followed by a second linear increase, albeit at a diminished rate (Figure 49). The higher initial rate in activity was associated with the segmental relaxation of the glassy PMMA host matrix at 40 °C. During the solvent casting process, PMMA undergoes "cooling" from above its T_g to below its T_g *(127)*. The phenomenon of structural relaxation is associated with the non-equilibrium state of the glassy polymer. The structural relaxation does not occur in polymers that are at a temperature above their T_g since the softened state has already been achieved *(128)*.

The conversion rate of OA and 1-NN to the NOc ester was dependent on the ability of the functionality to diffuse to the enzyme active site and the product to diffuse away. During the initial exposure at 40 °C, the excess free volume trapped from the solution casting process and slow evaporation rates manifested as increased catalytic turnover rate. When segmental relaxation achieves chain equilibrium configurations, the loss of excess free volume resulted in densification observed by an increase in T_g over time. We suspected that OA and 1-NN continued to diffuse to the active site, and upon conversion, the NOc ester diffused away from the active site. However, this process occurs with a diminished zero order rate, specifically five hours after the initial exposure to 40 °C. This suggested that the turnover rate was highly dependent on the rate of film formation (Figure 49). The glassy state processes in relation to reaction progress are further elucidated in Chapter VI.

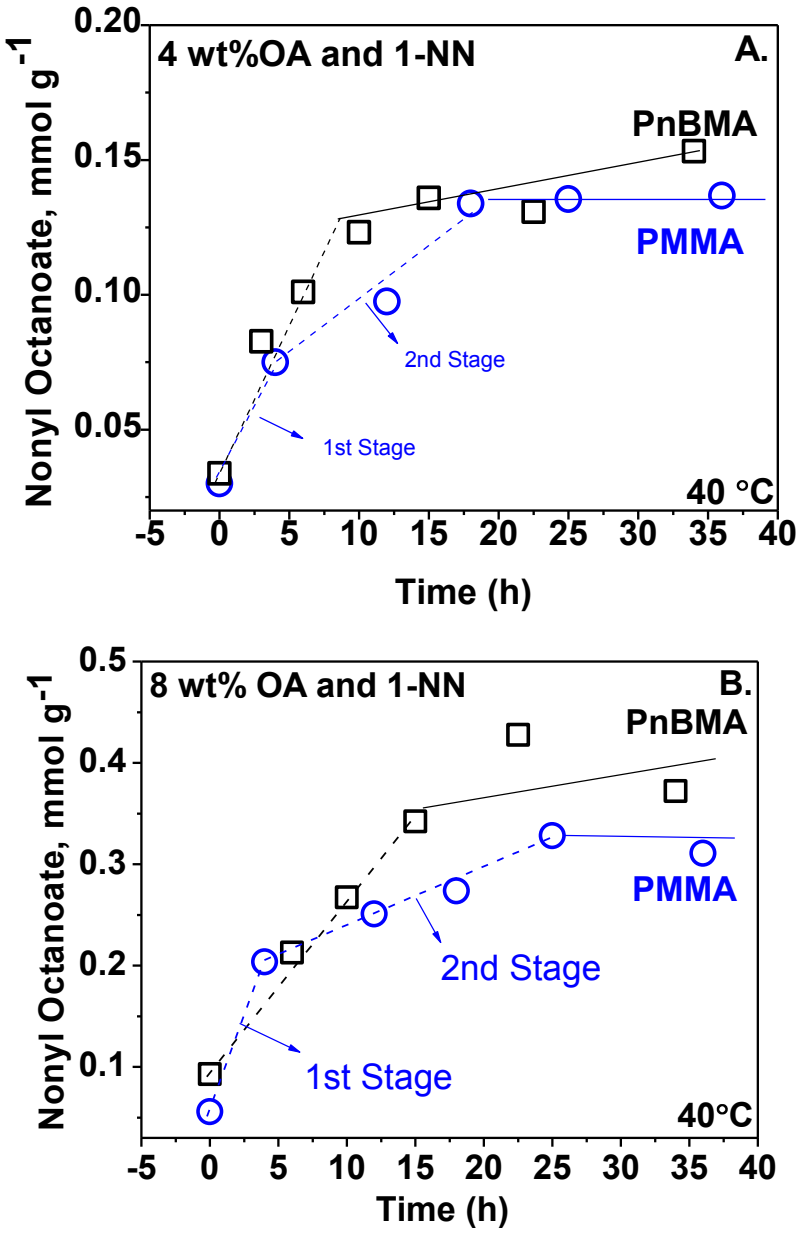

Figure 49. NOc synthesis over time at 40 °C in rubbery (PnBMA) and glassy polymer (PMMA) embedded with 1% (w/w) PPL biocatalyst and A) 4% (w/w) stoichiometric amounts of OA and 1-NN in rubbery (dashed line represents initial slope 4.1 μmol/g/h, R^2 = 0.92) and glassy (dashed line represents slope, 2nd stage, 8.6 μmol/g/h, R^2 = 0.95) polymers or B) 8% (w/w) stoichiometric amounts of OA and 1-NN in rubbery (dashed line represents initial slope, R^2 = 0.99) and glassy (dashed line represents initial slope, 2nd stage, R^2 = 0.99) polymers.

Effects of weight fraction of lipase and small molecule functionality on activity

Determining the effect of PPL weight fraction on the rate of ester synthesis was important to establish an optimum catalyst loading to observe zero order ester synthesis. The hypothesis was that the rate of ester synthesis would not increase beyond a threshold PPL weight fraction. PPL threshold would correspond to the weight fraction beyond which the enzyme packing density would render the active sites inaccessible to functional groups (Figure 50).

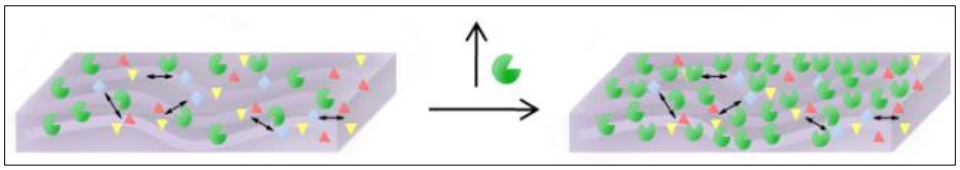

Figure 50. Effect of increasing enzyme weight fraction embedded in polymer films on the accessibility of embedded functionality to the active site. The following are depicted biocatalyst (●) and –COOH and –OH functionality (▲and ▼)

Ideally in heterogeneous catalysis, an optimum catalyst fraction and contact area would be required to obtain the maximum activity for the system. The optimal loading could vary between 0.1 to 10% by weight in traditional biocatalysis research (*34,129*). Considering a typical enzyme molecule to be 5 nm in diameter and assuming even enzyme distribution, 0.5% by weight of enzyme would correspond to approximately 1 enzyme per 15,242 nm^3 or per 25 nm x 25 nm x 25 nm cube. At the highest loading level, 4% by weight of PPL corresponded to one enzyme molecule in a 12.5 nm x 12.5 nm x 12.5 nm cube or twice as much enzyme density as in 0.5% by weight loading.

Figure 51 summarizes our results on the dependence of ester synthesis over time on the embedded enzyme weight fraction in PMMA films. The data

supported a dependence on the biocatalyst weight fraction early in the synthesis, i.e., prior to beginning the kinetic assay. Observations for high PPL weight fractions confirmed as much as 50% of ester synthesized before the films completed the drying/solvent evaporation process at room temperature. Therefore, above 2% PPL loading, the initially zero order rates as described by equation 38 were not able to be quantified. After the initial activity attributed to the presence of excess free volume, the rate of ester synthesis reached near the theoretical conversion at 40 °C in both the 3 and 4% by weight of embedded enzyme loading. At lower weight fractions of PPL, <2% by weight, linear increase in ester was observed after the initial activity. To practically observe the kinetic behavior of PPL catalyzed ester synthesis in polymers, the PPL loading had to be kept below 2% by weight; other combinations and systems were so rapid that the observations were consistently completed in advance of the film formation process.

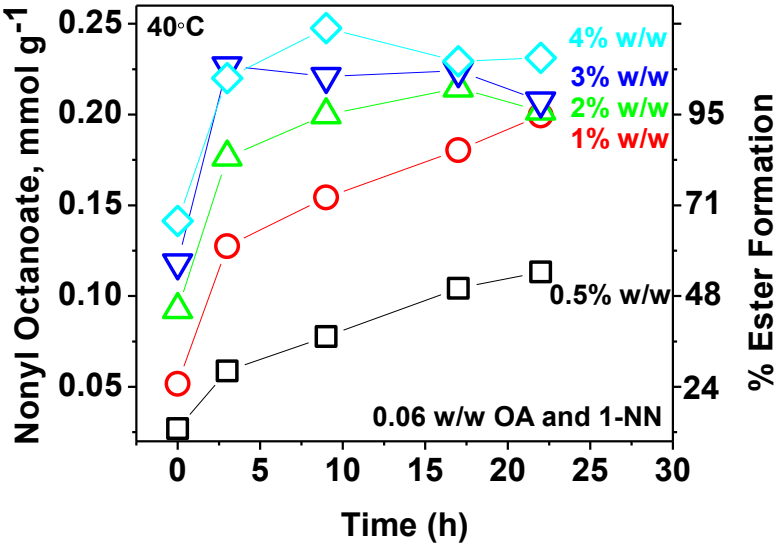

Figure 51. Dependence of biocatalyst activity on the weight fraction of embedded PPL in PMMA films with 0.06 w/w stoichiometric amount of OA and 1-NN at 40 °C. Zero order ester synthesis was observed in 0.5% w/w (black, R^2 = 0.999), 1% w/w (red, R^2 = 0.996), and 2% w/w (green, R^2 = 0.96). Films had an average thickness of 154 μm and 6 mm diameter top and bottom.

The dependence of enzyme activity on the weight fraction of stoichiometric OA and 1-NN in poly (alkyl methacrylate) films was also investigated. Our hypothesis was that enzyme catalysis would depend on the ability of the small molecules to migrate in volume not occupied by polymer chains, and enzyme activity would diminish drastically below a percolation threshold of OA and 1-NN wt% loading. Molecular transport in macromolecular materials relies on the continuous redistribution of free volume components within the material *(130)*. Various diffusion models based on free volume consider the diffusibility of a small molecule to be proportional to the probability of encountering a hole large enough into which the molecule can jump (*131,132*). Initially, we determined the effect of increasing the weight fraction of OA and 1-NN on polymer film physical properties. Figure 52 illustrates the effect of increasing the weight fraction of small molecules in polymer films. We expected

that the total free volume of the polymer-penetrant system would be higher than the free volume of the polymer alone. We hypothesized that higher weight fraction of OA and 1-NN would lead to higher probability for functionality transport to occur throughout the host polymer matrix.

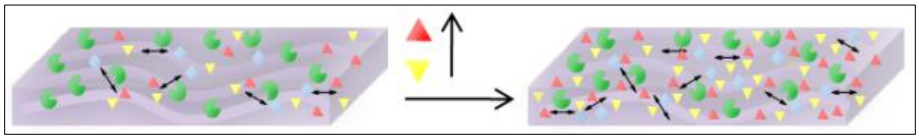

Figure 52. Effect of increasing functionality loading in PMMA films at constant PPL loading. The following are depicted biocatalyst (**e**) and –COOH and –OH functionality (▲and ▼)

Table 10 summarizes physical properties of poly (alkyl methacrylate) films containing different weight fractions of OA and 1-NN. We observed that increasing the amount of OA and 1-NN in films in advance of esterification lowers the T_g and the observed density. The characteristic changes in T_g and density for a combination of wt% functionality and type of polymer were more pronounced at loading levels above 8% by weight of OA and 1-NN. The specific volumes for PMMA, PEMA and PnBMA increased by 2.18%, 1.92%, and 4.53%, respectively, throughout the whole range of OA and 1-NN (4-16 wt%). PALS analysis was used to confirm that changes in density translated to changes in free volume after OA and 1-NN were embedded. The analysis was conducted at 0 wt% and 13.33 wt% loading of OA and 1-NN at room temperature for proof of concept and will be used more extensively in future examinations. We confirmed that PEMA films containing 13.33 wt% OA and 1-NN exhibited 1.46% increase in free volume relative to neat PEMA films, while PnBMA films containing the same amount of OA and 1-NN exhibited 14.8% increase in free volume. PALS results

corroborated that the observed density diminishment upon addition of OA and 1-NN translated in gain of the fraction free volume across poly (alkyl methacrylate) systems.

Table 10

Poly (alkyl methacrylate) T_gs and Observed Specific Volumes at Different Weight Fractions of OA and 1-NN

Poly (alkyl methacrylate)	OA and 1-NN weight fraction (%)	T_g (°C)	T_g (K)	Observed specific volume[a] (cm^3/g)	Standard deviation
PMMA	0	90.0	363	0.862	0.007
	4	58.7	332	0.871	0.003
	6	55.7	329	0.874	0.0008
	8	60.2	333	0.876	0.004
	12	57.7	331	0.881	0.002
	16	50.9	324	0.881	0.003
PEMA	0	58.0	331	0.911	0.007
	4	31.7	305	0.918	0.006
	6	31.0	304	0.919	0.002
	8	31.5	305	0.918	0.005
	12	27.2	300	0.926	0.009
	16	20.5	294	0.929	0.007
PnBMA	0	23.0	296	0.955	0.003
	4	14.2	287	0.954	0.003
	6	12.6	286	0.957	0.006
	8	1.60	275	0.962	0.009
	12	-2.10	271	0.973	0.005
	16	-9.70	263	0.999	0.004

[a] Measurements were conducted at room temperature

The zero order activity measurements in poly (alkyl methacrylate) films at different weight fractions of OA and 1-NN were shown in Figures 53-55. 4–16% weight fractions of OA and 1-NN exhibited the same effect on activity regardless of the type of poly (alkyl methacrylate) film used as matrix. Since these polymers traverse rubbery, leathery, and glassy physical states, the activity trend points to a universal behavior of activity dependence on increased loading of OA and 1-NN. The activity data shown in Figures 53-55 shows an exponential increase in

rate of ester formation with increasing loading of OA and 1-NN in the polymer phase. Surprisingly, the higher activity that resulted from 4-16% of functionality did not follow a common Michaelis-Menten behavior, i.e., a hyperbolic dependence that manifests as a linear increase in activity at low initial concentrations and an eventual plateau at higher initial concentrations. The observed exponential dependence supported that the zero-order rate was limited by the OA and 1-NN diffusion rates. We suspected that the exponential increase in activity observed in poly (alkyl methacrylate) films was due to increasingly higher total free volume driven by the partial solubilization with increased weight fraction of OA and 1-NN as seen in reduced T_g and density. Higher total free volume would increase the probability of OA and 1-NN to find holes and follow sequentially through the polymer, which would lead to higher frequency of effective jumping or increased mobility and higher probability for access of enzyme active sites.

Another result of increasing the weight fraction of OA and 1-NN is that the higher proportion of these molecules alters the interstitial space between polymer chains as reflected by T_g depression, again summarized in Table 10. The large difference in solubility parameters, 20 $(cal/cm^3)^{0.5}$ for OA and 21 $(cal/cm^3)^{0.5}$ for 1-NN, as compared to 9.3 $(cal/cm^3)^{0.5}$, 9.1 $(cal/cm^3)^{0.5}$, and 8.7 $(cal/cm^3)^{0.5}$ for PMMA, PEMA and PnBMA *(124)*, respectively, suggested stronger functionality–functionality attractive forces were available than the polymer–functionality forces. The difference favored the accumulation of OA and 1-NN in between polymer chains or in microphase separated domains. The potential for

microphase accumulation was thought to be driven by polymer exclusion and was an additional factor contributing to the observed activity over the 4-16% weight fraction range of OA and 1-NN.

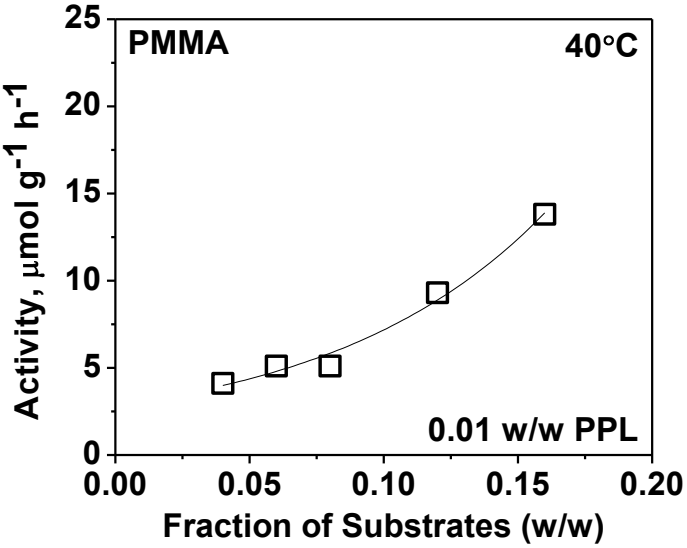

Figure 53. Effect of ester synthesis biocatalyst activity on the weight fraction of stoichiometric amounts of OA and 1-NN in PMMA films containing 0.01 w/w PPL at 40 °C. Activity was determined from initial zero order ester synthesis at 0.04 (w/w), R^2 = 0.95; 0.06 (w/w) R^2 = 0.94; 0.08 (w/w) R^2 = 0.99; 0.12 (w/w) R^2 = 0.99; 0.16 (w/w) R^2 = 0.91. Line represents the best fit of a single variable exponential growth function (R^2 = 0.99). Films had an average thickness of 188 μm and 6 mm diameter top and bottom.

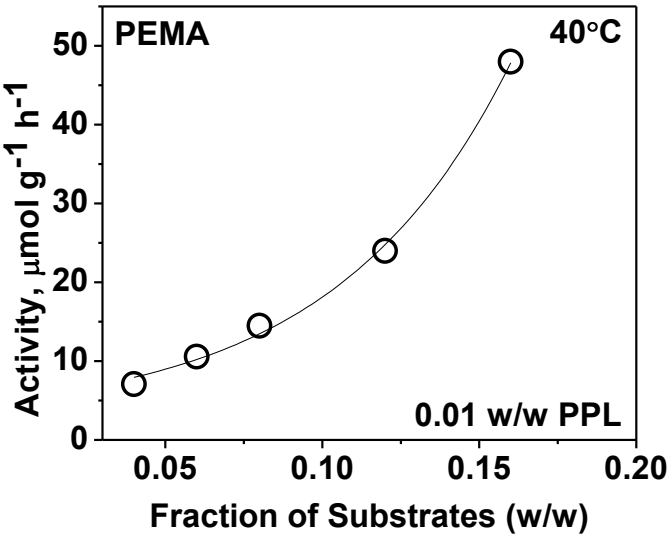

Figure 54. Effect of ester synthesis biocatalyst activity on the weight fraction of stoichiometric amounts of OA and 1-NN in PEMA films containing 0.01 w/w PPL at 40 °C. Activity was determined from initial zero order ester synthesis at 0.04 (w/w), R^2 = 0.98; 0.06 (w/w) R^2 = 0.97; 0.08 (w/w) R^2 = 0.98; 0.12 (w/w) R^2 = 0.97; 0.16 (w/w) R^2 = 0.99. Line represents the best fit of a single variable exponential growth function (R^2 = 0.99). Films had an average thickness of 138 μm and 6 mm diameter top and bottom.

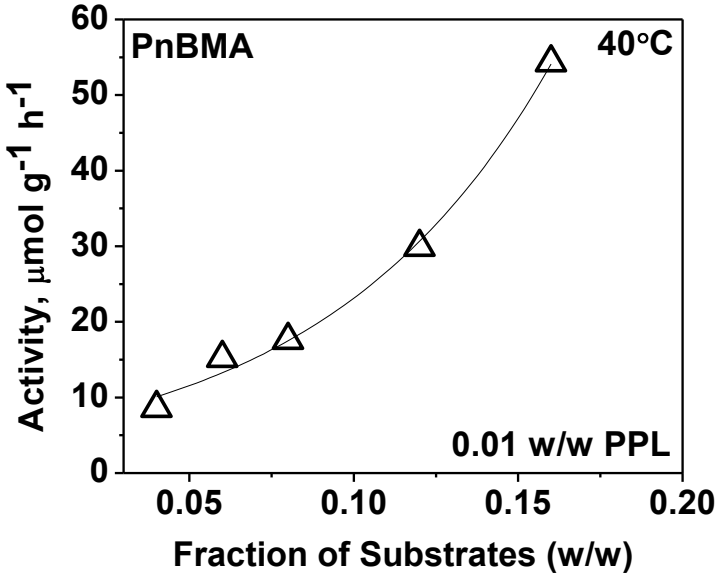

Figure 55. Effect of ester synthesis biocatalyst activity on the weight fraction of stoichiometric amounts of OA and 1-NN in PnBMA films containing 0.01 w/w PPL at 40 °C. Activity was determined from initial zero order ester synthesis at 0.04 (w/w), R^2 = 0.92; 0.06 (w/w) R^2 = 0.91; 0.08 (w/w) R^2 = 0.99; 0.12 (w/w) R^2 = 0.99; 0.16 (w/w) R^2 = 0.96. Line represents the best fit of a single variable exponential growth function (R^2 = 0.99). Films had an average thickness of 115 μm and 6 mm diameter top and bottom.

Free volume correlation to activity

The hypothesis that molecular transport is dependent on free volume was first introduced by Cohen and Turbull in 1959 and was further developed and applied to polymer-penetrant systems by Vrentas and Duda *(131,132,133,134)*. From these perspectives, translational motion occurs in "holes" or vacancies in the volume not occupied by the polymer chains. The nature of the hole free volume is different in rubbery and glassy amorphous polymers. In the rubbery state, polymer chains are capable of achieving equilibrium conformations, while in the glassy state, polymer chain motions are "frozen", at least in most experimental time scales, causing extra free volume to be trapped *(135)*. In addition, holes were attributed to: 1) both chain ends, or 2) either chain end, or 3) the polymer backbone. Chain end concentration was estimated using the following equation:

$$[\,CE\,] = \left(\frac{2}{M_n}\right)\cdot N_A \cdot \rho \quad \frac{10^{-21}\cdot cm^3}{nm^3} \qquad \text{Equation 39}$$

where [CE] is the chain end concentration (molecules/nm^3), M_n is the number-average molecular weight, N_A is Avogadro's number, and ρ is the density (g/cm^3) of polymer. Table 11 shows greater concentration of chain ends in the 40,000 g/mol PnBMA and PEMA samples than in the 996,000 g/mol PMMA sample; the ratio of chain end concentrations was 23:1 and 25:1, respectively.

Table 11

Relative Chain End Concentrations in Poly (alkyl methacrylate)s

Poly (alkyl methacrylate)s	M_n	Bulk density (g/cm^3)	Chain End Concentration ($molecules/nm^3$)	Ratio of Chain End Concentration[a]
PnBMA	40,122	1.052	0.0316	23
PEMA	37,922	1.102	0.035	25
PMMA	996,000	1.148	0.00139	1

[a] Ratio of chain end concentration to that in PMMA M_w 996,000.

Figure 56 shows the dependence of PPL ester synthesis activity on different poly (alkyl methacrylate) matrix materials and varying OA and 1-NN weight fractions. The data suggested that PPL activity at 40 °C and 0.01 w/w PPL loading was higher in poly (alkyl methacrylate)s with increasing softness (relative to 40 °C). Two main factors contributed to activity differences at the same wt% loading of OA and 1-NN. One driver was the diffusivity differences between polymers with varying free volume content that lead to higher PPL activity since the probability for finding holes is higher in polymer with increasing softness (PnBMA to PMMA). The other driver was the solubility differences between polymers at the same wt% loading of OA and 1-NN. For example, the solubility order of OA and 1-NN in poly (alkyl methacrylates) was determined to be PnBMA>PEMA>PMMA (see supplemental information). Thus, the drivers for activity difference among polymers at the same OA and 1-NN wt% loading were the increased diffusivity and solubility of OA and 1-NN in host matrices. In order to establish the relative effect of diffusivity and solubility on PPL activity, we determined the fraction of free volume at each wt% loading for each polymer.

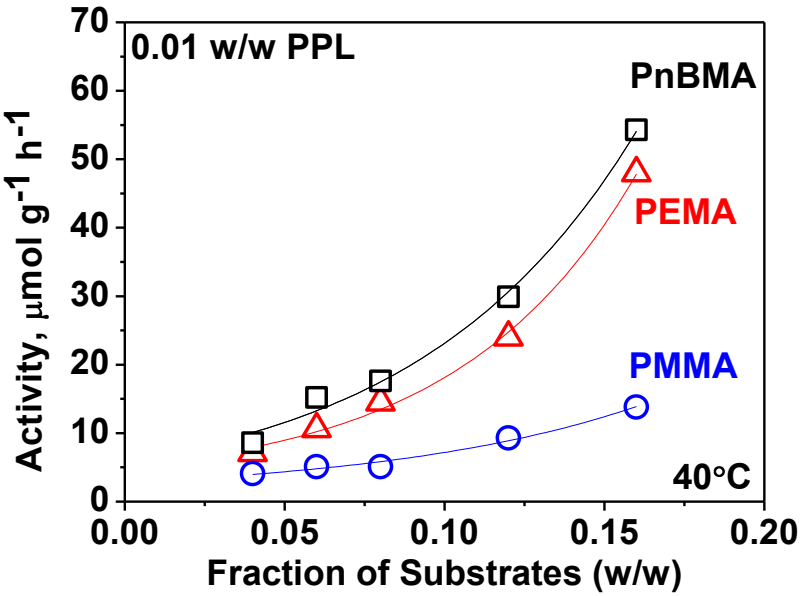

Figure 56. Effect of ester synthesis biocatalytic activity on the weight fraction of stoichiometric amounts of OA and 1-NN in poly (alkyl methacrylate) films containing 1% by weight PPL. Activity was determined from the initial rate of ester formation at 40 °C. Films were prepared by casting poly (alkyl methacrylate)s toluene solutions, each containing OA and 1-NN (0.04, 0.06, 0.08, 0.12, and 0.16 w/w) and PPL (0.01 w/w), onto glass substrates and drying at room temperature for 9 h. Lines represent the best fit of a single variable exponential growth function: PnBMA (R^2 = 0.995); PEMA (R^2 = 0.998); PMMA (R^2 = 0.990).

Since it was established that the observed diminishment of density also corresponded to an increase in the fraction of free volume as determined by PALS, we used the following method to estimate the fraction of free volume across various polymer systems and loadings of small molecule functionality. The free volume (V_F) of a polymer at any temperature T is typically explained as the difference between the specific volume of the polymer (V_T) and the specific volume of the equilibrium liquid or occupied volume (V_0) at 0 K.

$$V_F = V_T - V_0 \qquad \text{Equation 40}$$

According to the group contribution method, $V_0 = 1.3\ V_w$, where V_w is the van der Waals specific volume (*136*). Specific volume at any temperature T can

be determined from the specific volume at a reference temperature and the coefficient of thermal expansion at constant pressure:

$$V_T = V_{296} \exp [\alpha_T(T-296)] \qquad \text{Equation 41}$$

where $\alpha_T = d \ln V/dt$ is the coefficient of thermal expansion at constant pressure. Since increasing the weight fraction of OA and 1-NN will also result in a larger total free volume as described in the previous section, the fraction of activity increase was compared with the fractional increase in free volume (Figure 57).

At the lower limit(s) of OA and 1-NN loading, 4% and 6% weight fraction of the total film, the increase in enzyme activity resulted in a linear relationship with the increase in free volume fraction across PnBMA, PEMA, and PMMA. PPL activity correlated directly with the specific volume, validating that gains in activity across different poly (alkyl methacrylate)s are driven by increasing free volume available for small molecule functionality to diffuse to the active site. However, when OA and 1-NN levels were greater than 8% weight fraction, the PPL activity was not linear across various polymer systems at the same functionality loading. We attributed the lack of dependency of activity gains on fraction free volume, at 8% or higher weight fractions, on the clustering or pooling of the small molecule functionality limiting proportional access to biocatalyst as in the lower weight fractions of OA and 1-NN.

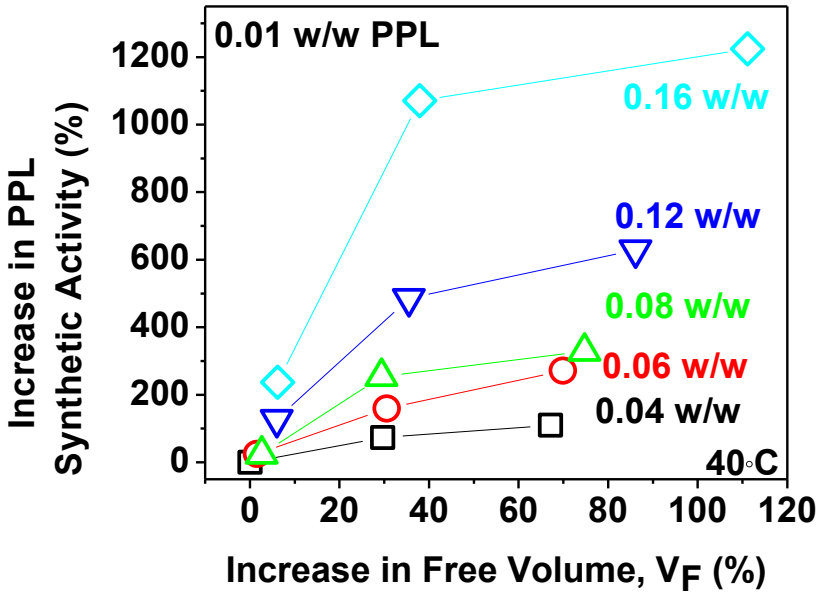

Figure 57. Dependence of % increase in ester synthesis biocatalytic activity on the % increase of free volume in poly (alkyl methacrylate)s at 0.04, 0.06, 0.08, 0.12, and 0.16 w/w fractions of stoichiometric amounts of OA and 1-NN. Films contained 1% by weight PPL and activity was determined from the initial rate of ester formation at constant temperature 40 °C. The 0.04 and 0.06 w/w specimen had a linear dependency with $R^2 = 0.94$ for the former and $R^2 = 0.98$ for the latter.

The questions then became *how* does OA and 1-NN interact with the polymer backbone or chain end free volume and *are* these interactions equivalent? The data provided some clarity through a comparison of the volumes for the OA (0.16 nm^3) and 1-NN (0.17 nm^3) molecules. It is clear that the small molecules *en masse* easily overwhelm all the available end group free volume when the weight fractions are between 4% and 16% by weight of both OA and 1-NN: PnBMA (0.041-0.05 nm^3), PEMA (0.031-0.033 nm^3), and PMMA (0.024-0.026 nm^3). We believe it was reasonable to assume that the OA and 1-NN will enter voids with either end first, i.e., with the $–CH_3$ end, –COOH, or the –OH, regardless of directional specificity. The volume of a $–CH_3$ unit is 20 cm^3/mol or 0.033 nm^3/molecule (diameter 0.38 nm), while the –OH unit has a

volume of 12 cm^3/mol or 0.02 nm^3/molecule (diameter of 0.32 nm). A comparison of an average hole diameter of 0.35 to 0.43 nm for PMMA to PnBMA with the diameter of $–CH_3$ end of 0.38 nm and the diameter of 0.32 nm of –OH end supported our thoughts that holes facilitated penetration of the OA and 1-NN end with the tail dangling outside. PnBMA can support more than one end per hole, which corroborated the higher PPL activity observed in PnBMA. Of course, the backbone or chain end holes may partially accommodate entry, but we think it was more likely that partial expansion of the polymers occurred upon OA and 1-NN entry. Specifically, one enters and the next enters more readily as the region becomes locally rich in functionality resulting in local density changes, T_g shifts, and heterogeneities depending upon interaction parameters. The chain ends were considered relatively mobile compared to the backbone, and therefore, the chain end specific voids could fluctuate to fit additional OA and 1-NN molecules. The rate and relative mobility of holes was further supported from the higher activity observed in PnBMA and PEMA as its ratio of chain end concentration is higher than in PMMA.

The combination of these results supported the tenet that higher total free volume directly drives higher PPL activity in both rubbery and glassy systems. The consistent data trends implied that PPL activity in a glassy matrix can be adjusted to the same activity level in rubbery systems by increasing the materials fractional free volume. One way of achieving higher free volume fractions and to test our hypothesis was to incorporate a tertiary non-reactive small molecule component. A plasticizer molecule is also able to increase the total free volume

since the combined free volume is higher than that of the polymer. To demonstrate that overall activity is driven by variations in free volume in a glassy polymer, additional PMMA films were cast containing 6% by weight of OA and 1-NN, and 1% by weight PPL. The films were cast at varying thicknesses using toluene as a slow evaporating solvent to result in dry film thicknesses between 88 to 362 μm and each to possess higher toluene concentrations as film thickness increased. The new materials were dried for 9 h, as previously reported for other films. Table 12 shows T_g at various thickness levels. The T_gs were unimodal and did not indicate any detectable broadening evidence of similar molecular level mixing across different systems (see supplemental Figure 63). We confirmed that the thinnest films (86 ± 31 μm) had the lowest amount of residual toluene at 5.81% by weight and the highest T_g at 82 °C. The thickest film in this study (362 ± 64 μm) possessed 9.73% by weight residual toluene and a T_g of 72 °C. The T_g depression in films with thicknesses ranging from 126 to 362 μm correlated poorly with the amount of the residual toluene, detected to be 9.3 to 10 wt%. The most significant increase in residual toluene content (from 5.81 to 9.28 wt%) occurred when the film thickness varied from 86 to 126 μm, and at higher film thicknesses the residual toluene content reached a plateau at 9.6-10 wt% with a slight depression in T_g.

Table 12

T_g of PMMA Films Containing 6% by Weight Fraction OA and 1-NN and 1% by Weight PPL at Different Thicknesses

Film Thickness (μm)	Wt% Residual Toluene[a]	T_g (°C)	T_g (K)
86 ± 31	5.81	82	355
126 ± 12	9.28	75	348
177 ± 20	9.58	76	349
262 ± 17	10.2	71	344
362 ± 64	9.73	72	345

[a] Determined by ^{1}H NMR

PPL activity was also determined at each thickness level without further drying at 40 °C, i.e., films contained residual toluene (Figure 58). PPL activity increased concurrently with film thicknesses from 3 μmol/g/h in 86 μm films to 22.6 μmol/g/h in 362 μm films. The 653% increase in activity in the 86-362 μm range occurred in a linear fashion, which suggested that increasingly thicker films contained more free volume sites even though the residual toluene content exhibited a concentration plateau. The higher total free volume resulted from the evaporation of relatively greater amounts of toluene per gram of film leaving behind more free volume sites large enough for the end groups of OA and 1-NN to permeate through the film until an enzyme active site was encountered. To our surprise, it appeared that the residual solvent acted as a temporary template by fixing the free volume positions. The toluene evaporated without relaxation of the free volume sites and occupancy by polymer chains, which ultimately led to higher enzyme activities. As the film thickness increased more free volume sites became available, which in turn increased the frequency of hole-jumping by OA and 1-NN and were supported by the incrementally higher enzyme activity (Figure 58).

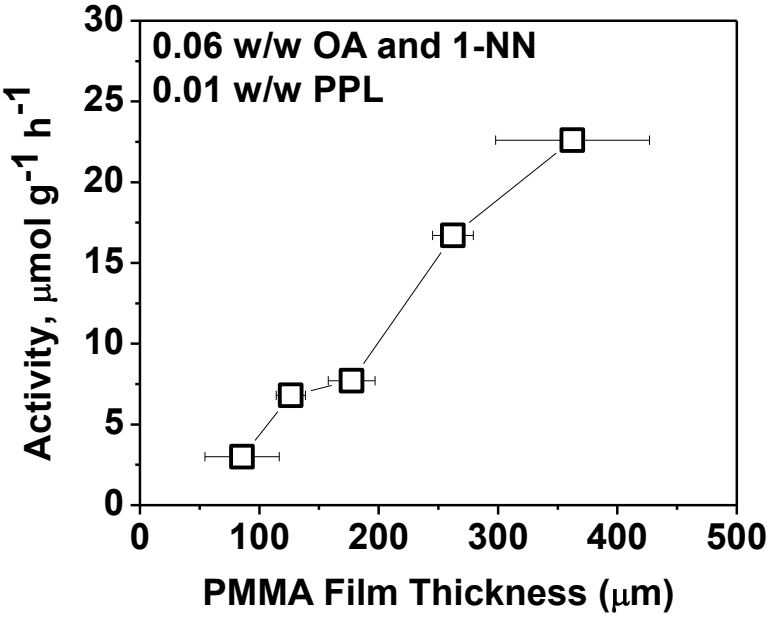

Figure 58. Dependence of ester synthesis biocatalyst activity on the PMMA film thickness with incorporated stoichiometric amounts of 6% by weight of OA and 1-NN and 1% by weight of PPL. Activity was determined from the initial rate of ester formation at 40 °C. Films were prepared by casting PMMA toluene solutions containing OA, 1-NN, and PPL onto a glass substrate and drying at room temperature for 9 hours.

Conclusions

In vivo, enzymes catalyze reactions efficiently and selectively in highly crowded cellular media. Typically, the excluded volume set by cellular macromolecular complexes drives biocatalyst activity by introducing diffusional resistance and concentration gradients of enzyme substrates within the cell. We were interested in developing a material platform with embedded functional components and enzymes in the same matrix. Upon environmental challenge, the matrix will adapt to stimuli and alter chemical or mechanical properties by leveraging enzyme catalysis. We examined mechanistically ester biosynthesis from –OH and –COOH functional small molecules and enzymes embedded in amorphous glassy or rubbery films before and after film solidification.

Biocatalytic films show high activity towards ester formation in bulk and film surface, although surface activity was approximately 30 times lower than bulk activity. The slower biosynthesis rate observed at the film surface was attributed to diminished access and diffusion limited sorption rate of OA and 1-NN towards biocatalyst. Direct comparison of surface activity and bulk activity in glassy and rubbery poly (alkyl methacrylate) films suggested that the rate of OA and 1-NN uptake was much slower that the rate of biocatalyzed conversion. Biocatalytic film activity was 16 times lower than organic media activity. The lower activity observed in films with embedded biocatalyst and small molecule functionality was attributed to the increase in diffusional resistance experienced by the –COOH and –OH functional molecules. In fact, the dimensionless modulus for OA and 1-NN was high in all poly (alkyl methacrylate) films indicating that the reaction rate was much faster than the self-diffusion coefficient of each functional component.

Typical reaction progress curves were characterized by a linear increase in ester synthesis and a plateau as the reaction reached near full conversion. In glassy polymers, the reaction progress curves resulted in two stages of ester formation with an initial stage that had a higher rate than the second stage. Higher rates in the first stage of the reaction were attributed to kinetically trapped polymer microstructures that favored the presence of excess free volume. The diminished rate of the second stage represented ester synthesis in quasi-equilibrium microstructures after sub-T_g aging of polymer chains consumed portions of excess free volume.

Glassy biocatalytic films with biocatalyst loadings higher than 2% by weight consistently exhibited greater than 50% conversion of OA and 1-NN during film formation stages, i.e., within the first 9 h after casting from solution. Thus, biocatalytic activity data could only be obtained for films with less than 2% PPL loading for practical reasons. Poly (alkyl methacrylate) films, glassy or rubbery, had increasing amounts of free volume with increased loadings of OA and 1-NN as determined by PALS and density measurements. Biocatalytic activity in PMMA, PEMA, and PnBMA films exhibited an exponential increase as a function of initial loading of OA and 1-NN. The activity trend was attributed to increased diffusivity and solubility of OA and 1-NN in the poly (alkyl methacrylate) matrices at higher OA and 1-NN loadings.

Biocatalyst activity was determined to be driven mainly by diffusivity of OA and 1-NN at loadings of less than 8%, while above this loading, biocatalyst activity was driven by increasing solubility of OA and 1-NN. It was proposed that diffusivity at low loading levels occurs by OA and 1-NN molecules entering polymer voids with either end regardless of directionality. To validate that biocatalytic activity in glassy polymers is free volume mediated, a tertiary inert fugitive molecule, which acts as solvent plasticizer, was employed to control biocatalyst activity. It was determined that slow solvent evaporation from films that are glassy at RT drove the presence of more trapped free volume sites as film thickness increased. This led to a linear increase in biocatalyst activity as a function of film thickness due to increased diffusivity of OA and 1-NN in glassy films.

Supplemental Information

The dimensionless observable modulus, *Φ*, was calculated to further corroborate that internal mass transfer is not negligible in the enzyme-catalyzed reaction of OA and 1-NN in poly (alkyl methacrylate) amorphous films (*137-138*).

$$\phi = \frac{v_o \cdot V_F^{\,2}}{D \cdot \left[M_o\right] \cdot A_F^{\,2}} \qquad \text{Equation 42}$$

v_o is initial zero order rate in mmol g^{-1} s^{-1}, D is the diffusion coefficient in cm^2 s^{-1}, V_F is the film volume in cm^3, A_F is area of the film in cm^2, and $[M_o]$ is the initial functionality concentration in mmol g^{-1}.

At Φ<0.3, OA and 1-NN diffusion is fast compared to its conversion, while at Φ>0.3, diffusion is slow compared to its conversion, therefore the reaction experiences mass transfer resistance (*139*). The diffusivity coefficient, D_e, was measured gravimetrically for each functionality and polymer system using sorption experiments to calculate Φ values. Upon polymer dissolution, self-diffusion coefficients were estimated using the Van Kravelen-Hoyftyzer method for estimating the viscosity of concentrated polymer solutions and the Einstein-Stokes equation:

$$D = \frac{k_B \cdot T(K)}{6 \cdot \pi \cdot \eta \cdot r} \qquad \text{Equation 43}$$

where D is diffusion coefficient in cm^2 s^{-1}, k_B is the Boltzmann constant in N m K^{-1}, T is the temperature in K, η is the media viscosity in N s m^{-2}, and r is the particle radius in cm (*124*).

Sorption experiments were conducted at 40 °C to determine D_e for each functionality and polymer. Results were plotted as the mass uptake fraction ($\Delta M/M_o$, $\Delta M = M_t - M_o$) versus the square root of time divided by the thickness squared $(t/L^2)^{0.5}$ where M_t is the current sample mass and M_o is the original sample mass. Figure 59 shows the results of a typical mass uptake fraction plot of PEMA films submerged in a 1-NN bath at constant temperature of 40 °C. D_e was obtained from linear regression analysis of the initial penetrant uptake while the gravimetric sorption content (U) was determined from the plateau region. At 30% by weight absorption of 1-NN, the blends became opaque at 40 °C, i.e., phase separation occurred, indicative of upper critical solution temperature (UCST) behavior.

Effective diffusivity coefficients for reaction components, OA and 1-NN, in poly (alkyl methacrylate) films were determined from gravimetric uptake experiments (Table 13). Water D_e values in PMMA were obtained from literature and appeared to be higher than D_e determined for 1-NN and OA. The lower D_e values of 1-NN and OA than water in PMMA were attributed to the relatively larger size of OA and 1-NN molecules. As expected, OA had consistently better compatibility than 1-NN with poly (alkyl methacrylate) films due to the acyl group in its structure bearing the most similarity to the polymer repeat unit structures. In addition, D_e for 1-NN in PEMA was higher than in PMMA due to the glassy nature of the latter.

PEMA dissolution occurs upon immersion in OA at 40 °C while PnBMA dissolution occurs upon immersion in both OA and 1-NN. Since diffusivity values

were inaccessible for PnBMA, self-diffusion coefficients for particles with molecular radius similar to OA and 1-NN were estimatied at various weight fractions in PnBMA (Table 14). The dimensionless modulus (Φ) values for PMMA, PEMA, and PnBMA as calculated from equation 42 (Table 15) reveal that the reaction is diffusion limited even as the weight fraction of OA and 1-NN in polymers increases.

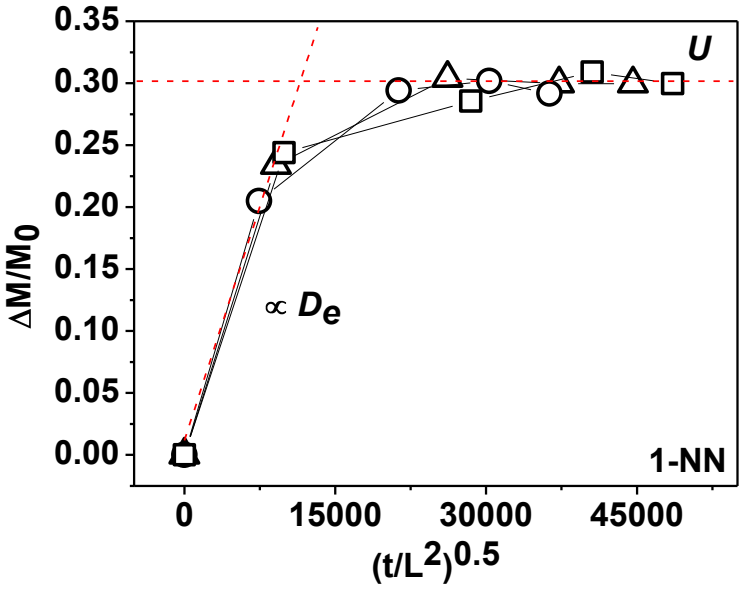

Figure 59. Mass uptake of PEMA films submerged in 1-NN at 40 °C. Dashed lines represent the initial slope, proportional to $D_e$and the gravimetric saturation content (*U*).

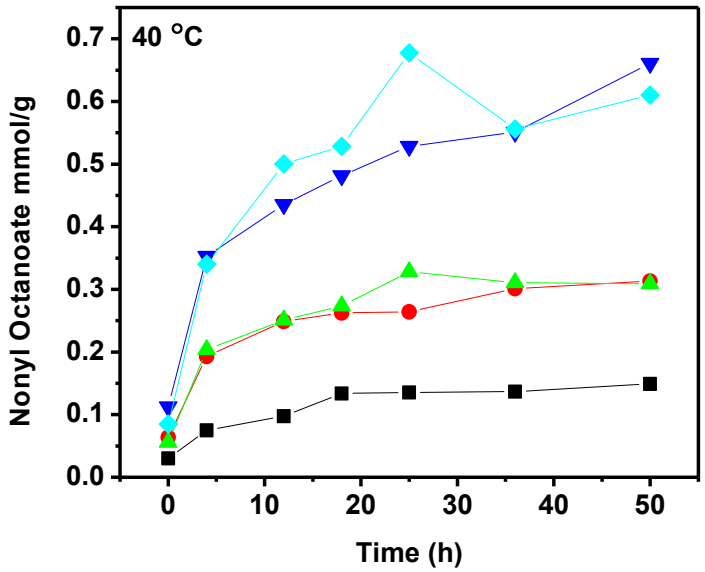

Figure 60. NOc synthesis as a function of time at 40 °C in glassy polymer (PMMA) with different stoichiometric amounts of OA and 1-NN and 1% (w/w) PPL biocatalyst. The following represent the weight percent loading of OA and 1-NN: 16 wt% (-♦-), 12 wt% (-▼-), 8 wt% (-▲-) 6 wt% (-●-), and 4 wt% (-■-).

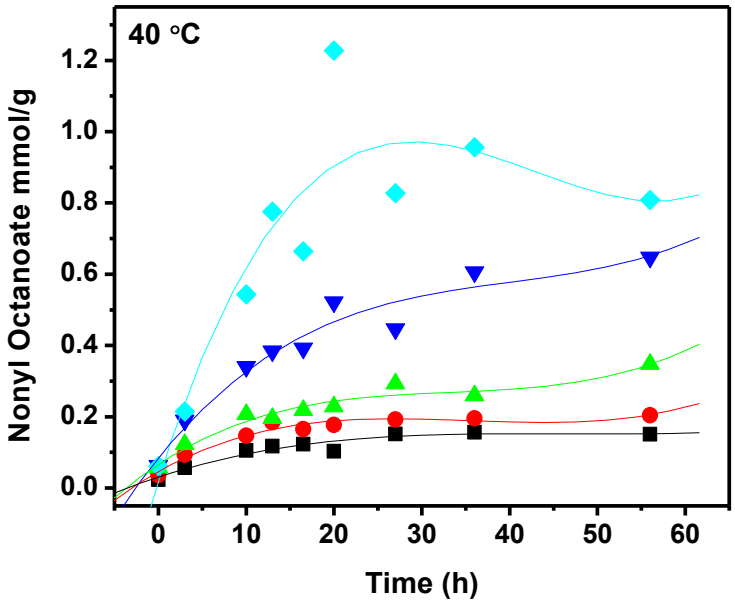

Figure 61. NOc synthesis as a function of time at 40 °C in rubbery polymer (PEMA) with different stoichiometric amounts of OA and 1-NN and 1% (w/w) PPL biocatalyst. The following represent the weight percent loading of OA and 1-NN: 16 wt% (-♦-), 12 wt% (-▼-), 8 wt% (-▲-) 6 wt% (-●-), and 4 wt% (-■-).

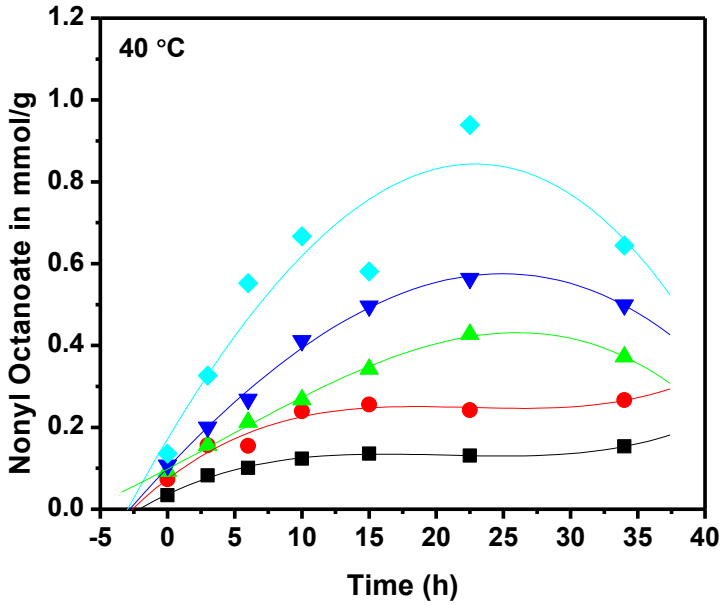

Figure 62. NOc synthesis as a function of time at 40 °C in rubbery polymer (PnBMA) with different stoichiometric amounts of OA and 1-NN and 1% (w/w) PPL biocatalyst. The following represent the weight percent loading of OA and 1-NN: 16 wt% (-♦-), 12 wt% (-▼-), 8 wt% (-▲-) 6 wt% (-●-), and 4 wt% (-■-).

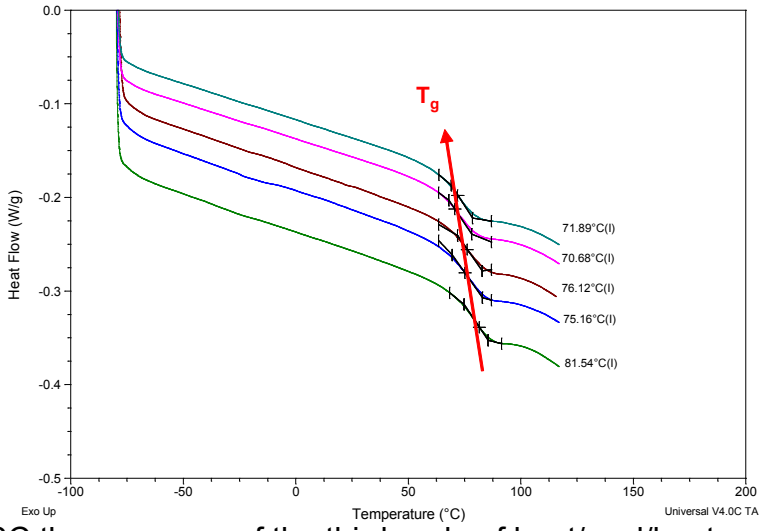

Figure 63. DSC thermograms of the third cycle of heat/cool/heat program of PMMA films embedded with 6% by weight initial loading of OA and 1-NN and 1% by weight PPL and different thicknesses from bottom to top corresponding to: 86 ± 31 µm, 126 ± 12 µm, 177 ± 20 µm, 262 ± 17 µm, 362 ± 64 µm, and exposed at 40 °C.

Table 13

D_e (cm^2/s) for Absorbed Liquids in Various Poly (alkyl methacrylate)s Films Determined from Sorption Experiments at 40 °C

Polymer/Absorbed	Octanoic Acid	1-Nonanol	Water
PMMA	[b] 1.39×10^{-13}	[b] 2.49×10^{-14}	[a] 1.52×10^{-10}
PEMA	Soluble	[b] 1.44×10^{-10}	[c] 2.9×10^{-7}
PnBMA	Soluble	Soluble	[c] 6.7×10^{-7}

[a] Average of reported literature values at 40 °C *(140,141)*
[b] Average calculated from sorption experiment
[c] Reported literature values at 40 °C *(142)*

Table 14

Estimated D (cm^2/s) for Different Compositions of PnBMA Films using the Van Kravelen-Hoyftyzer Method

Weight Fraction of OA and 1-NN	PnBMA Volume Fraction	log (η), Pa-s (calc.)	D, cm^2/s (calc.)
0.04	0.95	8.4	2.3×10^{-16}
0.06	0.93	7.4	5.1×10^{-16}
0.08	0.91	7.1	1.5×10^{-14}
0.12	0.87	5.7	1.9×10^{-14}
0.16	0.84	4.7	1.2×10^{-13}

Table 15

Dimensionless Modulus of Poly Alkyl (Methacrylate)s with Various Weight Fractions of OA and 1-NN Using Equation 42

OA and 1-NN Weight Fraction	0.04	0.06	0.08	0.12	0.16
PMMA	37,600	30,100	22,000	33,600	36,900
PEMA	4.4	5.7	5.1	5.2	6.9
PnBMA	2,160,000	1,620,000	46,300	35,600	10,400

CHAPTER VI

PROBING THERMAL AND SOLVENT EFFECTS ON THE SWITCHABLE BIOACTIVITY OF FREE-STANDING FILMS

Abstract

Biocatalytic activity of poly (alkyl methacrylate) free-standing films embedded with Porcine Pancreas Lipase alongside enzyme active –OH and –COOH functional small molecules was evaluated as a function of temperature and type of solvent cast system. Biocatalytic activity in the glassy state was seen to be largely dependent on the nature of free volume as determined indirectly by temperature studies of activity and compared to similar film compositions in the rubbery state. In addition, solvents in the glassy systems behaved as transient templates during film formation as determined by the correlation of biocatalytic activity with the difference between the solubility parameters of the film and the solvent. We also demonstrated that PMMA and PEMA films with embedded biocatalyst alongside functionality manifested reversible conversion of OA and 1-NN to NOc based on the equilibrium water content. These formulations exhibit potential as hybrid materials with switchable surface and bulk properties via reaction equilibrium control by altering environmental conditions.

Introduction

Reversibly controlling the surface and bulk properties of matter is advantageous to structural, separation, biomedical, and electronic applications of polymer materials. This capability would vastly expanding current polymer properties to have self-healing, sensing, actuating, phase/volume changing,

selective permeation, and shape-memory characteristics *(143)*. Typically, polymers are used as static monolithic or composite constructs blended with various additives to meet narrow and specific physical, chemical, electronic, optical, and processing property requirements *(144)*. However, most applications require dynamic polymer designs able to meet performance requirements in dissimilar environments throughout the polymer life-cycle. One strategy to attain such feat is the incorporation of functional components able to catalytically transform upon exposure to environmental stimuli. The reversible transformation would provide the material a tool to self-tune its surface and bulk properties, physical or chemical, by catalytic modification of the functionality *(145)*.

There are many examples of dynamic polymer systems in the open literature capable of supramolecular or covalent bond rearrangements upon exposure to stimuli *(146,147)*. Thermo-mechanical *(148)*, chemical *(149)*, and photo responsive polymers *(150)* have been developed based on reversible covalent or supramolecular assemblies; however, the majority of these materials have very low moduli despite exhibiting several orders of magnitude viscosity or modulus changes in response to the corresponding stimuli *(151)*. Glassy polymers, on the other hand, are employed in numerous industrial applications due to their mechanical properties. Designing and incorporating dynamic behavior in glassy systems would expand their utility in many applications that require adjustable bulk properties, such as impact strength, abrasion resistance, resilience, etc.

Thermoplastic amorphous glassy morphology is characterized by “frozen” configurations that arise during processing from the liquid to the solid state (vitrification) *(130)*. These configurations have transient micro- or nano- features due to kinetically driven trapped free volume often referred to as excess free volume. The excess free volume can be discrete or interconnected, and its size and distribution will largely determine the capability of the material to carry out extrinsic functions, such as catalysis, transport, sensing, and mechanical behavior. Traditionally, materials are classified as microporous when comprised of pore sizes smaller than 2 nm; mesoporous when pore sizes are in the range of 2-50 nm, and macroporous when pore sizes are above 50 nm *(152)*. Intrinsic microporosity is dictated by the presence of rotationally hindered bonds in the backbone *(153)* and pendant group size *(154)*. The interplay between these factors as well as the intermolecular interaction between chains and guest molecules has been used to optimize penetrant or additive transport through glassy polymers for industrial membrane, packaging, compounding, and coating applications *(155,156)*. Glassy polymers behave similarly to microporous materials if the excess free volume is high enough to become interconnected *(135)*.

Enzyme engineering has seen tremendous development since the rediscovery that enzymes function well in near anhydrous conditions *(4,5)*. Ability to optimize the highly specific and selective catalytic activity by altering enzyme microenvironment or structure has been an efficient tool in synthesis of pharmaceuticals, natural products, fine chemicals and food ingredients *(2,3)*.

Addition of polar or water-miscible solvents results in enzyme denaturation and activity loss as the solvents strip off the water molecules tightly bound to the enzyme surface. Barring some exceptions, low enzyme activity has been reported in solvents with logarithm of the partition, log (P), values less than 2, i.e., hydrophilic solvent. Activity is only moderately affected by solvents with log (P) values between 2-4, and high activity is observed in solvents with log (P) greater than 4, i.e., hydrophobic solvents *(157)*. The kinetic behavior of enzyme-catalyzed reactions is widely dependent on the chemical nature of functionality since the functional species must diffuse to the active site through the few nm thick aqueous shell enveloping the biocatalyst.

Enzyme immobilization in inert matrices has been widely used in applications demanding heterogeneous biocatalysts, selective adsorbents, controlled released protein drugs, and analytical devices *(8)*. Macroporous materials used in these applications are required to be an inert and supportive media for immobilization. Several review articles and books thoroughly describe enzyme immobilization technology for applications in the fields of biocatalysis and biosensors *(8,121,123)*. By leveraging enzyme catalysis, we are interested in developing a material platform with embedded functionality and biocatalyst within the same matrix that upon environmental challenge will adapt to stimuli by altering the matrix's chemical or mechanical properties. Lipase from porcine pancreas is an excellent model biocatalyst due to its well-defined and robust activity in polar and nonpolar organic solvents *(4,5,18)*.

In Chapter V, we reported on the catalytic behavior of enzymes in amorphous solids in rubbery and glassy state by evaluating the biocatalyzed esterification rate of OA and 1-NN. Upon film solidification, the enzyme remained active towards small molecule functionality. It was determined that the bioactivity was influenced by the glassy and rubbery nature of the final film composition and limited by the total free volume. The data indicated that biocatalyzed reactions occurred in glassy films if OA and 1-NN permeated through the free volume sites of the material. The biocatalyst activity was highly dependent on the residual solvent, which promoted bioactivity by increasing the fraction of free volume via chain plasticization and evaporation.

In this chapter, polymer glassy systems described earlier were investigated to understand the effect of the nature of excess free volume and polymer-solvent solubility parameters on the biocatalytic reaction (Figure 64). It was hypothesized that bioactivity spanning a temperature below and above the hybrid material T_g would mirror the behavior of segmental relaxation across the same temperature range due to the free-volume limited bioactivity. Additionally, we determined the effect on bioactivity of casting from solvents below and above the solubility parameter of the matrix. We also explored the long-term switchable nature of bioactivity to shift the hybrid material's bulk properties by driving the reaction either towards reactants or products via control of the equilibrium water content.

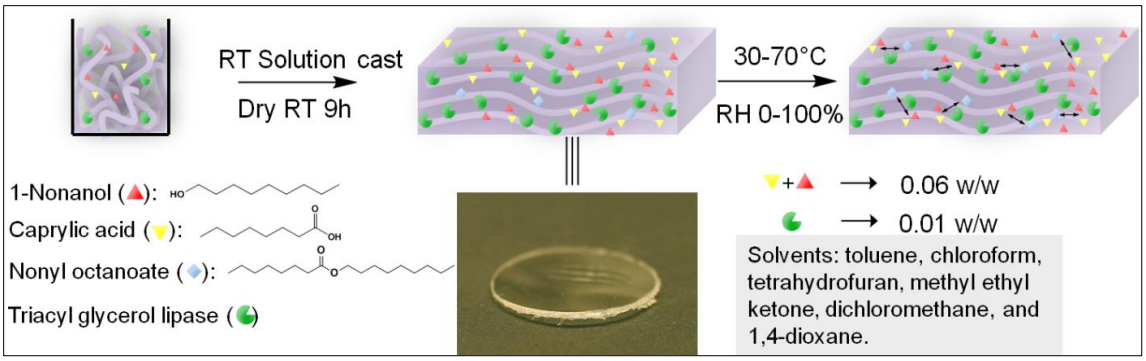

Figure 64. Formation of biocatalytic films upon incorporation of biocatalyst and stoichiometric amounts of small molecule functionality. Photograph shows a typical 6 mm diameter bioactive film.

Results and Discussion

Fox and Flory suggested that amorphous glassy materials are in an iso-free volume state, and the T_g occurs only at a critical fraction of free volume that allows the cooperative movement of polymer chains *(158)*. However, when rapidly cooled to below the T_g, the excess free volume is trapped due the inability of chains to reach equilibrium configurations. It has been experimentally determined that the mean size and number of holes is dictated by the presence of rotationally hindered bonds in the backbone *(153)*, the size of pendant groups *(154)* and the intermolecular interaction between chains and guest molecules *(155,156)*. As a glassy material approaches equilibrium, the excess free volume slowly dissipates spontaneously, i.e., undergoes physical aging. In the glassy state, relaxation times are very long and the segmental motions appear frozen, therefore it takes longer for the excess free volume loss to occur as it approaches thermodynamic equilibrium. In Chapter V, we reported that in glassy materials the enzymatic reaction manifested a dual stage behavior with higher initial zero order rate followed by a second lower zero order rate. We attributed

the first zero order rate of ester synthesis to the diffusion-limited translational motion of functionality within the excess free volume of the glassy host matrix. The slower rate of the second stage was attributed to greater extent of diffusion-limited translational motion, i.e., diminished probability for finding free volume holes, due to loss of excess free volume as the result of structural relaxation towards equilibrium configurations.

Temperature dependency of activity

Since isothermal consumption of excess free volume plays a role in biocatalyst activity, the probability that a small molecule functionality would find a similar size scale hole is expected to diminish as chains approach equilibrium configurations. To confirm this hypothesis, PMMA films containing 6% by weight OA and 1-NN, and 1% by weight PPL enzyme were evaluated. The 6% OA and 1-NN loading was used since we suspected that at low functionality loading clustering or pooling of OA and 1-NN was not significant as determined by the linear relationship between the increase in activity and the increase in specific volume described in Chapter V. At these low functionality loadings, it was concluded that bioactivity was due to transport of sorbed OA and 1-NN through a small molecule percolation pathway without pooling regions.

Figure 65 shows the progressive curves for the reaction conducted in glassy host matrices at various temperatures. The data confirmed the two-stage kinetics as observed in previous experiments with varying enzyme and small molecule functionality loading (Chapter V). Raising the reaction temperature shifted the onset of the zero order second stage at faster times though

conversions at the onset were drastically different, e.g., conversions varied from ~48% at 30 °C to ~80% at 60 °C. The observation confirmed that the onset of the second stage was dependent on the rate of structural relaxation, but not on the overall conversion. This indicated that after loss of excess free volume, the zero order rates diminish until reaching a plateau near full conversion.

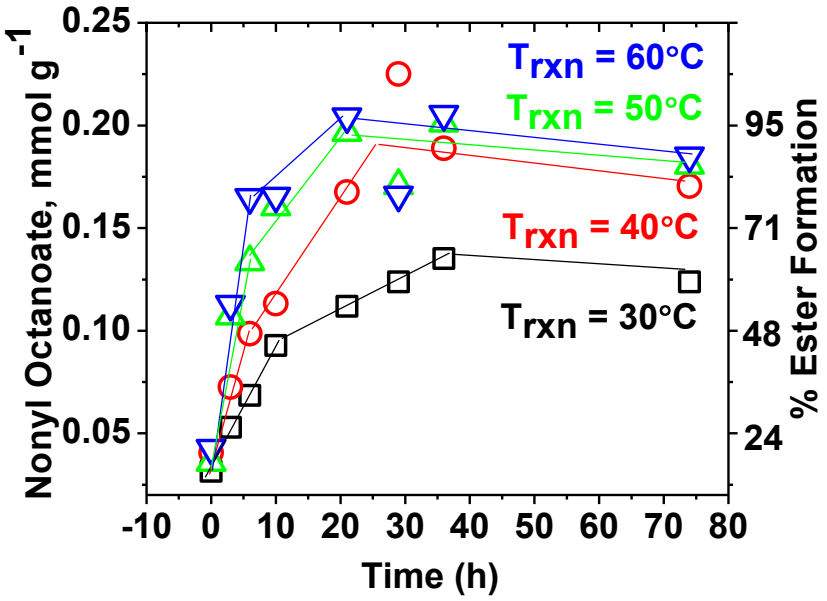

Figure 65. Dependence of ester synthesis biocatalytic activity on the reaction temperature (30–60 °C) in PMMA films containing 6 wt% stoichiometric amounts of OA and 1-NN, and 1 wt% PPL. The solid lines illustrated two-stage ester synthesis at various temperatures. The progressive curve obtained from curing at 70 °C was not included for clarity purposes. Films had an average thickness of 159 μm and 6 mm diameter top and bottom.

Figure 66a summarizes the dependency of PPL activity on temperature in PMMA films. PPL activity increased exponentially with temperature and reached a plateau above 60 °C. The abrupt change in activity occurred near the material T_g indicating that ester formation rate switched from being limited by excess free volume through an interconnected pathway of OA and 1-NN to being limited by ability of OA and 1-NN to diffuse from discrete functionality rich regions. The

Arrhenius plot of the catalytic rate was constructed to separate the contributions of temperature on reaction rate and consumption of excess free volume (Figure 66b). The Arrhenius plot resulted in a straight line with a correlation factor (R^2) of 0.976, but R^2 changed to 0.999 if the data was fitted to a concave second order polynomial. Interestingly, the concavity in the Arrhenius plot is identical to the behavior of the effects of sub-T_g aging temperature on the aging rate of PMMA as measured by changes in modulus and creep relaxation over similar time scale experiments *(159,160)*. The aging effect as the result of increasing sub-T_g temperature was also observed by the final T_g of the hybrid films, which increased incrementally from 64 °C to 76 °C for films exposed to 30-70 °C (see supplemental Figure 77).

A diminished standard energy of activation was observed above the T_g since annealing temperatures ($T_{rxn}>T_g$) were approached indicating that loss of excess free volume caused higher translational resistance relative to the reaction rate at 60-70 °C. Typically, as the reaction rate accelerates with temperature increments, the conversion of reactants to products occurs so rapidly that small molecule concentration in the enzyme microenvironment depletes faster than it can be replenished and hence, functionality diffusion through the diminished excess free volume to the enzyme becomes increasingly rate controlling. The standard energy of activation diminishes and reduces the effect of increased temperature on the reaction rate. The observed reduction in the standard energy of activation with increasing diffusion limitation has been reported extensively in the enzyme immobilization literature, where increasing temperature depletes

substrates within macroporous beads shifting the rate control from intrinsic to the enzyme to control by diffusion rate of fresh substrate from the substrate sink *(161,162)*. Despite the observed concavity, the general dependence of activity, expressed in µmol/g/h, on temperature was quantified using the Arrhenius equation:

$$\text{Activity} = A \cdot \exp\left(\frac{-E_a}{R \cdot T}\right) \qquad \text{Equation 44}$$

The activation energy (E_a) and the Arrhenius factor can be interpreted directly from a plot of log (Activity) versus 1/T, which yields a straight line with a slope of $-E_a/R$ and an intercept of log A. The Arrhenius plot of the conversion of OA and 1-NN in PMMA films (Figure 66b) indicated E_a and A values of 15.1 kJ/mol and 5.25×10^6, respectively. Mitchell and coworkers determined E_a for various fungal lipases towards the hydrolysis of triolein to be 56-77 kJ/mol in reverse micelles and 42 kJ/mol in aqueous emulsion *(163)*. These are typical E_a values for catalyzed reactions by enzymes in reverse micelles indicating enzyme kinetic control of the reaction *(164)*. Eriksson and coworkers determined that E_a for *Candida Antarctica* trapped in gels towards the synthesis of *R*-(-)-2-octyl hexanoate was 35-40 kJ/mol *(165)*. In comparison, the E_a value obtained in this study (15.1 kJ/mol) indicates that the reaction between OA and 1-NN was diffusion controlled in the 30-60 °C temperature regime.

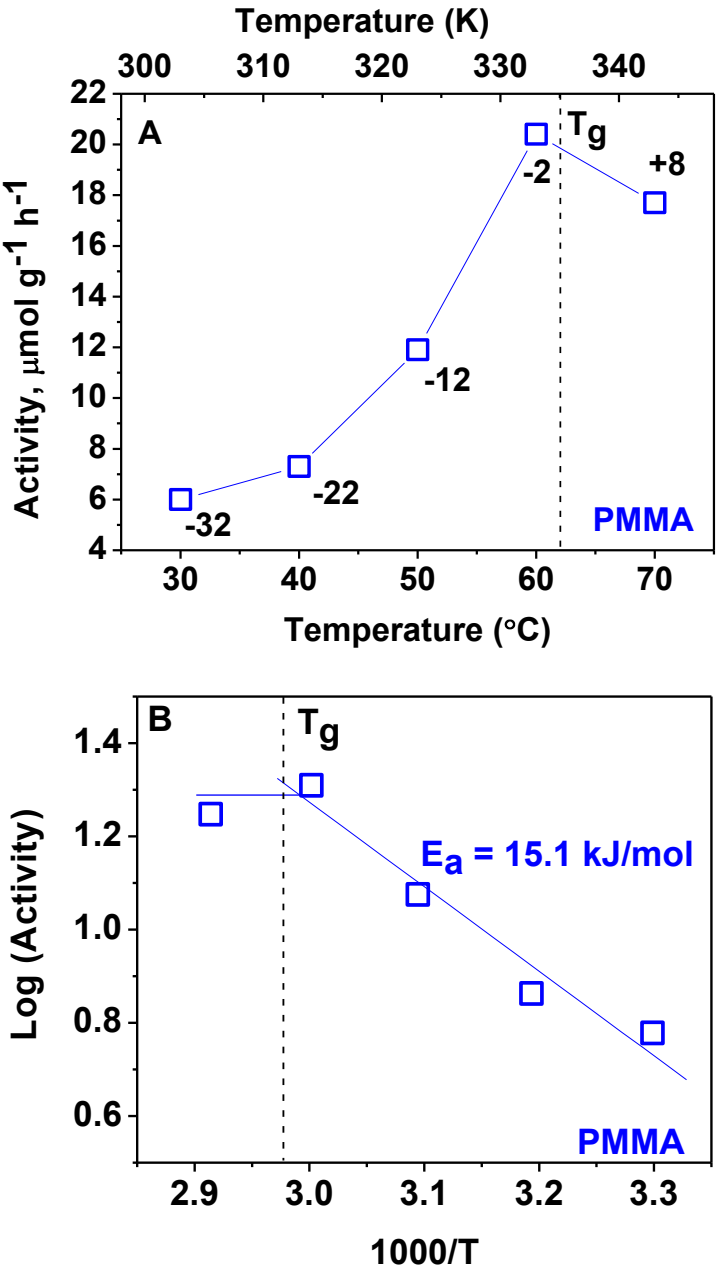

Figure 66. Dependency of ester synthesis biocatalyst activity on exposure temperature in PMMA films loaded with stoichiometric amounts of OA and 1-NN 6% by weight and PPL 1% by weight. Films had an average thickness of 159 μm and 6 mm diameter top and bottom. A) Activity plotted against temperature. Vertical dashed line indicates film T_g after 9 h drying time. Numbers associated with each activity measurement indicate T-T_g. B) Arrhenius plot of ester synthesis biocatalyst activity as a function of exposure temperature in PMMA films. Line represent best fit of linear function (R^2 = 0.976), and E_a was calculated to be 15.1 kJ/mol.

As a control experiment, we repeated the above studies in polymers that upon solution casting have T_gs lower than the assay temperature. In the rubbery regime, the long-range segmental motion is liquid-like and occurs at shorter or experimentally accessible time scales. Free volume distribution occurs in a dynamic manner facilitating the thermal hopping diffusive behavior of the small molecule functionality to occur throughout the rubbery regime. PnBMA films were cast containing 6% by weight OA and 1-NN, and 1% by weight PPL to confirm the magnitude of the contribution from hole-free volume and reaction rate. Figure 67a shows the dependency of PPL activity on temperature in PnBMA films. The progress curves do not manifest two-stage kinetics as observed in the glassy state, and the final T_g does not vary significantly with exposure temperature (see supplemental Figure 78).

At first glance, the system shows a linear increase in activity as a function of temperature. The Arrhenius plot for rubbery systems reveals that logarithm of activity as function of 1/T does not conform to a single straight line, but is best described by a dual activation energy model, i.e., the data can best be fitted by two straight lines. This kinetic type of temperature dependency is reminiscent of long-range secondary transitions in polymers where temperature dependent properties converge near T_g (Figure 67b). The dependency of the reaction rate diminishes at higher temperatures indicating that increased thermal hopping of small molecules is driving their clustering within the matrix; therefore, the rate is controlled by the small molecule functionality diffusion between discrete phase separated regions.

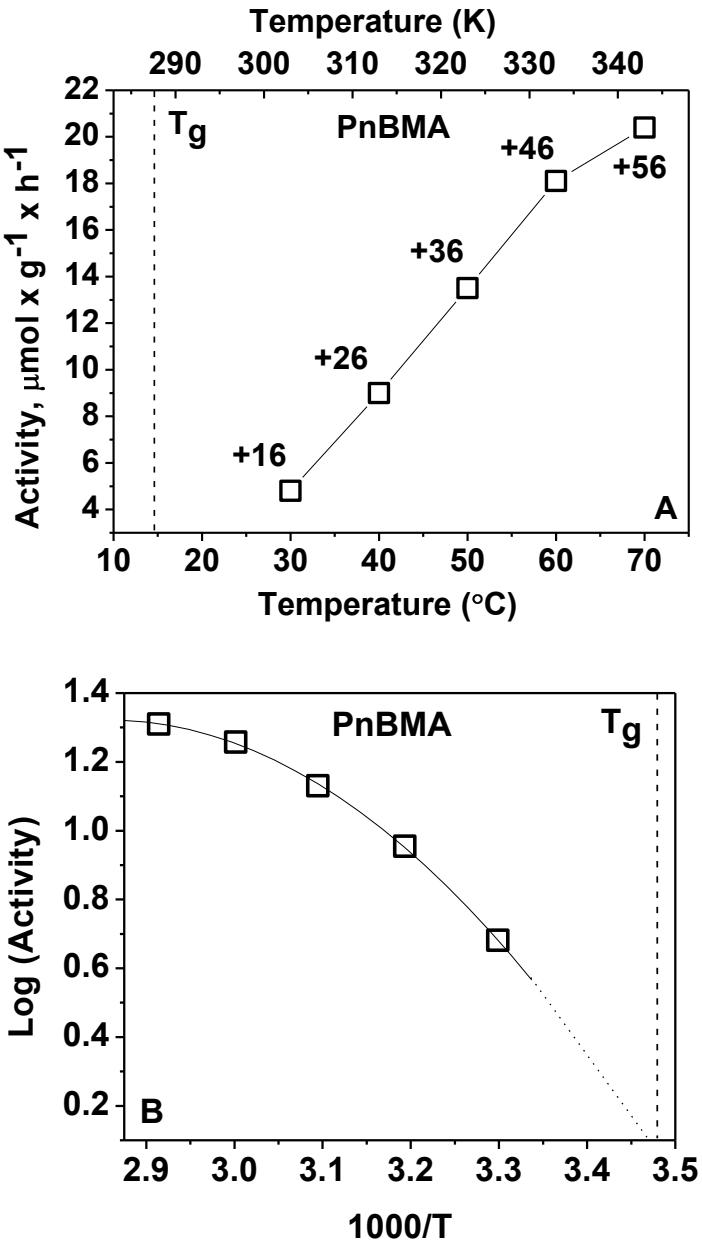

Figure 67. Dependency of ester synthesis biocatalyst activity on exposure temperature in PnBMA films loaded with stoichiometric amounts of OA and 1-NN 6% by weight and PPL 1% by weight. Films had an average thickness of 159 μm and 6 mm diameter top and bottom. A) Activity plotted against temperature. Vertical dashed line indicates film T_g after 9 h drying time. Numbers associated with each activity measurement indicate T-T_g. B) Arrhenius plot of ester synthesis biocatalyst activity on exposure temperature in PMMA films. Curve represents best of a two-variable polynomial function (R^2 = 0.99), and the extrapolation represent the activity limit for temperature approaching the host matrix T_g.

The non-Arrhenius behavior of PPL activity in PnBMA indicates that polymer long-range segmental relaxations dictate the enzyme-catalyzed conversion of OA and 1-NN to the NOc ester. The non-Arrhenius nature is typically modeled using the Vogel-Fulcher-Tammann (VFT) equation *(28)*:

$$\text{Activity} = A_V \cdot \exp\left(\frac{-E_{VFT}}{R(T - T_V)}\right) \qquad \text{Equation 45}$$

where Activity is the zero order rate (μmol/g/h), T_v is the Vogel temperature, the temperature at which chain segments become frozen in a hypothetical situation, where a polymer is cooled at a quasi-static rate from the rubbery state, A_V is the encounter frequency at T_v, E_{VFT} is the activation energy associated with polymer segmental relaxation, and R is gas constant in J/K mol. T_v is typically 50° below T_g *(28)*. Figure 68 shows the VFT plot for the logarithm of the rate of conversion of OA and 1-NN in PnBMA containing 6% by weight OA and 1-NN and 1% by weight PPL as a function of temperature. Values for E_{VFT} and A_v were determined to be 0.875 kJ/mol and 182, respectively. It was noted that the activation energy associated with segmental relaxation was much smaller than the Arrhenius activation energy. This is understandable since E_{VFT} is related to the temperature difference $T-T_v$ in equation 45, while in the Arrhenius equation 44, the activation energy is related to the absolute temperature T. The pre-exponential factor A_v can be regarded as the encounter frequency when $T_v = \infty$ or $E_{VFT} = 0$, although this could not be true in real systems.

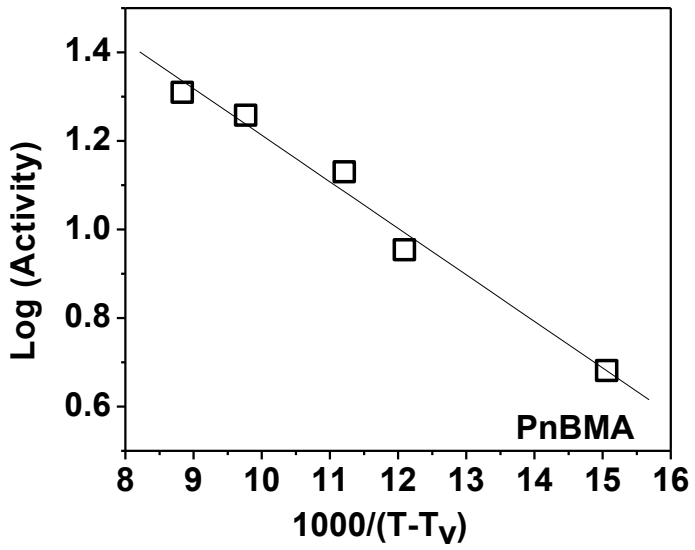

Figure 68. VFT plot of ester synthesis biocatalyst activity as a function of exposure temperature in PMMA films with incorporated stoichiometric amounts of OA and 1-NN 6% by weight and PPL 1% by weight. Line represents best fit of linear function (R^2 = 0.99), and E_{VFT} was calculated to be 0.875 kJ/mol.

The above results suggested that PPL activity in glassy systems was correlated to diminishing excess free volume which is driven by relaxation of polymer chains, i.e., densification. The enzyme activity was dictated from the ability of OA and 1-NN to diffuse via thermally induced hopping in the excess free volume until an active site was encountered, thereby effectively navigating interconnected phase separated regions. However, the glassy free volume is static relative to the translational motion of OA / 1-NN and is largely dependent on the thermal and mechanical history of the sample. As the excess free volume is consumed due to sub-T_g host matrix relaxations, the activity diminished since the OA and 1-NN functionality rich regions transitioned from being interconnected to discrete, which in turn increased the diffusional resistance of OA and 1-NN. In rubbery systems, PPL activity was observed to be of the same order of magnitude as the segmental relaxation processes. The activity depends on the

ability of OA and 1-NN to diffuse via hopping within free volume in interconnected OA and 1-NN rich regions, which is dynamic and constantly fluctuating due to thermal heterogeneities in the films. As the reaction temperatures approach the T_g, the available free volume and the interconnected OA and 1-NN regions approach a static state and deplete the PPL activity. The data was replotted in terms of reduced activity against the departure from T_g to summarize the contributions to activity of different regimes of the host poly (methyl methacrylate) matrices (Figure 69). The data revealed that near and at T_g there was an abrupt change in the rate of reduced activity, which indicated that the percolation pathway of OA and 1-NN and the free volume state were maintained since thermal energy was not causing thermal expansion but was contributing only to the cooperative motion of polymer chains.

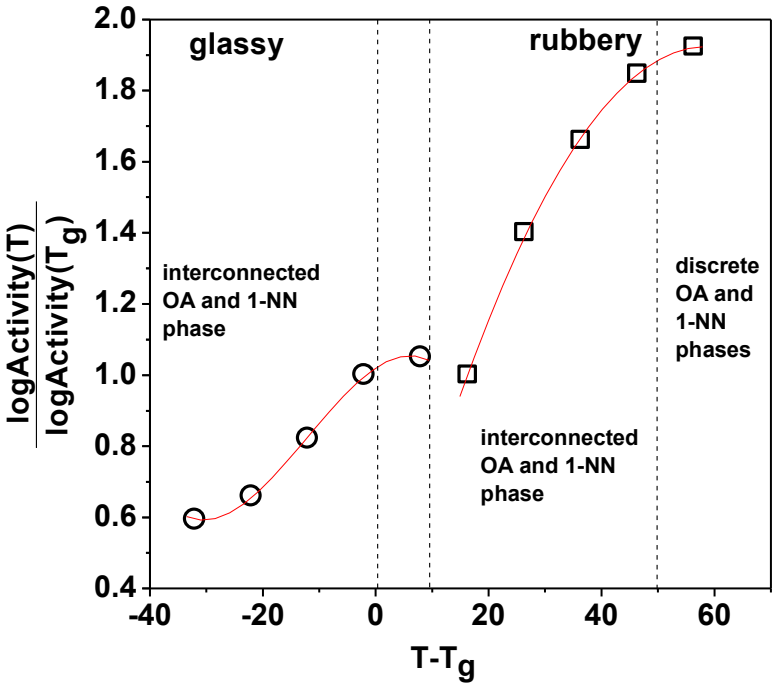

Figure 69. Ratio of activity at temperature, T, to activity at or near T_g , which is termed reduced activity, versus distance from equilibration temperature.

The temperature dependence of PPL activity observed in the amorphous PnBMA above its T_g implies that PPL activity reflects primarily the temperature dependence of internal segmental mobility. This mobility does not only affect the rates of all chain configurational arrangements, but also the combined arrangements of any motile components that interact favorably, i.e., plasticize or solubilize polymer segments. PPL activity reflects the internal mobility of OA and 1-NN and the observed dependence on temperature comes as the result of OA and 1-NN self-diffusion dependence on free volume. Using the same data to further illustrate the effects of departure from T_g, PPL activity at different temperature was analyzed using the Williams-Landel-Ferry (WLF) form *(166)*. The logarithm of the ratio of the PPL activity at temperature, T, to the PPL activity at 30 °C, T_{30} was plotted as the function $T-T_{30}$.

$$\log\left(\frac{\text{Activity}_{PPL}(T)}{\text{Activity}_{PPL}(T_{30})}\right) = \frac{C_1(T-T_{30})}{T-T_{30}+C_2} \qquad \text{Equation 46}$$

The WLF empirical parameters C_1 and C_2 were found to be 2.2 and 6.1 K, respectively. These parameters are specific for a penetrant size and a given polymer system and can be used to predict the dependency and shifts of PPL activity from below and above the T_g well into the rubbery state (T_g+50 °C). The closely coupled behavior of enzyme activity to the segmental relaxation processes in polymers and to the total amount of free volume as described in Chapters V and VI has vast implications on the behavior of reaction rates in confined environments, and understanding these implications are important to reaction design in the condensed polymer phase. In addition, the results provide

novel opportunities for harnessing enzyme-catalyzed chemistries as mesoscopic probes to study polymer behavior, segmental motion limits, and transitions as shown above.

Effects of casting solvent on biocatalyst activity

PPL activity in glassy systems is the result of OA and 1-NN self-diffusion by hopping through static holes in interconnected functional rich phases and is largely driven by the availability of the kinetic trapped excess free volume of the matrix. In glassy matrices, therefore, variations in polymer microstructure arising from the thermal and mechanical history of the sample will dictate PPL activity. Typically, in polymer blends, microstructure is determined only from enthalpic contributions since entropy, in free energy terms, is a relatively small component *(124)*. The enthalpic contributions are related to two portions: the binary interaction parameter (χ_{12}), and the volume fraction of each component *(124)*. The binary interaction parameter is related to the Hildebrand solubility parameter, δ, which estimates the attractive potential between two similar molecules.

To demonstrate that in a glassy polymer, overall activity is driven by non-equilibrium excess free volume, we cast additional PMMA films containing 6% by weight OA and 1-NN, and 1% by weight PPL from various solvents with solubility parameters from 8.8-10 $(cal/cm^3)^{1/2}$, both above and below the solubility parameter of the host glassy PMMA [δ_{PMMA} = 9.3 $(cal/cm^3)^{1/2}$] *(124)*. The hypothesis was that solvent molecules would behave as transient templates via intermolecular interactions with polymer chains during film solidification. Upon evaporation, the solvent would leave a trapped free volume that based on the

difference of $\delta_{solvent}$ and δ_{host} would give rise to various microstructures. Since, it was determined that any relaxation of these structures at 40 °C would be slow relative to the experimentation time scale, we expected to indirectly probe the dependence of PPL activity on the different glassy microstructures. Control experiments were also conducted in organic media with free enzyme to confirm that the observed activity was not due to conversion in the sol portions of the film.

Figure 70 shows the dependency of the host solubility parameter on PPL activity. The observed maxima in PPL activity was attributed to maximum interpenetration of the guest solvent molecules with the host polymer chains during film solidification via intermolecular interactions due to matching solubility parameters. Chloroform and methyl ethyl ketone have greater acidic character than acrylate groups, therefore, chloroform and methyl ethyl ketone interactions are favored relative to acrylate-acrylate interaction *(167)*. Upon solvent evaporation from the sorption sites, the excess free volume left behind was likely higher, thus decreasing the diffusional resistance of OA and 1-NN relative to other polymer-solvent systems and in turn manifesting as higher PPL activity. Active films had similar T_gs ~70 °C across all solvent systems but the dichloromethane system, which had a T_g of 82 °C suggesting that polymer microstructure comprised of lesser free volume relative to the other systems. It is likely that OA and 1-NN were limited to migration within discrete phase separated regions rather than in an interconnected pathway of OA and 1-NN, which lends to the lower observed activity in films cast from dichloromethane. Additionally, films cast from toluene solutions exhibited higher biosynthetic activities than expected.

Since toluene has a relatively basic character and the polymer has an amphoteric character due to the relatively low acidity of the methyl ester group, interactions between chains would be more favored than toluene-chain interactions *(167)*. Therefore, toluene would tend to cluster more than other solvents of this study, i.e., chloroform and MEK, which have relatively acidic character. However, toluene has the largest molar volume of the selected solvents, 106.3 cm^3/mol, compared to 1,4-dioxane, chloroform, THF, MEK (70-80 cm^3/mol), and DCM (63.3 cm^3/mol) *(124)*. Upon toluene evaporation and film solidification, the fraction of free volume would be relatively larger compared to other solvent cast systems lending to higher than expected biosynthetic activity. These results indicate that favorable intermolecular interactions and molar volume are important parameters for a transient template to promote higher biosynthetic activities by increasing the proportion of excess free volume within a polymer.

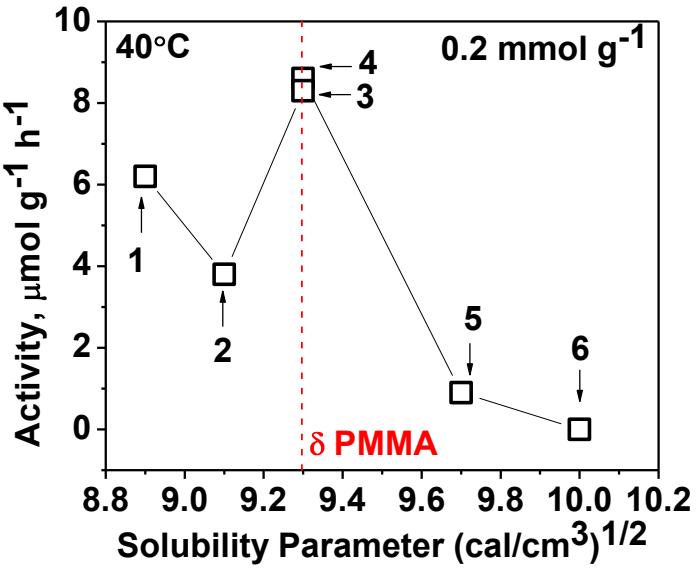

Figure 70. Dependence of ester synthesis biocatalyst activity on the guest Hildebrand solubility parameter in host PMMA film with embedded PPL at 1% by weight and 6% by weight stoichiometric amounts of OA and 1-NN, corresponding to 0.2 mmol/g. Assay was conducted at 40 °C. 1 - toluene, 2 - tetrahydrofuran, 3 - methyl ethyl ketone, 4 - chloroform, 5 - dichloromethane, and 6 - 1,4-dioxane. Films had an average thickness of 160 μm and 6 mm diameter top and bottom.

We examined the effect of solvent evaporation rate on PPL activity since fast evaporation rate could disrupt the enzyme conformation and render them inactive. Slow evaporation could result in high residual solvent content in the film, which would occupy free volume sites and manifest as lower activity. PPL activity was plotted versus the evaporation rate for the various solvents employed to cast the films (Figure 71a). The graph does not indicate an observable dependency on the evaporation rate of the solvent as an individual controlling factor of PPL activity in the 160 μm film thickness range. The strongest comparison is seen for films cast singularly from MEK and $CHCl_3$ that consistently proved to have similar activities. The results suggested that thicker films aid in the maintenance of active enzyme conformation during the drying stages by limiting enzyme exposure to the higher vapor pressure solvent in the

system. It is likely that solution cast thinner films would result in disruption of enzyme conformation and activity since film shielding of the enzyme from higher vapor pressure solvent molecules would diminish.

We also examined the effect of solvent partition to determine whether the observed trend in films cast from different solvents were due to the differential partitioning of reactants in the solvent phase within “sol” portions of the film based on solvent polarity. Solvent polarity is quantified by the logarithm of the partition coefficient, log (P), of the solvent, which is determined by the degree of the solvent partition (SP) in octanol relative to water *(168)*.

$$\log(P) = \log\left(\frac{SP_{octanol}}{SP_{water}}\right) \qquad \text{Equation 47}$$

The plot of log (P) of the guest solvent molecules on PPL activity is shown in (Figure 71b). The data did not indicate any correlation between the log (P) of the solvent and PPL activity. This confirmed that enzyme activity in glassy films is not driven by the preferential partition of OA and 1-NN within distinct sol phases but by the fraction of free volume resulting from enthalpic interactions among polymer chains and solvent molecules.

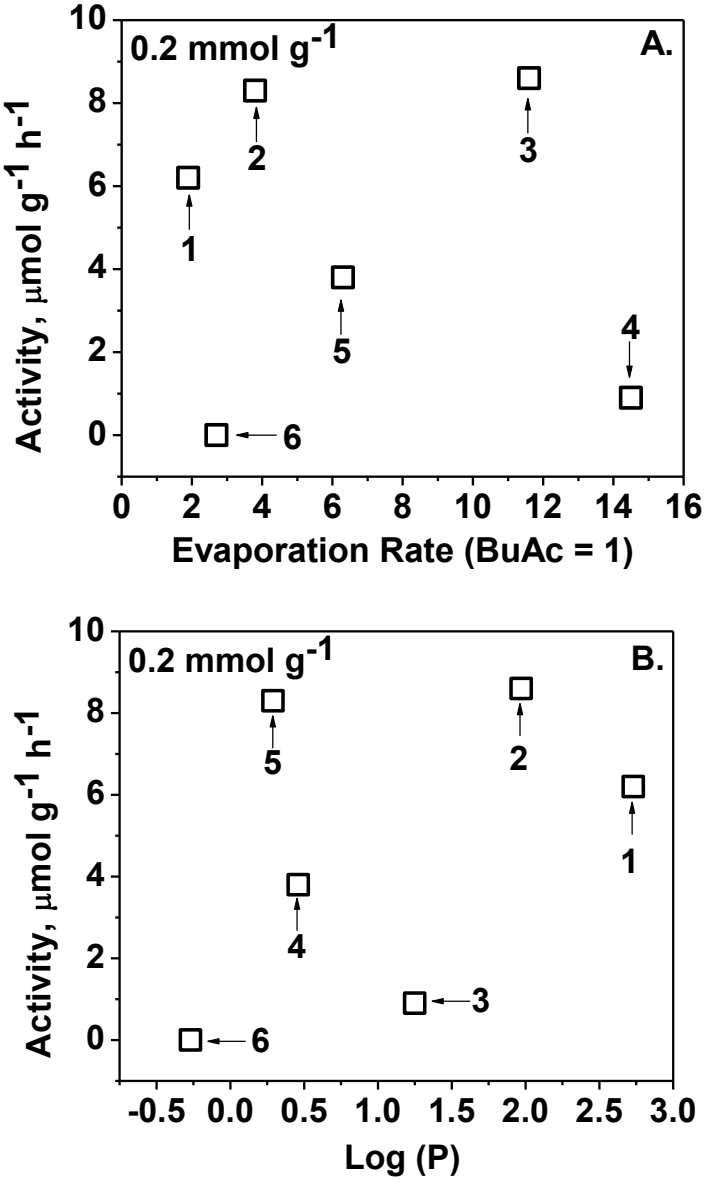

Figure 71. Data replotted to investigate the dependence of ester synthesis biocatalyst activity on: A) evaporation rate of the organic solvent used in film casting, and B) log (P) of the organic solvents used in film casting. PMMA films with embedded PPL at 1% by weight and 6% by weight of stoichiometric amounts of OA and 1-NN, corresponding to 0.2 mmol/g. Assay was conducted at 40 °C. 1 - toluene, 2 - methyl ethyl ketone, 3 - chloroform, 4 - dichloromethane, 5 - tetrahydrofuran, and 6 - 1,4-dioxane. Films had an average thickness of 160 μm and 6 mm diameter (top and bottom).

Interestingly, in organic solvent enzymology, the preferential partition of reactants and products in solvents versus enzyme microenvironment ,i.e.,

solution-enzyme interphase, is used to optimize enzyme activity *(157)*. Typically, similar log (P) values of reactants and enzyme microenvironment will drive the reactant to the interphase and to the enzyme active site for catalysis *(157)*. Additionally, similar log (P) values of the product and the organic phase will drive product diffusion to the organic phase, thereby clearing the active site for another reactant and avoiding saturation *(157)*. To demonstrate that drivers for catalysis are different in solution versus glassy films, we examined PPL activity in organic solvents while maintaining a similar relative molar ratio of OA and 1-NN to the total material weight, i.e., 6 wt% OA and 1-NN (0.2 mmol/g), and 1 wt% PPL. Figure 72 shows the plot of PPL catalyzed conversion of OA and 1-NN to NOc in an organic solvent at 40 °C versus the log (P) value of the solvent. The data indicated greater PPL activity for solvents with higher log (P) values, i.e., as the solvent becomes increasingly nonpolar. The results confirm that in nonpolar solvents, the polar OA and 1-NN molecules are driven to migrate to the polar enzyme microenvironment and result in higher observed activity.

We also evaluated the possibility that the lower activity observed in more hydrophilic solvents could be due to biocatalyst denaturation by the solvent stripping off the essential water layer around the enzyme. According to literature reports, PPL, unlike the majority of biocatalysts, is robust due to its hydrophobic nature, i.e., it has less tightly bound water, since *in vivo* it functions in extreme lipid-like environments *(4,157)*. Consequently, we did not expect significant loss of active enzyme conformation in hydrophilic solvents. However, in 1,4-dioxane,

no activity was observed in glassy films or organic media, indicating that it was the method of introducing PPL to 1,4-dioxane that caused denaturation.

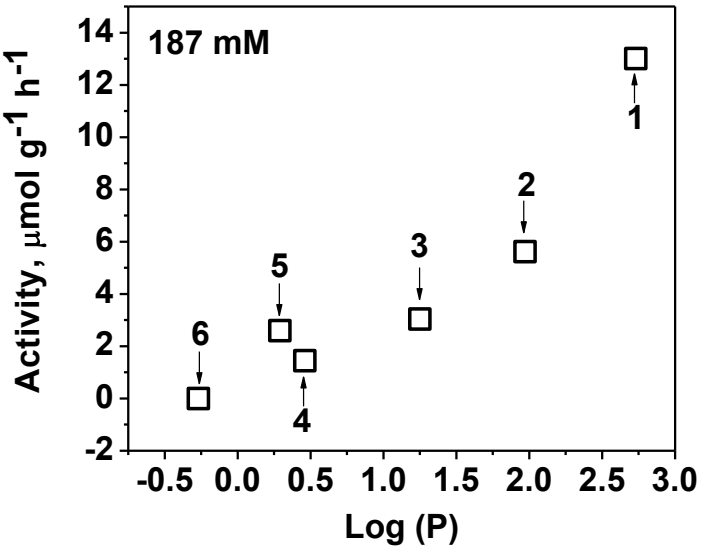

Figure 72. Ester synthesis biocatalyst activity versus log (P) of the organic solvents. 187 mM OA and 1-NN solutions (corresponding to 0.2 mmol/g) were prepared with 1% by weight PPL in organic media, and the assay was conducted at 40 °C. 1 - toluene, 2 - chloroform, 3 - dichloromethane, 4 - tetrahydrofuran, 5 - methyl ethyl ketone, and 6 - 1,4-dioxane.

The activity data shown in Figure 72 was replotted in terms of the Hansen solubility parameter, δ (Figure 73). The data did not manifest any trends of activity in terms of δ, which indicated that solubility parameters are not good predictor of enzyme activity in solution. Laane and coworkers determined that enzyme and immobilized cell activity did not show any discernible trends when compared to the δ parameters of organic solvents *(169)*. The lack of correlation was attributed to the dependency of δ on the solvent heat of evaporation, which stresses polar interactions more than nonpolar dispersion forces *(169)*. These results confirmed that drivers for biocatalyst activity in glassy film versus organic media are vastly different even though the same relative ratio of OA and 1-NN to the total weight was used throughout different systems. In glassy films, the

kinetically trapped microstructures dictate the ability of small molecule functionality to reach the enzyme active site. However, in organic media, the drivers of biocatalyst activity are the ability of the functionality to selectively partition in the enzyme-solution interphase region.

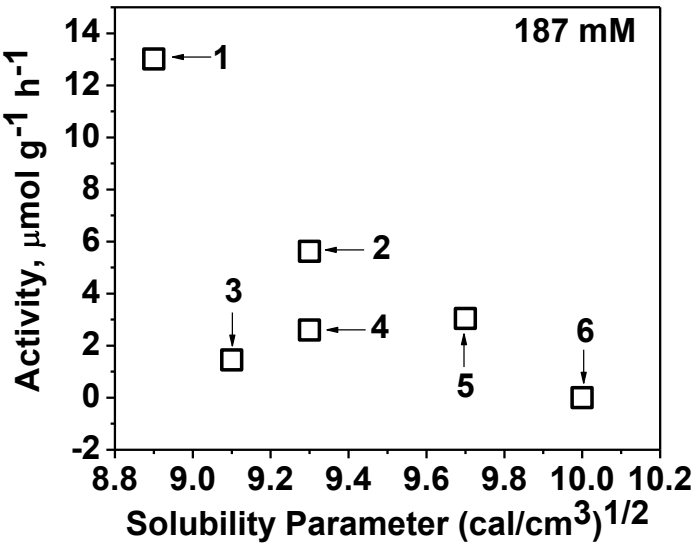

Figure 73. Solution activity data replotted versus Hildebrand solubility parameter, δ, of the organic solvents. 187 mM OA and 1-NN solutions (corresponding to 0.2 mmol/g) were prepared with 1% by weight PPL in organic media, and the assay was conducted at 40 °C. 1 - toluene, 2 - chloroform, 3 - tetrahydrofuran, 4 - methyl ethyl ketone, 5 - dichloromethane, and 6 - 1,4-dioxane.

Correlation of film water content to synthetic and hydrolytic activity

In many applications of polymers, it would be advantageous to reversibly alter the material's surface properties, e.g., hydrophobic and hydrophilic, bulk properties, e.g., modulus, degree of stiffness, resiliency, and impact strength. One route to reversibly alter the material's surface and bulk properties is to modify the chemistry of functional groups incorporated in the film, coating, or membrane. Equilibrium driven reactions with embedded functional groups have the potential to provide surface and bulk material property shifts on an environmental condition specific basis. We tested the hypothesis that the water

content of the glassy film determines whether the biocatalyst exhibits synthetic or hydrolytic activity. Equilibrium water content can be controlled by both environmental conditions and the polymer material properties. The experiments below were designed to test the practical limits for adjusting the ratio of reactants to products in polymer films by using external/environmental water content. PMMA films were solvent cast containing various weight fractions of OA and 1-NN, and 1% by weight PPL, initially maintained at 30% humidity, and after a period of time were exposed to 100% humidity. Figure 74 shows the amount of NOc synthesized in PMMA films at various humidity levels as a function of time.

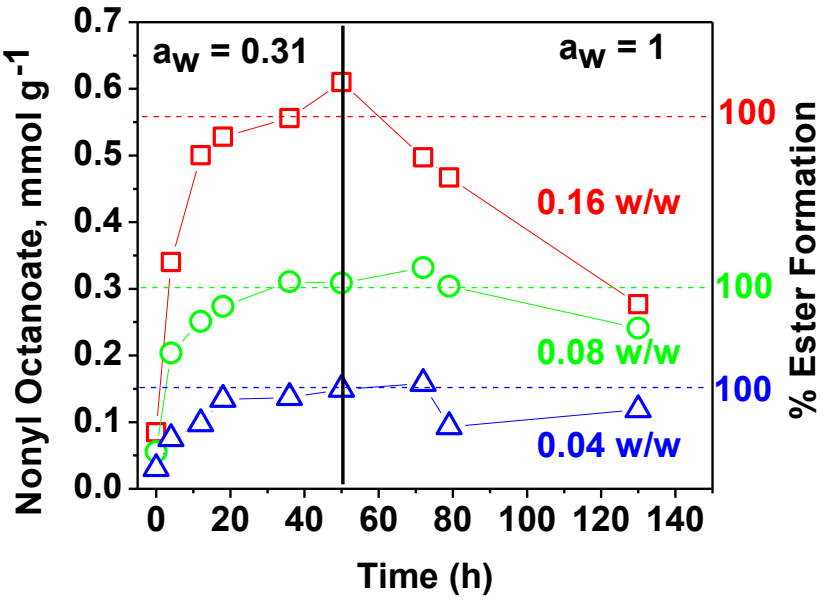

Figure 74. NOc synthesis as a function of time and humidity in PMMA films containing stoichiometric amounts of OA and 1-NN at different weight fractions and 1% by weight PPL. The solid vertical line indicates switching of the relative humidity (RH) from 0.31 to 1. The horizontal dashed lines indicate the theoretical yield for various initial OA and 1-NN loading.

The data suggested that at low humidity and during the initial stages of the reaction, NOc concentration in the film increased until it reached a plateau at different levels depending on the initial OA and 1-NN weight fractions. Once the

environmental chamber humidity was adjusted to 100% relative humidity (RH), depicted in Figure 74 by the solid black line, the NOc ester concentration diminished and exhibited higher rates of change at higher weight fractions of OA and 1-NN. By switching the environmental conditions, i.e., chamber humidity, the system's ester content was reduced.

To get a better understanding of the rate-limiting processes and parameters arising during repeated exposure to moisture and to determine the capacity for cyclic reversibility of the process, PEMA films containing 6% by weight, OA and 1-NN, and 1% by weight PPL were blended, cast, and evaluated by GC-MS and NIR spectroscopy for ester and water content, respectively (Figure 75). The following sentences describe the results, followed by a discussion in the next paragraph. Films were dried at ambient for 9 h and the water content of the films at t=0 h was set at 1. Upon exposure to 40 °C in a dessicator, the water content dropped ca. 20% relative to the starting value, while the ester content reached 80% of the theoretical yield. Films were then exposed to 100% RH chamber equilibrated at 40 °C, which caused the water content to increase to ca. 20% relative to the initial content, while ester content diminished by 50%. These values were maintained even after continuous exposure for 24 h. Next, films were exposed to a dessicator chamber at 40 °C again and exhibited a T_g of 46 °C. The water content diminished again, however only ca. 10% relative to the initial value during 100 h exposure. To drive water off and ester formation up at quicker pace, films were exposed to 50 °C or 4 °C above T_g, followed by exposure to 60 °C or 14 °C above T_g. Interestingly, exposure to 50 °C for 48 h

drove water content down by an additional 5%, while ester content reversed to similar values as prior exposure to 100% RH. At 60 °C, the water content was down ca. 30% relative to the starting amount, and the ester content exhibited increasing values. Films were exposed again to 100% relative humidity at 40 °C and water content increased by 30% of the initial value within 48 h of continuous exposure. Despite the quick increase in water content, ester content continued to increase, eventually dropping off 24 h after exposure at 100% RH. The observed lag time suggest the presence of distinct domains of ester and water and that the reaction was dependent on the diffusion of water from the water domains to the ester domains. The low ester value was maintained even after 48 h of the experiment completion.

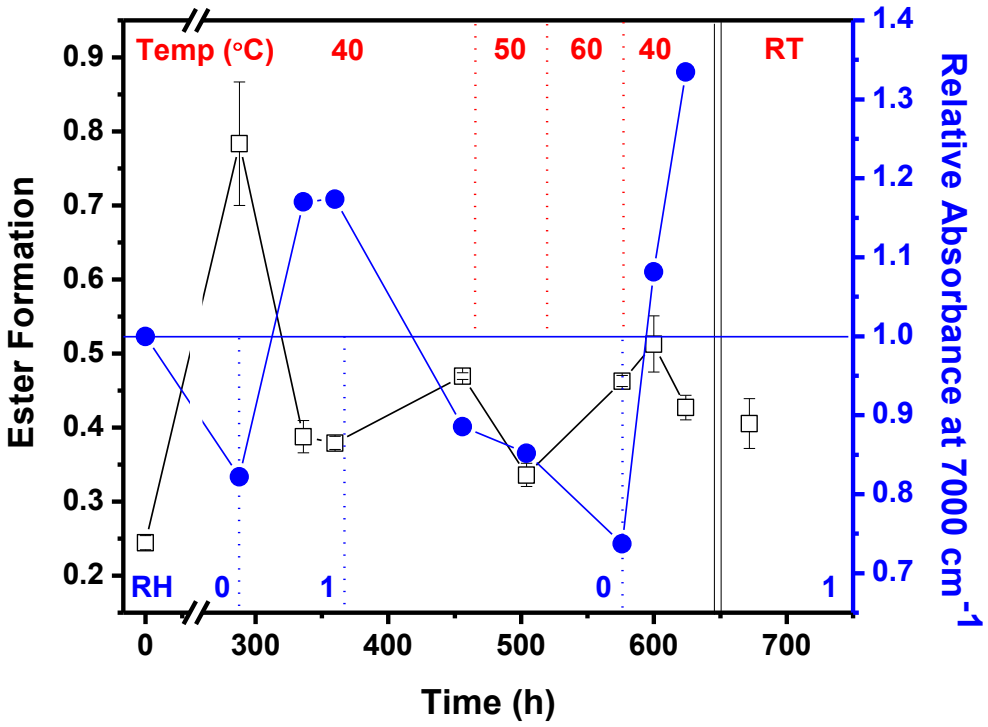

Figure 75. Dependence of NOc content on switching the chamber humidity "on" and "off" in PEMA films containing 6% weight fraction of OA and 1-NN and 1% weight fraction of PPL at 40 °C. The horizontal line represents water content at the beginning of the study. Values above or below depicted with –●–represent depletion or repletion relative to beginning water content. The fraction of ester formation is depicted with –■–. The top and bottom part of the graph depict the temperature and relative humidity regimes, respectively, that films were continuously exposed. Films had an average thickness of 140 μm and 6 mm diameter top and bottom

The analysis of the results was based on the free volume differences in the presence and absence of water in the glassy and the rubbery state. We believe PALS analysis of the films is important to confirm the free volume state of these materials. However, the following discussion is based on activity differences with the intent to serve as a hypothesis that addresses the activity differences that were observed.

These results again confirmed the NOc ester synthesis was dependent on the environmental conditions and was shown to be reversible by turning "on" and

"off" the chamber humidity. The data suggested that there was some control of the NOc concentration in the PEMA film by switching the humidity "on" and "off". However, a lag time in the response was observed after the first cycle. The presence of water changes the dynamics within the film as water acts both as a reactant and plasticizer. In the glassy state, upon initial exposure, water likely associated closely with OA and 1-NN domains changing the local equilibrium against ester synthesis. In addition, water also likely created water-only-domains as predicted by the dual-mode sorption theory *(170)*. Once exposed to a dry environment in the glassy state, water was driven away from small molecule domains, which shifted the equilibrium towards ester synthesis. At temperatures above T_g, the small molecule functional groups and water domains redistributed shifting the local equilibrium against ester synthesis, i.e., water-functional group domain mixed. Upon continuous exposure to dry environment and temperatures above T_g, water was driven away further from the film, i.e., 30% relative loss, which allowed ester synthesis to progress. Once the films were exposed to 40 °C, i.e., temperature below film T_g, and 100% relative humidity, water quickly occupied holes previously left behind in 48 h with 30% relative gain in water content. We suspected that water acted as transient template when removed in films above film T_g. When films were cooled to below T_g, the holes were preserved and occupied at faster pace by incoming water. In the first 24 h (ca.8% relative water gain), ester synthesis continued to occur in the OA and 1-NN domains as water was initially driven to empty space. Once the water

reached the 30% relative gain, ester synthesis reversed as water began to absorb in OA and 1-NN rich regions of the film.

Finally, a PEMA film containing 6 wt% OA and 1-NN and 1 wt% PPL was cast from solution, dried for 9 h, placed at 40 °C, and exposed in cyclic manner to 0% and 100% RH. During exposure to 0% RH the lipase-catalyzed reaction was driven towards NOc synthesis, while during exposure to 100% RH the reaction was driven towards the reformation of OA and 1-NN. It was determined that 12 h exposure at 100% RH was the effective time to hydrolyze at least 45% of the NOc dispersed in the film (Figure 76).

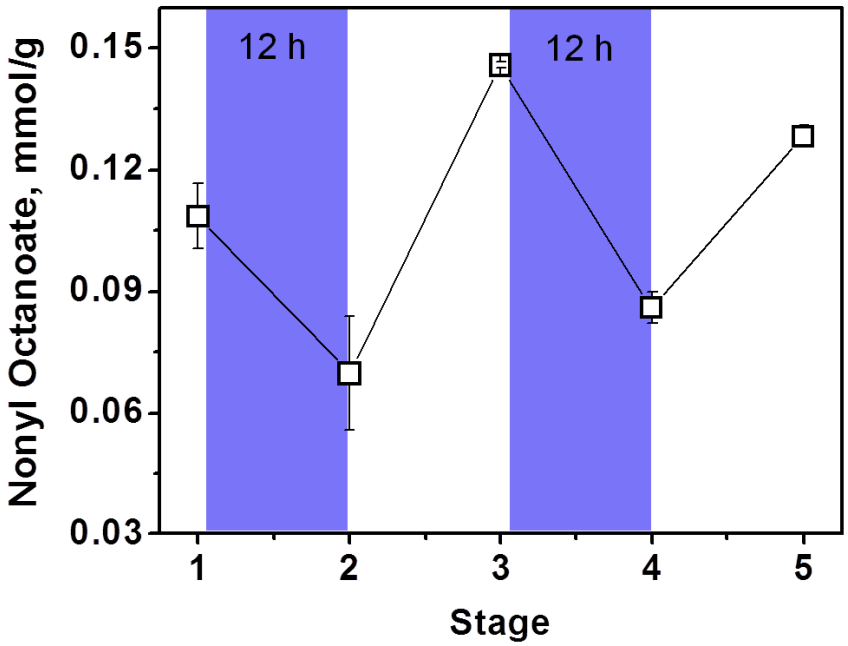

Figure 76. Dependence of NOc content on switching “on” and “off” the chamber humidity in PEMA films containing 6% weight fraction of substrates and 1% weight fraction of PPL at 40°C. The shaded regions represent exposure to 100% RH for 12 h, while the non-shaded region represents exposure to 0% relative humidity. Films had an average thickness of 150 μm and 6 mm diameter top and bottom

Conclusions

The temperature dependence of biocatalytic activity was examined in glassy and rubbery polymers. In glassy polymers, the first stage of ester formation rate exhibited a strong dependence on sub-T_g aging of polymer. Biocatalytic activity was driven by small molecule migration in kinetically trapped excess free volume within interconnected OA and 1-NN rich regions. It was found that when the glassy polymer was annealed ($T_{rxn} > T_g$), biocatalytic activity became increasingly diffusion controlled, which was attributed to polymer losing excess free volume and the formation of discrete OA and 1-NN rich regions. In rubbery polymer control systems, biocatalyst activity was driven by the diffusivity of OA and 1-NN within interconnected functional group rich regions as evidenced by activity temperature dependence best described by VFT and WLF models. At temperatures above 60 °C, corresponding to temperatures 50 °C above T_g, biocatalytic activity became dependent on the migration of OA and 1-NN from discrete functional group rich microphases corresponding to diminishing standard energy of activation.

Bioactivity studies in blends cast from various solvents validated that enzyme activity was largely dependent on glassy microstructure. A spike in bioactivity was observed when the solvent solubility parameter was matched with that of the host matrix indicating that solvent molecules act as transient templates, which upon evaporation leave behind free volume sites. Favorable attractive interactions and large transient molecule molar volume were identified as key parameters that promoted microstructures consisting of relatively high

fraction of free volume and interconnected OA and 1-NN pathways, which resulted in higher relative bioactivity. Additionally, the observed trend in activity was not dependent on solvent evaporation rate or selective partitioning of OA and 1-NN within discrete sol microphases determined by comparison with data from analogous studies in organic media.

The consistent near ambient activity characterized in these films containing enzyme and small molecules functional groups validate a broad range of conditions that support the biocatalytic reaction. The systems studied exhibit potential as materials with switchable surface properties, e.g., hydrophobic and hydrophilic, bulk properties, e.g., modulus, degree of stiffness, resiliency, and impact strength, via equilibrium control of environmental conditions to alter the ratio of reactants to products. We demonstrated that in PMMA and PEMA films with embedded biocatalyst alongside embedded functionality, the conversion of OA and 1-NN to NOc was reversible based on the equilibrium water content.

Supplemental Information

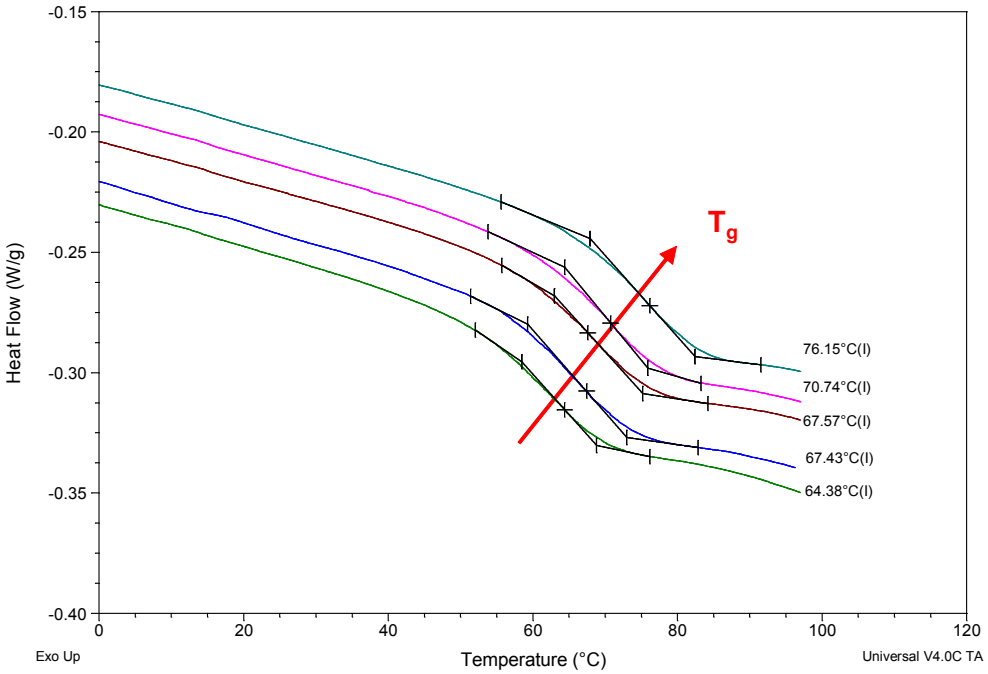

Figure 77. DSC thermograms of the third cycle of heat/cool/heat program of PMMA films embedded with 6% by weight initial loading of OA and 1-NN and 1% by weight PPL, and exposed to different temperatures from bottom to top corresponding to: 30 °C, 40 °C, 50 °C, 60 °C, and 70 °C for 75 h.

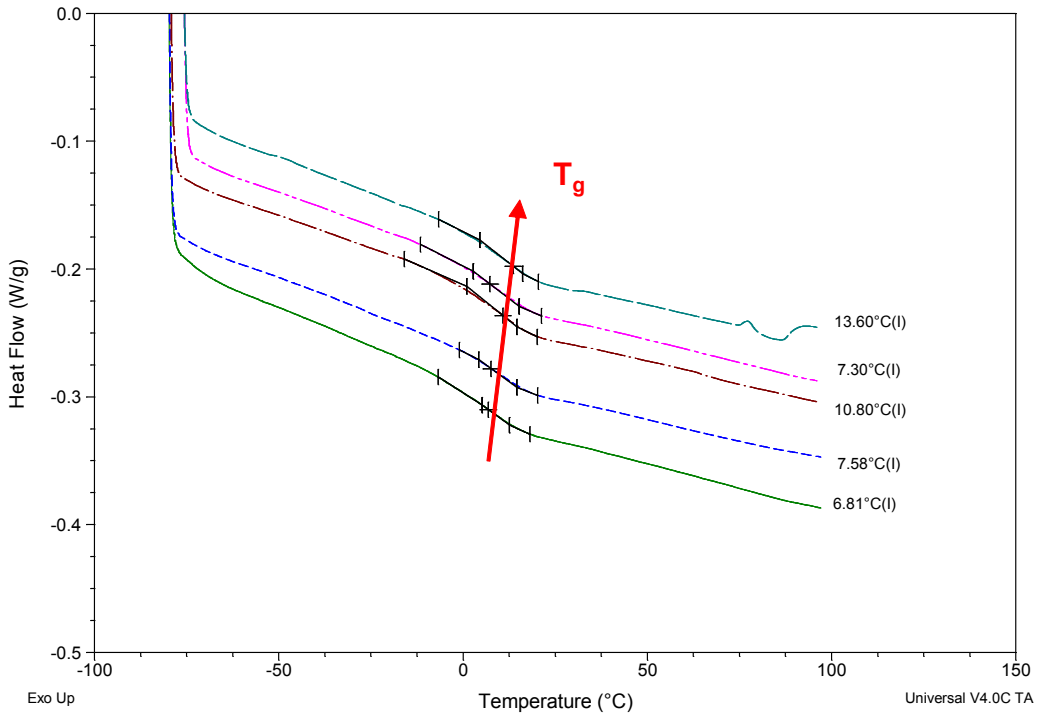

Figure 78. DSC thermograms of the third cycle of heat/cool/heat program of PnBMA films embedded with 6% by wt initial loading of OA and 1-NN and 1% by wt PPL, and exposed to different temperatures from bottom to top corresponding to: 30 °C, 40 °C, 50 °C, 60 °C, and 70 °C for for 50 h.

CHAPTER VII

BIOACTIVE COATINGS FROM POLYFUNCTIONAL COMB-LIKE COPOLYMER BLENDS

Abstract

Developing functional coatings and films to expand the utility of current organic materials has drawn considerable interest in literature. We investigated an approach to engineer materials capable of reversible crosslinking by immobilizing enzymes in matrices containing multifunctional comb-like –COOH and –OH copolymers for adhesives, elastomers, composites, and laminates applications. Coatings comprised of the polyfunctional polymer blend and lipase enzyme at 1-4 wt% by weight on solids were cast on glass and aluminum substrates. Acid equivalents, final molecular weight, and T_g progression over time were used to quantitatively assay the enzyme-catalyzed reaction between the two functionalized components up to 250 hours. In rubbery copolymer blends, the consumption of acid functionality corresponded to an increase in molecular weight with similar reactivity rates.

Introduction

Traditionally polymers are designed to have irreversible covalent bonds and repeat structures that afford fixed macromolecular architectures and translate to macroscopic properties required for a specific end-use application. The dynamic nature of the end-use environment and the inherent anisotropy of polymer materials inadvertently promote material vulnerabilities to compound over time and lead to diminished properties during end use, regardless of the

application. The loss in properties have been linked to chain pull out and chain scission events that originate from continuous or cyclic exposure to photochemical and mechanical energy *(171,172,173)*. Our research efforts have focused on developing strategies to prevent undesirable loss of properties by introducing catalytic mechanisms that support a steady-state number of covalent bonds for a defined period triggered by equilibrium shifts or changes in macromolecular architecture that result from failure mechanisms.

Research efforts to design mechanically dynamic materials stemming from controlling molecular events, such as chain coupling, chain scission, and non-covalent interactions, have led to the development of a plethora of materials that display remarkable property changes. In response to thermal, chemical, or electrical stimuli, these materials exhibit changes over several orders of magnitude ranging from low viscosity fluids to mechanically stable gels *(146)*. For example, a blend of oligomers containing ureas and amides derived from multifunctional fatty acids displayed a soft rubbery behavior due to intermolecular hydrogen bonding *(148)*. Despite its oligomeric nature, a non-tacky material with T_g of 8 °C was afforded that displayed rubber-like elastic behavior *(148)*. Interestingly, at RT, i.e. T-T_g of 18°C, the material was able to non-covalently re-tether upon fracture and gain initial properties without additional heating *(148)*. Although the majority of mending capability was afforded by the inherent flow characteristics of the oligomers, the reversible spatial arrangement of intermolecular hydrogen bonding did facilitate recovery subsequent to fracture *(148)*. The dynamic macroscopic behavior derived from the incorporation of

reversible covalent bonds was exemplified in solutions of alkoxyamine-functionalized polymers cast as thermoplastic and thermoset materials *(174,175)*. Upon heating, these materials dissociate into a stable nitroxide radical and a reactive radical capable of re-tethering inter- or intra- molecularly via radical exchange reactions to yield liquid-to-gel transitions or gels with adjustable mesh sizes *(174,175)*. Unfortunately, materials capable of stimuli-responsive transitions described in the open literature have very low moduli and have limited use for applications that depend on material toughness and stiffness.

Enzyme-catalyzed reactions in constricted media present the opportunity to access structurally adaptive films that use enzyme responsive bonds to maintain an equilibrium number of covalent bonds. Enzymes are very versatile catalysts in terms of types of functional group transformations and the range of operating conditions. Engineering systems to fully use enzyme catalytic properties has the potential to yield films and coatings with novel functionalities or combinations thereof. For example, organophosphorous hydrolase (OPH) has been incorporated in various coatings to impart the additional functionality of degrading chemical warfare agents *(61)*. The advent of enzyme immobilization can be traced to the need of a variety of applications, e.g., heterogeneous biocatalyst, selective adsorbents, controlled release protein drugs, analytical devices, and solid phase protein chemistry for insoluble enzymes *(8)*. In heterogeneous biocatalysis, immobilized enzymes are routinely used for a variety of polymer synthesis, e.g., polyesters, polyphenols, polyanilines, and poly(alkyl acrylates) *(85)*. Enzyme-catalyzed polymerizations have been shown to occur

both in bulk and solution conditions *(85)*. The immobilization matrices used in these previously mentioned applications are engineered to be inert and simply serve as catalyst supports *(8)*.

In the previous chapters, we established a theoretical and experimental framework for the kinetic behavior of enzyme-catalyzed reactions in glassy and rubbery polymers containing freely diffusing small molecule functionality. It was shown that the esterification reaction was dependent on the fraction of free volume and could be reversed in the presence of water. In this chapter, we extended the previous studies to rubbery and glassy polymer systems that contain tethered functional groups with the goal of engineering materials capable of reversible crosslinking reactions in the solid state. The immobilization matrix comprised of comb-like copolymers with a tethered functionality favored for catalytic action by an enzyme (Figure 79). Copolymers containing pendant hydroxyl and carboxylic acid functional groups along their backbone were synthesized via conventional free radical polymerization and cast with enzymes to yield stoichiometrically adjusted polyfunctional blends (Figure 80). The questions we set out to answer were *how* does polymer reactivity in the condensed polymer phase affect the final properties of the blend at temperatures above T_g, and *what* are the glassy limits for enzyme-catalyzed crosslinking to be observed?

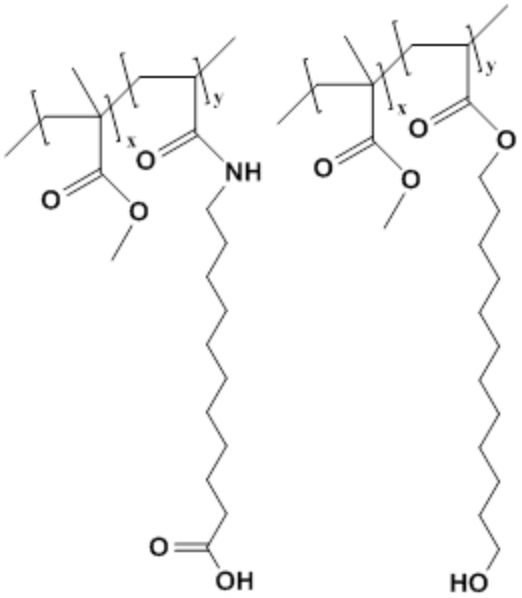

Figure 79. Scheme depicting pendant carboxylic acid functionalized polymer along acrylate/acrylamide backbone and pendant hydroxyl functionalized polymer along acrylate backbone.

The film T_g was systematically varied by the addition of butyl acrylate units in the final copolymer structure, while the functionality was controlled by adjusting the molar ratio of functional monomers to the total weight of functional and nonfunctional comonomers. The systematic variation in T_g and functional equivalent weight facilitated the identification of conditions under which enzymes could catalyze intermolecular reactions and produce crosslinked coatings. The experimental set up served as platform to study the kinetic behavior of enzyme-catalyzed conversions of functional groups tethered to the matrix. In addition, the developed raw materials and novel formulations serve as materials with reversible bulk properties for adhesives, elastomers, composites, and laminates applications.

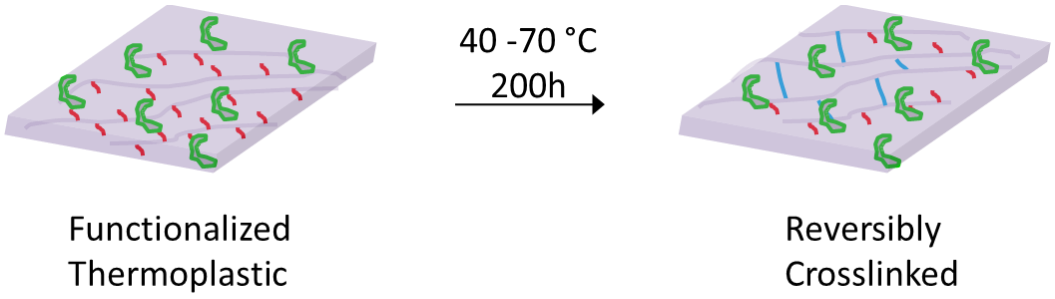

Figure 80. Coating from "comb-like" polyfunctional blend in the presence of lipase acrylic resin from *Candida Antarctica* (CAARC) at 70 °C for up to 200 hours. Biocatalyst (●) dispersed in a coating (rectangle) from polyfunctional blend comprised of –COOH and –OH functional pendant groups (lines).

Results and Discussion

Enzyme-catalyzed transformation of the polymer side chains require interactions of the reactive groups with the enzyme active site. Spacing of the reactive groups away from the polymer backbone would prevent the polymer chain from sterically hindering the enzyme from the reactive groups via van der Waals or dipole interactions. Solution studies of the α-chymotrypsin catalyzed hydrolysis of the *p*-nitroanilidine group in acrylamide copolymers has shown that the rate decreased sharply when the reactive site was less than five methylene units away from the polymer backbone *(126)*. In addition, the molecular weight of polymer solutions did not affect the rate of side chain hydrolysis *(176)*. Table 16 summarizes comb-like acrylic and acrylamide copolymers containing –COOH and –OH pendant groups synthesized with the reactive groups positioned at varying distances from the polymer backbone. The detailed synthetic procedures and labels for the monomer and the respective copolymers are described in Chapter III.

Table 16

The Distance of the Reactive Groups Expressed in Methylene Units from the Copolymer Backbone and the Nomenclature of Synthesized Polymers

"Comb-like copolymers"	**-OH functionalized**	**-COOH functionalized**
Polymer nomenclature	$AC(CH_2)_nOH$-MMA-BA $AC(CH_2)_{12}OH$-MMA	$AM(CH_2)_{10}COOH$-MMA-BA $AM(CH_2)_{10}COOH$-MMA
Methylene units from backbone	2, 8, 12	10

Effect of side chain length on the enzyme-catalyzed coupling in soft condensed matter above the T_g

Initial studies involved equal weight (–OH:–COOH molar ratio 1.7:1) blends of $AC(CH_2)_2OH$-MMA-BA (M_n = 17,218, FEW = 1,069, T_g = 0.83 °C) and $AM(CH_2)_{10}COOH$-MMA-BA (M_n = 11,494, FEW = 617, T_g = -2.24 °C) that were cast from a THF solution containing 1 wt% on solids PPL and cured at various temperatures. The blends registered a single T_g of 0.14 °C indicating that macrophase separation did not occur upon casting and vacuum drying for 24 h. Acid equivalents, T_g, and molecular weight were determined at specific intervals during exposure to different temperature regimes. Blends cured at 105 °C in the absence of PPL exhibited the most significant drop in acid equivalents, approximately 70% in 150 h and the quickest gain (30 °C) in T_g within 24 hours to reach 15 °C (Figure 81 and 82). Some of the T_g increase was attributed to equilibrium relaxation, i.e. physical aging, of the bulky polymer. However, the T_g increase was more pronounced than in samples that did not exhibit loss of –COOH equivalents. Since higher T_g values with cure were observed in all systems, we were unable to determine network structural characteristic such as crosslink density or M_c for samples cured at 105 °C. The crosslinking reaction

was confirmed by analyzing the coating solubility in THF. After 150 h, the coating was insoluble in THF, and the molecular weight of the soluble fraction was 4,960 g/mol (compared to the initial molecular weight of each component 17,218 and 11,494). The samples cured at 40 °C in the presence and absence of PPL did not result in significant loss of acid equivalents, which indicated that the enzyme catalyzed reaction of –COOH and –OH pendant reactive groups did not occur at 40 °C. The T_g reached approximately 10 °C in both low cure temperature blends. The observed T_g increase was attributed to volume relaxation of the coating since T_{cure}-T_g was 30 °C. The coatings remained soluble throughout the 250 h curing period, and the final molecular weight was 10,800 for the PPL containing blend, and 9,200 for the blend absent of PPL. The relaxation behavior observed as gain in T_g at low cure temperatures, i.e., 40 °C, indicated that polymer chains exhibited mobility, however, the polymer chains did not exhibit enzyme-catalyzed reactivity. We hypothesized that the lack of reactivity was due to the proximity of reactive hydroxyl groups to the polymer backbone (two methylene units), which sterically hindered the functionality from interacting with the enzyme active site. In addition, poor compatibility of the biocatalyst with the resin could have led to phase separation of biocatalyst and lack of accessibility of the functional groups to the enzyme active site. Both these issues were addressed in subsequent studies.

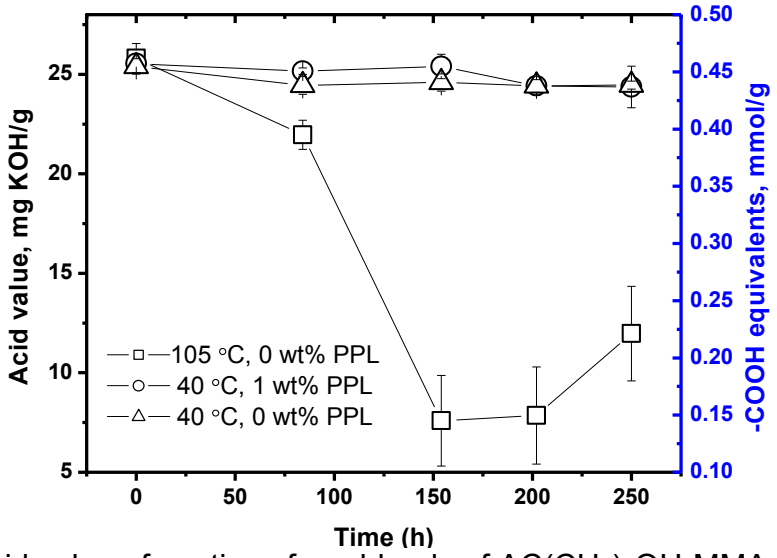

Figure 81. Acid value of coatings from blends of $AC(CH_2)_2OH$-MMA-BA (M_n = 17,218, FEW = 1,069, T_g = 0.83 °C) and $AM(CH_2)_{10}COOH$-MMA-BA (M_n = 11,494, FEW = 617, T_g = - 2.24 °C) cured at 40 °C with 1 wt% PPL (---O---), 40 °C (---Δ---), and 100 °C (---□---) in the absence of enzyme.

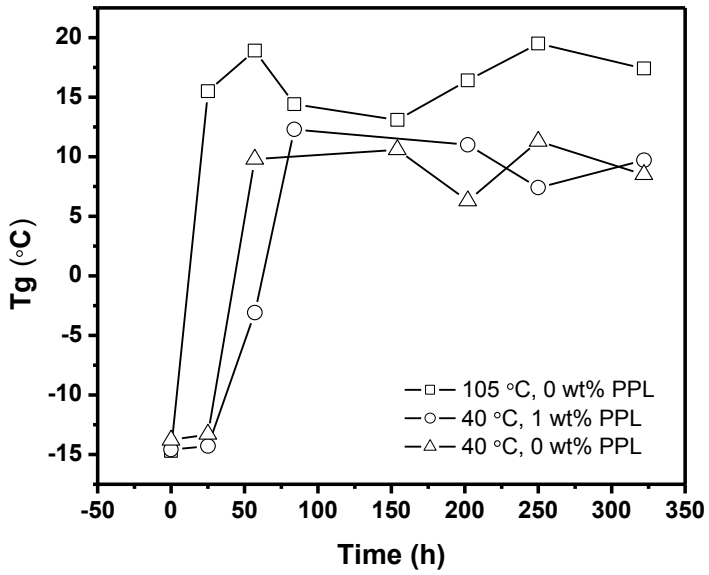

Figure 82. T_g of coatings from blends of $AC(CH_2)_2OH$-MMA-BA (M_n = 17,218, FEW = 1,069, T_g = 0.83 °C) and $AM(CH_2)_{10}COOH$-MMA-BA (M_n = 11,494, FEW = 617, T_g = - 2.24 °C) cured at 40 °C with 1 wt% PPL (---O---), 40 °C (---Δ---), and 100 °C (---□---) in the absence of enzyme.

Further studies focused on stoichiometric blends of $AC(CH_2)_{12}OH$-MMA-BA (M_n = 13,200, FEW = 990) and $AM(CH_2)_{10}COOH$-MMA-BA (M_n = 6,700, FEW = 1,250, T_g = -18.30 °C) where –OH and –COOH reactive sites were 12 and 10,

respectively, methylene units away from the backbone (synthesis and resulting properties are described in detail in Chapter III). Coatings were cast from THF solutions containing 1 wt% on solids Lipase acrylic resin from *Candida Antarctica.* The T_{cure} was set at 88 °C above the coating blend T_g, i.e., 70 °C, whereby sufficient mobility of polymer chains was expected to monitor the enzyme-catalyzed coupling of pendant groups. In addition, the biocatalyst used in this study is typically used as a heterogeneous catalyst in polyester synthesis, thus avoiding compatibility issues of the resin with the biocatalyst.

The progression of the enzyme-catalyzed transformation was followed via end-point titration for –COOH functional groups and GPC for the resulting molecular weight. The –COOH equivalents diminished over time reaching 30% conversion in 150 h (Figure 83). Since polyesterification reactions are assumed to be second-order reactions, the conversion was written in terms of Carothers equation and plotted versus time *(177)*. The observed second-order rate was 0.0033 h^{-1} based on the consumption of acid equivalents. As the acid equivalents were consumed in second-order fashion, a similar second-order trend was observed in increase of molecular weight by GPC (Figure 83). M_n and degree of polymerization were plotted as a function of reaction time and yielded a second-order rate of 0.0039 h^{-1}. The similarity in rates signifies that the diminishment of –COOH equivalents is related to the increase in observed molecular weight, and that a portion of the functionalized tethers in the blend reacted to form the corresponding coupled ester products. Control samples did

not show appreciable changes in acid equivalents, exhibiting only a 10% drop over 200 h.

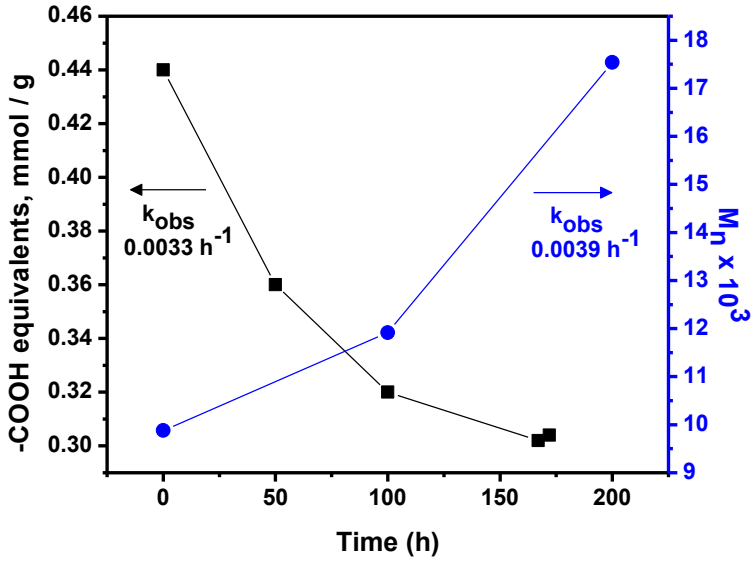

Figure 83. Molecular weight by GPC of stoichiometric –COOH:-OH polymer blend over time at 70 °C in bulk in the presence of Lipase acrylic resin from *Candida Antarctica* overlay with consumption of acid functionality over time by end-point titration. The rates were obtained from the corresponding second-order plots.

Table 17 summarizes the molecular weight data obtained at predetermined times. Interestingly, M_p did not change drastically over the 200 h period. However, M_w increased from 12,700 to 27,000, while PDI increased from 1.3 to 1.5. The lack of progression in M_p coupled with an increase in M_w indicated that lower molecular weight fractions, i.e., higher mobility fractions, participated to a greater extent in the reaction.

Table 17

M_n, M_w, M_p, and PDI of Blends at Different Intervals During Lipase Acrylic Resin from Candida Antarctica Catalyzed Reaction

Sample	M_n	M_w	M_p	PDI
Blend – 0 h	9,880	12,700	11,400	1.29
Blend –100 h	11,900	17,500	12,000	1.47
Blend – 200 h	17,540	27,000	11,900	1.54

Since the coatings were soluble in THF and did not exhibit any observable gel fraction, we investigated the change in –COOH average functionality (f_{avg}) and noted that it decreased by 0.5 over the 200 h evaluation period. After 100 hours f_{avg} reached a plateau despite increases in functional equivalent weight, which indicated that gains in M_n were not significant enough to dilute the functionality (Figure 84). We determined that the critical conversion to reach the gel point based on f_{avg} for –COOH and –OH polymers was 25%, which was similar to the conversion obtained during the 200 h study. These results raised the possibility that at some critical conversion, the functional groups will have diminished access to the enzyme active site due to the network limiting mobility of the unreacted tethered functionality.

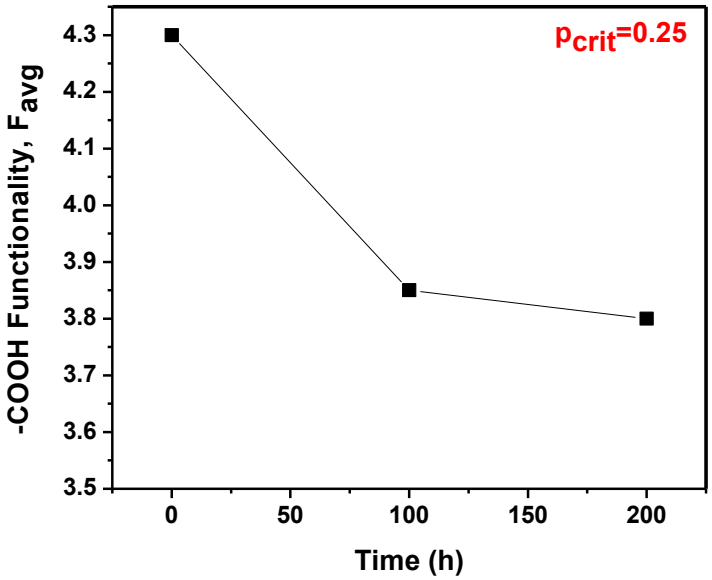

Figure 84. f_{avg} of stoichiometric –COOH:-OH polymer blend over time at 70 °C in bulk in the presence of lipase acrylic resin from *Candida Antarctica* as determined from M_n (GPC) and FEW (end-point titration).

Enzyme-catalyzed coupling of comb-like copolymers in soft condensed matter spanning the T_g

Previous experiments demonstrated that the reactive groups had to be some distance away from the polymer backbone to facilitate enzyme-catalyzed coupling of comb-like copolymers. However, previous studies were conducted at temperatures above the T_g of the copolymer blends to ensure cooperative segmental mobility. The next stage of research focused on understanding the glassy limits for enzyme-catalyzed crosslinking to be observed and the resulting properties such as T_g and crosslinking density. Local motions such as bending and twisting of the side chains groups predominate below T_g. In addition, we were interested in understanding whether slow rates due to the glassy state could be offset by increasing the volume fraction of the functional phase. Therefore, we synthesized a series of comb-like copolymers over a large range

of T_g (86 to – 29 °C) with varying volume fractions of the functional portion (0.23 – 0.73), while maintaining chain lengths below the entanglement molecular weight (40,000 g/mol) (Tables 18 and 19). The volume fractions were computed from the estimated van der Waals volumes using the functional group method according to the following:

$$V_f,FnC = \frac{V_w,FnC}{V_w} \qquad \text{Equation 48}$$

where $V_{w,FnC}$ is the van der Waals volume of only the functional component (either –OH or –COOH) in the copolymer. Likewise, V_w is the Van der Waals volume of the whole molecule. Both $V_{w,FnC}$ and V_w were estimated using the additive group method *(124,136)*. The detailed synthesis and the resulting properties of the copolymer series were included in Chapter III.

Table 18

Volume Fraction and T_g (°C) of $AM(CH_2)_{10}COOH$-MMA Copolymers

Polymer or Copolymer	$V_{w,\ AM(CH_2)_{10}COOH}$	Total V_w	$V_{f,\ AM(CH_2)_{10}COOH}$	T_g
MMA	0	56.1	0	100
$AM(CH_2)_{10}COOH$	151	151	1	n/a
$AM(CH_2)_{10}COOH$-MMA 10%	15.1	65.59	0.23	86
$AM(CH_2)_{10}COOH$-MMA 30%	45.3	84.57	0.54	83
$AM(CH_2)_{10}COOH$-MMA 50%	75.5	103.55	0.73	31

Table 19

Volume Fraction and T_g (°C) of $AM(CH_2)_{12}OH$-MMA Copolymers

Polymer or Copolymer	$V_{w,\ AM(CH_2)_{12}OH}$	Total V_w	$V_{f,\ AM(CH_2)_{12}OH}$	T_g
MMA	0	56.1	0	100
$AC(CH_2)_{10}OH$	163	163	1	n/a
$AC(CH_2)_{12}OH$-MMA 12%	19.56	68.93	0.28	55
$AC(CH_2)_{12}OH$-MMA 15%	24.49	72.14	0.34	59
$AC(CH_2)_{12}OH$-MMA 46%	74.90	131.50	0.57	-29

Initial thermal studies evaluated the blend compatibility of –COOH and –OH functional copolymers by casting from THF:DMF solution (9:1 by volume) containing stoichiometric amounts of each copolymer. The resulting coatings were dried at ambient conditions and T_g was evaluated for up to 120 h. Table 20 summarizes the T_g of the blends. 24 h after casting, blends of $AC(CH_2)_{12}OH$-MMA 12% + $AM(CH_2)_{10}COOH$-MMA 10% exhibited dual T_gs at 11 °C and 54 °C, while blends of $AC(CH_2)_{12}OH$-MMA 15% + $AM(CH_2)_{10}COOH$-MMA 30% and $AC(CH_2)_{12}OH$-MMA 46% + $AM(CH_2)_{10}COOH$-MMA 50% exhibited single T_gs at 13 °C and -39 °C, respectively. After 120 h of drying at ambient, all blends exhibited single T_gs indicating that the –COOH and –OH copolymers were phase compatible. In addition, the T_gs were higher than that observed after 24 h of drying; however, we suspected that some residual solvent was still present in the coating since the blend T_g was lower than the neat T_g of each copolymer.

Table 20

T_g of Copolymer Blend as a Function of Drying Time at Ambient

Ambient Drying Time	**$AC(CH_2)_{12}OH$-MMA 12% + $AM(CH_2)_{10}COOH$-MMA 10%**	**$AC(CH_2)_{12}OH$-MMA 15% + $AM(CH_2)_{10}COOH$-MMA 30%**	**$AC(CH_2)_{12}OH$-MMA 46% + $AM(CH_2)_{10}COOH$-MMA 50%**
22 h	11 °C 54 °C	13 °C	-39 °C
120 h	42 °C	40 °C	-15 °C

Biocatalyst compatibility with the copolymer blend was determined by acid equivalent measurements via end-point titration at predetermined times in stoichiometric blends of $AC(CH_2)_{12}OH$-MMA 12% (M_n = 9,500, FEW = 2,560, T_g = 55 °C) and $AM(CH_2)_{10}COOH$-MMA-BA 8.7% (M_n = 6,700, FEW = 1,250, T_g = -

18.30 °C) to yield a final blend T_g of 30 °C. 10 % w/v solutions of THF containing 1.39 % by weight on solids PPL were cast at ambient. Acid equivalents for samples with and without enzyme were evaluated prior to drying (Figure 85). Coatings were dried under vacuum for 48 h at room temperature and placed at 47 °C. T_{cure}-T_g was set at + 17 °C for preliminary evaluation of PPL compatibility with the coating. The acid equivalents in the sample containing 1.39 wt% PPL prior to drying in vacuum chamber at room temperature were 12% lower than coatings that did not contain PPL. However, after drying under vacuum at room temperature, both coatings had similar initial acid equivalents. During exposure at 47 °C, the acid equivalents did not vary significantly in the coatings containing PPL versus coatings absent of PPL. We hypothesized that PPL's incompatibility with the matrices prevented catalyzed coupling from occurring even at cure temperatures above the T_g of the final blend. We also evaluated the possibility that PPL was undergoing deactivation during exposure to the polymer solution prior to solution casting.

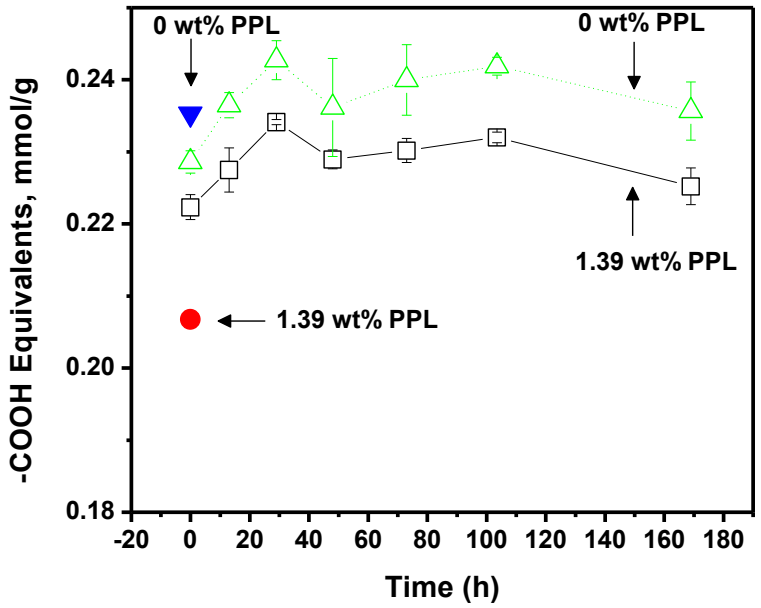

Figure 85. Acid value of coatings from blends of $AC(CH_2)_{12}OH$-MMA 12% (M_n = 9,500, FEW = 2,560, T_g = 55 °C) and $AM(CH_2)_{10}COOH$-MMA-BA 8.7% (M_n = 6,700, FEW = 1,250, T_g = -18.30 °C) cured at 47 °C with 1.39 wt% PPL (---□---); immediately after casting (---●---), in the absence of enzyme at 47 °C (---Δ---); immediately after casting (---▼---).

The detailed assay set up for determining enzyme activity in solutions of copolymer blends is provided in Chapter III. PPL activity is similar in neat THF and DMF, however, it diminishes by 50% in the solvent mixture of THF:DMF (9:1 by volume) shown in Figure 86. In the 20% w/v blend copolymer solutions, PPL activity maintained similar levels as in THF:DMF (9:1), while in the 20% w/v PMMA homopolymer, the activity reached values similar to that observed in neat THF and DMF. In addition, residence time in the homopolymer and copolymer solutions resulted in loss of PPL activity. The diminished relative activity in functionalized copolymer solutions indicated that copolymer functional groups were interacting with the amino acid side groups either on the enzyme shell or inside the active site. Interactions with the amino acid side groups would lead to

denaturation by unraveling the enzyme globular structure, while interactions with the active site would poison the catalyst.

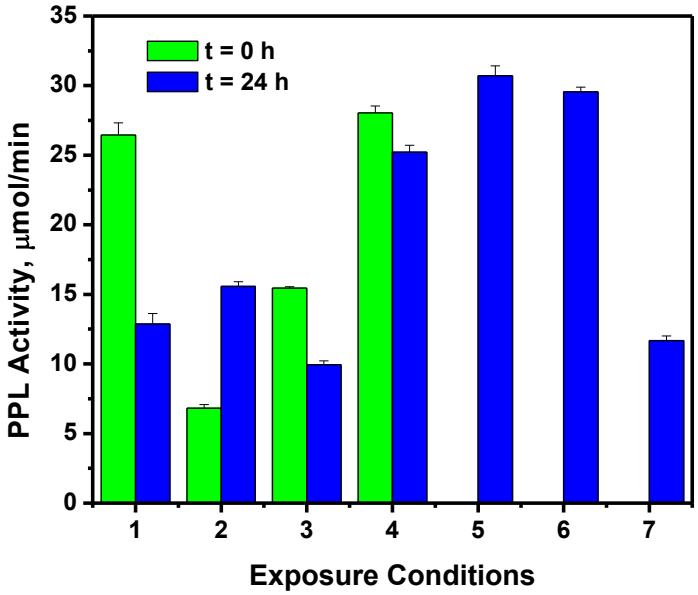

Figure 86. PPL activity as a function of exposure conditions and residence time at 2-8 °C in each of the following: 1 = $AC(CH_2)_{12}OH$-MMA 12% + $AM(CH_2)_{10}COOH$-MMA 10% in (THF:DMF 9:1); 2 = $AC(CH_2)_{12}OH$-MMA 15% + $AM(CH_2)_{10}COOH$-MMA 30% in (THF:DMF 9:1); 3 = $AC(CH_2)_{12}OH$-MMA 46% + $AM(CH_2)_{10}COOH$-MMA 50% in (THF:DMF 9:1); 4 20 wt% PMMA in (THF:DMF 9:1); 5 = THF; 6 = DMF; 7 = THF:DMF 9:1.

Similar activity studies were conducted for dioxane precipitated lipolase (P-Lipolase) and extracted CALB (E-CALB) (Figures 87 and 88). Procedures for preparing P-Lipolase and E-CALB are detailed in Chapter III. Both enzymes exhibited diminished activities when exposed to copolymer solutions. P-Lipolase exhibited activities in neat THF, DMF, and THF:DMF (9:1 by volume) that were similar to propylene glycol buffer environments. Exposure to functionalized copolymer solutions diminished lipolase activity by approximately 50%. Extracted CALB activity was completely depleted in neat THF and DMF relative to re-suspending in aqueous or surfactant containing organic solvents. Minimal

activity was observed in a THF:DMF blend (9:1 by volume), but the activity was 10 fold lower than in re-suspended aqueous or surfactant containing organic solvents. Interestingly, exposure to the THF:DMF blend (9:1 by volume) containing the highest functionalized copolymer blend improved E-CALB activity four fold compared to neat THD:DMF 9:1 by volume solution.

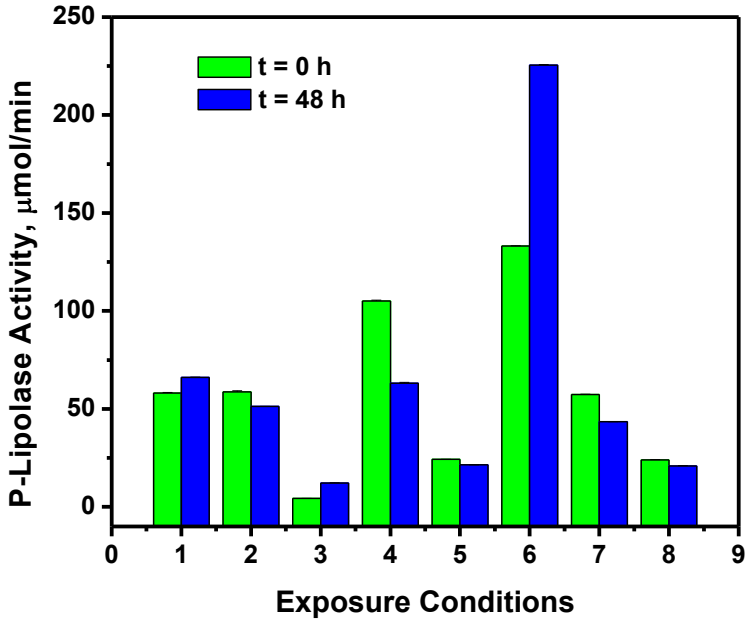

Figure 87. P-Lipolase activity as a function of exposure conditions and residence time at 2-8 °C in each of the following: 1 = $AC(CH_2)_{12}OH$-MMA 12% + $AM(CH_2)_{10}COOH$-MMA 10% in (THF:DMF 9:1); 2 = $AC(CH_2)_{12}OH$-MMA 15% + $AM(CH_2)_{10}COOH$-MMA 30% in (THF:DMF 9:1); 3 = $AC(CH_2)_{12}OH$-MMA 46% + $AM(CH_2)_{10}COOH$-MMA 50% in (THF:DMF 9:1); 4 20 wt% PMMA in (THF:DMF 9:1); 5 = DMF; 6 = THF:DMF 9:1; 7 = re-suspended in diH2O; 8 = re-suspended in dioxane.

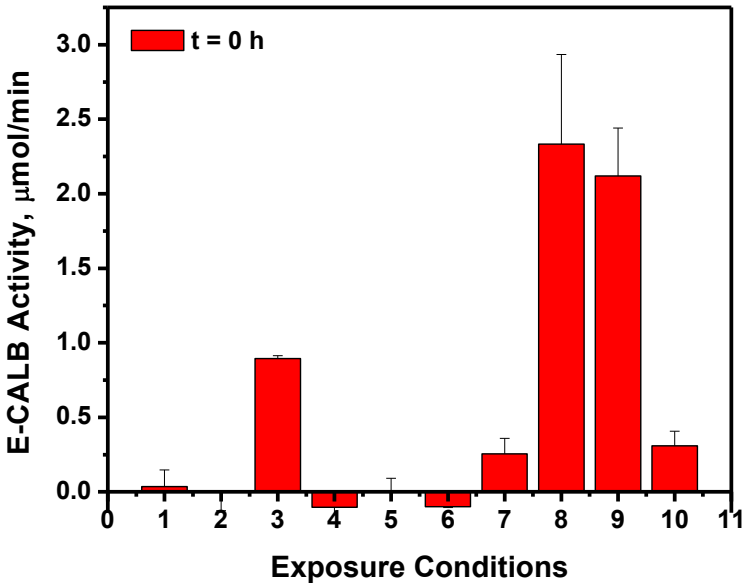

Figure 88. E-CALB activity as a function of exposure conditions in each of the following: 1 = $AC(CH_2)_{12}OH$-MMA 12% + $AM(CH_2)_{10}COOH$-MMA 10% in (THF:DMF 9:1); 2 = $AC(CH_2)_{12}OH$-MMA 15% + $AM(CH_2)_{10}COOH$-MMA 30% in (THF:DMF 9:1); 3 = $AC(CH_2)_{12}OH$-MMA 46% + $AM(CH_2)_{10}COOH$-MMA 50% in (THF:DMF 9:1); 4 20 wt% PMMA in (THF:DMF 9:1); 5 = THF; 6 = DMF; 7 = THF:DMF 9:1; 8 = re-suspended in diH2O; 9 = re-suspended in 2 mM AOT in isooctane; 10 = 2 mM AOT in isooctane after centrifuge.

Once organic soluble biocatalysts were obtained and characterized, stoichiometric blends of $AM(CH_2)_{10}COOH$-MMA 30% (T_g = 83 °C, M_n = 7,400) and $AC(CH_2)_{12}OH$-MMA 15% (T_g = 59 °C, M_n = 20,800) were cast on standard DSC aluminum pans with 4 wt% precipitated lipolase and dried at room temperature for 48 h. The coating preparation details are presented in Chapter III. Thermal analysis was performed periodically and the results are summarized in Figures 89 and 90. The initial T_g was similar to that of the control coatings dried for 120 h as described in Table 20. The blend T_g was lower than the T_g of each component indicating the presence of residual solvent in the coatings. Coatings that did not contain biocatalyst had consistently higher T_gs than coatings that contained 4 wt% lipolase. Coatings cured at 40 °C in the presence

of P-Lipolase did not exhibit changes with T_g, while coatings cured at 50-70 °C exhibited gains in T_g. The gains in T_g in the control coatings were attributed to physical aging of the blends due to the relatively bulky groups of each copolymer. In fact, regardless of exposure temperature, coatings that did not contain biocatalyst increased its T_g by ~20 °C (exception - control coatings cured at 70 °C gained 30 °C in T_g), while coatings that contained P-Lipolase exhibited T_g gains that were dependent on the cure temperature. Thus, coatings cured at 40 °C, 50 °C, 60 °C, and 70 °C exhibited T_g change after 228 h of cure of -2 °C, 11 °C, 15 °C, and 24 °C, respectively. We suspected that the T_g gains in coatings that contained P-Lipolase were not as pronounced due to biocatalyzed coupling reactions. Theoretically, if coupling occurred, it would yield a higher molecular weight sample with functionalized side chains unable to undergo the fast volume relaxation that led to higher T_gs (improved packing) in coatings in the absence of biocatalyst.

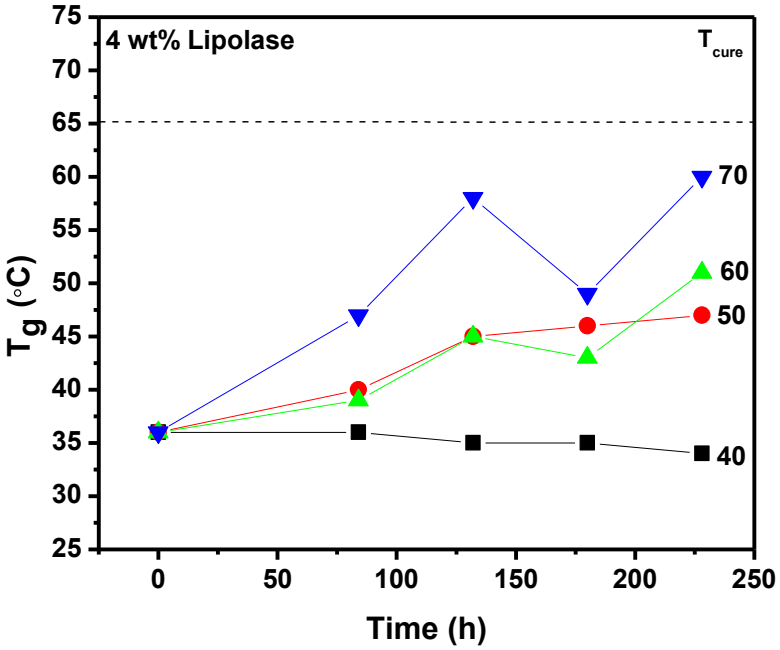

Figure 89. T_g evolution in copolymer blends from $AM(CH_2)_{10}COOH$-MMA 30% (T_g = 83 °C, M_n = 7,400) and $AC(CH_2)_{12}OH$-MMA 15% (T_g = 59 °C, M_n = 20,800) cured at different temperatures in the presence of 4 wt% on total resin solids P-Lipolase.

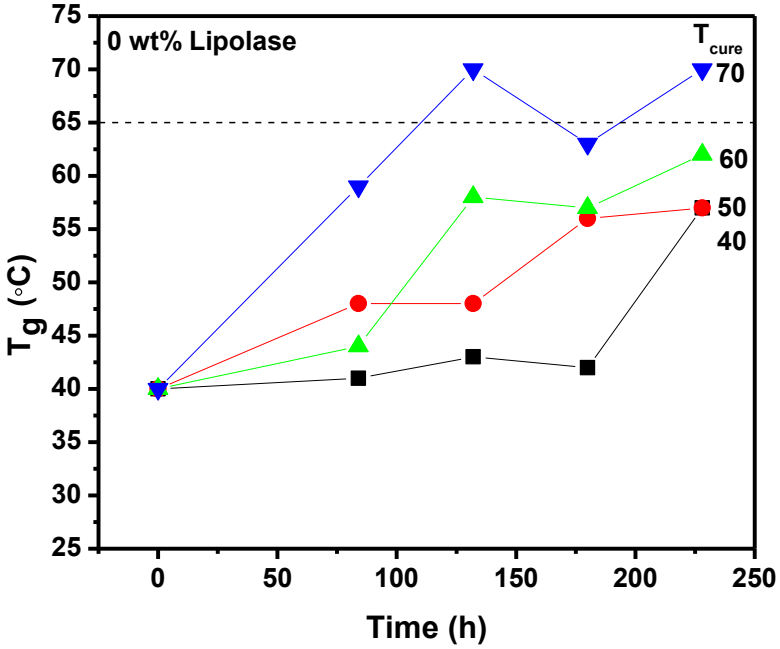

Figure 900. T_g evolution in copolymer blends from $AM(CH_2)_{10}COOH$-MMA 30% (T_g = 83 °C, M_n = 7,400) and $AC(CH_2)_{12}OH$-MMA 15% (T_g = 59 °C, M_n = 20,800) cured at different temperatures in the absence of biocatalyst.

The coatings were soluble in *N*,*N*-dimethylacetamide and THF after cure indicating that the critical conversion for gelation had not been achieved in these systems. Upon filtration of THF solutions, molecular weights of the copolymer blends in the presence and absence of biocatalyst were determined at fixed times during curing at various temperatures in order to gather more information on biocatalyst activity. Figure 91 and 92 illustrate the observed changes in M_n over time in copolymer blends in the presence and absence of P-Lipolase. Coatings in the presence of biocatalyst exhibited molecular growth at 50 °C and 60 °C and little to no change at 40 °C and 70 °C. Coatings in the absence of biocatalyst did not exhibit any observable trends that suggested molecular weight over time.

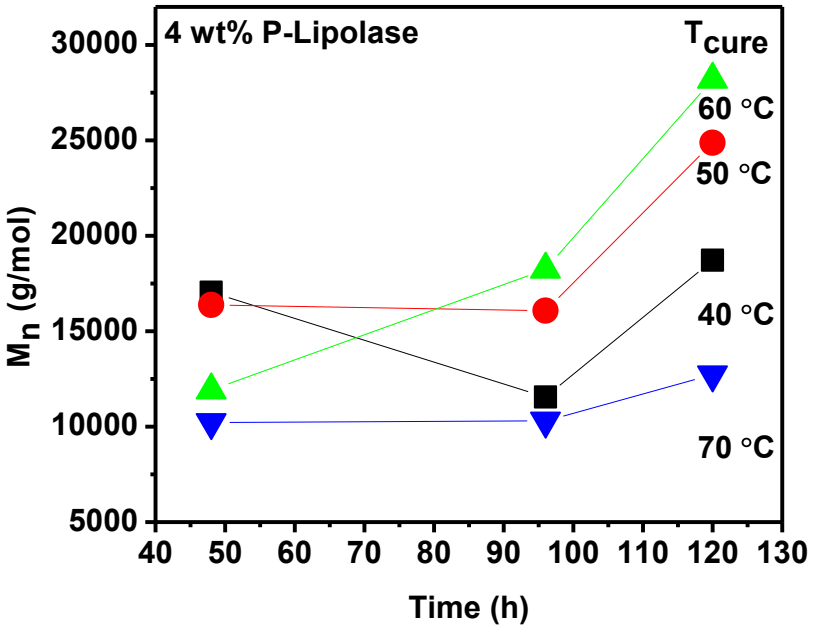

Figure 91. M_n evolution in copolymer blends from AM$(CH_2)_{10}$COOH-MMA 30% (T_g = 83 °C, M_n = 7,400) and AC$(CH_2)_{12}$OH-MMA 15% (T_g = 59 °C, M_n = 20,800) cured at different temperatures in the presence of 4 wt% on total resin solids P-Lipolase.

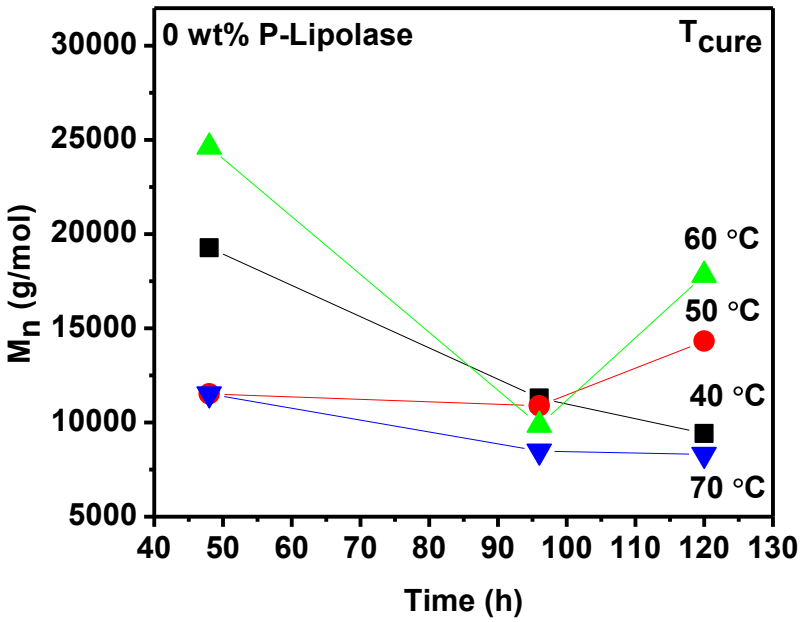

Figure 92. M_n evolution in copolymer blends from AM$(CH_2)_{10}$COOH-MMA 30% (T_g = 83 °C, M_n = 7,400) and AC$(CH_2)_{12}$OH-MMA 15% (T_g = 59 °C, M_n = 20,800) cured at different temperatures in the absence of biocatalyst.

The molecular weight and glass transition data suggested that biocatalyzed coupling of –COOH and –OH functional copolymer blends occurred in coatings with initial blend T_g of 40 °C. Molecular weight growth was more pronounced in coatings that were initially at 10 °C and 20 °C above the initial blend T_g. Overall, the changes in T_g and M_n were not very pronounced in polyfunctional coating blends containing P-Lipolase and did not lead to the formation of crosslinks, which indicated that further optimization in terms of biocatalyst compatibility and loading is necessary to obtain crosslinkable coatings.

Conclusions

We investigated enzyme-catalyzed kinetics in constrained environment by tethering the –COOH and –OH functional groups to an acrylate and acrylamide polymer backbone. The ability to control the reaction would give rise to self-

mendable or self-degradable materials and control over the material's rubber elastic behavior. These novel formulations would be advantageous as materials with reversible bulk properties for adhesives, elastomers, composites, and laminates applications. Enzyme activity assays in coatings from polyacid and polyalcohol blends indicated that the synthesized functional polymers act as substrate mimics in cases when the functional groups are at least 10 methylene units away from backbone. The synthesized comb-like –COOH and –OH copolymers were compatible with each other as signified by the presence of a single T_g.

Diminishment in activity was observed in solution of copolymers with increasing mole fraction of functionality and residence time in solution. P-lipolase activity dropped significantly in the copolymer functional series with the highest functionality, while E-CALB activity exhibited the highest activity in copolymer functional series with the highest functionality. The diminished relative activity in functionalized copolymer solutions indicated that copolymer functional groups were interacting with the amino acid side groups either on the enzyme shell or inside the active site. Interactions with the amino acid side groups would lead to denaturation by unraveling of the enzyme globular structure, while interactions with the active site would poison the biocatalyst.

We investigated reaction kinetics in copolymer blends at $T_{cure}>T_g$ and observed that the diminishment in acid equivalents follows similar rate as increase in molecular weight as determined by GPC when Lipase acrylic resin from *Candida Antarctica* was used as a biocatalyst. The gel point for Lipase

acrylic resin from *Candida Antarctica* catalyzed systems was 25% conversion, which was similar to the conversion obtained after 200 h of cure. This observation raised the possibility that at some critical conversion functional groups would have diminished access to the enzyme active site as network formation would limit the mobility of the unreacted tethered functionality. The f_{avg} value indicated that at the end of the evaluation, 0.5 acid functional chains had coupled with 0.5 hydroxyl functional chains. Molecular weight observations indicated that the lower molecular weight fraction, i.e., higher mobility species, participated in the reaction to a greater extent.

In blends cured at $T_{cure} \geq T_g$, the T_g of coatings containing P-lipolase was consistently lower than that of coatings without any enzyme. Increased T_g was observed in both systems, however, it progressed faster in the coatings without enzymes. The results indicated that a higher molecular weight polymer was obtained after cure since the functionalized side chains were unable to undergo the fast volume relaxation that led to higher T_gs in coatings in the absence of biocatalyst. GPC analysis confirmed the hypothesis since in copolymer blends in the presence of P-Lipolase M_n increased overtime, while no increase in M_n was observed in control coatings. However, gelation did not take place, which indicated that further optimization in terms of biocatalyst compatibility and loading is necessary to obtain crosslinkable coatings.

CHAPTER VIII

ENZYME-CATALYZED POLYMERIZATIONS OF POLY (ESTER AMIDE)S FROM NOVEL MONOMERS

Abstract

Immobilized lipase B from *Candida antarctica* (CAAR) was used to synthesize novel poly (ester amide)s (PEAs) with dual pendant and backbone amides. Polymerization kinetics, molecular weight, and structure of the resulting PEAs were determined via GPC and NMR spectroscopy. Rate constants for CAAR-catalyzed polyesterifications were examined as a function of monomer structure. Polymerization kinetics were characterized by initial linear molecular weight growth and a plateau in the later stages of polymerization. Thermal analysis of PEAs suggested that the pendant amide improved thermal stability. In addition, the polymerization of γ-acetamido-ε-caprolactone was carried out by a two-step, one-pot process, despite its lower reactivity as compared to the unsubstituted analog, ε-caprolactone. Initially, base catalyzed ring opening was conducted in methanol at room temperature followed by bulk polymerization in the presence of *Candida Antarctica* lipase acrylic resin at 60 °C for 150 h. The resulting polymer was determined to be amorphous in nature due to the presence of pendant groups along the polyester backbone.

Introduction

Biodegradable polymers are a promising class of materials with current commercial applications in drug delivery, sutures, dental devices, and vascular stents *(178)*. Aliphatic polyesters and their derivatives comprise the

biodegradable polymer class due to their excellent hydrolytic degradation properties *(179)*. However, commercial use of aliphatic polyesters is severely limited by their poor mechanical and thermal properties *(180)*. On the other hand, polyamides are widely used as engineering thermoplastics in commercial applications due to their excellent thermal stability, high modulus, and tensile strength *(181)*. Poly(ester amide)s (PEAs) are a promising candidate for use as biodegradable commodity thermoplastics since they combine the biodegradable behavior of polyesters and the mechanical and thermal properties of polyamides *(182,183,184)*.

PEAs are typically synthesized via thermal condensation of diamine, diacid, and glycol monomers using catalysts based on transition metals such as tin, titanium, platinum, magnesium, or strong acidic catalysts such as *p*-toluene sulfonic acid *(185,186)*. PEA microstructure impacts the mechanical properties and is controlled by judicious choice of synthetic strategy. For instance, the commercially available Bayer BAK®1095 has a random microstructure derived by copolymerization of ε-caprolactam, 1,4-butane diol, and adipic acid *(187)*. Highly segmented microstructures are obtained by copolymerizing amide-containing prepolymers, diesters/diacids, and glycols *(188)*. PEAs with pendant functional groups are desirable for use as biomaterials and are commonly derived from α-aminoacids *(189,190)*. Additional functional handles allow conjugation with drug or cell signaling molecules and enhance PEA biocompatibility, thus expanding their potential biomedical applications *(191)*.

Traditional catalysis in PEA synthesis often requires high temperatures that can result in side reactions due to amide alcoholysis and generate free primary amines, ester moieties, and macrocyclic products, all of which have a detrimental effect on mechanical properties *(187,192,193)*. Synthesizing PEAs with pendant functional groups requires additional synthetic steps to protect the latent functionality. The additional blocking and deblocking steps make PEA synthesis a cumbersome procedure *(190)*. Additionally, PEAs with predetermined ester-to-amide ratios are difficult to achieve due to the lower reactivity of the hydroxyl group relative to the amine group *(192)*.

Biocatalysis offers a mild, environmentally responsible route to PEA synthesis with high enantio- and regioselectivity that may otherwise be unobtainable. The use of environmentally benign procedures has been a growing trend in industrial practices. Such procedures include the use of monomers derived from natural feedstock, and often entail eliminating solvents, harsh acid and base catalysts, and transition metal catalysts. Moreover, biocatalyzed polymerizations are conducted at atmospheric pressure and lower temperatures, which reduce the occurrence of side reactions.

Lipases are prevalent in nature and have successfully been isolated and modified for use as catalysts. Although typically used for resolving alcohol chiral compounds, lipases have also been employed to synthesize polysaccharides, polyesters, polycarbonates, polyamides, polyphosphates, polythioesters, and a variety of polyaromatic compounds *(93)*. The immobilized lipase B from *Candida Antarctica* (CAAR) tolerates the presence of pendant functional groups in

monomers and has been the enzyme of choice for synthesizing various polyesters. Aliphatic polyesters have been synthesized via step-growth and ring opening lipase-catalyzed polymerization. Gross *et al.* reported CAAR-catalyzed polymerization of adipic acid and 1,8-octane diol in diphenyl ether that achieved a M_n of 2.9 x 10^4 after 48 h at 70 °C *(194)*. Under solvent-free conditions, the same monomers yielded a M_n of 2.1 x 10^4 after 48 h at 70 °C *(195)*. PEAs have been synthesized via lipase-catalyzed ring-opening polymerization of cyclic depsipeptide. Hocker *et al.* reported the Porcine Pancreas Lipase (PPL), *Pseudomonas* species, and *Pseudomonas Cepacia* (PC) catalyzed ring-opening polymerization of a variety of morpholine-2,5-dione monomers *(196,197,198)*. PEAs with alternating amide bonds in the backbone were synthesized at 100 - 130 °C with M_n values ranging from 3,500 to 12,000 after 72 hours. ε-caprolactone and its methyl-substituted derivatives have also been polymerized via CAAR catalysis *(199,200,201,202)*. Bulk polymerization of ε-caprolactone using 10 mg CAAR/mg at 60 °C achieved a M_n of 4,300 after 24 h at 99% conversion *(200)*. Similarly, bulk polymerization of α-methyl-ε-caprolactone using 50 mg CAAR / mmol at 60 °C attained a M_n of 4,800 after 24 h at 94% conversion *(201)*.

Lipase catalyzed polymerizations are generally accepted to proceed via an acyl-enzyme intermediate (EM) where the propagation step is the nucleophilic attack of a terminal hydroxyl group *(203)*. EM formation is the rate-determining step in lipase-catalyzed ring-opening polymerization of lactones *(96)*. However, if the majority of nucleophiles in the reaction mixture are sterically hindered and/or

the EM becomes structurally hindered during the polymerization, EM deacylation becomes the rate-determining step. In the lipase-catalyzed polymerizations of aliphatic diacids and diols, as the nucleophile end group concentration decreases at high conversions, molecular weight growth occurs primarily due to interchain transesterification and the rate determining step is the deacylation of the sterically crowded EM *(204)*. NMR analysis of lipase-catalyzed copolymerization of *ω*-methyl substituted lactones and unsubstituted lactones indicated relatively higher incorporation of unsubstituted nucleophiles, suggesting that the rate-determining step was EM deacylation due to steric hindrance of the *ω*-methyl substituted nucleophiles *(205)*. These studies suggested that nucleophiles and EM steric structures are likely to have a significant effect on the overall polymerization.

We report the CAAR-catalyzed synthesis and polymerization kinetics of PEAs containing γ-amide functionalities. To the best of our knowledge, transesterification polycondensation of sterically hindered monomers to produce PEAs has not been reported yet. A series of amide substituted and unsubstituted, monomeric and oligomeric diols were synthesized to determine the impact of steric effects on polymerization kinetics (Figure 93). Identifying specific parameters that impact the polymerization rate are invaluable for synthesizing high molecular weight PEAs and for expanding the monomer toolbox available to enzymatic polymerizations. The effects of sterically hindered nucleophile and EM on the overall polymerization kinetics were evaluated. The hypothesis that the thermal stability of monomers with pendant amide is higher

due to the intermolecular hydrogen bonding among polymer chains was also tested. The synthesized PEAs were compared to commercial aliphatic polyesters via thermal analysis. In addition, the polymerization of γ-acetamido-ε-caprolactone was carried out by a two-step, one-pot process, despite its lower reactivity relative to the unsubstituted analog, ε-caprolactone. Initially, base catalyzed ring opening was conducted in methanol at room temperature followed by bulk polymerization in the presence of *Candida Antarctica* lipase acrylic resin at 60 °C for 150 h. The resulting polymer was determined to be amorphous in nature due to the presence of pendant groups along the polyester backbone.

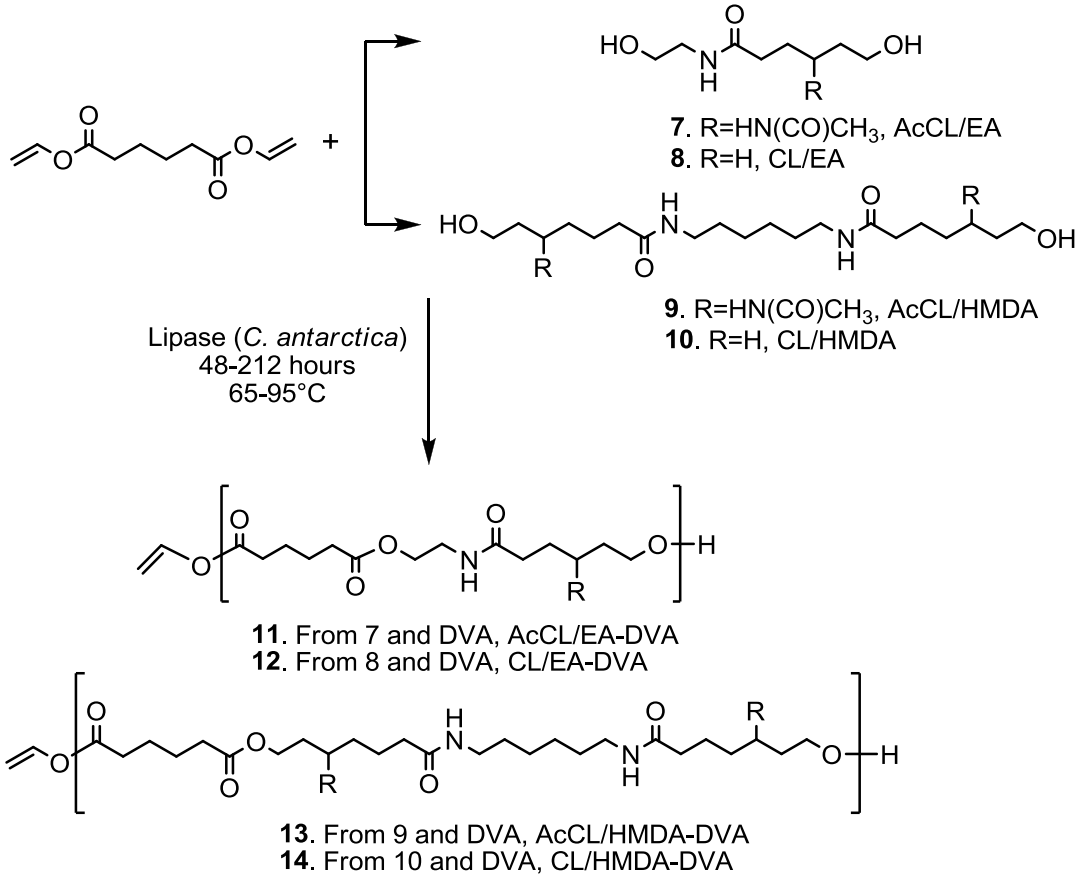

Figure 93. Generalized reaction scheme for the enzyme-mediated synthesis of poly(ester amide)s.

Results and Discussion

Polyesterification reactions of diols derived from γ-acetamido-ε-caprolactone and with divinyl adipate were examined using CAAR catalysis. Lipase-catalyzed polymerizations have typically been performed using 10% w/w immobilized lipase on monomer. Such loading levels have been determined to be optimal for various monomers in lipase-catalyzed polyesterification reactions. Several studies have examined optimal CAAR loading and determined that no significant change in molecular weight or polymerization rate was observed when the lipase loading level was increased to 20% w/w on monomer *(196)*. However, a loading level of 5% w/w resulted in lower molecular weights and slower polymerization rates *(197)*.

We investigated the use of divinyl adipate (DVA) as the acyl donor. Acyl transfer using enol esters has been shown to be about 10 times slower than the corresponding hydrolysis reaction and about 10-100 times faster than acyl transfer using alkylated esters such as ethyl acetate *(206)*. The vinyl functional group not only activates the ester end group for faster transesterification but also imparts inherent irreversibility to the process since it rapidly tautomerizes to the corresponding volatile aldehyde. Enzyme-free control experiments were performed using a 1:1 molar ratio of monomers to determine background esterification between DVA and **7** through **10**. GPC studies indicated that in the absence of enzyme catalyst, no polytransesterification was detected at temperatures below 95 °C. When **7** was copolymerized neat at 95 °C, the

background M_n reached 3,560. In this study, polymerization reactions were performed at temperatures below 95 °C.

Lipase-Catalyzed Synthesis of Poly(ester amide)s.

Polytransesterification reactions of amide containing diols with DVA were examined using CAAR catalysts in 1,4-dioxane or bulk, and analyzed for their final molecular weight by GPC and structure by NMR. Figure 94 shows the ^{13}C NMR spectra for the polymers and starting materials. Esterification was manifested by the appearance of a resonance peak from the acyl carbon at 173 ppm with slight shifts in the amide carbonyls upon incorporation in polymer. The resonance peaks for the carbons proximal to the hydroxyl group shifted downfield from 58 and 60 ppm to 61 and 63 ppm due to additional deshielding from the carbonyl ester (Figure 94). In addition, new carbon resonances appeared in the 20-35 ppm region due to DVA incorporation.

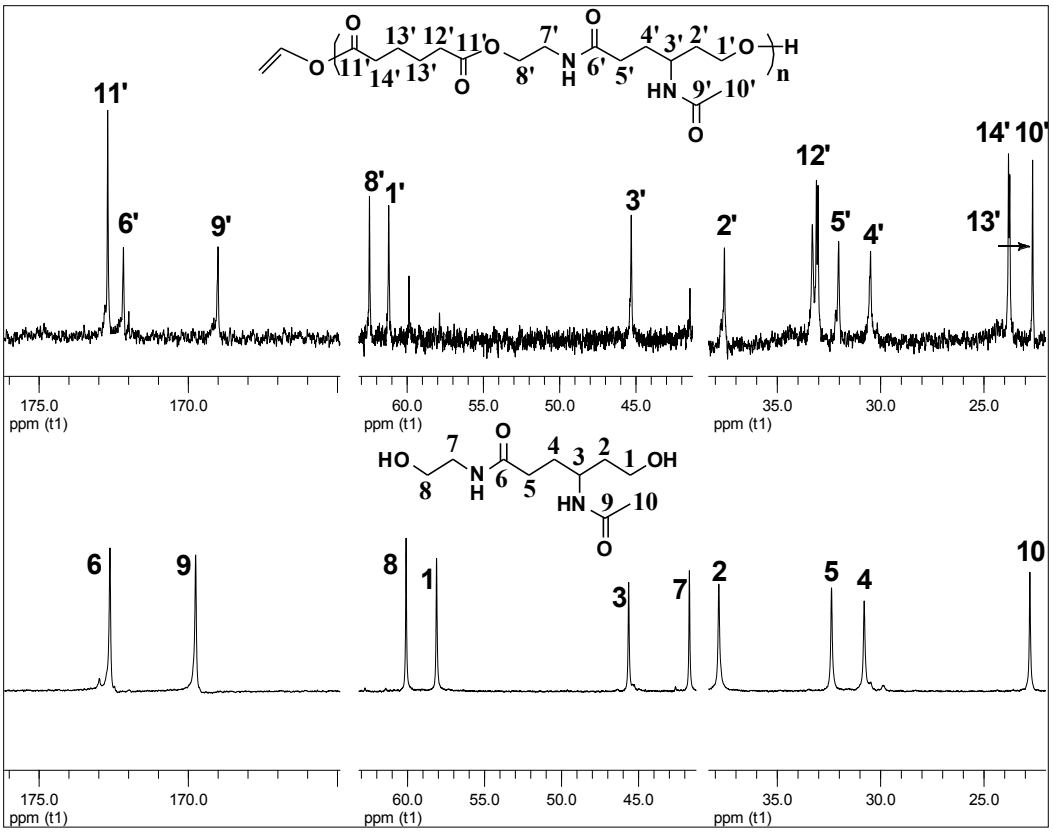

Figure 94. ^{13}C NMR of AcCL-EA/DVA (top) and AcCL/EA (bottom) in d_6-DMSO.

Neat polymerization of CL/EA and DVA reached a M_n of 7.8 x 10^3 in 48 h at 80 °C (Table 21). Hocker *et al.* reported that PPL and PS lipase catalyzed ring-opening polymerizations of morpholine-2,5-dione monomers achieved molecular weights of up to 12.5 x 10^3 at 100 °C after 72 h *(196)*. However, when CALB was used as the catalyst, no appreciable polymer was obtained *(196,197)*. The apparent lack of activity with CALB was attributed to the high reaction temperatures used during the polymerizations. However, the CAAR used in this study is thermally more stable than the lyophilized forms of lipase due to its immobilization on acrylic resin. We suspected that the observed lack of activity was due to inherent differences in water content among lyophilized and immobilized forms of the enzymes. PPL contains 3.6 % w/w of water that can act

as an initiator during ring-opening polymerizations (*4*). This was further corroborated by the lower molecular weights reported by Hocker at higher catalyst loading.

Neat polymerization of γ-substituted glycol, AcCL/EA, with DVA yielded a M_n of 5.0 x 10^3 in 48 h at 95 °C. The lower molecular weight is consistent with the hypothesis that EM deacylation occurs at a slower rate in the presence of a sterically hindered nucleophile. Polymerizations in 1,4-dioxane resulted in lower molecular weights than the corresponding neat polymerizations due to the lower reactive group concentration relative to the neat polymerizations (Table 21). Further analysis of polymerization kinetics was conducted to quantify the decrease in polymerization rate when nucleophiles with higher molecular weights and hindered versus unhindered steric structures were used in the transesterification polycondensation polymerizations.

Table 21

Final Copolymer Molecular Weight as Determined by GPC

Polymer	Solvent	Temperature (°C)	Time (h)	M_n x 10^{-3}	M_w x 10^{-3}	PDI
11	1,4-dioxane	80	48	4.0	4.9	1.2
12	1,4-dioxane	80	48	4.1	5.3	1.3
13	1,4-dioxane	80	48	3.5	4.1	1.2
14	1,4-dioxane	80	48	2.6	3.0	1.2
11	Bulk	95	48	5.0	7.0	1.4
12	Bulk	70	48	7.8	12.2	1.6

The difunctional compounds formed by the reaction of γ-acetamido-ε-caprolactone with alcohol amines or alcohols were excellent monomers for enzyme-catalyzed condensation polymerizations. Since γ-acetamido-ε-caprolactone could not be polymerized in the presence of biocatalyst and initiator

via a ring opening polymerization, we designed a one-pot / two-step enzymatic polycondensation reaction to obtain polyesters with pendant acetamide groups (Figure 95).

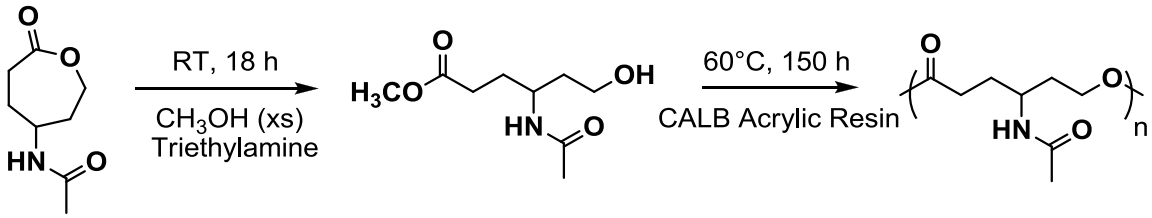

Figure 95. One-pot / two-step lipase catalyzed polycondensation.

Figure 96 shows the ^{1}H NMR spectra after the ring-opening step and the reaction in the presence of lipase at 60 °C for 150 h. The oxomethylene protons labeled **g** shifted downfield as the result of the acyl transfer reaction. Their presence in the polymer product was attributed to chains that contain hydroxyl end groups and residual unreacted compound **8**. Polymerization resulted in broadening of amide proton peaks indication of changes in proton microenvironment resulting from disruption of intramolecular hydrogen bonding.

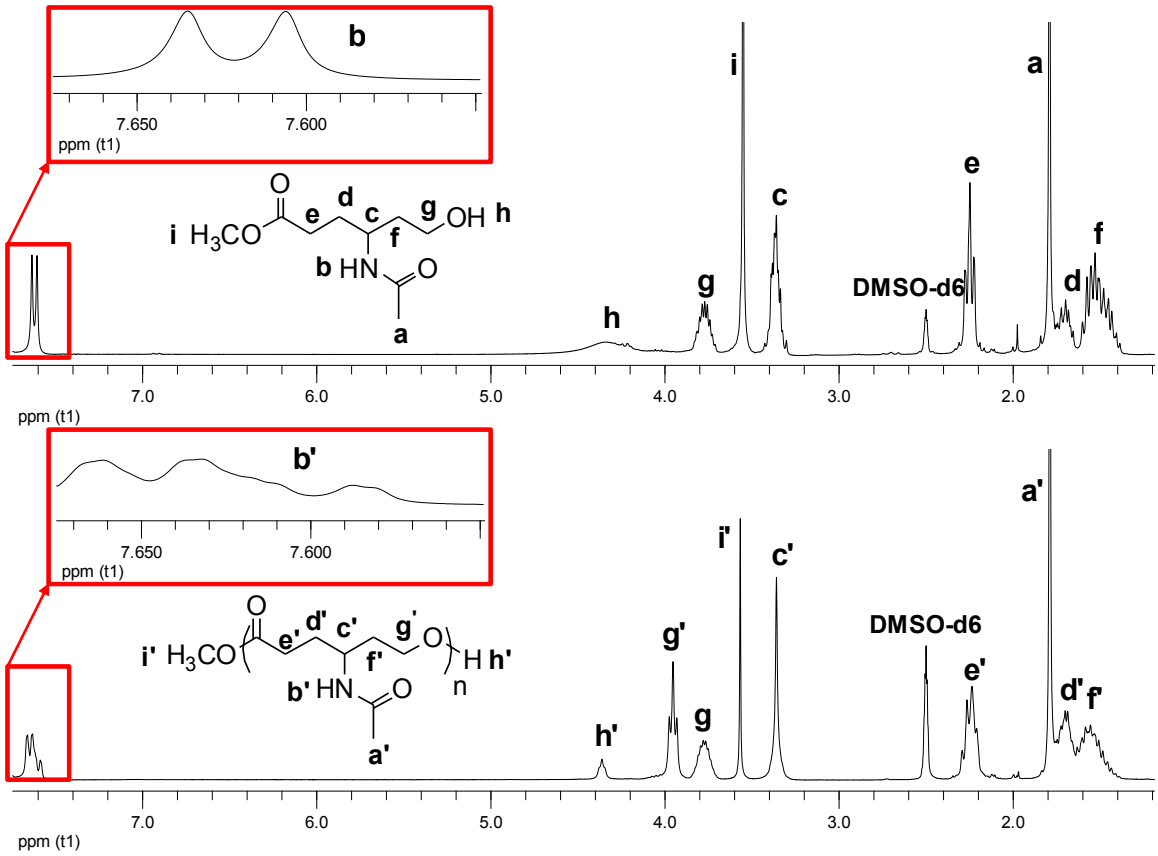

Figure 96. ^{1}H NMR in DMSO-d_6 of the methanol ring opening product (top) and the resulting spectra of the lipase-catalyzed polymerization (bottom).

Analysis of the ^{13}C NMR spectra revealed the presence of multiple and intense signals for the ester and amide carbonyl carbons due to neighboring group effects (Figure 97). In addition, slight shifts were observed in the carbon signals corresponding to methyl 4-acetamido-6-hydroxyhexanoate as compared to the lipase-catalyzed polymerization product. For example, ester carbonyl shifted from 173.3 to 170 ppm, while the oxomethylene carbon shifted from 57.9 to 57.8 ppm. Peak splitting and a shift from 45.1 to 44.9 ppm were also observed for the -CH_2-NH carbons. The α and β carbon signals labeled as 5' and 4' shifted further downfield, and the intensity of the amide α carbon labeled as 9' increased significantly after the lipase-catalyzed polymerization.

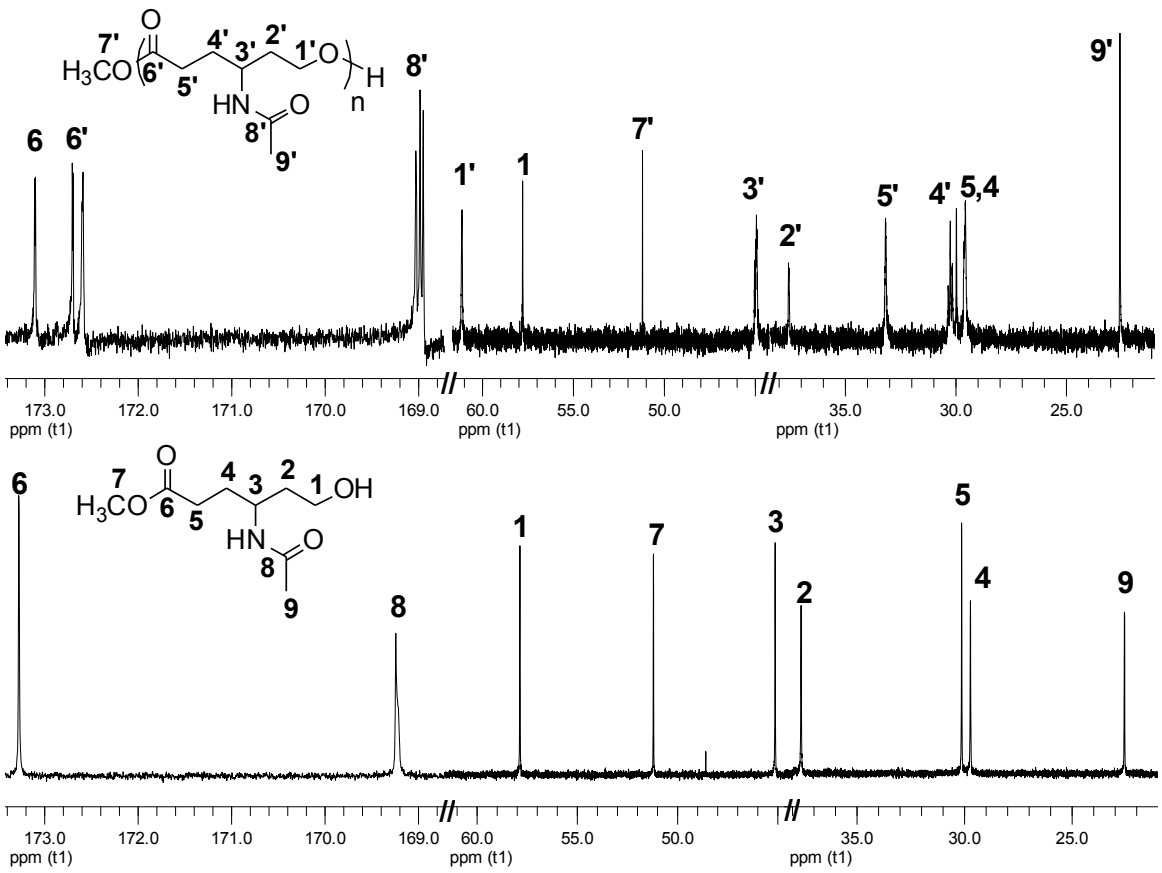

Figure 97. ^{13}C NMR spectra in DMSO-d_6 of the methanol ring opening product (bottom) and the resulting spectra of the lipase-catalyzed polymerization (top).

GPC indicated that the number average molecular weight, M_n, was 2,600, peak molecular weight, M_p, was 2,800, and weight average molecular weight, M_w, was 3,100. Figure 98 shows the shift to lower elution times as the result of the lipase-catalyzed polymerization of the CH_3OH ring-opened γ-acetamido-ε-caprolactone. The shoulder observed in the polymer trace corresponds to the elution of unreacted compound **8**.

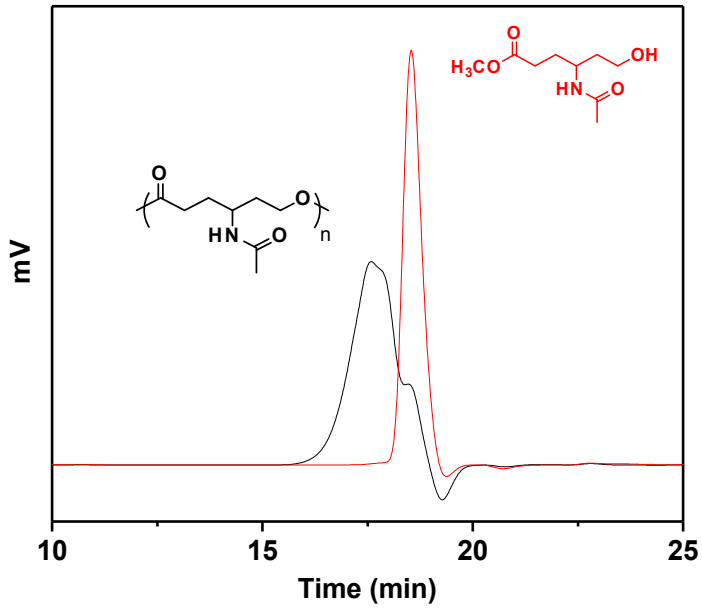

Figure 98. GPC chromatograms of the sequential polymerization of γ-acetamido-ε-caprolactone.

The results of the thermal analysis of the starting compound 8, methyl 4-acetamido-6-hydroxyhexanoate, and the product of lipase-catalyzed polymerization, poly(γ-acetamido-ε-caprolactone) are shown in Figures 99 and 100. DSC thermograms indicate that poly(γ-acetamido-ε-caprolactone) has an amorphous character (no T_m) due to the presence the pendant groups along the polyester backbone and a glass transition at -2 °C. The observed thermal behavior is markedly different from that of saturated polyesters that form crystalline regions due to their regular backbone. TGA analysis indicated that the onset of degradation increased by 40 °C upon the lipase-catalyzed polymerization of compound **8**.

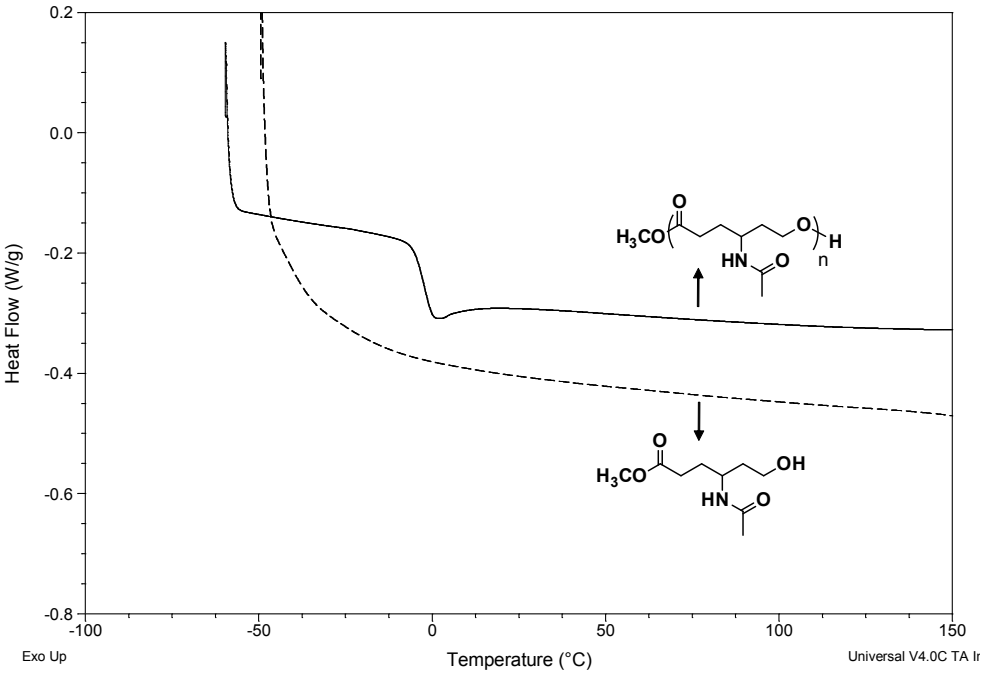

Figure 99. DSC thermograms of the second heating run of poly(γ-acetamido-ε-caprolactone) and methyl 4-acetamido-6-hydroxyhexanoate (compound 8) undergoing a heat/cool/heat cycle under N_2 atmosphere with a heating rate of 10 °C/min and a cooling rate of 5 °C/min.

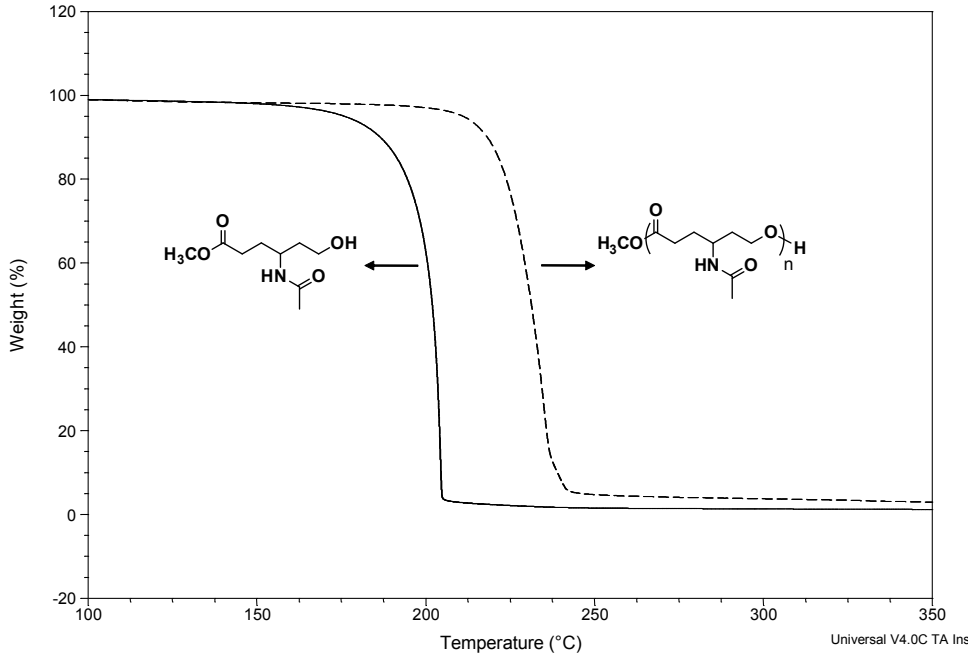

Figure 100. TGA thermograms of poly(γ-acetamido-ε-caprolactone) and methyl 4-acetamido-6-hydroxyhexanoate (compound 8) under N_2 atmosphere using a dynamic mode with a heating rate of 50 °C/min.

Enzyme esterification kinetic analysis

Enzymatic transesterification in organic solvents follows the acyl-enzyme mechanism where the free enzyme binds with the enol ester to form an acyl-enzyme intermediate (EM). In the next step, the alcohol nucleophile deacylates the enzyme ester complex to form the transesterified product, PEA, and free enzyme (*203*). The general reaction scheme is given by the following equation:

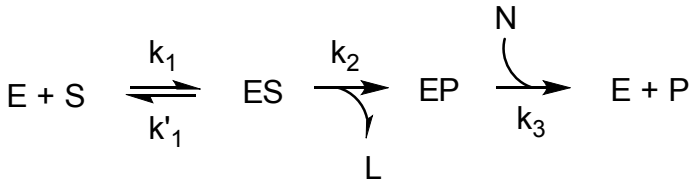

where S and N denote the acyl donor and nucleophile, while E and P denote enzyme and polymer formed. Since monomers were used in equal molar quantities, $S_0 = N_0 = M_0$, and the monomer association with enzyme can be considered to be random, the polymer linkage kinetics are:

$$\frac{dP}{dt} = \frac{k_{cat} \cdot [E] \cdot [M]}{K^{app} + [M]} \qquad \text{Equation 49}$$

where [M] is the concentration of the acyl donor or nucleophiles, [E] represent enzyme concentration, and k_{cat} is the turnover rate. To borrow terms common to Michaelis-Menten kinetics, K^{app} is equal ($K_m + k_2/k_3$) where K_m is , the ratio of (k'_1+k_2/k_1). To get the observable reaction rate, k_{obs} we can let:

$$k_{obs} = \frac{k_{cat} \cdot [E]}{K^{app} + [M]} \qquad \text{Equation 50}$$

and rewrite equation 49 in a first-order form as:

$$\frac{dP}{dt} = k_{obs} \cdot [M] \qquad \text{Equation 51}$$

During the initial stages of the reaction when [M]>> K^{app}, k_{obs} of equation 50 can be regarded as a zero order rate constant. The integrated form of equation 51 was written in terms of average number of structural units, X_n, given that the total number of structural units equals the total number of bifunctional monomers present

$$X_n = k_{obs} \cdot t \qquad \text{Equation 52}$$

In the initial stages of the CAAR-catalyzed polymerization, this was shown to be the case from the GPC analysis data of aliquots removed from the reaction mixture at fixed intervals (Figure 101). As polymerization progressed, **14** displayed increasingly lower solubility in dioxane due to the higher density of amide bonds in the backbone per monomer addition, resulting in polymers with greater crystallinity relative to **12**. Since only the soluble fraction could be detected via GPC, a correct k_{obs} value could not be determined for the polymerization of **14**.

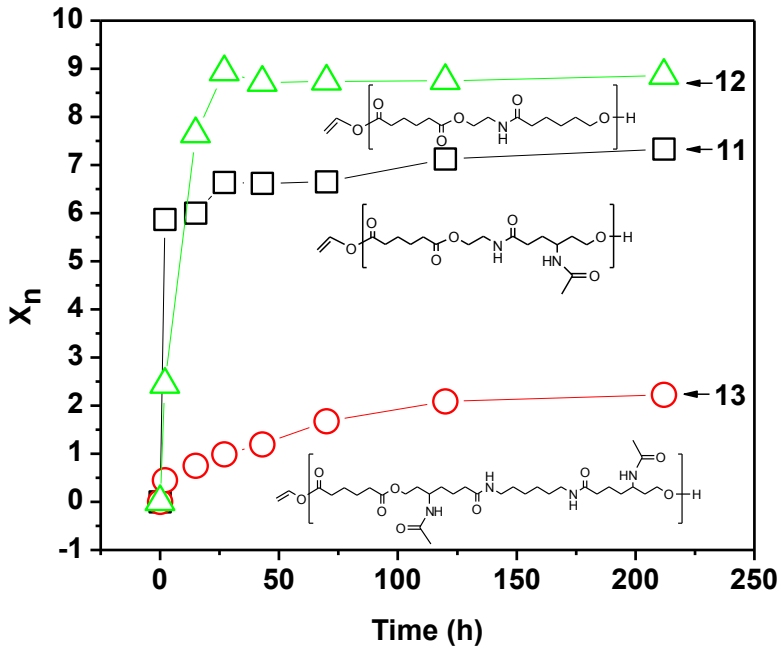

Figure 101. Degree of polymerization over time for a series of substituted and unsubstituted glycol with DVA.

The k_{obs} value for the polymerization of **11** and **13** was calculated to be 0.031 h^{-1} and 0.018 h^{-1}, respectively. Deviation from linearity in the polymerization of **11** was attributed to differences in the reactivity of the hydroxyl functional groups in the AcCL/EA nucleophile (**7**). The presence of unsubstituted –OH and a γ-substituted –OH in **7** results in a nucleophile with functional groups of unequal reactivity due to their steric differences. Polymerization of **12** exhibited a k_{obs} value of 0.47 h^{-1}, or 15 times higher than that of the polymerization of **11,** and 26 times higher than the polymerization of **13**. These results supported the hypothesis that the use of sterically unhindered nucleophiles yielded higher polytransesterification rates in PEA synthesis (Table 22).

Table 22

Rate Constants for CAAR-Catalyzed Determined from Line Fitting of Experimental Data

Polymerization	k_{obs} (h^{-1})	R^2
11	0.031	0.86
12	0.47	0.96
13	0.018	0.98

We also observed that the final molecular weights were vastly different among polymers even between polymers derived from sterically hindered diol monomers. Polymers **11** and **12** from monomeric diols **7** and **8** reached higher final molecular weights than polymer **13** from oligomeric diol **9** (Figure 101). The higher molecular weight and quick cessation in molecular weight growth observed in the polymerization of monomeric diols suggested that during the propagation step monomeric diols move more freely inside the biocatalytic particle relative to oligomeric diols. A similar phenomenon was also observed in the immobilized lipase-catalyzed polycondensation of diacids, diols, and polysiloxane based polyesters *(194,207)*. We suspected that the cessation of growth in molecular weight of **11** and **12** after 50 h was not due to biocatalyst denaturation since X_n in the polymerization of **13** continues to increase up 125 h into the reaction suggesting that some fraction of the original enzyme activity remains.

PDI as a function of diol structure and chain length are shown in Figure 102. PDI values were independent of chain length and reached a plateau of 1.2 - 1.3 for the unsubstituted diols. However, PDI values for γ-substituted diols registered a linear increase throughout the polymerization time. These data

suggests asymmetric growth in molecular weight along with coupling of higher molecular weight fractions during polymerization due to the varied reactivity of the hydroxyl functional groups in the substituted nucleophile. The PDI value of 1.35 after 212 hours is consistent with literature reported PDI values for enzyme-catalyzed polytransesterifications.

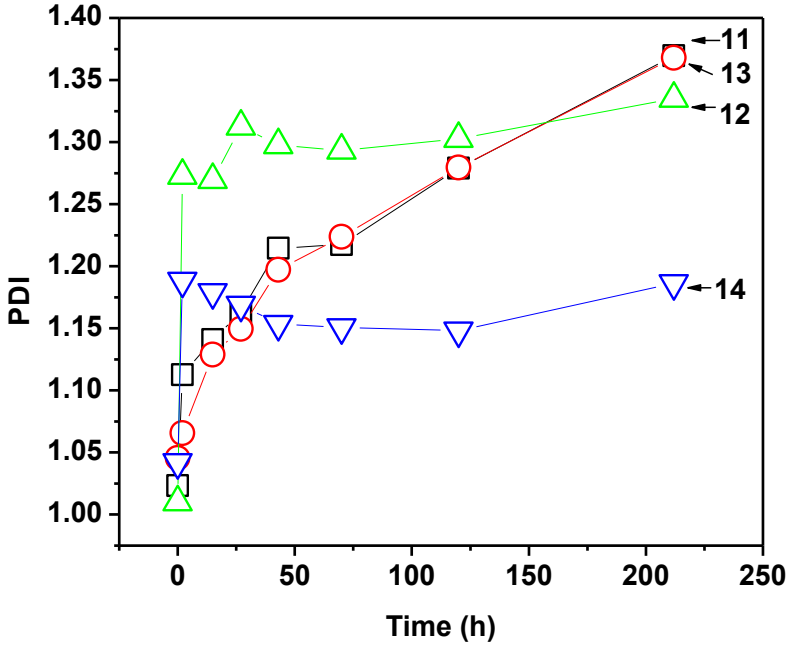

Figure 102. Polydispersity Index (PDI) over time for a series of substituted and unsubstituted glycols with DVA.

Thermal analysis of PEAs

Figures 103 and 104 summarize the thermal properties of PEAs derived from unsubstituted and γ-substituted diol monomers. The PEAs derived from the γ-substituted diols did not exhibit sharp melting transitions. We suspected that the incorporation of the pendant amide group diminished the propensity for the backbone to crystallize. On the other hand, the linear PEA (CL/EA-DVA) exhibited a broad melting transition. A low temperature T_g transition was observed in CL/EA-DVA which corresponded to approximately the theoretical T_g

considering the broad melting transition observed at temperatures >100 °C and the empirical relationship for unsymmetrical polymer T_g/T_m ~ 0.67(*124*). Thermogravimetric analysis confirmed that PEAs derived from the γ-substituted diols exhibited similar onset of degradation temperatures among each other. However, the onset of degradation temperature was higher than in the PEA derived from the unsubstituted diol. The transitions observed above 500 °C in all PEAs were attributed to loss of char.

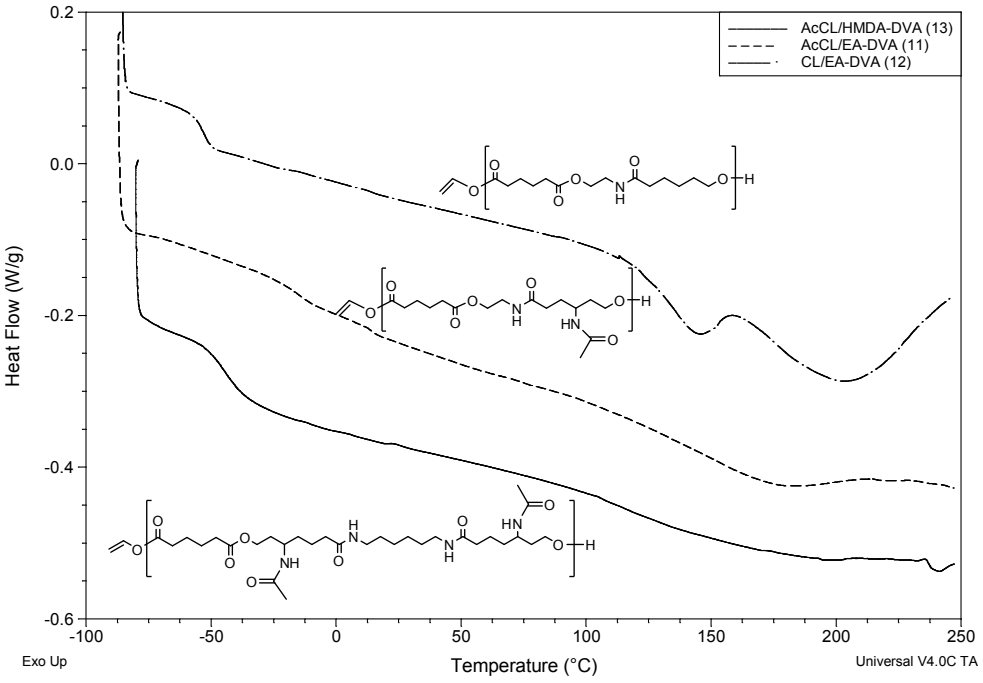

Figure 103. Thermal properties of PEAs with pendant functional groups. DSC thermograms are from 2nd heating cycle of a heat/cool/heat schedule.

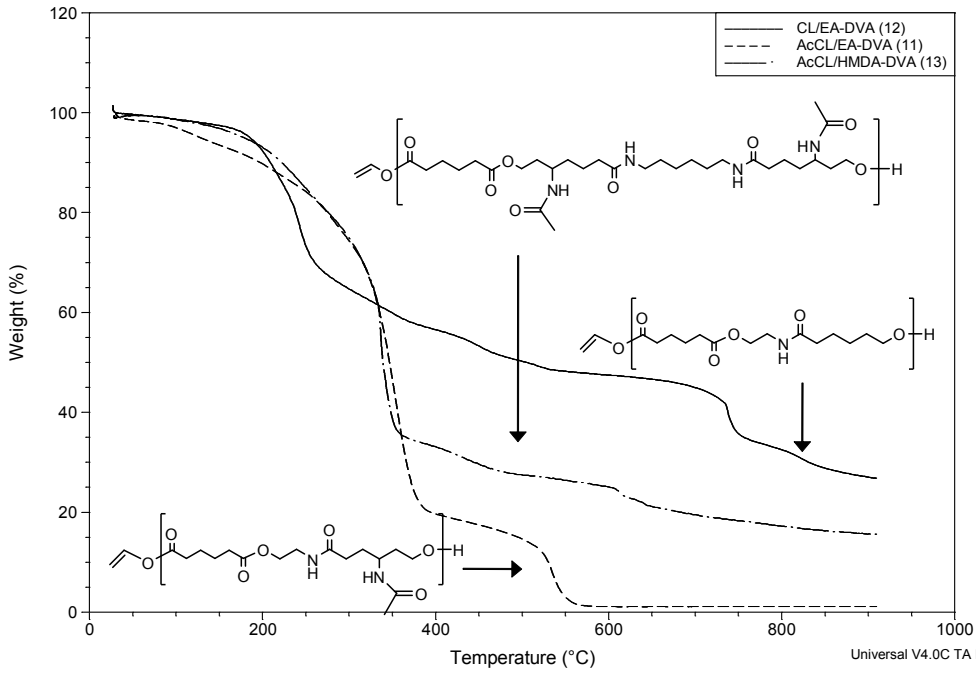

Figure 104. Thermal stability of PEAs with pendant functional groups. TGA thermograms were obtained using a heating of 50 °C/min under nitrogen.

Conclusions

Poly (γ-acetamido-ε-caprolactone) was synthesized with M_n 2,600 g/mol via one pot, two-step process using *Candida Antarctica* lipase acrylic resin as catalyst. Initially, base catalyzed ring opening was conducted in methanol at room temperature followed by bulk polymerization in the presence of *Candida Antarctica* lipase acrylic resin at 60 °C for 150 h. The resulting polymer was determined to be amorphous in nature due to the presence of pendant groups along the polyester backbone.

Rate constants for CAAR-catalyzed polyesterifications were examined as a function of monomer structure. Polymerization kinetics were characterized by initial linear molecular weight growth and a plateau in the later stages of polymerization. We observed that sterically hindered nucleophiles by the γ-

substitution exhibited lower polymerization rates relative to unhindered nucleophiles. In addition, the polymerization of monomeric diols yielded higher molecular weight PEAs due to higher relative mobility inside the biocatalytic particle relative to oligomeric diols. PDI values for γ-substituted diols exhibited a linear increase suggesting asymmetric growth in molecular weight due to difference in reactivity of the sterically hindered and unhindered hydroxyl functional groups. Thermal analysis of PEAs suggested that the pendant amide improved thermal stability.

CHAPTER IX

CONCLUSIONS AND FUTURE WORK

This dissertation describes a novel strategy to render materials capable of "smart" surface and bulk properties with the aid of embedded biocatalyst and latent functional groups that are selectively activated in the presence of biocatalyst to undergo chemical transformation. The research presented herein focused on experimentally characterizing the activity of lipase catalysts embedded in poly (alkyl methacrylate)s alongside with functional groups, either as freely diffusing within the polymeric matrix or tethered to the matrix. Lipase activity, ester forming (synthetic) or ester breaking (hydrolytic), will provide the pathway for the polymer matrix to self-modulate its properties by catalytic transformation of the untethered or tethered functionality. The research established that regardless of bond forming or breaking, matrices containing hydroxyl, carboxylic acid, and/or ester groups can be modified *in situ* at ambient.

In solution, biocatalyzed ester formation followed the rate law derived from theory based on the accepted serine hydrolase (lipase) mechanism. The Michaelis-Menten form of the rate law was shown to be valid regardless of whether one monomer is in excess or the monomers are in stoichiometric proportions. This mathematical treatment and correlation of variables to achieve the same result set the precedent for the expected enzyme intrinsic kinetic behavior of the synthetic or hydrolytic reaction. In toluene solutions, when the initial OA and 1-NN concentrations were >200 mM, the derived rate law did not hold in the initial stages of the reaction due to a delay in ester production. The

observed lag time was attributed partly to the cooperative binding with both OA and 1-NN and partly to inhibitory effects of the nucleophile as determined by end-point titration studies. When OA and 1-NN concentrations were less than 200 mM, GC characterization indicated initial zero order behavior as expected by the Michaelis-Menten equation. The values for k_{cat} and K^{app} for the model reaction in toluene were determined to be 3.29 μM/h and 115 mM, respectively.

Several enzyme sources were studied for internal comparison and the activity of a P-Lipolase and E-CALB was compared to the activity of other commercially available lipases such as PPL and PFL in neat organic solvents and solutions containing monomer or functionalized copolymers. Upon solubilization, modified enzymes remained largely active in nonpolar solvents and solutions of monomer or functionalized copolymers. The presence of thiol-terminated compounds, i.e., polymer precursors negatively affected lipase activity and we suspected that thiols were disrupting biocatalyst conformation via the thiol-disulfide exchange reaction(s). PPL remained active in 20 wt% copolymer solutions up to 46 mol% functional content. Diminishment in activity was observed in solution of copolymers with increasing mole fraction of functionality and residence time in solution. P-Lipolase activity dropped significantly in the copolymer functional series with the highest functionality, while E-CALB activity exhibited the highest activity in copolymer functional series with the highest mol% functional content. The diminished relative activity in functionalized copolymer solutions indicated that copolymer functional groups were interacting with the amino acid side groups either on the enzyme shell or

inside the active site. Interactions with the amino acid side groups would lead to denaturation by unraveling the enzyme globular structure, while interactions with the active site would poison the biocatalyst.

In vivo, enzymes catalyze reactions efficiently and selectively in highly crowded cellular media. Typically, the excluded volume set by cellular macromolecular complexes drives biocatalyst activity by introducing diffusional resistance and concentration gradients of functional groups within the cell. Since the research platform focused on embedding functional components and enzymes in the same matrix to alter chemical or mechanical properties based on the reaction kinetics, we focused on understanding the kinetic behavior as a function of increasing constrains. We demonstrated that PPL catalytic activity in viscous solutions of toluene comprised of 1% solid to 20% solids of PMMA was similar to the PPL activity in neat toluene. By using simple scaling law arguments, we confirmed that the reason for similarity in activity despite higher solution macroviscosity was that the solution mesh sizes established by the excluded volume of polymer segments were larger in diameter than the OA / 1-NN and the enzyme. Since screening did not occur in the 1% to 20% solid PMMA solutions, we suspected that OA / 1-NN and enzyme diffusion rates in polymer solutions were similar to the diffusion rates in neat toluene.

In more constrained systems comprised of amorphous glassy or rubbery films with embedded enzymes and small molecule –OH and –COOH functionality, we observed biocatalytic ester synthetic activity after film solidification. Biocatalytic films exhibited high activity towards ester formation in

the bulk and film surface though surface activity was approximately 30 times lower than the bulk activity. The slower biosynthesis rate observed at the film surface was attributed to diminished access and diffusion limited rate of sorption for OA and 1-NN to reach the biocatalyst. Direct comparison of surface activity and bulk activity in glassy and rubbery poly (alkyl methacrylate) films suggested that the rate of OA and 1-NN uptake was much slower that the rate of biocatalyzed conversion. Biocatalytic film activity was ca. 16 times lower than organic media activity. The lower activity observed in films with embedded biocatalyst alongside embedded small molecule functionality was attributed to the increase in diffusional resistance experienced by the –COOH and –OH functional molecules. In fact, the dimensionless modulus for the OA /1-NN was high in all poly (alkyl methacrylate) films indicating that the reaction rate was much faster than the self-diffusion coefficient of OA/1-NN.

We explored reaction kinetics in matrices embedded with biocatalyst along with small molecule functionality and observed that typical progress curves were characterized by a zero order increase in ester synthesis until a plateau was reached at high conversion ca.80-95 % depending on temperature, reactant, and enzyme loading. In glassy polymers, typical progress curves manifested two stages of ester formation with an initial stage that had higher rates than the second stage. Higher rates in the first stage of the reaction were attributed to kinetically trapped polymer microstructures that favored the presence of excess free volume. The diminished rate of the second stage represented ester

synthesis in quasi-equilibrium microstructures after sub-T_g aging of polymer chains consumed portions of excess free volume.

Glassy biocatalytic films with biocatalyst loadings higher than 2% by weight converted more than 50% of the functionality during film drying stages, i.e., within the first 9 h after casting from solution. Thus, biocatalytic activity could only be obtained for films with less than 2% PPL loading. Poly (alkyl methacrylate) films, glassy or rubbery, had increasing amounts of free volume with increased loadings of OA and 1-NN. The exponential increase in biocatalytic activity with increased loading of OA and 1-NN was attributed to increased diffusivity and solubility of the small molecule functionality.

Biocatalytic activity was determined to be driven mainly by OA and 1-NN diffusivity at loadings of less than 8%, while above this loading, biocatalytic activity was driven by increasing OA and 1-NN solubility. We proposed that diffusivity at low loading levels occurs by OA / 1-NN entering polymer voids with end using relative volume measurements via density and PALS. To validate that biocatalytic activity in glassy polymers is free volume mediated, a tertiary inert small molecule, i.e., solvent plasticizer, was employed to control biocatalytic activity. It was determined that solvent evaporation from films drove the presence of more free volume site as film thickness increased, which led to a linear increase in biocatalyst activity due to ease of OA / 1-NN diffusivity in glassy films.

The temperature dependence of biocatalytic activity was examined in glassy and rubbery polymers. In glassy polymers, the first stage of ester

formation rate exhibited a strong dependence on sub-T_g aging of polymer. Biocatalytic activity was driven by small molecule migration in kinetically trapped excess free volume within interconnected OA and 1-NN rich regions. It was found that when the glassy polymer was annealed ($T_{rxn} > T_g$), biocatalytic activity became increasingly diffusion controlled, which was attributed to polymer losing excess free volume and the formation of discrete OA and 1-NN rich regions. In rubbery polymer control systems, biocatalyst activity was driven by the diffusivity of OA and 1-NN within interconnected functional group rich regions as evidenced by activity temperature dependence best described by VFT and WLF models. At temperatures above 60 °C, corresponding to temperatures 50 °C above T_g, biocatalytic activity became dependent on the migration of OA and 1-NN from discrete functional group rich microphases corresponding to diminishing standard energy of activation.

Bioactivity studies in blends cast from various solvents validated that enzyme activity was largely dependent on glassy microstructure. A spike in bioactivity was observed when the solvent solubility parameter was matched with that of the host matrix indicating that solvent molecules act as transient templates, which upon evaporation leave behind free volume sites. Favorable attractive interactions and large transient molecule molar volume were identified as key parameters that promoted microstructures consisting of relatively high fraction of free volume and interconnected OA and 1-NN pathways, which resulted in higher relative bioactivity. Additionally, the observed trend in activity was not dependent on solvent evaporation rate or selective partitioning of OA

and 1-NN within discrete sol microphases determined by comparison with data from analogous studies in organic media.

The consistent near ambient activity characterized in these films containing enzyme and small molecules functional groups validate a broad range of conditions that support the biocatalytic reaction. The systems studied exhibit potential as materials with switchable surface properties, e.g., hydrophobic and hydrophilic, bulk properties, e.g., modulus, degree of stiffness, resiliency, and impact strength, via equilibrium control of environmental conditions to alter the ratio of reactants to products. We demonstrated that in PMMA and PEMA films with embedded biocatalyst alongside embedded functionality, the conversion of OA and 1-NN to NOc was reversible based on the equilibrium water content.

The degrees of freedom were further constrained by tethering the –COOH and –OH functional groups to an acrylate and acrylamide polymer backbone. The ability to control the reaction would give rise to self-mendable or self-degradable materials and control over the material's rubber elastic behavior. Enzyme activity assays in coatings from polyacid and polyalcohol blends indicated that the synthesized functional polymers act as substrate mimics in cases when the functional groups are at least 10 methylene units away from backbone. The synthesized comb-like –COOH and –OH copolymers were compatible with each other as signified by the presence of a single T_g.

We investigated reaction kinetics in copolymer blends at $T_{cure}>T_g$ and observed that the diminishment in acid equivalents follows similar rate as increase in molecular weight as determined by GPC when Lipase acrylic resin

from *Candida Antarctica* was used as a catalyst. The gel point for Lipase acrylic resin from *Candida Antarctica* catalyzed systems was 25% conversion, which was similar to the conversion obtained after 200 h of cure, raising the possibility that at some critical conversion, functional groups will have diminished access to the enzyme active site as network formation will limit the mobility of the unreacted tethered functionality. The f_{avg} value indicated that at the end of the evaluation, 0.5 acid functional chains had coupled with 0.5 hydroxyl functional chains. Molecular weight observations indicated that the lower molecular weight fraction, i.e., higher mobility species, participated in the reaction to a greater extent.

In blends cured at $T_{cure} \geq T_g$, the T_g of coatings containing P-Lipolase was consistently lower than that of coatings without any enzyme. Increased T_g was observed in both systems, however, it progressed faster in the coatings without enzymes. The results indicated that a higher molecular weight sample was obtained after cure since the functionalized side chains were unable to undergo the fast volume relaxation that led to higher T_gs in coatings in the absence of biocatalyst. GPC analysis confirmed the hypothesis since in copolymer blends in the presence of P-Lipolase M_n increased overtime, while no increase in M_n was observed in control coatings. However, gelation did not take place, which indicated that further optimization in terms of biocatalyst compatibility and loading is necessary to obtain crosslinkable coatings.

Finally, a series of novel monomers were polymerized via enzyme catalysis to yield poly (ester amide)s. Poly (γ-acetamido-ε-caprolactone) was

synthesized with M_n 2,600 g/mol via one pot, two-step process using *Candida Antarctica* lipase acrylic resin as catalyst. Initially, base catalyzed ring opening was conducted in methanol at room temperature followed by bulk polymerization in the presence of *Candida Antarctica* lipase acrylic resin at 60 °C for 150 h. The resulting polymer was determined to be amorphous in nature due to the presence of pendant groups along the polyester backbone.

Rate constants for CAAR-catalyzed polyesterifications were examined as a function of monomer structure. Polymerization kinetics were characterized by initial linear molecular weight growth and a plateau in the later stages of polymerization. We observed that sterically hindered nucleophiles by the γ-substitution exhibited lower polymerization rates relative to unhindered nucleophiles. In addition, the polymerization of monomeric diols yielded higher molecular weight PEAs due to higher relative mobility inside the biocatalytic particle relative to oligomeric diols. PDI values for γ-substituted diols exhibited a linear increase suggesting asymmetric growth in molecular weight due to difference in reactivity of the sterically hindered and unhindered hydroxyl functional groups.

In general, the research demonstrated that regardless of bond forming or breaking, matrices containing hydroxyl, carboxylic acid, and/or ester groups either blended in or covalently tethered can be modified *in situ* at temperature ranging from ambient up to 70 °C. In diffusion-limited systems, the reaction rate was controlled by the fraction of free volume and exhibited temperature dependence that mirrored the temperature dependence of polymer chain

relaxations. Despite this characterization, a large amount of work remains before the transformation of functional groups either blended or covalently attached can be directly related to the final properties of the polymeric material.

In this regard, several areas should be explored. Coupling biocatalyzed kinetics and mechanical properties would provide valuable information about the influence of functionality on the properties of the polymer. A variety of thermoplastic coating/composite systems and additives should be scanned for compatibility with biocatalyst and property changes upon transformation of the functionality. In addition, the observed kinetic behavior should be compared across various polymer systems to determine the universality of the effects of polymer structure and processing conditions on the catalyzed transformation.

From the catalyst perspective, many orthogonal catalyst systems should be investigated using as a framework the experimental study put forth. Catalyst choice should not be limited to biocatalysts given the size, mobility, and compatibility considerations that are prerequisites for reactions to occur under a large variety of conditions and polymer materials. In addition, biocatalyst conjugation with photo- , mechanico-, thermo-, electro- responsive polymers that reversibly block access to the enzyme active site should be explored to engineer triggers in catalyst activity that are independent of the use environment.

Finally, incorporating biocatalyst in thermosets containing catalytically active linkages would produce systems able to undergo physical and chemical changes post network formation. One important engineering requirement for these systems is that the mesh size of the network has to match the biocatalyst

diameter to allow biocatalyst access to the reactive bonds. These systems would exhibit unique mechanical properties bestowed from the reversible arrangement of the covalent bonds.

BIBLIOGRAPHY

(1) Berg, J. M.; Tymoczko, J. L.; Stryer, L. *Biochemistry* 5th ed.; Freeman Company: New York, 2001.

(2) Tischer, W.; Kasche, V. Immobilized Enzymes: Crystals or Carriers? *Trends in Biotechnology* **1999**, *17*, 326.

(3) Schulze, B.; Wubbolts, M. G. Biocatalysis for Industrial Production of Fine Chemicals. *Current Opinion in Biotechnology* **1999**, *10*, 609.

(4) Zaks, A.; Klibanov, A. M. Enzyme-Catalyzed Processes in Organic Solvents. *Proceedings to the National Academy of Sciences* **1985**, *82*, 3192.

(5) Zaks, A.; Klibanov, A. M. Enzymic Catalysis in Nonaqueous Solvents. *Journal of Biological Chemistry* **1988**, *263*, 3194.

(6) Fox, R. J.; Davis, S. C.; Mundorff, E. C.; Newman, L. M.; Gavrilovic, V.; Ma, S. K.; Chung, L. M.; Ching, C.; Tam, S.; Muley, S.; Grate, J.; Gruber, J.; Whitman, J. C.; Sheldon, R. A.; Huisman, G. W. Improving Catalytic Function by ProSAR-driven Enzyme Evolution. *Nature Biotechnology* **2007**, *25*, 338.

(7) Roessl, U.; Nahalka, J.; Nidetzky, B. Carrier-free Immobilized Enzymes for Biocatalysis. *Biotechnology Letters* **2010**, *32*, 341.

(8) Cao, L. *Carrier-bound Immobilized Enzymes: Principles, Application and Design*; Wiley-Vch Verlag GmbH & Co. KGaA: Weinheim, 2005.

(9) Trevan, M. D. *Immobilized Enzymes*; John Wiley & Sons Ltd.: New York, 1980.

(10) *Biosensors and Their Applications*; Victor C. Yang, That T. Ngo, Ed.; Kluwer Academic/Plenum Publishers: New York, 1999.

(11) *Handbook of Affinity Chromatography*; Hage, D. S., Ed.; Taylor & Francis Group: Boca Raton, Florida, 2006; Vol. 92.

(12) Koepsel, R. R.; Russell, A. J. Directed Capture of Enzymes and Bacteria on Bioplastic Films. *Biomacromolecules* **2003**, *4*, 850.

(13) McDaniel, C. S.; McDaniel J. M.; Wales, M. E.; Wild, J. R. Biocatalytic Coatings. *Paints & Coatings Industry* **2005**, 26.

(14) Ganesh, M.; Dave, R. N.; L'Amoreaux, W.; Gross, R. A. Embedded Enzymatic Biomaterial Degradation. *Macromolecules* **2009**, *42*, 6836.

(15) Dinu, C. Z.; Zhu, G.; Bale, S. S.; Anand, G.; Reeder, P. J.; Sanford, K.; Whited, G.; Kane, R. S.; Dordick, J. S. Enzyme-Based Nanoscale Composites for Use as Active Decontamination Surfaces. *Advanced Functional Materials* **2010**, *20*, 392.

(16) Singh, A.; Lee, Y.; Dressick, W. J. Self-Cleaning Fabrics for Decontamination of Organophosphorous Pesticides and Related Chemical Agents. *Advanced Materials* **2004**, *16*, 2112.

(17) Lambourne, R.; Strivens, T. A. *Paint and Surface Coatings: Theory and Practice*; Second ed.; Woodhead Publishing Limited: Cambridge England, 1999.

(18) Zaks, A.; Klibanov, A. M. Enzymatic Catalysis in Organic Media at 100 °C. *Science* **1984**, *224*, 1249.

(19) Sitnitsky, A. E. Solvent Viscosity Dependence for Enzymatic Reactions. *Physica A: Statistical Mechanics and its Applications* **2008**, *387*, 5483.

(20) Pocker, Y.; Janjic, N. Enzyme Kinetics in Solvents of Increased Viscosity. Dynamic Aspects of Carbonic Anhydrase Catalysis. *Biochemistry* **1987**, *26*, 2597.

(21) Muramatsu, N.; Minton, A. P. Tracer Diffusion of Globular Proteins in Cocentrated Protein Solutions. *Proceedings to the National Academy of Sciences* **1988**, *85*, 2984.

(22) Gavish, B.; Werber, M. M. Viscosity-Dependent Structural Fluctuations in Enzyme Catalysis. *Biochemistry* **1979**, *18*, 1269.

(23) Meste, M. L.; Champion, D.; Roudaut, G.; Blond, G.; Simatos, D. Glass Transition and Food Technology: A Critical Appraisal. *Journal of Food Science* **2002**, *67*, 2444.

(24) Bell, L.; White, K. Thiamin Stability in Solids as Affected by the Glass Transition. *Journal of Food Science* **2000**, *65*, 498.

(25) Kouassi, K.; Roos, Y. H. Glass Transition and Water Effects on Sucrose Inversion by Invertase in a Lactose−Sucrose System. *Journal of Agricultural and Food Chemistry* **2000**, *48*, 2461.

(26) Kouassi, K.; Roos, Y. H. Glass Transition and Water Effects on Sucrose Inversion in Noncrystalline Carbohydrate Food Systems. *Food Research International* **2001**, *34*, 895.

(27) Gedde, U. W. *Polymer Physics*; Chapman and Hall, 1995.

(28) Rubinstein, M.; Colby, R. H. *Polymer Physics*; Oxford University Press, 2003.

(29) Bosley, J. Turning Lipases into Industrial Biocatalysts. *Biochemical Society Transactions* **1997**, *2*, 174.

(30) Bosley, J. A.; Clayton, J. C. Blueprint for a Lipase Support: Use of Hydrophobic Controlled-Pore Glasses as Model Systems. *Biotechnology and Bioengineering* **1994**, *43*, 934.

(31) Fonseca, L. P.; Cardoso, J. P.; Cabral, J. M. S. Immobilization Studies of an Industrial Penicillin Acylase Preparation on a Silica Carrier. *Journal of Chemical Technology & Biotechnology* **1993**, *58*, 27.

(32) D'Urso, E. M.; Fortier, G. Albumin-Poly(Ethylene Glycol) Hydrogel as Matrix for Enzyme Immobilization: Biochemical Characterization of Crosslinked Acid Phosphatase. *Enzyme and Microbial Technology* **1996**, *18*, 482.

(33) Novick, S. J.; Dordick, J. S. Investigating the Effects of Polymer Chemistry on Activity of Biocatalytic Plastic Materials. *Biotechnology and Bioengineering* **2000**, *68*, 665.

(34) Chen, B.; Miller, M. E.; Gross, R. A. Effects of Porous Polystyrene Resin Parameters on Candida antarctica Lipase B Adsorption, Distribution, and Polyester Synthesis Activity. *Langmuir* **2007**, *23*, 6467.

(35) Burton, A. F. M. *CRC Handbook of Solubility Parameters and Other Cohesion Parameters*; 2nd ed.; CRC Press, 1991.

(36) Abe, H.; Doi, Y.; Aoki, H.; Akehata, T.; Hori, Y.; Yamaguchi, A. Physical Properties and Enzymic Degradability of Copolymers of (R)-3-Hydroxybutyric and 6-Hydroxyhexanoic Acids. *Macromolecules* **1995**, *28*, 7630.

(37) Novick, S. J.; Dordick, J. S. Protein-containing Hydrophobic Coatings and Films. *Biomaterials* **2002**, *23*, 441.

(38) Tweddell, R. J.; Kermasha, S.; Combes, D.; Marty, A. Immobilization of Lipase from Rhizopus Niveus: A Way to Enhance its Synthetic Activity in Organic Solvent. *Biocatalysis and Biotransformation* **1999**, *16*, 411.

(39) Cao, L. Immobilised Enzymes: Science or Art? *Current Opinion in Chemical Biology* **2005**, *9*, 217.

(40) Kamei, S.; Okubo, M.; Matsuda, T.; Matsumoto, T. Adsorption of Trypsin onto Styrene-2-hydroxyethyl Methacrylate Copolymer Microspheres and its Enzymatic Activity. *Colloid and Polymer Science* **1986**, *264*, 743.

(41) Penzol, G.; Armisén, P.; Fernández-Lafuente, R.; Rodés, L.; Guisán, J. M. Use of Dextrans as Long and Hydrophilic Spacer Arms to Improve the Performance of Immobilized Proteins Acting on Macromolecules. *Biotechnology and Bioengineering* **1998**, *60*, 518.

(42) Weisman, G. R.; Sundberg, D. C.; Cimini, R. A.; Brown, M. G.; Beno, B. R.; Eighmy, T. Controlled Release Antifouling Coatings. I. Approaches for Controlled Release of 2,4-dinitrophenolate and Benzoate into Seawater. *Biofouling* **1992**, *6*, 123.

(43) (EPA), E. P. A., Ed.; Federal Register: 1999; Vol. 64, p 60194.

(44) Olsen, S. M.; Pedersen, L. T.; Laursen, M. H.; Kiil, S.; Dam-Johansen, K. Enzyme-based Antifouling Coatings: a review. *Biofouling* **2007**, *23*, 369.

(45) Yebra, D. M.; Kiil, S.; Dam-Johansen, K. Antifouling Technology-Past, Present and Future Steps Towards Efficient and Environmentally Friendly Antifouling Coatings. *Progress in Organic Coatings* **2004**, *50*, 75.

(46) Asuri, P.; Karajanagi, S. S.; Kane, R. S.; Dordick, J. S. Polymer-Nanotube-Enzyme Composites as Active Antifouling Films. *Small* **2007**, *3*, 50.

(47) Grundmann, H.; Aires-de-Sousa, M.; Boyce, J.; Tiemersma, E. Emergence and Resurgence of Meticillin-resistant Staphylococcus Aureus as a Public-health Threat. *The Lancet* **2006**, *368*, 874.

(48) Klibanov, A. M. Permanently Microbicidal Materials Coatings. *Journal of Materials Chemistry* **2007**, *17*, 2479.

(49) Haldar, J.; An, D.; Cienfuegos, L. A.; Chen, J.; Klibanov, A. M. Polymeric Coatings that Inactivate Both Influenza Virus and Pathogenic Bacteria. *Proceedings to the National Academy of Sciences* **2006**, *103*, 17667.

(50) Conte, A.; Sinigaglia, M.; Nobile, M. A. Antimicrobial Effectiveness of Lysozyme Immobilized on Polyvinylalcohol-Based Film against *Alicyclobacillus Acidoterrestris*. *Journal of Food Protection* **2006**, *69*, 861.

(51) Lichter, J. A.; Van Vliet, K. J.; Rubner, M. F. Design of Antibacterial Surfaces and Interfaces: Polyelectrolyte Multilayers as a Multifunctional Platform. *Macromolecules* **2009**, *42*, 8573.

(52) Kumar, R.; Münstedt, H. Silver Ion Release from Antimicrobial Polyamide/silver Composites. *Biomaterials* **2005**, *26*, 2081.

(53) Tang, J.; Xiong, L.; Wang, S.; Wang, J.; Liu, L.; Li, J.; Wan, Z.; Xi, T. Influence of Silver Nanoparticles on Neurons and Blood-brain Barrier via Subcutaneous Injection in Rats. *Applied Surface Science* **2008**, *255*, 502.

(54) Cudic, M.; Otvos, L. Intracellular Targets of Antibacterial Peptides. *Current Drug Targets* **2002**, *3*, 101.

(55) Wu, J. A.; Kusuma, C.; Mond, J. J.; Kokai-Kun, J. F. Lysostaphin Disrupts Staphylococcus aureus and Staphylococcus epidermidis Biofilms on Artificial Surfaces. *Antimicrobial Agents and Chemotherapy* **2003**, *47*, 3407.

(56) Fischetti, V. A. Bacteriophage Lytic Enzymes: Novel Anti-infectives. *Trends in Microbiology* **2006**, *13*, 491.

(57) Loeffler, J. M.; Nelson, D.; Fischetti, V. A. Rapid Killing of Streptococcus pneumoniae with a Bacteriophage Cell Wall Hydrolase. *Science* **2001**, *294*, 2170.

(58) Schuch, R.; Nelson, D.; Fischetti, V. A. A Bacteriolytic Agent that Detects and Kills Bacillus anthracis. *Nature* **2002**, *418*, 884.

(59) Pangule, R. C.; Brooks, S. J.; Dinu, C. Z.; Bale, S. S.; Salmon, S. L.; Zhu, G.; Metzger, D. W.; Kane, R. S.; Dordick, J. S. Antistaphylococcal Nanocomposite Films Based on Enzyme-Nanotube Conjugates. *ACS Nano* **2010**, *4*, 3993.

(60) Drevon, G. F.; Danielmeier, K.; Federspiel, W.; Stolz, D. B.; Wicks, D. A.; Yu, P. C.; Russell, A. J. High-Activity Enzyme-Polyurethane Coatings. *Biotechnology and Bioengineering* **2002**, *79*, 785.

(61) McDaniel, C. S.; McDaniel, J.; Wales, M. E.; Wild, J. R. Enzyme-based Additives for Paints and Coatings. *Progress in Organic Coatings* **2006**, *55*, 182.

(62) Lele, B. S.; Papworth, G.; Katsemi, V.; Ruterjans, H.; Martyano, I.; Klabunde, K. J.; Russell, A. J. Enhancing Bioplastic–Substrate Interaction Via Pore Induction and Directed Migration of Enzyme Location. *Biotechnology and Bioengineering* **2004**, *86*, 628.

(63) Tong, X.; Trivedi, A.; Jia, H.; Zhang, M.; Wang, P. Enzymic Thin Film Coatings for Bioactive Materials. *Biotechnology Progress* **2008**, *24*, 714.

(64) Ulijn, R. V. Enzyme-responsive Materials: A New Class of Smart Biomaterials. *Journal of Materials Chemistry* **2006**, *16*, 2217.

(65) Yang, Z.; Xu, B. A Simple Visual Assay Based on Small Molecule Hydrogels for Detecting Inhibitors of Enzymes. *Chemical Communications* **2004**, 2424.

(66) Hassan, C. M.; Doyle, F. J.; Peppas, N. A. Dynamic Behavior of Glucose-Responsive Poly(methacrylic acid-g-ethylene glycol) Hydrogels. *Macromolecules* **1997**, *30*, 6166.

(67) Toledano, S.; Williams, R. J.; Jayawarna, V.; Ulijn, R. V. Enzyme-Triggered Self-Assembly of Peptide Hydrogels via Reversed Hydrolysis. *Journal of American Chemical Society* **2006**, *128*, 1070.

(68) Andreana, P. R.; Xie, W.; Wang, P. G. *Biocatalysis in Polymer Science*; Gross, R. A., Cheng, H. N., Eds.; ACS Symposium Series: Washington DC, 2003, p 188.

(69) Xie, J.; Hsieh, Y.-L. *Biocatalysis in Polymer Science*; Gross, R. A., Cheng, H. N., Eds.; ACS Symposium Series: Washington DC, 2002; Vol. 840, p 217.

(70) Gubitz, G. M.; Paulo, A. C. New Substrates for Reliable Enzymes: Enzymatic Modification of Polymers. *Current Opinion in Biotechnology* **2003**, *14*, 577.

(71) Vertommen, M. A. M. E.; Nierstrasz, V. A.; Veer, M. V. D.; Warmoeskerken, M. M. C. G. Enzymatic Surface Modification of Poly(ethylene terephthalate). *Journal of Biotechnology* **2005**, *120*, 376.

(72) Rizzarelli, P.; Impallomeni, G.; Montaudo, G. Evidence for Selective Hydrolysis of Aliphatic Copolyesters Induced by Lipase Catalysis. *Biomacromolecules* **2003**, *5*, 433.

(73) Abe, H.; Doi, Y.; Aoki, H.; Akehata, T. Solid-State Structures and Enzymatic Degradabilities for Melt-Crystallized Films of Copolymers of (R)-3-Hydroxybutyric Acid with Different Hydroxyalkanoic Acids. *Macromolecules* **1998**, *31*, 1791.

(74) Sambasivam, M.; Klein, A.; Sperling, L. H. The Molecular Basis of Fracture in Polystyrene Films: Role of molecular weight. *Journal of Applied Polymer Science* **1995**, *58*, 357.

(75) Haacke, G.; Andrawes, F. F.; Campbell, B. H. *Migration of light Stabilizers in Acrylic/melamine Clearcoats*; Federation of Societies for Coatings Technology: Blue Bell, PA, ETATS-UNIS, 1996; Vol. 68.

(76) White, S. R.; Sottos, N. R.; Geubelle, P. H.; Moore, J. S.; Kessler, M. R.; Sriram, S. R.; Brown, E. N.; Viswanathan, S. Autonomic Healing of Polymer Composites. *Nature* **2001**, *409*, 794.

(77) Chen, X.; Dam, M. A.; Ono, K.; Mal, A.; Shen, H.; Nutt, S. R.; Sheran, K.; Wudl, F. A Thermally Re-Mendable Cross-Linked Polymeric Material. *Science* **2002**, *295*, 1698.

(78) Sijbesma, R. P.; Beijer, F. H.; Brunsveld, L.; Folmer, B. J. B.; Hirschberg, J. J. K. K.; Lange, R. F. M.; Lowe, J. K. L.; Meijer, E. W. Reversible Polymers Formed from Self-Complementary Monomers Using Quadruple Hydrogen Bonding. *Science* **1997**, *278*, 1601.

(79) Beck, J. B.; Rowan, S. J. Multistimuli, Multiresponsive Metallo-Supramolecular Polymers. *Journal of the American Chemical Society* **2003**, *125*, 13922.

(80) Niu, W.; O'Sullivan, C.; Rambo, B. M.; Smith, M. D.; Lavigne, J. J. Self-repairing Polymers: Poly(dioxaborolane)s Containing Trigonal Planar Boron. *Chemical Communications* **2005**, 4342.

(81) Kwisnek, L.; Kaushik, M.; Hoyle, C. E.; Nazarenko, S. Free Volume, Transport, and Physical Properties of n-Alkyl Derivatized Thiol-Ene Networks: Chain Length Effect. *Macromolecules* **2010**, *43*, 3859.

(82) Marra, K. G.; Winger, T. M.; Hanson, S. R.; Chaikof, E. L. Cytomimetic Biomaterials. 1. In-Situ Polymerization of Phospholipids on an Alkylated Surface. *Macromolecules* **1997**, *30*, 6483.

(83) Sells, T. D.; O'Brien, D. F. Two-dimensional Polymerization of Lipid Bilayers: Degree of Polymerization of Acryloyl Lipids. *Macromolecules* **1994**, *27*, 226.

(84) Tarkin-Tas, E., Design, Synthesis, and Polymerization of Novel Heterocyclic Monomers as Precursors for Functional Polyesters, Poly(ester amide)s and Polyamides, The University of Southern Mississippi, 2010.

(85) Kobayashi, S.; Makino, A. Enzymatic Polymer Synthesis: An Opportunity for Green Polymer Chemistry. *Chemical reviews* **2009**, *109*, 5288.

(86) Kobayashi, S.; Uyama, H.; Ohmae, M. Enzymatic Polymerization for Precision Polymer Synthesis. *Bulletin of the Chemical Society of Japan* **2001**, *74*, 613.

(87) Matsumura, S. Enzymatic Synthesis of Polyesters via Ring-opening Polymerization. *Advances in Polymer Science* **2006**, *194*, 95.

(88) Reihmann, M.; Ritter, H. Synthesis of Phenol Polymers using Peroxidases. *Advances in Polymer Science* **2006**, *194*, 1.

(89) Singh, A.; Kaplan, D. L. In Vitro Enzyme-induced Vinyl Polymerization. *Advances in Polymer Science* **2006**, *194*, 211.

(90) Uyama, H.; Kobayashi, S. Enzymatic Synthesis and Properties of Polymers from Polyphenols. *Advances in Polymer Science* **2006**, *194*, 51.

(91) Uyama, H.; Kobayashi, S. Enzymatic Synthesis of Polyesters via Polycondensation. *Advances in Polymer Science* **2006**, *194*, 133.

(92) Simon, G. M.; Cravatt, B. F. Activity-based Proteomics of Enzyme Superfamilies: Serine Hydrolases as a Case Study. *Journal of Biological Chemistry* **2010**, *285*, 11051.

(93) Varma, I. K.; Albertsson, A.C.; Rajkhowaa, R.; Srivastava, R. K. Enzyme Catalyzed Synthesis of Polyesters. *Progress in Polymer Science* **2005**, *30*, 949.

(94) Martinelle, M.; Hult, K. Kinetics of Acyl Transfer Reactions in Organic Media Catalysed by *Candida Antarctica* Lipase B. *Biochimica et Biophysica Acta* **1995**, *1251*, 191.

(95) Chulalaksananukul, W.; Condoret, J. S.; Delorme, P.; Willemot, R. M. Kinetic Study of Esterification by Immobilized Lipase in n-hexane. *FEBS Letters* **1990**, *276*, 181.

(96) Kobayashi, S.; Uyama, H. In Vitro Polyester Synthesis via Enzymatic Polymerization. *Current Organic Chemistry* **2002**, *6*, 209.

(97) Hermoso, J.; Pignol, D.; Kerfelec, B.; Crenon, I.; Chapus, C.; Fontecilla-Camps, J. C. Lipase Activation by Nonionic Detergents. *The Journal of Biological Chemistry* **1996**, *271*, 18007.

(98) Reis, P.; Holmberg, K.; Watzke, H.; Leser, M. E.; Miller, R. Lipases at Interfaces: A review. *Advances in colloid and interface science* **2009**, *147-148*, 237.

(99) Cook, P. F.; Cleland, W. W. *Enzyme Kinetics and Mechanism*; Garland Science: New York, NY, 2007.

(100) Choi, Y.J.; Chae, H. J.; Kim, E. Y. Steady-State Oxidation Model by Horseradish Peroxidase for the Estimation of the Non-Inactivation Zone in the Enzymatic Removal of Pentachlorophenol. *Journal of Bioscience and Bioengineering* **1999**, *88*, 368.

(101) Frieden, C. Slow Transitions and Hysteretic Behavior in Enzymes. *Annual Review of Biochemistry* **1979**, *48*, 471.

(102) Case, A.; Huskey, P. W.; Stein, R. L. Enzymatic Reaction of Silent Substrates: Kinetic Theory and Application to the Serine Protease Chymotrypsin. *Biochemistry* **2003**, *42*, 4727.

(103) Marangoni, A. G. Enzyme Kinetics of Lipolysis Revisited: The Role of Lipase Interfacial Binding. *Biochemical and Biophysical Research Communications* **1994**, *200*, 1321.

(104) Verger, R. *Methods in Enzymology*; Daniel, L. P., Ed.; Academic Press: 1980; Vol. Volume 64, p 340.

(105) Pattus, F.; Slotboom, A. J.; De Haas, G. H. Regulation of Phospholipase A2 Activity by the Lipid-water Interface: a Monolayer Approach. *Biochemistry* **1979**, *18*, 2691.

(106) Chahinian, H.; Sarda, L. Distinction Between Esterases and Lipases: Comparative Biochemical Properties of Sequence-related Carboxylesterases. *Protein & Peptide Letters* **2009**, *16*, 1149.

(107) Rakels, J. L. L.; Romein, B.; Straathof, A. J. J.; Heijnen, J. J. Kinetic Analysis of Enzymatic Chiral Resolution by Progress Curve Evaluation. *Biotechnology and Bioengineering* **1994**, *43*, 411.

(108) Akbar, U.; Aschenbrenner, C. D.; Harper, M. R.; Johnson, H. R.; Dordick, J. S.; Clark, D. S. Direct Solubilization of Enzyme Aggregates with Enhanced Activity in Nonaqueous Media. *Biotechnology and Bioengineering* **2006**, *96*, 1030.

(109) Gilbert, H. F. Thiol/disulfide Exchange Equilibria and Disulfide Bond Stability. *Methods in Enzymology* **1995**, *251*, 8.

(110) Alexander, K. M. Improving Enzymes by Using them in Organic Solvents. *Nature* **2001**, *409*, 241.

(111) Anderegg, J. W.; Beeman, W. W.; Shulman, S.; Kaesberg, P. An Investigation of the Size, Shape and Hydration of Serum Albumin by Small-Angle X-Ray Scattering. *Journal of the American Chemical Society* **1955**, *77*, 2927.

(112) Tanford, C. *Physical Chemistry of Macromolecules*; John Wiley & Sons: New York, 1961.

(113) Martin, S. F.; Hergenrother, P. J. Catalytic Cycle of the Phosphatidylcholine-Preferring Phospholipase C from Bacillus Cereus. Solvent Viscosity, Deuterium Isotope Effects, and Proton Inventory Studies. *Biochemistry* **1999**, *38*, 4403.

(114) Tokarev, I.; Minko, S. Stimuli-responsive Hydrogel Thin Films. *Soft Matter* **2009**, *5*, 511.

(115) Lee, H.; Lee, B. P.; Messersmith, P. B. A Reversible Wet/Dry Adhesive Inspired by Mussels and Geckos. *Nature* **2007**, *448*, 338.

(116) Jeong, K.-H.; Kim, J.; Lee, L. P. Biologically Inspired Artificial Compound Eyes. *Science* **2006**, *312*, 557.

(117) Feng, L.; Li, S.; Li, H.; Zhai, J.; Song, Y.; Jiang, L.; Zhu, D. Super-Hydrophobic Surface of Aligned Polyacrylonitrile Nanofibers. *Angewandte Chemie International Edition* **2002**, *41*, 1221.

(118) Zhai, L.; Berg, M. C.; Cebeci, F. C.; Kim, Y.; Milwid, J. M.; Rubner, M. F.; Cohen, R. E. Patterned Superhydrophobic Surfaces: Toward a Synthetic Mimic of the Namib Desert Beetle. *Nano Letters* **2006**, *6*, 1213.

(119) Nam, K. T.; Kim, D.-W.; Yoo, P. J.; Chiang, C.-Y.; Meethong, N.; Hammond, P. T.; Chiang, Y.-M.; Belcher, A. M. Virus-Enabled Synthesis and Assembly of Nanowires for Lithium Ion Battery Electrodes. *Science* **2006**, *312*, 885.

(120) Minton, A. P. The Influence of Macromolecular Crowding and Macromolecular Confinement on Biochemical Reactions in Physiological Media. *The Journal of Biological Chemistry* **2001**, *276*, 10667.

(121) Betancor, L.; Luckarift, H. R. Bioinspired Enzyme Encapsulation for Biocatalysis. *Trends in Biotechnology* **2008**, *26*, 566.

(122) Kim, J.; Jia, H.; Wang, P. Challenges in Biocatalysis for Enzyme-Based Biofuel Cells. *Biotechnology Advances* **2006**, *24*, 296.

(123) Sarma, A. K.; Vatsyayan, P.; Goswami, P.; Minteer, S. D. Recent Advances in Material Science for Developing Enzyme Electrodes. *Biosensors and Bioelectronics* **2009**, *24*, 2313.

(124) Van Krevelen, D. W. *Properties of Polymers*; Fourth ed.; Elsevier: Amsterdam, 2009.

(125) Rawlins, J. W.; Wales, M. E. Putting Nature to Work: Using Enzymes for Decontamination and Polymer Modification. *European Coatings Journal* **2008**, 26.

(126) Fu, T. Y.; Morawetz, H. Enzymatic Attack on Side Chains of Synthetic Polymers. Chymotrypsin-catalyzed Hydrolysis of Specific Substrate Groups Attached to Acrylamide or Acrylic Acid Co-polymers. *Journal of Biological Chemistry* **1976**, *251*, 2083.

(127) Romdhane, I. H.; Price, P. E.; Miller, C. A.; Benson, P. T.; Wang, S. Drying of Glassy Polymer Films. *Industrial & Engineering Chemistry Research* **2001**, *40*, 3065.

(128) Hutchinson, J. M. Physical Aging of Polymers. *Progress in Polymer Science* **1995**, *20*, 703.

(129) Van Roon, J. L.; Joerink, M.; Rijkers, M. P. W. M.; Tramper, J.; Schroen, C. G. P. H.; Beeftink, H. H. Enzyme Distribution Derived from Macroscopic Particle Behavior of an Industrial Immobilized Penicillin-G Acylase. *Biotechnology Progress* **2003**, *19*, 1510.

(130) Neogi, P. *Diffusion in Polymers*; Marcel Dekker: New York, 1996.

(131) Cohen, M. H.; Turnbull, D. Molecular Transport in Liquids and Glasses. *The Journal of Chemical Physics* **1959**, *31*, 1164.

(132) Vrentas, J. S.; Duda, J. L.; Ling, H. C. Free-Volume Theories for Self-Diffusion in Polymer-Solvent Systems. I. Conceptual Differences in

Theories. *Journal of Polymer Science: Polymer Physics Edition* **1985**, *23*, 275.

(133) Vrentas, J. S.; Vrentas, C. M. Solvent Self-Diffusion in Glassy Polymer-Solvent Systems. *Macromolecules* **1994**, *27*, 5570.

(134) Vrentas, J. S.; Duda, J. L. Diffusion of Small Molecules in Amorphous Polymers. *Macromolecules* **1976**, *9*, 785.

(135) Budd, P. M.; McKeown, N. B.; Fritsch, D. Free Volume and Intrinsic Microporosity in Polymers. *Journal of Materials Chemistry* **2005**, *15*, 1977.

(136) Bondi, A. van der Waals Volumes and Radii. *The Journal of Physical Chemistry* **1964**, *68*, 441.

(137) Levenspiel, O. *Chemical Reaction Engineering*; 3rd ed. ed.; John Wiley & Sons, Inc., 1999.

(138) Bailey, J. E.; Ollis, D. F. *Biochemical Engineering Fundamentals*; McGraw-Hill: New York, 1977.

(139) Berendsen, W. R.; Lapin, A.; Reuss, M. Investigations of Reaction Kinetics for Immobilized Enzymes-Identification of Parameters in the Presence of Diffusion Limitation. *Biotechnology Progress* **2006**, *22*, 1305.

(140) Unemoria , M.; Matsuyaa, Y.; Matsuyab, S.; Akashia, A.; Akaminea, A. Water Absorption of Poly(methyl methacrylate) Containing 4-Methacryloxyethyl Trimellitic Anhydride. *Biomaterials* **2003**, *24*, 1381.

(141) Ordaz, I.; Singh, L.; Ludovice, P. J.; Henderson, C. L. Small Molecule Diffusion in Polymer Ultra-Thin Films In *Materials Research Society Symposia Proceedings 2006*; Vol. 899E, p 0899.

(142) Barrie, J. A.; Machin, D. Diffusion and Association of Water in Some Polyalkylmethacrylates. Part 1 - Equilibrium Sorption and Steady State Permeation. *Transactions of the Faraday Society* **1971**, *67*, 244.

(143) *Intelligent Materials*; Shahinpoor, M.; Schneider, H.J., Eds.; The Royal Society of Chemistry: Cambridge, UK, 2008.

(144) Sperling, L. H. *Introduction to Physical Polymer Science*; 4th ed.; John Wiley & Sons, Inc.: Hoboken, NJ, 2006.

(145) Riggleman, R. A.; Douglas, J. F.; Pablo, J. J. Tuning Polymer Melt Fragility with Antiplasticizer Additives. *The Journal of Chemical Physics* **2007**, *126*.

(146) Wojtecki, R. J.; Meador, M. A.; Rowan, S. J. Using the Dynamic Bond to Access Macroscopically Responsive Structurally Dynamic Polymers. *Nature Materials* **2011**, *10*, 14.

(147) Roy, D.; Cambre, J. N.; Sumerlin, B. S. Future Perspectives and Recent Advances in Stimuli-Responsive Materials. *Progress in Polymer Science* **2010**, *35*, 278.

(148) Cordier, P.; Tournilhac, F.; Soulie-Ziakovic, C.; Leibler, L. Self-healing and Thermoreversible Rubber from Supramolecular Assembly. *Nature* **2008**, *451*, 977.

(149) Deng, G.; Tang, C.; Li, F.; Jiang, H.; Chen, Y. Covalent Cross-Linked Polymer Gels with Reversible Sol−Gel Transition and Self-Healing Properties. *Macromolecules* **2010**, *43*, 1191.

(150) Scott, T. F.; Schneider, A. D.; Cook, W. D.; Bowman, C. N. Photoinduced Plasticity in Cross-linked Polymers. *Science* **2005**, *308*, 1615.

(151) Yoshida, R. Design of Functional Polymer Gels and Their Application to Biomimetic Materials. *Current Organic Chemistry* **2005**, *9*, 1617.

(152) Innocenzi, P.; Malfatti, L.; Soler-Illia, G. J. A. A. Hierarchical Mesoporous Films: From Self-Assembly to Porosity with Different Length Scales. *Chemistry of Materials* **2011**, *23*, 2501.

(153) McKeown, N. B.; Budd, P. M. Exploitation of Intrinsic Microporosity in Polymer-Based Materials. *Macromolecules* **2010**, *43*, 5163.

(154) Nagai, K.; Masuda, T.; Nakagawa, T.; Freeman, B. D.; Pinnau, I. Poly[1-(trimethylsilyl)-1-propyne] and Related Polymers: Synthesis, Properties and Functions. *Progress in Polymer Science* **2001**, *26*, 721.

(155) George, S. C.; Thomas, S. Transport Phenomena through Polymeric Systems. *Progress in Polymer Science* **2001**, *26*, 985.

(156) Van der Wel, G. K.; Adan, O. C. G. Moisture in Organic Coatings - A Review. *Progress in Organic Coatings* **1999**, *37*, 1.

(157) Laane, C.; Boeren, S.; Vos, K.; Veeger, C. Rules for Optimization of Biocatalysis in Organic Solvents. *Biotechnology and Bioengineering* **1987**, *30*, 81.

(158) Fox, T. G.; Flory, P. J. Second-Order Transition Temperatures and Related Properties of Polystyrene. I. Influence of Molecular Weight. *Journal of Applied Physics* **1950**, *21*, 581.

(159) Venditti, R. A.; Gillham, J. K. Isothermal Physical Aging of Poly(methyl methacrylate): Localization of Perturbations in Thermomechanical Properties. *Journal of Applied Polymer Science* **1992**, *45*, 501.

(160) Kovacs, A. J.; Stratton, R. A.; Ferry, J. D. Dynamic Mechanical Properties of Polyvinyl Acetate in Shear in the Glass Transition Temperature Range. *The Journal of Physical Chemistry* **1963**, *67*, 152.

(161) Brahim, S.; Narinesingh, D.; Guiseppi-Elie, A. Kinetics of Glucose Oxidase Immobilized in p(HEMA)-hydrogel Microspheres in a Packed-Bed Bioreactor. *Journal of Molecular Catalysis B: Enzymatic* **2002**, *18*, 69.

(162) Narinesingh, D.; Stoute, V. A.; Davis, G.; Ngo, T. T. b-Galactosidase Covalently Immobilized on Fractogel Derivative: Preparation, Bioreactor Flow Kinetics, Solvent Effects and Stability. *Journal of Molecular Catalysis* **1988**, *45*, 285.

(163) Fernandes, M. L. M.; Krieger, N.; Baron, A. M.; Zamoraa, P. P.; Ramosa, L. P.; Mitchell, D. A. Hydrolysis and Synthesis Reactions Catalysed by *Thermomyces lanuginosa* Lipase in the AOT/Isooctane Reversed Micellar System. *Journal of Molecular Catalysis B: Enzymatic* **2004**, *30*, 43.

(164) Biasutti, M. A.; Abuin, E. B.; Silber, J. J.; Correa, N. M.; Lissi, E. A. Kinetics of Reactions Catalyzed by Enzymes in Solutions of Surfactants. *Advances in Colloid and Interface Science* **2008**, *136*, 1.

(165) Hedstrom, G.; Backlund, S.; Eriksson, F. Influence of Diffusion on the Kinetics of an Enzyme-Catalyzed Reaction in Gelatin-Based Gels. *Journal of Colloid and Interface Science* **2001**, *239*, 190.

(166) Williams, M. L.; Landel, R. F.; Ferry, J. D. The Temperature Dependence of Relaxation Mechanisms in Amorphous Polymers and Other Glass-forming Liquids. *Journal of American Chemical Society* **1955**, *77*, 3701.

(167) Bistac, S.; Schultz, J. Solvent Retention in Solution-cast Films of PMMA: Study by Dielectric Spectroscopy. *Progress in Organic Coatings* **1997**, *31*, 347.

(168) Leo, A.; Hansch, C.; Elkins, D. Partition Coefficients and their Uses. *Chemical Reviews* **1971**, *71*, 525.

(169) Laane, C.; Boeren, S.; Vos, K. On Optimizing Organic Solvents in Multi-Liquid-Phase Biocatalysis. *Trends in Biotechnology* **1985**, *3*, 251.

(170) Fredrickson, G. H.; Helfand, E. Dual-Mode Transport of Penetrants in Glassy Polymers. *Macromolecules* **1985**, *18*, 2201.

(171) Wypych, G. *Handbook of Material Weathering*; 4th ed.; ChemTech Publishing: Toronto, 2008.

(172) *Service Life Prediction: Challenging the Status Quo*; Martin, J. W.; Ryntz, R. A.; Dickie, R. A., Eds.; Federation of Societies for Coatings Technology, 2005.

(173) Casale, A.; Porter, R. S. *Polymer Stress Reactions*; Academic Press: New York, 1978.

(174) Higaki, Y.; Otsuka, H.; Takahara, A. A Thermodynamic Polymer Cross-linking System Based on Radically Exchangeable Covalent Bonds. *Macromolecules* **2006**, *39*, 2121.

(175) Amamoto, Y.; Kikuchi, M.; Masunaga, H.; Ogawa, H.; Sasaki, S.; Otsuka, H.; Takahara, A. Mesh-size Control and Functionalization of Reorganizable Chemical Gels by Monomer Insertion into their Cross-linking Points. *Polymer Chemistry* **2011**, *2*, 957.

(176) Drobník, J.; Kopeček, J.; Labský, J.; Rejmanová, P.; Exner, J.; Saudek, V.; Kálal, J. Enzymatic Cleavage of Side Chains of Synthetic Water-soluble Polymers. *Die Makromolekulare Chemie* **1976**, *177*, 2833.

(177) Odian, G. *Principles of Polymerization*; Fourth ed.; John Wiley & Sons: Hoboken, New Jersey, 2004.

(178) Naira, L. S.; Laurencin, C. T. Biodegradable Polymers as Biomaterials. *Progress in Polymer Science* **2007**, *32*, 762.

(179) Tamada, J. A.; Langer, R. Erosion Kinetics of Hydrolytically Degradable Polymers. *Proceedings to the National Academy of Sciences* **1993**, *90*, 552.

(180) Okada, M. Chemical Synthesis of Biodegradable Polymers. *Progress in Polymer Science* **2002**, *27*, 87.

(181) García, J. M.; García, F. C.; Serna, F.; Pena, J. L. d. l. High-performance Aromatic Polyamides. *Progress in Polymer Science* **2010**, *35*, 623.

(182) Garg, P.; Keul, H.; Klee, D.; Moller, M. Thermal Properties of Poly(ester amide)s with Isolated, Two Adjacent and Three Adjacent Amide Groups within a Polyester Chain. *Macromolecular Chemistry and Physics* **2009**, *210*, 1754.

(183) Bettinger, C. J.; Bruggeman, J. P.; Borenstein, J. T.; Langer, R. S. Amino Alcohol-based Degradable Poly(ester amide) Elastomers. *Biomaterials* **2008**, *29*, 2315.

(184) Botines, E.; Franco, L.; Puiggali, J. Thermal Stability and Degradation Studies of Alternating Poly(ester amide)s Derived from Glycolic Acid and ω-amino acids. *Journal of Appied Polymer Science* **2006**, *102*, 5545.

(185) Botines, E.; Rodriguez-Galan, A.; Puiggali, J. Poly(ester amide)s Derived from 1,4-butanediol, Adipic Acid and 1,6-aminohexanoic acid: Characterization and Degradation Studies. *Polymer* **2002**, *43*, 6073.

(186) Flores, A.; Pietkiewicz, D.; Stribeck, N.; Roslaniec, Z.; Calleja, F. J. B. Structural Features of Random Polyester-Amide Copolymers As Revealed by X-ray Scattering and Microindentation Hardness. *Macromolecules* **2001**, *34*, 8094.

(187) Garg, P.; Keul, H.; Klee, D.; Moller, M. Concept and Synthesis of Poly(ester amide)s with One Isolated, Two or Three Consecutive Amide Bonds Randomly Distributed Along the Polyester Backbone. *Designed Monomers and Polymers* **2009**, *12*, 405.

(188) Serrano, P. J. M.; Van, B. A. C. M.; Gaymans, R. J. Alternating Polyester Amides Based on 1,4-butylene terephthalamide: 1. Synthesis of the Bisester Diamide. *Polymer* **1998**, *39*, 5773.

(189) De Wit, M. A.; Wang, Z.; Atkins, K. M.; Mequanint, K.; Gillies, E. R. Syntheses, Characterization, and Functionalization of Poly(ester amide)s

with Pendant Amine Functional Groups. *Journal of Polymer Science, Part A: Polymer Chemistry* **2008**, *46*, 6376.

(190) Deng, M.; Wu, J.; Reinhart-King, C. A.; Chu, C.C. Synthesis and Characterization of Biodegradable Poly(ester amide)s with Pendant Amine Functional Groups and in Vitro Cellular Response. *Biomacromolecules* **2009**, *10*, 3037.

(191) Del, V. L. J.; Sepulcre, F.; Gamez, A.; Rodriguez-Galan, A.; Puiggali, J. New Poly(ester amide)s Containing Glycolic Acid Units: Evaluation of Biocompatibility. *Current Trends in Polymer Science* **2008**, *12*, 27.

(192) Regaño, C.; Alla, A.; Ilarduya, A. M. d.; Muñoz-Guerra, S. Poly(ester amide)s Derived from L-Malic Acid. *Macromolecules* **2004**, *37*, 2067.

(193) Stapert, H. R.; Bouwens, A.M.; Dijkstra, P. J.; Feijen, J. Environmentally Degradable Aliphatic Poly(ester-amide)s Based on Short, Symmetrical, and Uniform Bisamide-diol Blocks. Part 1. Synthesis and Interchange Reactions. *Macromolecular Chemistry and Physics* **1999**, *200*, 1921.

(194) Mahapatro, A.; Kalra, B.; Kumar, A.; Gross, R. A. Lipase-Catalyzed Polycondensations: Effect of Substrates and Solvent on Chain Formation, Dispersity, and End-Group Structure. *Biomacromolecules* **2003**, *4*, 544.

(195) Mahapatro, A.; Kumar, A.; Kalra, B.; Gross, R. A. Solvent-Free Adipic Acid/1,8-Octanediol Condensation Polymerizations Catalyzed by Candida Antarctica Lipase B. *Macromolecules* **2004**, *37*, 35.

(196) Feng, Y.; Knufermann, J.; Klee, D.; Hocker, H. Enzyme-Catalyzed Ring-Opening Polymerization of 3(S)-isopropylmorpholine-2,5-dione. *Macromolecular Rapid Communications* **1999**, *20*, 88.

(197) Feng, Y.; Knufermann, J.; Klee, D.; Hocker, H. Lipase-Catalyzed Ring-Opening Polymerization of 3(S)-isopropylmorpholine-2,5-dione. *Macromolecular Chemistry and Physics* **1999**, *200*, 1506.

(198) Feng, Y.; Klee, D.; Keul, H.; Hocker, H. Lipase-Catalyzed Ring-Opening Polymerization of Morpholine-2,5-dione Derivatives: A Novel Route to the Synthesis of Poly(ester amide)s. *Macromolecular Chemistry and Physics* **2000**, *201*, 2670.

(199) MacDonald, R. T.; Pulapura, S. K.; Svirkin, Y. Y.; Gross, R. A.; Kaplan, D. L.; Akkara, J.; Swift, G.; Wolk, S. Enzyme-Catalyzed ε-Caprolactone Ring-Opening Polymerization. *Macromolecules* **1995**, *28*, 73.

(200) Uyama, H.; Suda, S.; Kikuchi, H.; Kobayashi, S. Extremely Efficient Catalysis of Immobilized Lipase in Ring-Opening Polymerization of Lactones. *Chemistry Letters* **1997**, *26*, 1109.

(201) Küllmer, K.; Kikuchi, H.; Uyama, H.; Kobayashi, S. Lipase-Catalyzed Ring-Opening Polymerization of α-methyl-δ-valerolactone and α-methyl-ε-caprolactone. *Macromolecular Rapid Communications* **1998**, *19*, 127.

(202) Kikuchi, H.; Uyama, H.; Kobayashi, S. Lipase-Catalyzed Ring-Opening Polymerization of Substituted Lactones. *Polymer Journal* **2002**, *34*, 835.

(203) Chaudhary, A. K.; Beckman, E. J.; Russell, A. J. *Enzymes for Polyester Synthesis*; American Chemical Society Series, 1998.

(204) Kumar, A.; Gross, R. A. Candida Antarctica Lipase B-Catalyzed Transesterification: New Synthetic Routes to Copolyesters. *Journal of American Chemical Society* **2000**, *122*, 11767.

(205) Kobayashi, S. Enzymatic Ring-Opening Polymerization of Lactones by Lipase Catalyst: Mechanistic Aspects. *Macromolecular Symposia* **2006**, *240*, 178.

(206) Wang, Y.F.; Lalonde, J. J.; Momongan, M.; Bergbreiter, D. E.; Wong, C.-H. Lipase-Catalyzed Irreversible Transesterifications Using Enol Esters as Acylating Reagents: Preparative Enantio- and Regioselective Syntheses of Alcohols, Glycerol Derivatives, Sugars, and Organometallics. *Journal of American Chemical Society* **1988**, *110*, 7200.

(207) Guo, L.; Zhang, Z.; Zhu, Y.; Li, J.; Xie, Z. Synthesis of Polysiloxane–Polyester Copolymer by Lipase-Catalyzed Polycondensation. *Journal of Applied Polymer Science* **2008**, *108*, 1901.